Mechanical Engineering Series

Frederick F. Ling
Series Editor

Springer Science+Business Media, LLC

Mechanical Engineering Series

Introductory Attitude Dynamics
F.P. Rimrott

Balancing of High-Speed Machinery
M.S. Darlow

Theory of Wire Rope, 2nd ed.
G.A. Costello

Theory of Vibration: An Introduction, 2nd ed.
A.A. Shabana

Theory of Vibration: Discrete and Continuous Systems, 2nd ed.
A.A. Shabana

Laser Machining: Theory and Practice
G. Chryssolouris

Underconstrained Structural Systems
E.N. Kuznetsov

Principles of Heat Transfer in Porous Media, 2nd ed.
M. Kaviany

Mechatronics: Electromechanics and Contromechanics
D.K. Miu

Structural Analysis of Printed Circuit Board Systems
P.A. Engel

Kinematic and Dynamic Simulation of Multibody Systems: The Real-Time Challenge
J. García de Jalón and E. Bayo

High Sensitivity Moiré: Experimental Analysis for Mechanics and Materials
D. Post, B. Han, and P. Ifju

Principles of Convective Heat Transfer
M. Kaviany

(continued after index)

Wodek K. Gawronski

Dynamics and Control of Structures

A Modal Approach

With 126 Figures

Springer

Wodek K. Gawronski
Jet Propulsion Laboratory
California Institute of Technology
Pasadena, CA 91109, USA

Series Editor
Frederick F. Ling
Ernest F. Gloyna Regents Chair in Engineering
Department of Mechanical Engineering
The University of Texas at Austin
Austin, TX 78712-1063, USA
and
William Howard Hart Professor Emeritus
Department of Mechanical Engineering,
Aeronautical Engineering and Mechanics
Rensselaer Polytechnic Institute
Troy, NY 12180-3590, USA

Library of Congress Cataloging-in-Publication Data
Gawronski, Wodek, 1944–
Dynamics and control of structures : a modal approach / Wodek K. Gawronski.
p. cm. — (Mechanical engineering series)
Includes bibliographical references and index.
ISBN 978-1-4757-5033-1 ISBN 978-0-387-21855-7 (eBook)
DOI 10.1007/978-0-387-21855-7
1. Modal analysis. 2. Structural analysis (Engineering)
3. Structural control (Engineering) I. Title. II. Series:
Mechanical engineering series (Berlin, Germany)
TA654.15.G39 1998
624.1′71—dc21 98-16914

Printed on acid-free paper.

Originally published by Springer-Verlag New York, Inc. in 1998

Production managed by Victoria Evarretta; manufacturing supervised by Jeffrey Taub.
Photocomposed copy prepared from the author's Microsoft Word files.

9 8 7 6 5 4 3 2 1

ISBN 978-1-4757-5033-1 SPIN 10678009

To Barbara, Jakub, and Kaja

Although this may seem a paradox, all exact science
is dominated by the idea of approximation.

Bertrand Russell

Mechanical Engineering Series

Frederick F. Ling
Series Editor

Advisory Board

Applied Mechanics	F.A. Leckie University of California, Santa Barbara
Biomechanics	V.C. Mow Columbia University
Computational Mechanics	H.T. Yang University of California, Santa Barbara
Dynamical Systems and Control	K.M. Marshek University of Texas, Austin
Energetics	J.R. Welty University of Oregon, Eugene
Mechanics of Materials	I. Finnie University of California, Berkeley
Processing	K.K. Wang Cornell University
Production Systems	G.-A. Klutke Texas A&M University
Thermal Science	A.E. Bergles Rensselaer Polytechnic Institute
Tribology	W.O. Winer Georgia Institute of Technology

Preface

Robots, aerospace structures, active earthquake-damping devices of tall buildings, and active sound suppression are examples of the application of structural dynamics and control methods. This book addresses the structural dynamics and control problems encountered by mechanical, civil, and control engineers. Many problems presented in this book originated in recent applications in the aerospace industry, and have been solved using the approach presented here.

Dynamics analysis and controller design for flexible structures require a special approach due to the large size of structural models, and because flexible structure testing and control typically requires massive instrumentation (sensors and actuators). But the rapid development of new technologies and the increased power of computers allows for the formulation and solution of engineering problems that seemed to be unapproachable not so very long ago.

The modal approach was chosen in this book. It has a long tradition in structural engineering (see, e.g., [84], [87], and [26]) and is also used in control system analysis, e.g., [93]. Its usefulness, thoroughly tested, does not need extensive justification. Both structural testing and analysis give priority to the modal representation, due to its compactness, simplicity, and explicit physical interpretation. Also, many useful structural properties are properly exposed only in modal coordinates. In this book the modal approach, preferred by structural engineers, is extended into control engineering, giving new analytical results, and narrowing the gap between structural and control analysis.

The structural dynamics problems presented in this book include system modeling using either structural equations (derived from the laws of physics), or computer software (using finite-element tools), or field test data (using the system identification approach). System norms, as a means of measuring the "size" of a system and its modes, form a base for the system performance evaluation. Properties of norms of modes and of structures (including H_2, H_∞, and Hankel norms) are derived and used to solve the optimal model reduction problem. Reduction of the structural model is important not only to reduce computational effort, but is a key issue in system identification (allowing one to

avoid the inclusion of noise into the structural model), and in controller design (simplification of controller software and hardware). The actuator/sensor location for structural testing and control is another important issue. It is often required to locate sensors at a large number of candidate locations. Search procedures typically used for this purpose are computationally expensive, fail to perform for a large number of candidate locations, and do not guarantee the optimal solution. The actuator/sensor placement methods presented in this book are optimal, and allow for the quick location of sensors and actuators, even for a large number of candidate locations. The example of the International Space Station structure, with a choice of four actuators and 341 accelerometers out of 11,804 candidate locations, illustrates the advantages of the presented approach.

The control issues include the properties, analysis, and design of the dissipative, LQG, and H_∞ controllers. It is assumed in this book that the controllers are of low authority, i.e., that the controller action does not completely destroy the structural properties. This is a typical approach in the design of the controllers for flexible structures, since the low-authority controller for the flexible part of the structure preserves its tracking properties that should not deteriorate. The connections between structural parameters, controller gains, and the root-locus have been derived. This approach is illustrated with the dissipative, LQG, and H_∞ controller design for a simple structure, for the two-dimensional (2D) and three-dimensional (3D) trusses, and for the tracking control of the NASA Deep Space Network antenna. In the latter case the controllers were tested and implemented to serve the current NASA missions.

Several books on structural dynamics and control have been published. Meirovitch's graduate college textbook [84] covers methods of structural dynamics (virtual work, d'Alambert's principle, Hamilton's principle, Lagrange's and Hamilton's equations, and modal analysis of structures) and control, including pole placement methods, LQG design, and modal control. Ewins [26] presents the methods of modal testing of structures. Natke's book [87] on structural identification also contains excellent material on structural dynamics. Fuller, Elliot, and Nelson [30] cover problems of structural active control and structural acoustic control. Inman's book [60] introduces the basic concepts of vibration control. The book by Preumont [94] introduces modern approaches to structural control, including LQG controllers, sensors, and actuator placement, and piezoelectric materials with numerous applications in aerospace and civil engineering. The Junkins and Kim book [67] is a graduate-level textbook on dynamics and control of flexible structures. The Porter and Crossley book [93] is one of the first books on modal control. The Skelton book [98], on the control of general linear systems, introduces methods designed specifically for the control of flexible structures. For example, the component cost approach to model or controller reduction is frequently used in this field. The monograph by Joshi [64] on control flexible space structures presents developments on dissipative and LQG controllers supported by numerous

applications. The book by Kwon and Bang [72] is dedicated mainly to the development and analysis of structural finite-element models, but part of it is dedicated to structural dynamics and to structural control. My previous book [34] approached structural dynamics and control problems in balanced coordinates.

In this book, modal coordinates have been chosen. They are commonly used by structural engineers, and are also useful in control system analysis. Modal representation can be approximately balanced (open- or closed-loop) by choosing the appropriate scale factors. The connection between balanced and modal coordinates is derived here. This book also differs from [34] not only in its approach, but also by its content: new methods, properties, applications, and examples are presented.

The purpose of this book is to introduce the methods of structural dynamics (such as modal properties and modal models) to structural control analysis and design, and to incorporate the control concepts and methods (such as system norms, or controllability and observability properties) in structural dynamics analysis. The combination of control and structural concepts allows one to unveil new structural properties and gives new insight on the well-known control laws. Also, it makes it easier for structural engineers to design control laws for flexible systems, and allows control engineers to operate in the structural dynamics environment. In short, it should serve as a bridge between the structural and control engineering.

Chapter 1 defines the term "flexible structure" (in brief, a structure), and presents examples of structures, including a simple structure, 2D and 3D trusses, the NASA Deep Space Network antenna, and the International Space Station structure.

Chapter 2 discusses in detail structural models: second-order and state-space models. Models are either derived from the laws of physics (e.g., force equilibrium, d'Alambert's principle, Lagrange's equations), obtained from the finite-element codes, or from structural test data. All three approaches are illustrated in this book. A simple structure model is derived from the force equilibrium laws, while models of 2D and 3D trusses, and the International Space Station structure are obtained from the finite-element codes. The structural model of the Deep Space Network antenna was identified from the field test data.

System controllability and observability properties are extensively used in system dynamics evaluation. The controllability and observability grammians are introduced in Chapter 3, and the balanced system representation obtained. Also, the controllability and observability properties of structures are derived.

Chapter 4 defines the system H_2, H_∞, and Hankel norms, and specifies them (in terms of structural parameters) for each individual mode, as well as for the entire structure. Properties of norms, used later in system dynamics and control, are derived.

Chapter 5 describes model reduction in modal coordinates, in terms of H_2, H_∞, and Hankel norms. The purpose of model reduction is to obtain a structural reduced model as small as possible, so that the dynamic response of the reduced model is close to the response of the full model within a given threshold. Modes of structural models are almost independent. Therefore, the structural norm can be expressed approximately as a combination of modal norms. This property easily translates to the almost-optimal model reduction.

Chapter 6 introduces the choice of sensor and actuator locations such that the prescribed degree of controllability and observability is achieved. If all states are equally controllable and observable, the system is uniformly balanced. Also, the properties of the uniformly balanced system are derived.

The problem of locations of sensors and actuators for structural testing and control is discussed in Chapter 7. This problem is of importance in structural tests since they often require massive instrumentation. The choice of location is neither straightforward nor an easy task. The methods proposed in this book are comparatively simple, allowing for the almost-optimal location of actuators and sensors for large structures, as is illustrated with the International Space Station structure, where 341 sensors have been chosen out of 11,804 candidate locations.

Chapter 8 presents the design of dissipative controllers in modal coordinates. The root-locus depends on modal controllability and observability properties, and these properties are used to shape the closed-loop system properties.

Chapter 9 discusses the LQG controller design issues. The LQG analysis and design is performed using modal coordinates. The performance of the LQG controller depends of the choice of weights of the performance index. Typically, there is no a priori knowledge available to relate the weights and the required performance. In this book, the relationship in modal coordinates between the structural weights and performance is derived, allowing the designer to shape the closed-loop performance. In implementation, the size of the controller is a critical issue. Large-size controllers make the controller software complex, and may introduce parasitic dynamics that can deteriorate the closed-loop performance. We show that in the modal coordinates the LQG controller can be reduced in a simple manner using modal criteria.

Chapter 10 presents the analysis and design of H_∞ and H_2 controllers. The modal coordinates allow for the straightforward implementation of the input and output shaping filters and for shaping the closed-loop performance. Also, this chapter introduces the controller reduction method, and illustrates the approach with the H_∞ controller design for the Deep Space Network antenna. This controller features excellent tracking performance with the wind disturbance rejection properties that meet the stringent antenna performance requirements.

Matlab codes of selected methods and procedures from this book are presented in Appendix A. This includes transformation to the modal coordinates, the open-loop balanced coordinates, the LQG balanced coordinates, and the H_∞ balanced coordinates. Also, the determination of the almost-balanced

modal representation (open-loop, LQG, and H_∞) is given. Finally, the Matlab function for the determination of the H_2 and H_∞ norms for the given actuator and sensor placement (including displacement, rate, and acceleration sensors) is included.

Appendix B includes the parameters of the 2D truss and the Deep Space Network antenna. This allows the reader to check the methods, and to exercise his/her own ideas and modifications, since no result is final and no approach is perfect.

Acknowledgments

I would like to acknowledge the contributions of my colleagues who have had an influence on this work. Kyong Lim (NASA Langley Research Center) in the sensor/actuator placement technology, filter design, and H_∞ controller analysis. Hagop Panossian (Boeing North American, Inc., Rocketdyne), in the sensor/actuator placement of the International Space Station structure. Jer-Nan Juang (NASA Langley Research Center), in the model identification of the Deep Space Network antenna. Jerzy Sawicki (Cleveland State University) in the modal error estimation of the nonproportional damping. And Abner Bernardo (Jet Propulsion Laboratory, California Institute of Technology) for data collection of the antenna.

I am obliged to my managers: Scott Morgan, Chris Yung, Al Bhanji, and Joseph Statman (Jet Propulsion Laboratory, California Institute of Technology) for their support of the Deep Space Network antenna study, part of which is included in this book.

Part of the research described in this book was carried out by the Jet Propulsion Laboratory, California Institute of Technology, under contract with the National Aeronautics and Space Administration.

Wodek Gawronski

Pasadena, California
April 1998

Contents

PART 2. CONTROL

List of Symbols

General

A^T	transpose of matrix A
A^*	complex-conjugate transpose of matrix A
A^{-1}	inverse of square nonsingular matrix A
$\mathrm{tr}(A)$	trace of a matrix A, $\mathrm{tr}(A) = \sum_i a_{ii}$
$\|A\|_2$	Euclidean (Frobenius) norm of a real-valued matrix A: $\|A\|_2 = \sqrt{\sum_{i,j} a_{ij}^2} = \sqrt{\mathrm{tr}(A^T A)}$
$\mathrm{diag}(a_i)$	diagonal matrix with elements a_i along the diagonal
$\mathrm{eig}(A)$	eigenvalue of a square matrix A
$\lambda_i(A)$	ith eigenvalue of a square matrix A
$\lambda_{\max}(A)$	maximal eigenvalue of a square matrix A
$\sigma_i(A)$	ith singular value of a matrix A
$\sigma_{\max}(A)$	maximal singular value of a matrix A
I_n	identity matrix, $n \times n$
$0_{n\times m}$	zero matrix, $n \times m$

Linear Systems

(A,B,C,D)	quadruple of the system state-space representation
(A,B,C)	triple of the system state-space representation
$(A_{lqg},B_{lqg},C_{lqg})$	LQG controller state-space representation
$(A_\infty,B_\infty,C_\infty)$	H_∞ controller state-space representation
(A_o,B_o,C_o)	closed-loop state-space representation
G	transfer function
x	system state
x_e	system estimated state
u	system (control) input
y	system (measured) output
z	performance output
w	disturbance input
B_1	matrix of disturbance inputs
B_2	matrix of control inputs
C_1	matrix of performance outputs
C_2	matrix of measured outputs
$\|G\|_2$	system H_2 norm
$\|G\|_\infty$	system H_∞ norm
$\|G\|_h$	system Hankel norm
$\mathcal{C}$	controllability matrix
$\mathcal{O}$	observability matrix
W_c	controllability grammian
W_o	observability grammian
γ_i	ith Hankel singular value
$\gamma_{\max}$	the largest Hankel singular value of a system
Γ	matrix of Hankel singular values
CARE	controller algebraic Riccati equation
FARE	filter (or estimator) algebraic Riccati equation
HCARE	H_∞ controller algebraic Riccati equation
HFARE	H_∞ filter (or estimator) algebraic Riccati equation
S_c	solution of CARE
S_e	solution of FARE
$S_{\infty c}$	solution of HCARE
$S_{\infty e}$	solution of HFARE
μ_i	ith LQG singular value
$\mu_{\infty i}$	ith H_∞ singular value

$\mathrm{M} = \mathrm{diag}(\mu_i)$	matrix of the LQG singular values
$\mathrm{M}_\infty = \mathrm{diag}(\mu_{\infty i})$	matrix of the H_∞ singular values
ρ	parameter of the H_∞ controller
K_c	controller gain
K_e	estimator gain
ε	tracking error
t	time sequence
N	number of states
s	number of inputs
r	number of outputs

Structures

D	damping matrix
K	stiffness matrix
M	mass matrix
D_m	modal damping matrix
K_m	modal stiffness matrix
M_m	modal mass matrix
q	structural displacement (nodal)
q_m	structural displacement (modal)
q_{ab}	structural displacement (almost-balanced)
q_i	displacement of the *i*th degree of freedom
q_{mi}	displacement of the *i*th mode
q_{abi}	displacement of the *i*th almost-balanced mode
ϕ_i	*i*th structural mode
ϕ_{abi}	almost-balanced *i*th structural mode
Φ	modal matrix
Φ_{ab}	almost-balanced modal matrix
ω_i	*i*th natural frequency
Ω	matrix of natural frequencies
ζ_i	*i*th modal damping
Z	matrix of modal damping coefficients
B_o	nodal input matrix
C_{oq}	nodal displacement output matrix
C_{ov}	nodal velocity output matrix

B_m	modal input matrix
C_{mq}	modal displacement output matrix
C_{mv}	modal velocity output matrix
C_m	modal output matrix, $C_m = C_{mq}\Omega^{-1} + C_{mv}$
b_{mi}	input matrix of the ith mode, ith row of B_m
c_{mi}	output matrix of the ith mode, ith row of C_m
$\|B_m\|_2$	modal input gain
$\|C_m\|_2$	modal output gain, $\|C_m\|_2^2 = \|C_{mq}\Omega^{-1}\|_2^2 + \|C_{mv}\|_2^2$
$\|b_{mi}\|_2$	input gain of the ith mode
$\|c_{mi}\|_2$	output gain of the ith mode
$\Delta\omega_i$	ith half-power frequency, $\Delta\omega_i = 2\zeta_i\omega_i$
σ_{2ij}	H_2 placement index for the ith actuator (sensor) and the kth mode
$\sigma_{\infty ij}$	H_∞ placement index for the ith actuator (sensor) and the kth mode
Σ_2	H_2 placement matrix
Σ_∞	H_∞ placement matrix
$I(k)$	membership index of the kth sensor
β_i	pole shift factor
n_d	number of degrees of freedom
n	number of modes
N	number of states
s	number of inputs
r	number of outputs
S	number of candidate actuator locations
R	number of candidate sensor locations

Part 1

Dynamics

1
Introduction

A flexible structure is a linear system of specific properties. What are the special features that distinguish a flexible structure from other systems? For structural or mechanical engineers its special properties include periodic vibrations with dominating few frequencies, resonances, and natural modes of vibrations. The term "flexible structure" is commonly used within the control engineering community to refer to a linear system with oscillatory properties characterized by strong amplification of a harmonic signal for certain frequencies, a system with weakly correlated states, and which complex conjugate poles have small real parts.

1.1 Flexible Structure Definition

The term *flexible structure* has different interpretations depending on source and application; and for the purposes of this book, a flexible structure is

- a linear system;
- finite-dimensional;
- controllable, and observable; and
- its poles are complex with small real parts;
- its poles are non-clustered.

This definition narrows the class of linear systems under consideration, and based on this definition, many interesting properties of structures and their controllers will be derived. However, our experience shows that even if this definition of a flexible structure is violated or extended the derived properties

W. K. Gawronski, *Dynamics and Control of Structures*

may still hold. For example, for structures with heavy damping, with some of the poles being real, or close to each other, one still obtains reasonable results.

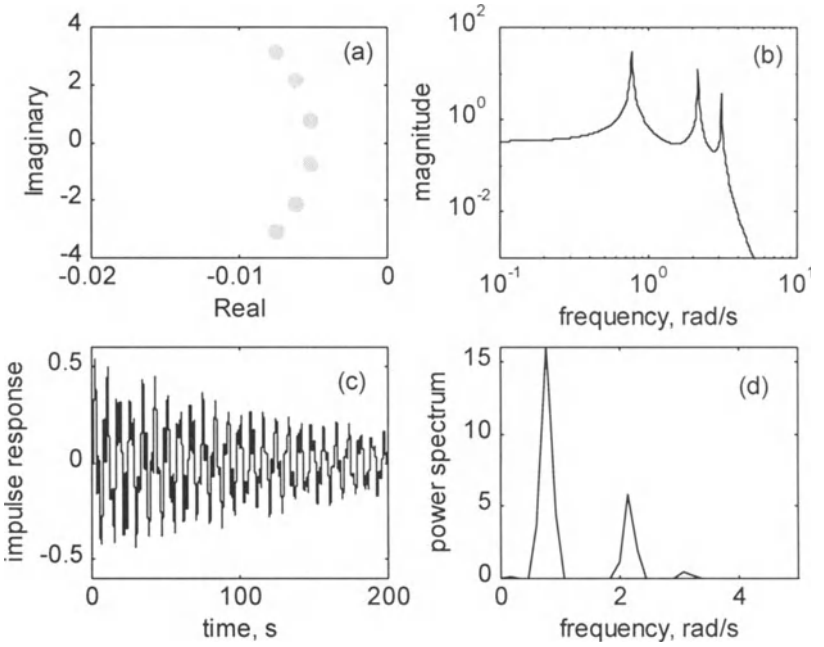

Figure 1.1. Properties of a typical flexible structure: (a) poles; (b) magnitude of a transfer function;(c) impulse response; and (d) power spectrum of the impulse response.

The properties of a typical flexible structure are illustrated in Fig. 1.1. Poles are complex conjugate, with small real parts, and their locations are shown in Fig. 1.1(a). The magnitude of a flexible structure transfer function is shown in Fig. 1.1(b), and is characterized by the presence of resonance peaks. The impulse response of a flexible structure is shown in Fig. 1.1(c), which consists of harmonic components, related to complex poles, or to resonance peaks. These components are clearly visible in the power spectrum of the impulse response as shown in Fig. 1.1(d).

1.2 Examples

In this book five examples of flexible structures are investigated: a simple structure, two-dimensional (2D) and three-dimensional (3D) trusses, the Deep Space Network (DSN) antenna, and the International Space Station structure. They represent different levels of complexity.

1.2.1 A Simple Structure

A three-mass system – a simple flexible structure – is used mainly for illustration purposes. Its simplicity allows for easy analysis, and straightforward interpretation. Also, in this case, solution properties and numerical data can be displayed in a compact form. The system is shown in Fig. 1.2. In this figure m_1, m_2, and m_3 are system masses, k_1, k_2, k_3, and k_4 are stiffness coefficients, while d_1, d_2, d_3, and d_4 are damping coefficients.

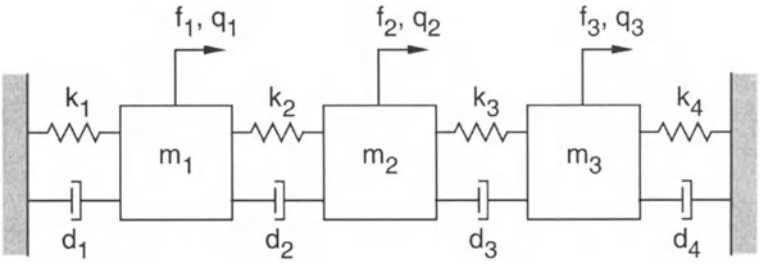

Figure 1.2. A simple flexible structure.

1.2.2 A 2D Truss

The truss structure in Fig. 1.3 is another example of a flexible structure. It is more complex than the simple structure, yet can easily be simulated by the reader, if necessary. For this structure, $l_1 = 15$ cm, $l_2 = 20$ cm, each truss has a cross-sectional area of $1\ \text{cm}^2$, elastic modulus of $2.0\times10^7\ \text{N/cm}^2$, and mass density of $0.00786\ \text{kg/cm}^3$. The system has 32 states (or 16 degrees of freedom), two inputs, and two outputs. Its stiffness and mass matrices are given in Appendix B.1.

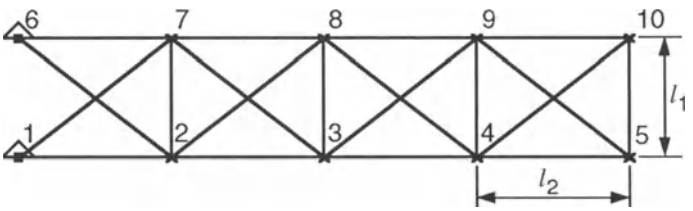

Figure 1.3. A 2D truss structure.

1.2.3 A 3D Truss

A three-dimensional truss is shown in Fig. 1.4. For this truss, the length is 60 cm, the width 8 cm, the height 10 cm, the elastic modulus $2.1 \times 10^7 \text{N/cm}^2$, and the mass density 0.00392 kg/cm^3. The truss has 72 degrees of freedom (or 144 states).

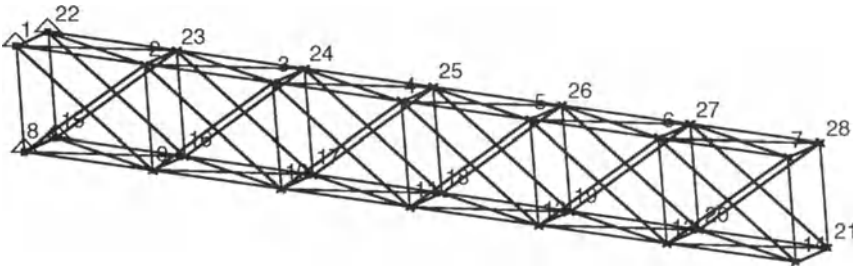

Figure 1.4. A 3D truss structure.

1.2.4 The Deep Space Network Antenna

The NASA Deep Space Network antenna structure illustrates a real-world flexible structure. The Deep Space Network antennas, operated by the Jet Propulsion Laboratory, consist of several antenna types and are located at Goldstone (California), Madrid (Spain), and Canberra (Australia). The Deep Space Network serves as a communication tool for space exploration. A new generation Deep Space Network antenna with 34-m dish is shown in Fig. 1.5. This antenna is an articulated large flexible structure, which can rotate around azimuth and elevation axes. The rotation is controlled by azimuth and elevation servos, as shown in Fig. 1.6. The combination of the antenna structure and its azimuth and elevation drives is the open-loop model of the antenna. The open-loop plant has two inputs (azimuth and elevation rates) and two outputs (azimuth and elevation position), and the position loop is closed between the encoder outputs, and the rate inputs. The drives consist of gearboxes, electric motors, amplifiers, and tachometers. For more details about the antenna, see [46]. The finite element model of the antenna structure consists of about 5000 degrees of freedom, with some nonlinear properties (dry friction, backlash, and imposed limits on its rates, and accelerations). However, the model of the structure and the drives used in this book are obtained from the field test data using system identification procedures.

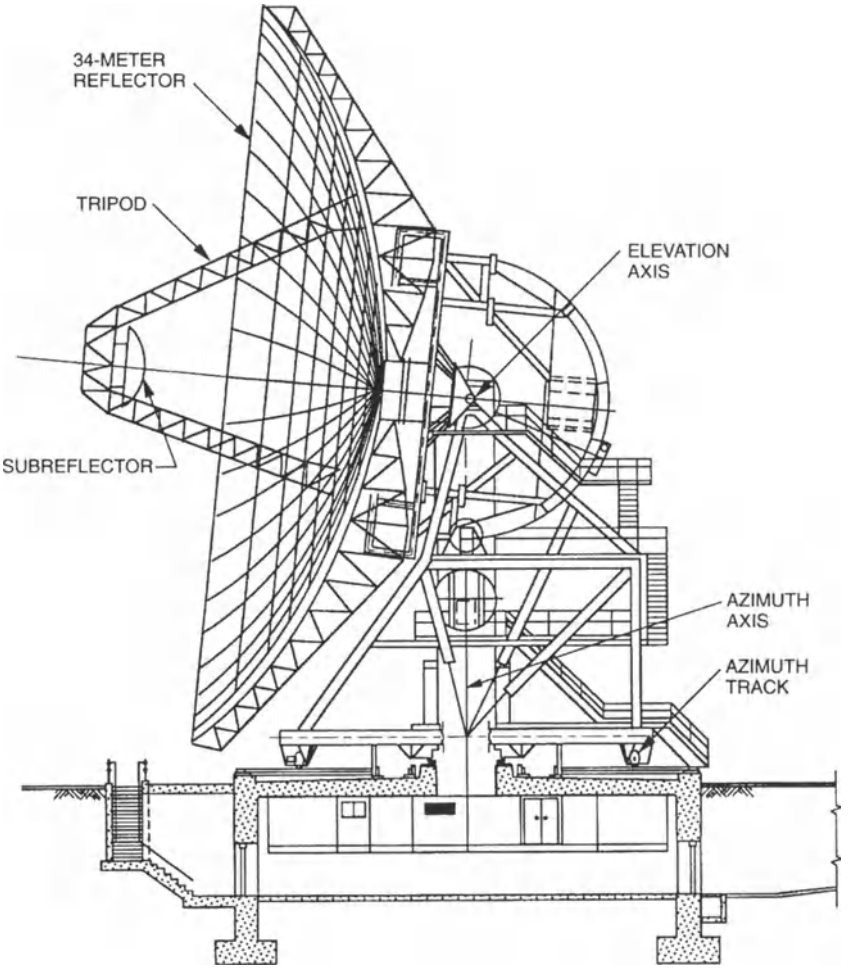

Figure 1.5. The Deep Space Network antenna.

The antenna was tested using the white noise input signal of sampling frequency 20 Hz, as shown in Fig. 1.7(a). The antenna azimuth encoder output record is shown in Fig. 1.7(b). From these records the transfer function, from the antenna rate input to the encoder output was determined, see Fig. 1.8(a,b), dashed line. The ERA identification algorithm, see [65], was used to determine the antenna state-space representation. For this representation the plot of the transfer function was obtained, and shown as a solid line in Fig. 1.8(a,b). The flexible properties are clearly visible in the identified model. The identified state-space representation of the antenna model is given in Appendix B.2.

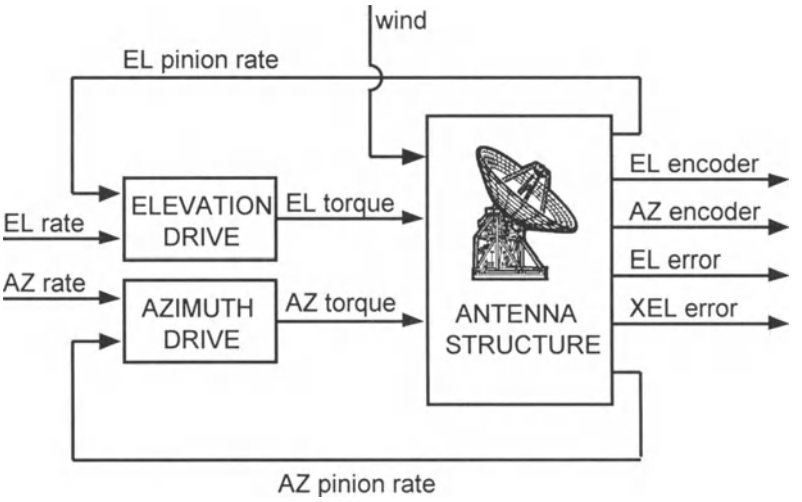

Figure 1.6. The open-loop model of the Deep Space Network antenna (AZ = azimuth, EL = elevation, XEL = cross-elevation).

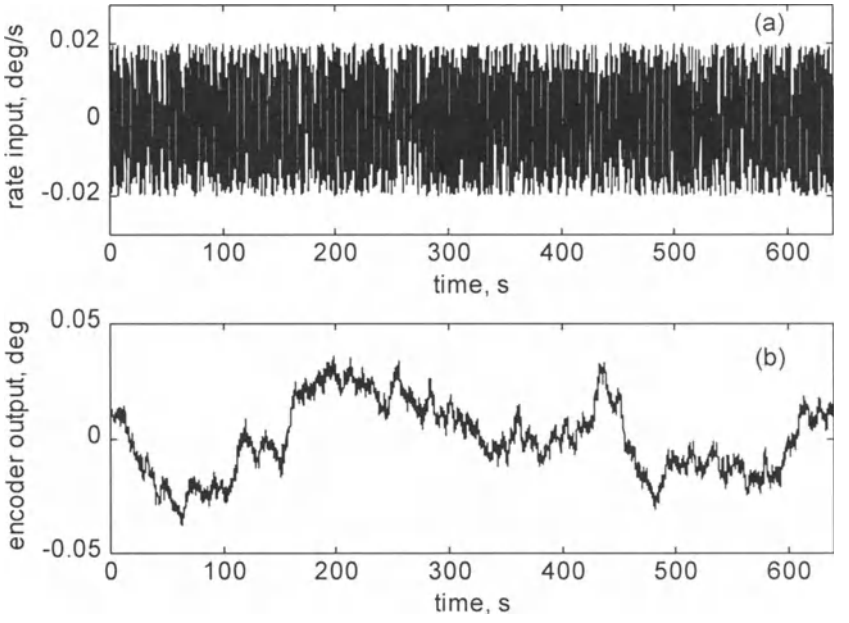

Figure 1.7. The identification of the antenna model: (a) input and (b) output signals.

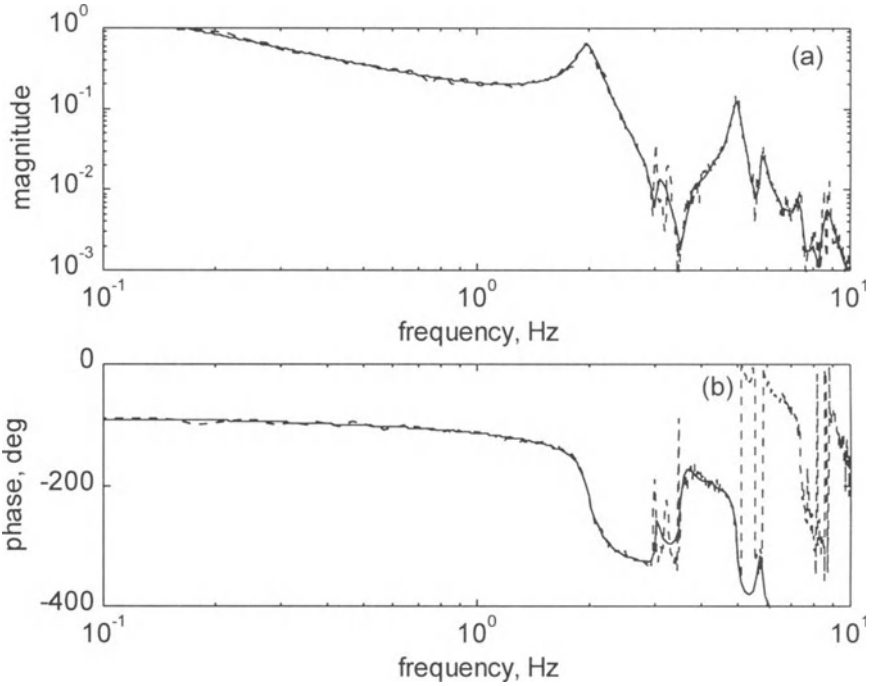

Figure 1.8. The antenna transfer functions from the data (dashed line), and identified (solid line): (a) magnitude; and (b) phase.

1.2.5 The International Space Station Structure

The Z1 module of the International Space Station structure is a large structure of a cubical shape with a basic truss frame and numerous appendages and attachments such as control moment gyros and a cable tray. Its finite element model is shown in Fig. 1.9. The total mass of the structure is around 14,000 kG. The finite-element model of the structure consists of 11,804 degrees of freedom with 56 modes, which natural frequencies are below 70 Hz. This structure is analyzed for preparation of the modal tests: the optimal locations of shakers and accelerometers are determined.

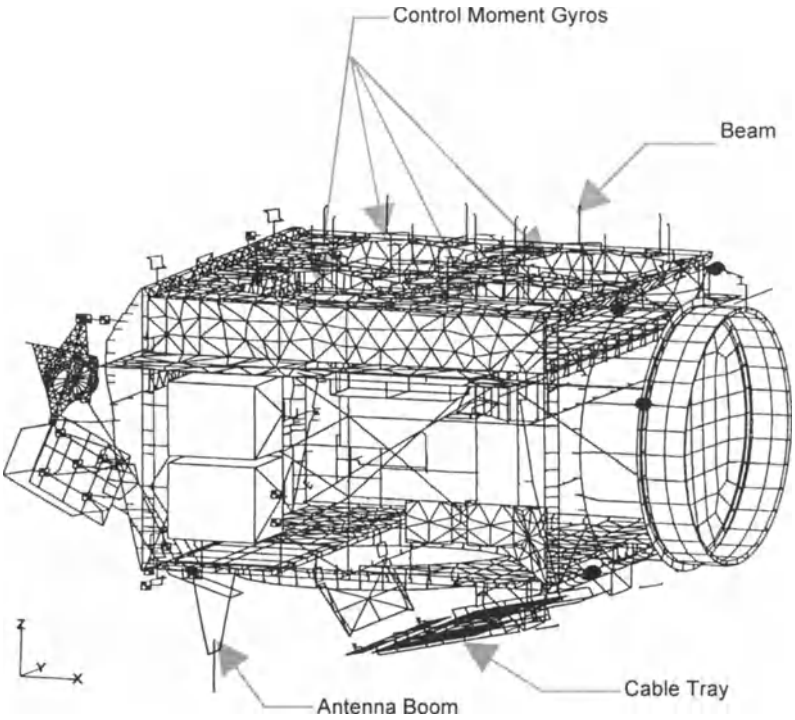

Figure 1.9. The International Space Station structure.

2
Models

System analytical models are given in the form of equations. Linear models are represented by linear differential equations. Structural models are represented in the form of second-order differential equations or in the form of first-order differential equations as a state-space representation. In the first case, the system dynamics is typically represented by the system degrees of freedom, and in the second case by the system states. Preferred by structural engineers, second-order differential equations of structural dynamics have a series of nice mathematical and physical properties. In this representation of a long tradition many important results have been derived. The state-space model is a standard model used by control engineers. Most linear control system analysis and design methods are given in state-space form. In this chapter we use both: second-order and state-space models.

The choice of coordinates in which the system model is represented is arbitrary. However, two coordinate systems, nodal and modal, are commonly used. Nodal coordinates are defined through displacements and velocities of selected structural locations, called nodes; and modal coordinates are defined through the displacements and velocities of structural (or natural) modes. The modal coordinate system is primarily used in this book.

The structural analytical models are derived either from physical laws, such as Newton's motion laws, Lagrange's equations of motion, or D'Alembert's principle [84], and [87]; or from finite-element models; or from test data using system identification methods. All three approaches are illustrated in this book.

W. K. Gawronski, *Dynamics and Control of Structures*

At the beginning of this chapter a state-space system model and its transfer function are presented. Next the second-order models of flexible structures are followed by structural state-space models.

2.1 Models of a Linear System

A linear time-invariant system of finite dimensions is described by the following linear constant coefficient differential equations:

$$\dot{x} = Ax + Bu, \qquad x(0) = x_o, \tag{2.1a}$$

$$y = Cx, \tag{2.1b}$$

where the N-dimensional vector x is called the state vector, x_o is the initial condition of the state, the s-dimensional vector u is the system input, and the r-dimensional vector y is the system output. The A, B, and C matrices are real constant matrices of appropriate dimensions, and (A, B, C) is the system triple. The triple is called the system state-space representation.

The state-space representation and the state vector are not unique, and one can introduce a new state variable, x_n, such that $x = Rx_n$. For a nonsingular transformation matrix R a new state representation (A_n, B_n, C_n) is obtained

$$A_n = R^{-1}AR, \qquad B_n = R^{-1}B, \qquad C_n = CR. \tag{2.2}$$

In this representation the input–output relationship is the same as in the original representation (A, B, C). Although input–output relations remain invariant, it makes a difference for system analysis or controller design what state or representation is chosen. Some representations have useful physical interpretations, others are more suitable for analysis and design.

A linear system can be alternatively represented by its transfer function. The transfer function $G(s)$ is defined as

$$y(s) = G(s)u(s), \tag{2.3}$$

where $y(s)$ and $u(s)$ are the Laplace transforms of $y(t)$ and $u(t)$, respectively. For zero initial condition, $x(0) = 0$, one obtains

$$G(s) = C(sI - A)^{-1}B. \tag{2.4}$$

The transfer function is invariant under the coordinate transformation, which can be checked by introducing (2.2) into the above equation.

2.2 Second-Order Structural Models

The second-order structural models are the ones represented by the second-order linear differential equations. They are commonly used in the analysis of structural dynamics. The model representation depends on the choice of coordinates. Typically, the second-order models are represented either in the nodal coordinates, and are called nodal models, or in the modal coordinates, called modal models.

2.2.1 Nodal Models

The nodal models are derived in nodal coordinates, in terms of nodal displacements and velocities. The model is characterized by the mass, stiffness, and damping matrices, and by the sensors and actuators locations. These models are typically obtained from the finite-element codes or from other CAD-type software.

As a convention, we denote a dot as a first derivative with respect to time (i.e., $dx / dt = \dot{x}$), and a double dot as a second derivative with respect to time (i.e., $d^2x / dt^2 = \ddot{x}$). Let n_d be a number of degrees of freedom of the system (linearly independent coordinates describing the finite-dimensional structure), let r be a number of outputs, and let s be a number of inputs. A flexible structure in nodal coordinates is represented by the following second-order matrix differential equation:

$$M\ddot{q} + D\dot{q} + Kq = B_o u \qquad y = C_{oq}q + C_{ov}\dot{q}\,. \tag{2.5}$$

In this equation q is the $n_d \times 1$ displacement vector, u is the $s \times 1$ input vector, y is the output vector, $r \times 1$, M is the mass matrix, $n_d \times n_d$, D is the damping matrix, $n_d \times n_d$, and K is the stiffness matrix, $n_d \times n_d$. The input matrix B_o is $n_d \times s$, the output displacement matrix C_{oq} is $r \times n_d$, and the output velocity matrix C_{ov} is $r \times n_d$. The mass matrix is positive definite, and the stiffness and damping matrices are positive semidefinite.

Example 2.1. The simple system from Fig. 1.2 is considered. For this system with masses $m_1 = m_2 = m_3 = 1$, stiffness $k_1 = k_2 = k_3 = 3$, $k_4 = 0$, and a damping matrix is proportional to the stiffness matrix, $D = 0.01K$, or $d_i = 0.01k_i$, $i = 1, 2, 3, 4$. There is a single input force at mass 3, and three outputs: displacement and velocity of mass 1, and velocity of mass 3.

For this system, the nodal model is as follows: the mass matrix is $M = I_3$, the stiffness and damping matrices are

$$K = \begin{bmatrix} 6 & -3 & 0 \\ -3 & 6 & -3 \\ 0 & -3 & 3 \end{bmatrix}, \qquad D = \begin{bmatrix} 0.06 & -0.03 & 0.00 \\ -0.03 & 0.06 & -0.03 \\ 0.00 & -0.03 & 0.03 \end{bmatrix}.$$

The input and output matrices are

$$B_o = \begin{bmatrix} 0 \\ 0 \\ 1 \end{bmatrix}, \qquad C_{oq} = \begin{bmatrix} 1 & 0 & 0 \\ 0 & 0 & 0 \\ 0 & 0 & 0 \end{bmatrix}, \qquad \text{and} \qquad C_{ov} = \begin{bmatrix} 0 & 0 & 0 \\ 1 & 0 & 0 \\ 0 & 0 & 1 \end{bmatrix}.$$

2.2.2 Modal Models

The second-order models are also obtained in modal coordinates, for example, from the system identification procedures, or by the transformation of the nodal models. This transformation is derived as follows.

Consider free vibrations (i.e., $u \equiv 0$) of a system without damping (i.e., $D = 0$). In this case the solution of (2.5) is of the form $q = \phi e^{j\omega t}$, hence, $\ddot{q} = -\omega^2 \phi e^{j\omega t}$, and (2.5) is now

$$(K - \omega^2 M)\phi e^{j\omega t} = 0. \tag{2.6}$$

The nontrivial solution of the above equation exists if

$$\det(K - \omega^2 M) = 0. \tag{2.7}$$

One can find n values of $\omega : \{\omega_1, \omega_2, ..., \omega_n\}$ such that the above equation is satisfied, where $n \le n_d$. The frequency ω_i is called the ith natural frequency. Substituting ω_i into (2.6) yields the corresponding set of solutions $\{\phi_1, \phi_2, ..., \phi_n\}$, and ϕ_i is called the ith natural mode, or mode shape. Note that the natural modes are not unique, since they can be arbitrary scaled. Indeed, if ϕ_i satisfies (2.6), so does $\alpha\phi_i$, where α is an arbitrary scalar.

Define the matrix of natural frequencies

$$\Omega = \mathrm{diag}(\omega_1, \omega_2, \ldots, \omega_n) \tag{2.8a}$$

and the modal matrix Φ $(n_d \times n)$, which consists of n natural modes of a structure

$$\Phi = \begin{bmatrix} \phi_1 & \phi_2 & \ldots & \phi_n \end{bmatrix}. \tag{2.8b}$$

The modal matrix diagonalizes mass and stiffness matrices M and K

$$M_m = \Phi^T M \Phi, \tag{2.9a}$$

$$K_m = \Phi^T K \Phi, \tag{2.9b}$$

obtaining diagonal matrices of modal mass M_m, and stiffness K_m. Additionally, if the damping matrix can be diagonalized

$$D_m = \Phi^T D \Phi \tag{2.9c}$$

it is called a matrix of proportional damping. The proportionality of damping is commonly assumed for analytical convenience. This approach is justified by the fact that the nature of damping is not known exactly, and that its values are rather roughly approximated.

Introducing a new variable, q_m, such that

$$q = \Phi q_m \tag{2.10}$$

and by left-multiplying (2.5) by Φ^T, one obtains

$$\Phi^T M \Phi \ddot{q}_m + \Phi^T D \Phi \dot{q}_m + \Phi^T K \Phi q_m = \Phi^T B_o u, \tag{2.11a}$$

$$y = C_{oq} \Phi q_m + C_{ov} \Phi \dot{q}_m,$$

or, equivalently,

$$M_m \ddot{q}_m + D_m \dot{q}_m + K_m q_m = \Phi^T B_o u, \tag{2.11b}$$

$$y = C_{oq} \Phi q_m + C_{ov} \Phi \dot{q}_m.$$

Left multiplication of the last equation by M_m^{-1} gives

$$\ddot{q}_m + M_m^{-1} D_m \dot{q}_m + M_m^{-1} K_m q_m = M_m^{-1} \Phi^T B_o u \,, \tag{2.11c}$$

$$y = C_{oq} \Phi q_m + C_{ov} \Phi \dot{q}_m \,,$$

thus the second-order modal model is obtained in its final form

$$\ddot{q}_m + 2Z\Omega \dot{q}_m + \Omega^2 q_m = B_m u \,, \tag{2.12}$$

$$y = C_{mq} q_m + C_{mv} \dot{q}_m \,,$$

where

$$\Omega^2 = M_m^{-1} K_m \,, \tag{2.13a}$$

$$Z = 0.5 M_m^{-1} D_m \Omega^{-1} = 0.5 M_m^{-1/2} K_m^{-1/2} D_m \,. \tag{2.13b}$$

The modal input matrix B_m is introduced

$$B_m = M_m^{-1} \Phi^T B_o, \tag{2.14}$$

and C_{mq}, C_{mv} are the modal displacement and rate matrices, respectively

$$C_{mq} = C_{oq} \Phi, \tag{2.15a}$$

$$C_{mv} = C_{ov} \Phi \,. \tag{2.15b}$$

For applications introduced later in this book (e.g., in the determination of modal norms) the modal equivalent output matrix C_m is defined as

$$C_m = C_{mq} \Omega^{-1} + C_{mv} \tag{2.16a}$$

which has the following property:

$$\|C_m\|_2^2 = \left\|C_{mq} \Omega^{-1}\right\|_2^2 + \|C_{mv}\|_2^2 \,. \tag{2.16b}$$

Structural Transfer Function. The transfer function of a structure is obtained from (2.12)

$$G(\omega) = (C_{mq} + j\omega C_{mv})(\Omega^2 - \omega^2 I_n + 2j\omega Z\Omega)^{-1} B_m . \tag{2.17}$$

Mode Representation. The modal equation (2.12) can be written as a set of n independent equations for each modal displacement

$$\ddot{q}_{mi} + 2\zeta_i \omega_i \dot{q}_{mi} + \omega_i^2 q_{mi} = b_{mi} u , \tag{2.18a}$$

$$y_i = c_{mqi} q_{mi} + c_{mvi} \dot{q}_{mi} , \qquad i = 1, \ldots, n, \tag{2.18b}$$

and c_{mi} is defined as the ith mode equivalent output matrix

$$c_{mi} = \frac{c_{mqi}}{\omega_i} + c_{mvi} . \tag{2.19}$$

In the above equations y_i is the system output due to the ith mode dynamics, while b_{mi} is the ith row of B_m, and c_{mqi}, c_{mvi}, and c_{mi} are the ith columns of C_{mq}, C_{mv}, and C_m, respectively. The quadruple $(\omega_i, \zeta_i, b_{mi}, c_{mi})$ that corresponds to (2.18) represents the ith natural mode, while $\|b_{mi}\|_2$ and $\|c_{mi}\|_2$ are the input and output gains of the ith mode. It is easy, but important, to see that the system gains are the root-mean-square (rms) sum of the modal gains

$$\|B_m\|_2 = \sqrt{\sum_{i=1}^{n} \|b_{mi}\|_2^2}, \qquad \|C_m\|_2 = \sqrt{\sum_{i=1}^{n} \|c_{mi}\|_2^2} . \tag{2.20}$$

Mode Transfer Function. The transfer function of the ith mode is obtained from (2.18)

$$G_i(\omega) = \frac{(c_{mqi} + j\omega c_{mvi}) b_{mi}}{\omega_i^2 - \omega^2 + 2j\zeta_i \omega_i \omega} . \tag{2.21}$$

The structural and modal transfer functions are related as follows:

Property 2.1(a) ***Transfer Function in Modal Coordinates.*** *The structural transfer function is a sum of modal transfer functions*

$$(a)\quad G(\omega)=\sum_{i=1}^{n} G_i(\omega) \tag{2.22a}$$

and the structural transfer function at the ith resonant frequency is approximately equal to the ith modal transfer function at this frequency

$$(b)\quad G(\omega_i)\cong G_i(\omega_i),\qquad i=1,\ldots,n. \tag{2.22b}$$

Proof. By inspection of Eqs.(2.17) and (2.21). ❑

Example 2.2. The modal model of the simple structure from Example 2.1 is determined. The natural frequency matrix is

$$\Omega=\begin{bmatrix} 3.1210 & 0 & 0 \\ 0 & 2.1598 & 0 \\ 0 & 0 & 0.7708 \end{bmatrix},$$

the modal matrix is

$$\Phi=\begin{bmatrix} 0.5910 & 0.7370 & 0.3280 \\ -0.7370 & 0.3280 & 0.5910 \\ 0.3280 & -0.5910 & 0.7370 \end{bmatrix},$$

the modal mass $M_m = I_3$, the modal stiffness $K_m = \Omega^2$, and the modal damping, from (2.13b), is

$$Z=\begin{bmatrix} 0.0156 & 0 & 0 \\ 0 & 0.0108 & 0 \\ 0 & 0 & 0.0039 \end{bmatrix}.$$

The modal input and output matrices are obtained from (2.14) and (2.15)

$$B_m=\begin{bmatrix} 0.3280 \\ -0.5910 \\ 0.7370 \end{bmatrix},$$

$$C_{mq} = \begin{bmatrix} 0.5910 & 0.7370 & 0.3280 \\ 0 & 0 & 0 \\ 0 & 0 & 0 \end{bmatrix}, \quad C_{mv} = \begin{bmatrix} 0 & 0 & 0 \\ 0.5910 & 0.7370 & 0.3280 \\ 0.3280 & -0.5910 & 0.7370 \end{bmatrix},$$

$$C_m = \begin{bmatrix} 0.1894 & 0.3412 & 0.4255 \\ 0.5910 & 0.7370 & 0.3280 \\ 0.3280 & -0.5910 & 0.7370 \end{bmatrix}.$$

2.3 State-Space Structural Models

For control system analysis and design purposes, it is convenient to represent the flexible structure equations in a state-space form, as in (2.1). The triple (A, B, C) is a state-space representation of a system, and x is the state vector. The state representation and the state vector are not unique. For example, by introducing a new state variable, x_n, such that $x = Rx_n$ and R is nonsingular, a new state representation $(A_n, B_n, C_n) = (R^{-1}AR, R^{-1}B, CR)$ is obtained as in (2.2). The input–output relationship has not been changed by the transformation. However, it makes a difference what state representation is chosen for system analysis or for controller design. It is shown in this book that modal representation is specifically useful for the purpose of dynamics and control of flexible structures.

2.3.1 Nodal Models

In order to obtain a state representation from the nodal model as in (2.5) the latter equation is rewritten as follows (mass matrix is assumed nonsingular):

$$\ddot{q} + M^{-1}D\dot{q} + M^{-1}Kq = M^{-1}B_o u \ , \tag{2.23a}$$

$$y = C_q q + C_v \dot{q} \ . \tag{2.23b}$$

Define the state vector x

$$x = \begin{Bmatrix} q \\ \dot{q} \end{Bmatrix}, \tag{2.24}$$

in which the first component is the system displacement, and the second component is the system velocity. In this case, after elementary manipulations, one obtains the following state-space representation:

$$A = \begin{bmatrix} 0 & I \\ -M^{-1}K & -M^{-1}D \end{bmatrix}, \qquad B = \begin{bmatrix} 0 \\ M^{-1}B_o \end{bmatrix}, \qquad C = \begin{bmatrix} C_{oq} & C_{ov} \end{bmatrix}, \tag{2.25}$$

where A is $N \times N$, B is $N \times s$, and C is $r \times N$. The dimension of the state model N is twice the number of degrees of freedom of the system n_d, i.e., $N = 2n_d$.

Example 2.3. The nodal state-space model for the simple structure from Example 2.1 is obtained from (2.25)

$$A = \begin{bmatrix} 0 & 0 & 0 & 1 & 0 & 0 \\ 0 & 0 & 0 & 0 & 1 & 0 \\ 0 & 0 & 0 & 0 & 0 & 1 \\ -6 & 3 & 0 & -0.06 & 0.03 & 0 \\ 3 & -6 & 3 & 0.03 & -0.06 & 0.03 \\ 0 & 3 & -3 & 0 & 0.03 & -0.03 \end{bmatrix}, \qquad B = \begin{bmatrix} 0 \\ 0 \\ 0 \\ 0 \\ 0 \\ 1 \end{bmatrix},$$

$$C = \begin{bmatrix} 1 & 0 & 0 & 0 & 0 & 0 \\ 0 & 0 & 0 & 1 & 0 & 0 \\ 0 & 0 & 0 & 0 & 0 & 1 \end{bmatrix}.$$

2.3.2 Modal Models

The order N of the nodal representation is often unacceptably high. For example, the number of degrees of freedom of the finite-element model is very large. Therefore the nodal state representation is seldom used in engineering practice. An alternative approach to obtain the state-space representation is to use the second-order modal form (2.12). Defining the state variable consisting of modal displacement and velocities

$$x = \begin{Bmatrix} x_1 \\ x_2 \end{Bmatrix} = \begin{Bmatrix} q_m \\ \dot{q}_m \end{Bmatrix}, \tag{2.26}$$

equation (2.12) is presented as a set of first-order equations

$$\dot{x}_1 = x_2 , \tag{2.27a}$$

$$\dot{x}_2 = -\Omega^2 x_1 - 2Z\Omega x_2 + B_m u , \tag{2.27b}$$

$$y = C_{mq} x_1 + C_{mv} x_2 , \tag{2.27c}$$

or, in the state-space form, with the state triple as follows:

$$A = \begin{bmatrix} 0 & I \\ -\Omega^2 & -2Z\Omega \end{bmatrix}, \qquad B = \begin{bmatrix} 0 \\ B_m \end{bmatrix}, \qquad C = \begin{bmatrix} C_{mq} & C_{mv} \end{bmatrix} . \tag{2.28}$$

In this representation x_1 is the vector of the modal displacements, and x_2 is the vector of modal velocities. The dimension of this state-space representation is $2n$, while the nodal state-space representation, as in (2.25), is $2n_d$, and $n << n_d$. While the mass and stiffness matrices are typically derived in the nodal coordinates (e.g., from a finite-element model), the damping matrix is commonly evaluated in the modal coordinates. Usually, the damping estimation is more accurate in modal coordinates.

Example 2.4. The state-space model for the simple structure from Example 2.2 is obtained from (2.28)

$$A = \begin{bmatrix} 0 & 0 & 0 & 1 & 0 & 0 \\ 0 & 0 & 0 & 0 & 1 & 0 \\ 0 & 0 & 0 & 0 & 0 & 1 \\ -9.7409 & 0 & 0 & -0.0974 & 0 & 0 \\ 0 & -4.6649 & 0 & 0 & -0.0466 & 0 \\ 0 & 0 & -0.5942 & 0 & 0 & -0.0059 \end{bmatrix},$$

$$B = \begin{bmatrix} 0 \\ 0 \\ 0 \\ 0.328 \\ -0.591 \\ 0.737 \end{bmatrix}, \qquad C = \begin{bmatrix} 0.591 & 0.737 & 0.328 & 0 & 0 & 0 \\ 0 & 0 & 0 & 0.591 & 0.737 & 0.328 \\ 0 & 0 & 0 & 0.328 & -0.591 & 0.737 \end{bmatrix}.$$

Presented above, state-space representation is not a modal state representation (although it was obtained using modal displacements, q_m). The modal state-space representation has a triple (A_m, B_m, C_m) characterized by the block-diagonal matrix, A_m, and the related input and output matrices

$$A_m = \text{diag}(A_{mi}), \qquad B_m = \begin{bmatrix} B_{m1} \\ B_{m2} \\ \vdots \\ B_{mn} \end{bmatrix}, \qquad C_m = \begin{bmatrix} C_{m1} & C_{m2} & \cdots & C_{mn} \end{bmatrix}, \tag{2.29}$$

$i = 1, 2, \ldots, n$, where A_{mi}, B_{mi}, and C_{mi} are 2×2, $2 \times s$, and $r \times 2$ blocks, respectively. The blocks A_{mi} are in four different forms:

- modal form 1

$$A_{mi} = \begin{bmatrix} 0 & \omega_i \\ -\omega_i & -2\zeta_i\omega_i \end{bmatrix}; \tag{2.30a}$$

- modal form 2

$$A_{mi} = \begin{bmatrix} -\zeta_i\omega_i & \omega_i \\ -\omega_i & -\zeta_i\omega_i \end{bmatrix}; \tag{2.30b}$$

- modal form 3

$$A_{mi} = \begin{bmatrix} 0 & 1 \\ -\omega_i^2 & -2\zeta_i\omega_i \end{bmatrix}; \tag{2.30c}$$

- modal form 4

$$A_{mi} = \begin{bmatrix} -\zeta_i\omega_i + j\omega_i\sqrt{1-\zeta_i^2} & 0 \\ 0 & -\zeta_i\omega_i - j\omega_i\sqrt{1-\zeta_i^2} \end{bmatrix}, \tag{2.30d}$$

where $j = \sqrt{-1}$.

The state x of the modal representation consists of n independent components, x_i, that represent a state of each mode

$$x = \begin{Bmatrix} x_1 \\ x_2 \\ \vdots \\ x_n \end{Bmatrix}. \tag{2.31}$$

The ith mode has the state-space representation

$$(A_{mi}, B_{mi}, C_{mi}), \tag{2.32a}$$

and is independently obtained from the state equations

$$\dot{x}_i = A_{mi} x_i + B_{mi} u, \tag{2.32b}$$

$$y_i = C_{mi} x_i, \tag{2.32c}$$

such that $y = \sum_{i=1}^{n} y_i$. This is justified by the block-diagonal form of the matrix A_m. The ith state component of the first modal form is as follows:

$$x_i = \begin{Bmatrix} q_{mi} \\ \dot{q}_{mi} / \omega_i \end{Bmatrix}, \tag{2.33a}$$

of the second modal form is

$$x_i = \begin{Bmatrix} q_{mi} \\ q_{moi} \end{Bmatrix}, \tag{2.33b}$$

of the third modal form is

$$x_i = \begin{Bmatrix} q_{mi} \\ \dot{q}_{mi} \end{Bmatrix}, \tag{2.33c}$$

and of the fourth form is

$$x_i = \begin{Bmatrix} q_{mi} - jq_{moi} \\ q_{mi} + jq_{moi} \end{Bmatrix}, \tag{2.33d}$$

where q_{mi} and $\dot{q}_{mi}$ are the ith modal displacement and velocity, as defined in (2.10), and $q_{moi} = \zeta_i q_{mi} + \dot{q}_{mi} / \omega_i$. Note that each component consists of modal displacement and velocity, which, by (2.10), gives the original (nodal) displacement q and velocity $\dot{q}$.

The modal form 3 is obtained from the representation (A, B, C) as in (2.28), simply by rearranging the columns of A and C and the rows of A and B. In this way, the state vector $x^T = \begin{bmatrix} q_m^T & \dot{q}_m^T \end{bmatrix}$, consisting of modal displacements followed by modal rates, is transformed to the new state $x_n^T = \begin{bmatrix} q_{m1} & \dot{q}_{m1} & q_{m2} & \dot{q}_{m2} & \cdots & q_{mn} & \dot{q}_{mn} \end{bmatrix}$, where the modal displacement for each component stays next to its rate. This is done by using the transformation matrix R in the form

$$R = \begin{bmatrix} 0 & e_1 \\ e_1 & 0 \\ 0 & e_2 \\ e_2 & 0 \\ \vdots & \vdots \\ 0 & e_n \\ e_n & 0 \end{bmatrix}, \tag{2.34}$$

where e_i is an n row vector with all elements equal to zero except the ith which is equal to one.

Denote A_{mk} as the state matrix A_m in the modal form k, where k = 1, 2, 3, or 4. The transformation matrix, R_{kl}, transforms the modal state variable, x_k, into x_l,

$$x_l = R_{kl} x_k, \qquad k, l = 1, 2, 3, \text{ or } 4, \tag{2.35}$$

where

$$R_{kl} = \text{diag}(R_{kli}). \tag{2.36}$$

Assuming small damping, i.e., $\zeta_i << 1$, i = 1, ..., n, one obtains

$$R_{12i} = \begin{bmatrix} 1 & 0 \\ \zeta_i & 1 \end{bmatrix}, \qquad R_{13i} = \begin{bmatrix} 1 & 0 \\ 0 & \omega_i \end{bmatrix}, \qquad R_{14i} = \begin{bmatrix} 1 - j\zeta_i & -j \\ 1 + j\zeta_i & j \end{bmatrix}, \tag{2.37a}$$

$$R_{23i} = \begin{bmatrix} 1 & 0 \\ -\zeta_i\omega_i & \omega_i \end{bmatrix}, \quad R_{24i} = \begin{bmatrix} 1 & -j \\ 1 & j \end{bmatrix}, \quad R_{34i} = \begin{bmatrix} 1-j\zeta_i & -j/\omega_i \\ 1+j\zeta_i & j/\omega_i \end{bmatrix}. \quad (2.37b)$$

The remaining transformations can easily be derived from the above transformations by using the following relationship:

$$R_{kpi} = R_{pji}^{-1}, \quad (2.38a)$$

or by noting that

$$R_{kji} = R_{lji}R_{kli}, \qquad l, k, j = 1, 2, 3, 4. \quad (2.38b)$$

The Matlab subroutine *cdf2rdf.m* transforms the modal form 4 into the modal form 2. The subroutine *realdiag.m* given in Appendix A.1 transforms any state-space representation into the modal representation 2.

The first three are real modal representations, while the last one is a complex one. In this book the first two forms are used extensively, in contrast to the last form, where a complex matrix, A_{mi}, obviously creates unnecessary analytical and numerical difficulties.

Example 2.5. The modal model of form 2 is obtained using *realdiag.m* subroutine.

$$A_m = \begin{bmatrix} -0.0487 & 3.1207 & 0 & 0 & 0 & 0 \\ -3.1207 & -0.0487 & 0 & 0 & 0 & 0 \\ 0 & 0 & -0.0233 & 2.1597 & 0 & 0 \\ 0 & 0 & -2.1597 & -0.0233 & 0 & 0 \\ 0 & 0 & 0 & 0 & -0.0030 & 0.7708 \\ 0 & 0 & 0 & 0 & -0.7708 & -0.0030 \end{bmatrix},$$

$$B_m = \begin{bmatrix} -0.0161 \\ 0.3441 \\ 0.0162 \\ 0.6511 \\ -1.2070 \\ -0.0191 \end{bmatrix}, \quad C_m = \begin{bmatrix} 0.1801 & 0.0084 & -0.0041 & 0.2597 & -0.3095 & 0.0077 \\ -0.0351 & 0.5617 & -0.2002 & -0.0039 & -0.0094 & -0.6687 \\ -0.0195 & 0.3117 & -0.4498 & -0.0088 & 0.0075 & 0.5363 \end{bmatrix}.$$

The input and output gains are $\|B_{m1}\|_2 = 0.3445$, $\|C_{m1}\|_2 = 0.6685$, $\|B_{m2}\|_2 = 0.6513$, $\|C_{m2}\|_2 = 0.9115$, $\|B_{m3}\|_2 = 1.2072$, and $\|C_{m3}\|_2 = 0.5568$.

Finally, consider a transfer function of a structure in modal coordinates. The transfer function of a structure is defined in (2.3). The transfer function of the ith mode follows from (2.32)

$$G_i(\omega) = C_i(j\omega I - A_i)^{-1} B_i, \qquad i = 1, \ldots, n \tag{2.39}$$

then, for a system with distinct natural frequencies one obtains the following property of the transfer function

Property 2.1(b) ***Transfer Function in Modal Coordinates.*** *The structural transfer function is a composition of modal transfer functions:*

$$(a) \quad G(\omega) = \sum_{i=1}^{n} G_i(\omega) \tag{2.40a}$$

and the value of the transfer function at the ith resonant frequency is approximately equal to the value of the ith mode transfer function at this frequency:

$$(b) \quad G(\omega_i) \cong G_i(\omega_i) \tag{2.40b}$$

Proof. Introducing A, B, and C as in (2.28) to the definition of the transfer function one obtains

$$G(\omega) = C(j\omega I - A)^{-1} B = \sum_{k=1}^{n} C_k(j\omega I - A_k)^{-1} B_k = \sum_{k=1}^{n} G_k(\omega), \tag{2.41}$$

which proves part (a). Part (b) follows from part (a), by noting that for flexible structures with distinct natural frequencies and low damping, $\|G_j(\omega_i)\|_2 << \|G_i(\omega_i)\|_2$ for $i \neq j$. ❐

Example 2.6. For the simple system from Example 2.1, the transfer function G is given in Fig. 2.1, solid line. The plots of the transfer functions, of the first mode G_1 (mode of frequency $\omega_1 = 0.7708$ rad/s – dashed line), of the second

mode G_2 (mode of frequency $\omega_2 = 2.1597$ rad/s – dash–dot line), and of the third mode G_3 (mode of frequency $\omega_3 = 3.1207$ rad/s – dotted line), show that Property 2.1 holds.

2.4 Models with Small Nonproportional Damping

The damping properties of structures are often assumed in the form of modal damping. This is done not only for the sake of analytical simplicity, but also because it is the most favorable way to measure or estimate it. This is the way, for example, to estimate the material damping in the finite-element analysis of large flexible structures. The resulting damping is a proportional one. In another approach, a damping matrix proportional either to the mass, or to the stiffness matrix, or to both, is introduced. This technique produces proportional damping as well.

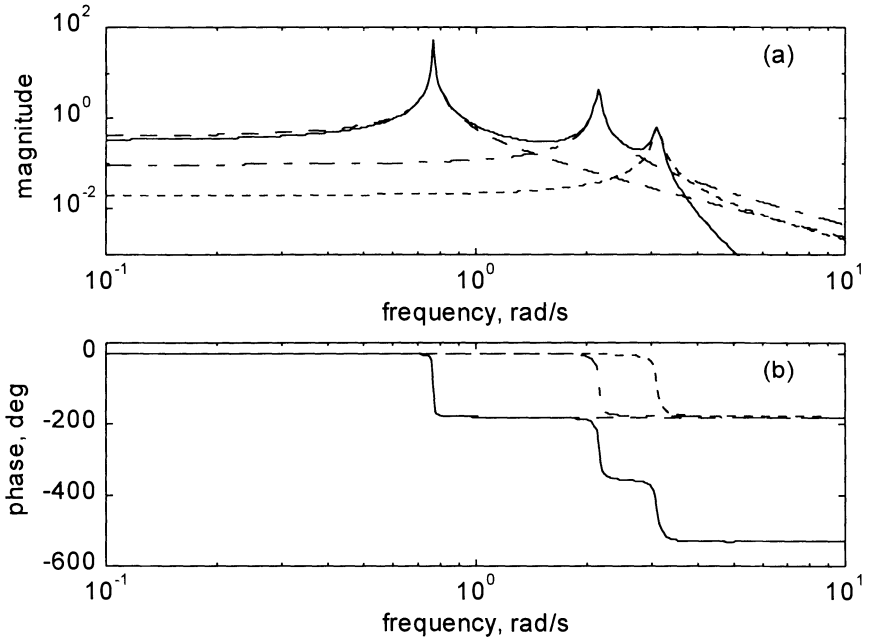

Figure 2.1. Transfer function G of the simple system (solid line) and its modes G_1 (dashed line), G_2 (dash–dot line), and G_3 (dotted line).

However, in many practical problems structural damping is not proportional. In this book, we analyze structural dynamics and design controllers for the proportional damping only. The question arises: Are the analysis and the design procedures valid for the case of nonproportional damping? In this section we

shall show that small nonproportional damping can be replaced with proportional damping without causing a significant error.

Replacement of nonproportional damping with proportional damping was considered by several authors, including Cronin [18], Chung and Lee [14], Bellos and Inman [8], Yae and Inman [113], Nicholson [88], Felszeghy [27]. The simplest and most common approach to the problem is to replace the full damping matrix with a diagonal one by neglecting the off-diagonal terms of the nonproportional damping matrix. Several researchers studied the error bounds generated by this simplified approach, see, for example, Shahruz and Ma [96], Uwadia and Esfandiari [103], Hwang and Ma [57], Bhaskar [11], and Gawronski and Sawicki [50].

In order to analyze the impact of nonproportional damping on system dynamics consider (2.12) - the second-order modal equation of a structure. Replace the proportional damping matrix $2Z\Omega$ with the full matrix D. This matrix can be decomposed into the diagonal ($2Z\Omega$) and off-diagonal (D_o) components $D = 2Z\Omega + D_o$, so that the equation of motion is as follows:

$$\ddot{q} + 2Z\Omega\dot{q} + D_o\dot{q} + \Omega^2 q = Bu \ . \tag{2.42}$$

Now, q is the displacement of the nonproportionally damped structure, and q_m is the displacement of the proportionally damped structure, a solution of equation (2.12).

Denote by e_i the ith modal error between non-proportionally damped and proportionally damped structures, $e_i = q_i - q_{mi}$. Subtracting (2.12) from (2.42), one obtains for the ith mode

$$\ddot{e}_i + 2\zeta_i\omega_i\dot{e}_i + \omega_i^2 e_i = -d_{oi}\dot{q}\,, \tag{2.43}$$

where d_{oi} is the ith row of D_o. A question arises as to when the error is small (compared to the system displacement q) so that the nonproportional part, D_o, can be ignored.

We will show the following property:

Property 2.2 ***Error of a Mode with Nonproportional Damping.*** *For non-clustered natural frequencies the error e_i of the ith mode is limited as follows:*

$$\|e_i\|_2 << \|q\|_2\,, \qquad i = 1,\ldots,n. \tag{2.44}$$

Proof. Note that (2.43) can be written in the frequency domain as

$$e_i(\omega) = g_i(\omega) d_{oi} q_o(\omega)\,, \tag{2.45}$$

where

$$g_i(\omega) = \frac{-j\omega}{\omega_i^2 - \omega^2 + 2j\zeta_i\omega_i\omega}\,, \tag{2.46}$$

and q_o is equal to a displacement vector q except the ith component, which is equal to zero. From (2.45) it follows that

$$\begin{aligned}
\|e_i\|_2^2 &= \frac{1}{4\pi^2}\int_{-\infty}^{\infty} |e_i|^2 d\omega = \frac{1}{4\pi^2}\int_0^{\infty} |g_i(\omega)|^2 \operatorname{tr}(d_{oi} q_o(\omega) q_o^*(\omega) d_{oi}^T) d\omega \\
&= \|d_{oi}\|_2^2 \frac{1}{4\pi^2}\int_0^{\infty} |g_i(\omega)|^2 \operatorname{tr}(q_o(\omega) q_o^*(\omega)) d\omega \\
&\le \|d_{oi}\|_2^2 |g_{i\max}|^2 \frac{1}{4\pi^2}\int_0^{\infty} \operatorname{tr}(q_o(\omega) q_o^*(\omega)) d\omega \\
&= \|d_{oi}\|_2^2 |g_i(\omega_i)|^2 \|q_o\|_2^2\,.
\end{aligned} \tag{2.47a}$$

However,

$$|g_i(\omega_i)| = \frac{1}{2\zeta_i\omega_i} \qquad \text{and} \qquad \|q_o\|_2 << \|q\|_2\,, \tag{2.47b}$$

therefore

$$\|e_i\|_2^2 << \frac{\|d_{oi}\|_2^2}{4\zeta_i^2\omega_i^2}\|q\|_2^2 \le \|q\|_2^2 \tag{2.47c}$$

since $d_{oik} \le 2\zeta_i\omega_i$. ❑

The above property implies that for separate natural frequencies the off-diagonal elements of the damping matrix can be neglected regardless of their values.

The following example illustrates the insignificance of the nonproportional damping terms.

Example 2.7. Consider a flexible truss as in Fig. 1.3, with the damping matrix proportional to the stiffness matrix, $D = 2\times10^{9}\,K$, and with added damping at node 5, see Fig. 2.2. This addition makes the damping nonproportional. The structural damping is about 1.5% of the critical damping and the concentrated viscous damping in a vertical direction at node 5 is ten times larger than the structural damping at this location.

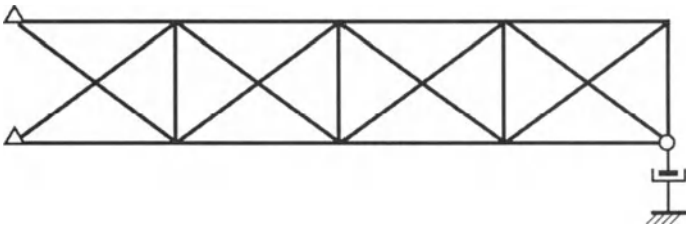

Figure 2.2. The 2D truss with a damper.

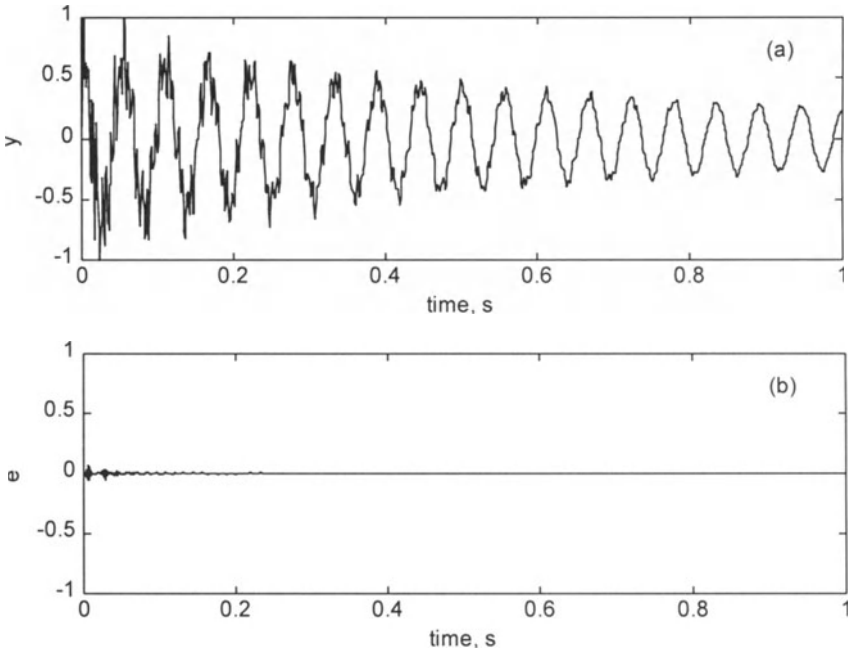

Figure 2.3. The impulse responses: (a) of the nonproportionally damped system; and (b) of the response error of the system with the equivalent proportional damping.

The impulse force is applied at node 10 and the response is measured at node 9 in a vertical direction. A comparison is made between the exact solution (i.e., with full damping matrix) and the approximate solution obtained by neglecting off-diagonal terms in the damping matrix. In Fig. 2.3(a) the exact response (y) is shown, while in Fig. 2.3(b) the difference, $e = y - y_d$, between the exact response and the response of the system with the proportional damping (y_d) is plotted. This difference is small, since the approximate solution has the error $\|y - y_d\|_2 / \|y\|_2 = 0.019$. Let D and D_d stand for the full damping matrix and the diagonal part of the same matrix, then the damping matrix diagonality index defined as $\|D - D_d\|_2 / \|D\|_2$ is not a small number in this case, it is equal to 0.760.

3
Controllability and Observability

Controllability and observability are structural properties that carry useful information for structural testing and control, yet are often overlooked by structural engineers. A structure is controllable if the installed actuators excite all its structural modes. It is observable if the installed sensors detect the motions of all the modes. This information, although essential in many applications, is too limited: it answers the question of excitation or detection in terms of yes or no. The quantitative answer is supplied by the controllability and observability grammians, which represent a degree of controllability and observability of each mode. In this chapter the controllability and observability properties of flexible structures are discussed. The fundamental property of a flexible structure in modal coordinates consists of a set of weakly coupling of the modes, as shown in Property 2.1. The weak coupling allows one to treat each individual mode separately specifically, to combine the controllability and observability properties of the whole system out of the properties of individual modes. These controllability and observability properties are used later in this book in the evaluation of structural testing and in control analysis and design.

3.1 Definition

Controllability and observability properties of a linear time-invariant system can be heuristically described as follows. The system dynamics described by the state variable (x) is excited by the input (u) and measured by the output (y).

W. K. Gawronski, *Dynamics and Control of Structures*

However, the input may not be able to excite all states (or, equivalently, move it in an arbitrary direction), and not all states are represented at the output (or, equivalently, the system states cannot be recovered from a record of the output measurements). If the input excites all states, the system is controllable. If all the states are represented in the output, the system is observable. More precise definitions follow.

Controllability, as a coupling between the input and the states, involves the system matrix A and the input matrix B. A linear system, or the pair (A, B), is controllable at t_o if it is possible to find a piecewise continuous input $u(t)$, $t \in [t_o, t_1]$, that will transfer the system from the initial state, $x(t_o)$, to the origin $x(t_1) = 0$, at finite time $t_1 > t_o$. If this is true for all initial moments t_o and all initial states $x(t_o)$ the system is completely controllable. Otherwise, the system, or the pair (A, B), is uncontrollable.

Observability, as a coupling between the states and the output, involves the system matrix A and the output matrix C. A linear system, or the pair (A, C), is observable at t_o if the state $x(t_o)$ can be determined from the output $y(t)$, $t \in [t_o, t_1]$, where $t_1 > t_o$ is some finite time. If this is true for all initial moments t_o and all initial states $x(t_o)$ the system is completely observable. Otherwise, the system, or the pair (A, C), is unobservable.

There are many criteria to determine system controllability and observability see, for example, [68] and [115]. We consider two of them. A linear time-invariant system (A, B, C), with s inputs is completely controllable if and only if the $N \times sN$ matrix of

$$\mathcal{C} = \begin{bmatrix} B & AB & A^2B & \dots & A^{N-1}B \end{bmatrix} \tag{3.1}$$

has rank N. A linear time-invariant system (A, B, C) with r outputs is completely observable if and only if the $rN \times N$ matrix of

$$\mathcal{O} = \begin{bmatrix} C \\ CA \\ CA^2 \\ \vdots \\ CA^{N-1} \end{bmatrix} \tag{3.2}$$

has rank N.

The above criteria, although simple, have two serious drawbacks. First, they answer to the controllability and observability question in terms of yes or no. Second, they are useful only for a system of small dimensions. Assume, for example, that the system is of dimension $N = 100$. In order to answer the

controllability and observability question one has to find powers of A up to 99. Finding A^{99} for a 100×100 matrix is a numerical task that easily results in numerical overflow.

The alternative approach uses grammians to determine the system properties. Grammians express the controllability and observability properties qualitatively, and avoid numerical difficulties. The controllability and observability grammians are defined as follows, see, for example, [68],

$$W_c(t) = \int_0^t \exp(At)BB^T \exp(A^T t)\,dt, \qquad W_o(t) = \int_0^t \exp(A^T t)C^T C \exp(At)\,dt\,. \tag{3.3}$$

They can be determined alternatively from the following differential equations:

$$\dot{W}_c = AW_c + W_c A^T + BB^T, \qquad \dot{W}_o = A^T W_o + W_o A + C^T C\,. \tag{3.4}$$

For a stable system, the stationary solutions of the above equations are obtained by assuming $\dot{W}_c = \dot{W}_o = 0$. In this case, the grammians are determined from the following Lyapunov equations:

$$AW_c + W_c A^T + BB^T = 0, \qquad A^T W_o + W_o A + C^T C = 0\,. \tag{3.5}$$

For stable A, the grammians W_c and W_o are positive definite.

The grammians depend on the system coordinates, and for a linear transformation of a state, $\bar{x} = Rx$, they are transformed as follows:

$$\overline{W}_c = R^{-1} W_c R^{-T}, \qquad \overline{W}_o = R^T W_o R. \tag{3.6}$$

The eigenvalues of the grammian product are invariant under linear transformation. It can be shown as follows:

$$\lambda_i(\overline{W}_c \overline{W}_o) = \lambda_i(R^{-1} W_c R^{-T} R^T W_o R) = \lambda_i(R^{-1} W_c W_o R) = \lambda_i(W_c W_o)\,. \tag{3.7}$$

These invariants, denoted γ_i,

$$\gamma_i = \sqrt{\lambda_i(W_c W_o)}, \qquad i = 1, \ldots, N\,, \tag{3.8}$$

are called the Hankel singular values of the system.

3.2 Balanced Representation

The system triple is open-loop balanced, if its controllability and observability grammians are equal and diagonal, as defined by Moore in [85],

$$W_c = W_o = \Gamma, \qquad \Gamma = \mathrm{diag}(\gamma_1,...,\gamma_N), \qquad \gamma_i \geq 0, \qquad i = 1, \ldots, N, \tag{3.9}$$

where γ_i is the ith Hankel singular value of the system. The transformation R to the balanced representation, such that $A_b = R^{-1}AR$, $B_b = R^{-1}B$, and $C_b = CR$, is as follows, see [40]:

$$R = PU\Gamma^{-1/2}. \tag{3.10}$$

The matrices Γ and U are obtained from the singular value decomposition of the matrix H

$$H = V\Gamma U^T, \tag{3.11}$$

where H is obtained as a product of the matrices P and Q

$$H = QP \tag{3.12}$$

and P, Q, in turn, are obtained from the decomposition of the controllability and observability grammians, respectively,

$$W_c = PP^T, \qquad W_o = Q^TQ. \tag{3.13}$$

The Cholesky, or the singular value decomposition can be used to decompose W_c and W_o.

The Matlab function *bal_op_loop.m* which transforms a representation (A, B, C) to the open-loop balanced representation is given in Appendix A.2.

3.3 Balanced Systems with Integrators

Some plants (e.g., plants of tracking systems) include integrators. A linear system is called a system with integrators if its N–m poles are stable, the remaining m poles are at zero, and if it is observable and controllable (see [23]). It is also assumed that A is nondefective (c.f. [56]), i.e., that the geometric multiplicity of poles at zero is m. Grammians for systems with integrators do not

exist, although the systems with integrators are controllable and observable. Here we show how to represent the grammians so that the infinite values of some of their components do not prevent the analysis.

A system with integrators can be represented by the following state-space representation:

$$A = \begin{bmatrix} 0_m & 0_{m\times(N-m)} \\ 0_{(N-m)\times m} & A_o \end{bmatrix}, \qquad B = \begin{bmatrix} B_r \\ B_o \end{bmatrix}, \qquad C = \begin{bmatrix} C_r & C_o \end{bmatrix}, \tag{3.14}$$

where $0_{m\times N}$ is an $m \times N$ zero matrix. Matrix A in the form as above always exists since it has m poles at zero, and matrices B, C exist too, due to the nondefectiveness of A_o.

The system matrix of the balanced system with integrators is block-diagonal, $A_b = \text{diag}(0_m, A_{bo})$. And the balanced representation (A_b, B_b, C_b) is obtained by the transformation R

$$A_b = R^{-1}AR, \qquad B_b = R^{-1}B, \qquad C_b = CR \ . \tag{3.15}$$

The transformation R is in the form $R = \text{diag}(I_m, R_o)$ where I_m is an identity matrix of order m, and R_o balances A_o, i.e.,

$$A_{bo} = R_o^{-1} A_o R_o \ . \tag{3.16}$$

In order to obtain the system Hankel singular values one needs to balance the triple (A_o, B_o, C_o) that has no poles at zero, and add to these values the infinity Hankel singular values that correspond to the poles at zero. Let γ_o represent the vector of Hankel singular values of (A_o, B_o, C_o), then

$$\gamma = \{\text{inf}, \gamma_o\} \tag{3.17}$$

represents the vector of Hankel singular values of (A, B, C), where $\text{inf} = \{\infty \quad \infty \quad \ldots \quad \infty\}$ contains m values at infinity.

3.4 Structural Properties

In this section the controllability and observability properties of structures are discussed. The modal state-space representation of flexible structures has

specific controllability and observability properties, and its grammians are of specific form.

In the following the approximate relationships are denoted with the equality sign "$\cong$" , used in the following sense. Two variables, x and y are approximately equal ($x \cong y$) if $x = y + \varepsilon$, and $\|e\| << \|y\|$. For example, if D is a diagonal matrix, then S is diagonally dominant, then $S \cong D$ if the terms s_{ij} satisfy the condition $s_{ij} + \varepsilon = d_{ij}$, $i, j = 1,..., n$, and ε is small when compared to d_{ii}.

3.4.1 The State-Space Modal Model

Assuming small damping, such that $\zeta << 1$, $\zeta = \max(\zeta_i)$, $i = 1, ..., n$, the balanced and modal representations of flexible structures are closely related. One symptom of this relationship is expressed in the following property:

Property 3.1 ***Diagonally Dominant Grammians in Modal Coordinates.*** *In modal coordinates controllability and observability grammians are diagonally dominant, i.e.,*

$$W_c \cong \text{diag}(w_{ci} I_2), \qquad w_{ci} > 0, \qquad i = 1,..., n, \tag{3.18a}$$

$$W_o \cong \text{diag}(w_{oi} I_2), \qquad w_{oi} > 0, \qquad i = 1,..., n, \tag{3.18b}$$

where w_{ci} and w_{oi} are the modal controllability and observability coefficients. The approximate Hankel singular values are obtained as a geometric mean of the modal controllability and observability

$$\gamma_i \cong \sqrt{w_{cii} w_{oii}}\ . \tag{3.19}$$

Proof. Consider a flexible structure in the modal representation 1, as in (2.29) and (2.30a). The diagonal dominance of the controllability and observability grammians is proved by the introduction of this modal representation to the Lyapunov equations (3.5). By inspection, for $\zeta \to 0$ one obtains finite values of the off-diagonal terms w_{cij} and w_{oij}, for $i \neq j$, i.e., $\lim_{\zeta \to 0} w_{cij} < \infty$ and $\lim_{\zeta \to 0} w_{oij} < \infty$, while the diagonal terms tend to infinity, $\lim_{\zeta \to 0} w_{cii} = \infty$ and $\lim_{\zeta \to 0} w_{oii} = \infty$. Moreover, the difference between the diagonal terms in each

block is finite, $\lim_{\zeta \to 0} | w_{cii} - w_{ci+1,i+1} | < \infty$, thus for small ζ the grammians in modal coordinates are diagonally dominant, having 2×2 blocks on the diagonal with almost identical diagonal entries of each block. Equation (3.19) is a direct consequence of the diagonal dominance of W_c and W_o, and the fact that the eigenvalues of the grammian product are invariant. ❐

The profiles of grammians and system matrix A in modal coordinates are drawn in Fig. 3.1.

The controllability grammian is, at the same time, a covariance matrix of the states x excited by the white noise input, i.e., $W_c = E(xx^T)$. Thus, the diagonal dominance results in the following conclusion that under white noise or impulse, excitation modes are almost independent, or almost orthogonal.

Example 3.1. The grammians were determined for the modal model from Example 2.5

$$W_{mc} = \begin{bmatrix} 0.6095 & 0.0095 & 0.0122 & -0.0946 & 0.0350 & 0.0048 \\ 0.0095 & 0.6086 & 0.1370 & 0.0114 & -0.0014 & 0.1418 \\ 0.0122 & 0.1370 & 4.5464 & 0.0491 & 0.1489 & 0.0016 \\ -0.0946 & 0.0114 & 0.0491 & 4.5475 & -0.0013 & 0.4171 \\ 0.0350 & -0.0014 & 0.1489 & -0.0013 & 122.6197 & -0.4726 \\ 0.0048 & 0.1418 & 0.0016 & 0.4171 & -0.4726 & 122.0863 \end{bmatrix},$$

$$W_{mo} = \begin{bmatrix} 2.2922 & -0.0305 & -0.0057 & -0.1227 & -0.0373 & -0.0008 \\ 0.0305 & 2.2952 & 0.1517 & -0.0065 & -0.0007 & -0.0903 \\ -0.0057 & 0.1517 & 8.9050 & -0.0740 & 0.0223 & 0.0003 \\ -0.1227 & -0.0065 & -0.0740 & 8.9039 & 0.0002 & -0.0417 \\ -0.0373 & -0.0007 & 0.0223 & 0.0002 & 26.0878 & 0.0568 \\ -0.0008 & -0.0903 & 0.0003 & -0.0417 & 0.0568 & 26.0863 \end{bmatrix}.$$

Indeed, the grammians are diagonally dominant. The approximate grammians, from (3.18)

$$w_{c1} = 0.6095, \qquad w_{c2} = 4.5464, \qquad w_{c3} = 122.6197,$$

$$w_{o1} = 2.2922, \qquad w_{o2} = 8.9050, \qquad w_{o3} = 26.0878,$$

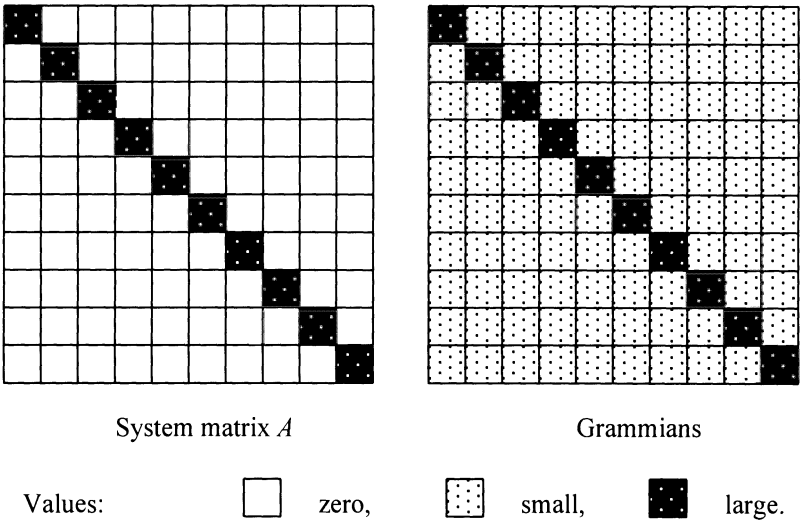

Figure 3.1. Profiles of the system matrix A and the grammians in the modal coordinates.

are close to the actual ones:

$$w_{c1} = 0.6090, \quad w_{c2} = 4.5469, \quad w_{c3} = 122.6243,$$

$$w_{o1} = 2.2937, \quad w_{o2} = 8.9045, \quad w_{o3} = 26.0871.$$

The approximate Hankel singular values for each mode are obtained from (3.19)

$$\Gamma_{ap} = \text{diag}(1.1818,\ 1.1818,\ 6.3625,\ 6.3625,\ 56.5579,\ 56.5579)$$

and are close to the actual Hankel singular values

$$\Gamma = \text{diag}(1.1756,\ 1.1794,\ 6.3575,\ 6.3735,\ 56.5110,\ 56.5579).$$

For flexible structures the grammians of each mode can be expressed in closed form. This allows for their speedy determination for structures with a large number of modes, and allows for physical insight into the grammian meaning. Let B_i and C_i be the $2 \times s$ and $r \times 2$ blocks of modal B and C, respectively, and the latter matrices are part of the modal representation, (2.29). In this case the following property is valid:

Property 3.2 ***Closed-Form Controllability and Observability Grammians.*** *In modal coordinates the diagonal entries of the controllability and observability grammians as in (3.18) are as follows:*

$$w_{ci} = \frac{\|B_i\|_2^2}{4\zeta_i\omega_i}, \qquad w_{oi} = \frac{\|C_i\|_2^2}{4\zeta_i\omega_i}, \tag{3.20}$$

and the approximate Hankel singular values are obtained from

$$\gamma_i \cong \frac{\|B_i\|_2\|C_i\|_2}{4\zeta_i\omega_i}. \tag{3.21}$$

Proof. By inspection, introducing the modal representation (2.29) and (2.30a) to the Lyapunov equations (3.5). ❐

The above equations show that the controllability grammian of the *i*th mode is proportional to the square of the *i*th modal input gain, and inversely proportional to the *i*th modal damping and modal frequency. Similarly, the observability grammian is proportional to the square of the *i*th modal output gain, and inversely proportional to the *i*th modal damping and modal frequency. Finally, the Hankel singular value is the geometric mean of the previous two, and is proportional to the *i*th input and output gains and is inversely proportional to the *i*th modal damping and modal frequency.

Example 3.2. The closed form Hankel singular values for the modal model from Example 2.5 are determined: $\gamma_1 = 1.1817$, $\gamma_2 = 6.3627$, and $\gamma_3 = 56.5585$, which are close to the actual values obtained in Example 3.1.

Example 3.3. The exact and approximate Hankel singular values of the International Space Station structure are compared. The input is a force at node 8583 (marked by the black dot at the top of Fig. 1.9), and the output is a rate at this node. The results in Fig. 3.2 show good coincidence between the exact and approximate Hankel singular values.

The closeness of the balanced and modal representations can be observed in the diagonally dominant form of the system matrix A in the balanced representation.

Property 3.3 ***Diagonal Dominance of the System Matrix in the Balanced Coordinates.*** *In the balanced representations the system matrix A is block diagonally dominant with 2 × 2 blocks on the diagonal, and B, C are divided into 2×s and r×2 blocks*

$$A \cong \text{diag}(A_i), \qquad B = \begin{bmatrix} B_1 \\ B_2 \\ \vdots \\ B_n \end{bmatrix}, \qquad C = \begin{bmatrix} C_1 & C_2 & \cdots & C_n \end{bmatrix}, \tag{3.22}$$

where i = 1, ..., n, and

$$A_i = \begin{bmatrix} -\zeta_i\omega_i & \omega_i \\ -\omega_i & -\zeta_i\omega_i \end{bmatrix}. \tag{3.23}$$

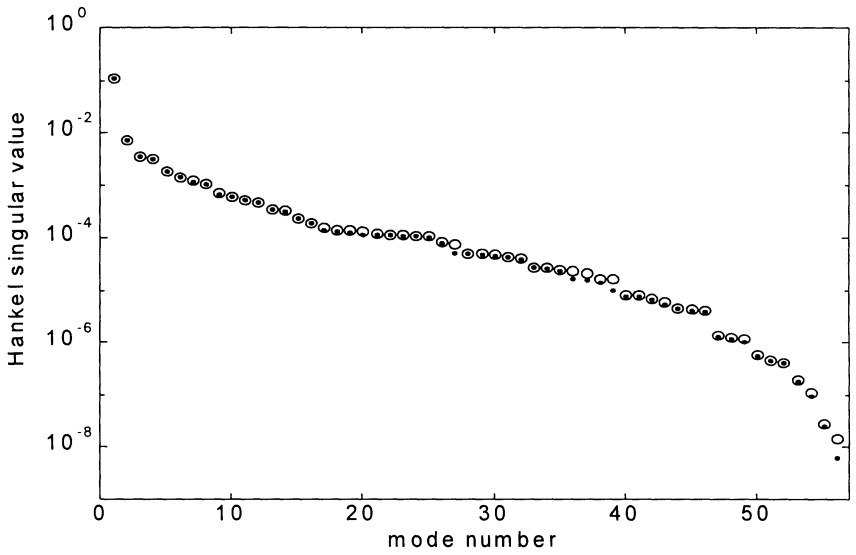

Figure 3.2. Exact (o) and approximate (•) Hankel singular values for the International Space Station structure.

Proof. Since the grammians in modal coordinates are diagonally dominant, the transformation matrix R from the modal to the balanced coordinates is diagonally dominant itself. The system matrix in the balanced coordinates is $A = R^{-1}A_mR$, therefore it is diagonally dominant. ❐

The profiles of the grammians and a system matrix A are drawn in Fig. 3.3.

Example 3.4. The balanced representation of a simple system from Example 2.3 is as follows:

$$A_b = \begin{bmatrix} -0.0029 & 0.7685 & 0.0003 & 0.0015 & -0.0032 & 0.0006 \\ -0.7731 & -0.0030 & 0.0014 & 0.0004 & 0.0028 & -0.0018 \\ -0.0059 & 0.0058 & -0.0263 & -2.1400 & 0.0243 & -0.0047 \\ 0.0050 & -0.0052 & 2.1807 & -0.0203 & -0.0174 & 0.0105 \\ -0.0044 & 0.0044 & -0.0441 & 0.0380 & -0.0805 & -3.0883 \\ 0.0020 & -0.0020 & 0.0190 & -0.0179 & 3.1523 & -0.0170 \end{bmatrix},$$

$$B_b = \begin{bmatrix} 0.5772 \\ -0.5822 \\ 0.5790 \\ -0.5074 \\ 0.4357 \\ -0.2001 \end{bmatrix},$$

$$C_b = \begin{bmatrix} 0.2707 & 0.2703 & -0.1649 & -0.2029 & 0.0414 & 0.1222 \\ 0.2082 & -0.2088 & -0.4373 & 0.3568 & 0.3814 & -0.1318 \\ 0.4654 & -0.4715 & 0.3418 & -0.2983 & 0.2064 & -0.0881 \end{bmatrix},$$

showing the diagonally dominant matrix A_b.

Define a state-space representation as almost balanced if its grammians are almost equal and diagonally dominant, $\Gamma \cong W_c \cong W_o$. The question arises: Can the modal representation be almost-balanced. Well, almost, as stated in the following property:

Property 3.4 ***Approximate Balancing by Scaling the Modal Coordinates.*** *By re-scaling the modal representation* (A_m, B_m, C_m) *one obtains an almost balanced representation* (A_{ab}, B_{ab}, C_{ab})*, such that its grammians are almost equal and diagonally dominant*

$$A_{ab} = A_m, \quad B_{ab} = R_{ab}^{-1} B_m, \quad C_{ab} = C_m R_{ab}, \tag{3.24}$$

$$x_m = R x_{ab}. \tag{3.25}$$

Above, R_{ab} is a diagonal matrix

$$R_{ab} = \mathrm{diag}(R_{abi}), \qquad R_{abi} = r_i I_2, \qquad i = 1,...,n, \tag{3.26a}$$

and

$$r_i = \left(\frac{w_{ci}}{w_{oi}}\right)^{1/4} = \sqrt{\frac{\|B_{mi}\|_2}{\|C_{mi}\|_2}}\,. \tag{3.26b}$$

Note that the transformation matrix R_{ab} leaves matrix A_m almost unchanged, and scales matrices B_m and C_m.

Proof. This property is proved by inspection. Introducing (3.26) to (3.6) one obtains

$$\overline{W}_c \cong \overline{W}_o \cong \Gamma = \mathrm{diag}(\gamma_i I_2), \qquad \gamma_i = \sqrt{w_{ci} w_{oi}}, \tag{3.27}$$

hence, by using transformation (3.24), the approximately balanced representation (A_{ab}, B_{ab}, C_{ab}) is obtained from the modal representation (A_m, B_m, C_m). ❐

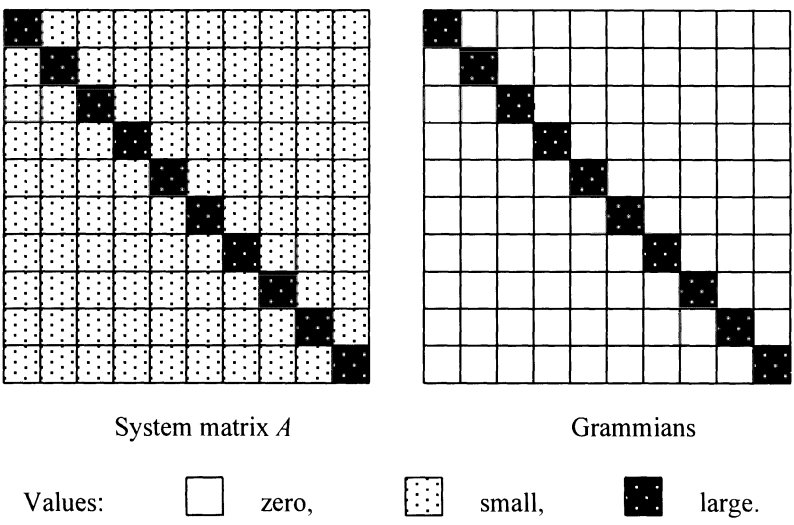

Figure 3.3. Profiles of the system matrix A and the grammians in the balanced coordinates.

A similar property can be derived for the modal representation 2. The closeness of these two modal representations follows from the fact that the transformation R_{12} from modal representation 1 to 2 is itself diagonally dominant, as in (2.37a). The closeness of the modal, balanced and almost-balanced, coordinates is illustrated in Fig. 3.4.

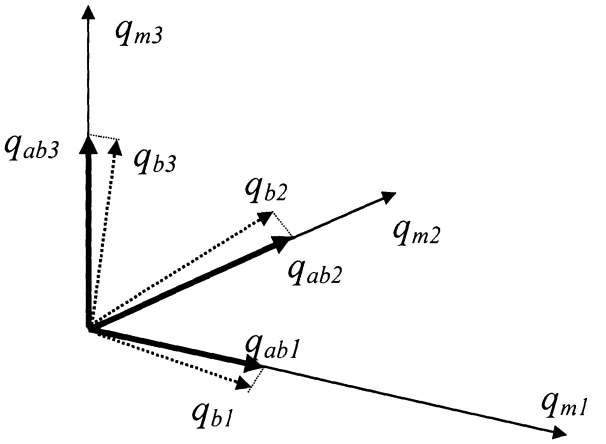

Figure3.4. Modal, balanced, and almost-balanced coordinates.

Similarly to the modal representation, the almost-balanced state-vector x_{ab} is divided into n components,

$$x_{ab} = \begin{Bmatrix} x_{ab1} \\ x_{ab2} \\ \vdots \\ x_{abn} \end{Bmatrix} . \tag{3.28}$$

Components are independent, which is justified by the diagonal matrix A_{ab} of the almost-balanced representation. The state-space representation $(A_{abi}, B_{abi}, C_{abi})$ is associated with the component x_{abi}.

Consider the state-space representation $(A_{abi}, B_{abi}, C_{abi})$ of the ith balanced mode, then $\|B_{abi}\|_2$ is its input gain, and $\|C_{abi}\|_2$ is its output gain.

Property 3.5 ***Input and Output Gains.*** *In the almost-balanced representation the input and output gains are equal:*

$$\|B_{abi}\|_2 = \|C_{abi}\|_2 . \tag{3.29}$$

Proof. This can be shown by introducing transformation R_{ab} as in (3.26)–(3.24), obtaining

$$\|B_{abi}\|_2 = \|C_{abi}\|_2 = \sqrt{\|B_{mi}\|_2 \|C_{mi}\|_2} \,. \tag{3.30}$$

❐

In the almost-balanced representation the grammians are almost equal, $w_{ci} \cong w_{oi}$, or $\Gamma \cong W_c \cong W_o$, where the matrix of the Hankel singular values is as follows $\Gamma \cong \text{diag}(\gamma_1, \gamma_1, \gamma_2, \gamma_2, \ldots, \gamma_n, \gamma_n)$, and

$$w_{ci} \cong w_{oi} \cong \gamma_i \cong \frac{\|B_{abi}\|_2^2}{4\zeta_i \omega_i} = \frac{\|C_{abi}\|_2^2}{4\zeta_i \omega_i} \tag{3.31}$$

Example 3.5. The almost-balanced state-space representation of the simple system is obtained. Starting from the state-space modal representation, as in Example 2.5, one finds the transformation matrix R_{ab} as in (3.26),

$$R_{ab} = \text{diag}\begin{pmatrix} 0.7178 & 0.7178 & 0.8453 & 0.8453 & 1.4724 & 1.4724 \end{pmatrix}.$$

The state matrix $A_{ab} = A_m$, while the B_{ab} and C_{ab} are found from (3.25)

$$B_{ab} = \begin{bmatrix} -0.4798 \\ 0.0075 \\ -0.7704 \\ -0.0083 \\ -0.0025 \\ -0.8198 \end{bmatrix},$$

$$C_{ab} = \begin{bmatrix} -0.0020 & -0.1294 & -0.0028 & 0.2617 & 0.3825 & -0.0012 \\ -0.4038 & 0.0126 & 0.5653 & 0 & -0.0020 & -0.2948 \\ -0.2241 & 0.0070 & -0.4534 & 0 & -0.0045 & -0.6625 \end{bmatrix}.$$

In this representation (3.29) holds:

$$\|B_{ab1}\|_2 = \|C_{ab1}\|_2 = 0.4798,$$
$$\|B_{ab2}\|_2 = \|C_{ab2}\|_2 = 0.7705,$$

$$\|B_{ab3}\|_2 = \|C_{ab3}\|_2 = 0.8198,$$

The grammians obtained for this model are almost equal, i.e., $\Gamma \cong W_o \cong W_c = \text{diag}(1.1817,\ 1.1817,\ 6.3627,\ 6.3627,\ 56.5585,\ 56.5585)$.

3.4.2 The Second-Order Modal Model

The grammians and the balanced models are defined exclusively in the state-space representation, and they do not exist in the second-order form. This is a certain disadvantage since the second-order structural equations are the most popular form of modeling. However, for flexible structures one can find a second-order model which is almost balanced, and for which Hankel singular values can be approximately determined without using a state-space representation.

Property 3.6 ***Controllability and Observability Grammians of the Second-Order Modal Model.*** *The controllability (w_c) and observability (w_o) grammians of the second-order modal model are given as*

$$w_c = 0.25\mathrm{Z}^{-1}\Omega^{-1}\,\text{diag}(B_m B_m^T), \qquad w_o = 0.25\mathrm{Z}^{-1}\Omega^{-1}\,\text{diag}(C_m^T C_m) \tag{3.32}$$

where $\text{diag}(B_m B_m^T)$ *and* $\text{diag}(C_m^T C_m)$ *denote the diagonal part of* $B_m B_m^T$ *and* $C_m^T C_m$, *respectively,* B_m *is given by (2.14), and* C_m *is defined as in (2.16a). Therefore, the ith diagonal entries of* w_c *and* w_o *are*

$$w_{ci} = \frac{\|b_{mi}\|_2^2}{4\zeta_i\omega_i}, \qquad w_{oi} = \frac{\|c_{mi}\|_2^2}{4\zeta_i\omega_i}, \tag{3.33}$$

and b_{mi} *is the ith row of* B_m, *and* c_{mi} *is the ith column of* C_m.

Proof. In order to show this we use a state-space representation. Define the following state vector:

$$x_m = \begin{bmatrix} \Omega q_m \\ \dot{q}_m \end{bmatrix} \tag{3.34}$$

associated with the following state-space representation

$$A = \begin{bmatrix} 0 & \Omega \\ -\Omega & -2Z\Omega \end{bmatrix}, \qquad B = \begin{bmatrix} 0 \\ B_m \end{bmatrix}, \qquad C = \begin{bmatrix} C_{mq}\Omega^{-1} & C_{mv} \end{bmatrix} \tag{3.35}$$

By inspection, for this representation, the grammians are diagonally dominant, in the form

$$W_c \cong \begin{bmatrix} w_c & 0 \\ 0 & w_c \end{bmatrix}, \qquad W_o \cong \begin{bmatrix} w_o & 0 \\ 0 & w_o \end{bmatrix}, \tag{3.36}$$

where w_c and w_o are the diagonally dominant matrices, $w_c \cong \text{diag}(w_{ci})$ and $w_o \cong \text{diag}(w_{oi})$. Introducing (3.35) and (3.36) to the Lyapunov equations (3.5) one obtains (3.33). ❐

The Hankel singular values are determined approximately from (3.33) as

$$\gamma_i \cong \sqrt{w_{ci} w_{oi}} = \frac{\|b_{mi}\|_2 \|c_{mi}\|_2}{4\zeta_i \omega_i}, \qquad i = 1, \ldots, n \tag{3.37}$$

Second-order modal models are nonunique, since the modes can be arbitrarily scaled. By a proper choice of the scaling factors we introduce a model that is almost balanced, i.e., its controllability and observability grammians are approximately equal, and diagonally dominant. The second-order almost-balanced model is obtained by scaling the modal displacement (q_m) such that

$$q_{ab} = R^{-1} q_m \quad \text{or} \quad q_m = R q_{ab} \tag{3.38}$$

and q_{ab} is the almost-balanced displacement.

The transformation R is defined as follows. Denote $\|b_{mi}\|_2$ and $\|c_{mi}\|_2$ as the input and output gains, then

$$R = diag(r_i), \qquad i = 1, \ldots, n \tag{3.39a}$$

and the ith entry r_i is defined as a square root of the gain ratio

$$r_i = \sqrt{\frac{\|b_{mi}\|_2}{\|c_{mi}\|_2}}. \tag{3.39b}$$

Using (2.19) one obtains

$$\|c_{mi}\|_2^2 = \frac{\|c_{qi}\|_2^2}{\omega_i^2} + \|c_{vi}\|_2^2, \tag{3.39c}$$

while

$$\|c_{qi}\|_2^2 = c_{qi}^T c_{qi}, \quad \text{and} \quad \|c_{vi}\|_2^2 = c_{vi}^T c_{vi}. \tag{3.39d}$$

In the above equations b_{mi} is the ith row of B_m, and c_{qi}, c_{vi}, c_{mi} are the ith columns of C_{mq}, C_{mv}, and C_m, respectively.

Introducing (3.38) and (3.39) to the modal equation (2.12) one obtains the almost-balanced second-order modal model

$$\ddot{q}_{ab} + 2Z\Omega\dot{q}_{ab} + \Omega^2 q_{ab} = B_{ab}u, \tag{3.40}$$

$$y = C_{abq}q_{ab} + C_{abv}\dot{q}_{ab},$$

where

$$B_{ab} = R^{-1}B_m, \tag{3.41a}$$

and

$$C_{abq} = C_{mq}R, \qquad C_{abv} = C_{mv}R, \tag{3.41b}$$

while the output matrix C_{ab} is defined as

$$C_{ab} = C_{abq}\Omega^{-1} + C_{abv}. \tag{3.42}$$

It has the following property

$$\|C_{ab}\|_2^2 = \|C_{abq}\Omega^{-1}\|_2^2 + \|C_{abv}\|_2^2. \tag{3.43}$$

A flexible structure in modal coordinates is described by its *natural modes*, ϕ_i, $i = 1, \ldots, n$. Similarly the almost-balanced modal representation is described

by the *almost-balanced modes*, ϕ_{abi}, $i = 1, \ldots, n$. The latter ones are obtained by re-scaling the natural modes

$$\phi_{abi} = r_i \phi_i, \qquad i = 1, \ldots, n, \tag{3.44}$$

with the scaling factor r_i given by (3.39b). Let Φ be the modal matrix, as in (2.8b), and let $\Phi_{ab} = \left[\phi_{ab1} \quad \phi_{ab2} \quad \ldots \quad \phi_{abn}\right]$ be the almost-balanced mode matrix, then

$$\Phi_{ab} = \Phi R. \tag{3.45}$$

In order to show this note that from (2.10) one obtains $q = \Phi q_m$, or equivalently

$$q = \sum_{i=1}^{n} \phi_i q_{mi}. \tag{3.46}$$

But, from (3.38) it follows that $q_{mi} = r_i q_{abi}$, thus (3.48) is now

$$q = \sum_{i=1}^{n} r_i \phi_i q_{abi} = \sum_{i=1}^{n} \phi_{abi} q_{abi}, \tag{3.47}$$

where ϕ_{abi} is a balanced mode as in (3.44).

Property 3.7 ***Grammians of the Almost-Balanced Model.*** *In the almost-balanced model the controllability and observability grammians are approximately equal*

$$w_{cabi} \cong w_{oabi} \cong \frac{\sqrt{\|b_{mi}\|_2 \|c_{mi}\|_2}}{4\zeta_i \omega_i} \cong \gamma_i. \tag{3.48}$$

Proof. From (3.33) one obtains

$$w_{cabi} = \frac{\|b_{abi}\|_2}{4\zeta_i \omega_i}, \qquad w_{oabi} = \frac{\|c_{abi}\|_2}{4\zeta_i \omega_i}. \tag{3.49}$$

However, from (3.41) it follows that

$$b_{abi} = b_{mi}\sqrt{\frac{\|c_{mi}\|_2}{\|b_{mi}\|_2}}, \qquad c_{abi} = c_{mi}\sqrt{\frac{\|b_{mi}\|_2}{\|c_{mi}\|_2}}. \tag{3.50}$$

Introducing the above equation to (3.49) one obtains approximately equal grammians as in (3.48). ❐

Define $\|b_{abi}\|_2$ as the input gain of the ith almost-balanced mode, and define $\|c_{abi}\|_2$ as the output gain of the same mode.

Property 3.8 ***Gains of the Almost-Balanced Model.*** *In the second-order almost-balanced model, the input and output gains are equal:*

$$\|b_{abi}\|_2 = \|c_{abi}\|_2 . \tag{3.51}$$

Proof. The transformation R as in (3.39) is introduced to (3.41a,b) obtaining

$$\|b_{abi}\|_2 = \frac{1}{\|r_i\|}\|b_{mi}\|_2 = \sqrt{\frac{\|c_{mi}\|_2}{\|b_{mi}\|_2}}\|b_{mi}\|_2 = \sqrt{\|b_{mi}\|_2\|c_{mi}\|_2}, \tag{3.52a}$$

$$\|c_{abi}\|_2 = \|c_{mi}\|_2 r_i = \|c_{mi}\|_2\sqrt{\frac{\|b_{mi}\|_2}{\|c_{mi}\|_2}} = \sqrt{\|b_{mi}\|_2\|c_{mi}\|_2} . \tag{3.52b}$$

❐

Example 3.6. The almost-balanced model of a simple structure from Example 2.2 is determined. The transformation matrix R from (3.39a,b) is R=diag(0.6836, 0.7671, 0.8989). Almost-balanced input and output matrices are obtained from (3.41)

$$B_{ab} = \begin{bmatrix} 0.4798 \\ -0.7705 \\ 0.8198 \end{bmatrix},$$

$$C_{abq} = \begin{bmatrix} 0.4040 & 0.5653 & 0.2948 \\ 0 & 0 & 0 \\ 0 & 0 & 0 \end{bmatrix}, \qquad C_{abv} = \begin{bmatrix} 0 & 0 & 0 \\ 0.4040 & 0.5653 & 0.2948 \\ 0.2242 & -0.4534 & 0.6625 \end{bmatrix},$$

$$C_{ab} = \begin{bmatrix} 0.1294 & 0.2617 & 0.3825 \\ 0.4040 & 0.5653 & 0.2948 \\ 0.2242 & -0.4534 & 0.6625 \end{bmatrix}.$$

The almost-balanced mode matrix is obtained from (3.45)

$$\Phi_{ab} = \begin{bmatrix} 0.4040 & 0.5653 & 0.2948 \\ -0.5038 & 0.2516 & 0.5313 \\ 0.2242 & -0.4534 & 0.6625 \end{bmatrix}.$$

Finally, it is easy to check that the input and output gains are equal

$$\|b_{ab1}\|_2 = \|c_{ab1}\|_2 = 0.4798,$$
$$\|b_{ab2}\|_2 = \|c_{ab2}\|_2 = 0.7705,$$
$$\|b_{ab3}\|_2 = \|c_{ab3}\|_2 = 0.8198.$$

Also, from (3.49) one obtains $w_{c1} = w_{o1} = 1.1821$, $w_{c2} = w_{o2} = 6.3628$, $w_{c3} = w_{o3} = 55.8920$, which shows that the model is almost balanced, since the exact Hankel singular values for this system are $\gamma_1 = 1.1794$, $\gamma_2 = 6.3736$, and $\gamma_3 = 56.4212$.

3.5 Three Ways to Compute Hankel Singular Values

Based on the above analysis one can see that there are three ways to obtain Hankel singular values for flexible structures in modal coordinates.

1. From the algorithm in Section 3.2. This algorithm gives the exact Hankel singular values. However, for large structures it could be time consuming. Also, the relationship between the Hankel singular value and the natural mode it represents is not an obvious one: it requires one to examine the system matrix A in order to find the natural frequency related to the Hankel singular value in question.
2. From (3.18) and (3.19). This is an approximate value, and its determination can be time consuming for large structures. However, there is a straightforward relationship between the Hankel singular values and natural frequencies (the Hankel singular value from (3.19) is found for the ith frequency).

3. From (3.21) or (3.37). This is an approximate value, but is determined fast, regardless of the size of the structure. Also, it is immediately known what mode it is associated with.

4
Norms

System norms serve as a measure of system "size" and in this capacity they are used in the model reduction and in the actuator/sensor placement procedures. Three system norms: H_2, H_∞, and Hankel are analyzed in this book. It is shown that for flexible structures the H_2 norm has an additive property: it is a root-mean-square (rms) sum of the norms of individual modes. The H_∞ and Hankel norms are also determined from the corresponding modal norms, by choosing the largest one. All three norms of a structure with multiple inputs (or outputs) can be decomposed into the rms sum of norms of a structure with a single input (or output). These two properties allow for the development of unique and efficient model reduction methods and actuator/sensor placement procedures.

4.1 Definition

Three system norms, H_2, H_∞, and Hankel, are analyzed in this book. Their properties are derived and specified for structural applications.

4.1.1 The H_2 Norm

Let (A, B, C) be a system state-space representation of a linear system, and let $G(\omega) = C(j\omega I - A)^{-1}B$ be its transfer function. The H_2 norm of the system is defined as

W. K. Gawronski, *Dynamics and Control of Structures*

$$\|G\|_2^2 = \frac{1}{2\pi}\int_{-\infty}^{+\infty} \mathrm{tr}(G^*(\omega)G(\omega))\,d\omega\,. \tag{4.1a}$$

A convenient way to determine its numerical value is to use the following formulas

$$\|G\|_2 = \sqrt{\mathrm{tr}(C^T C W_c)}\,, \tag{4.1b}$$

$$\|G\|_2 = \sqrt{\mathrm{tr}(BB^T W_o)}\,, \tag{4.1c}$$

where W_c and W_o are the controllability and observability grammians.

4.1.2 The H_∞ Norm

The H_∞ norm of a stable system is defined as

$$\|G\|_\infty = \max_\omega \sigma_{\max}(G(\omega))\,, \tag{4.2}$$

where $\sigma_{\max}(G(\omega))$ is the largest singular value of $G(\omega)$. The H_∞ norm of a single-input–single-output system is the peak of the transfer function magnitude (in terms of its singular values).

4.1.3 The Hankel Norm

The Hankel norm of a system is a measure of the effect of its past input on its future output, or the amount of energy stored in, and subsequently retrieved from, the system [12, p. 103], and given by

$$\|G\|_h = \sqrt{\lambda_{\max}(W_c W_o)}\,, \tag{4.3}$$

where $\lambda_{\max}(.)$ denotes the largest eigenvalue, and W_c, W_o are the controllability and observability grammians, respectively. Thus, it follows from the definition of the Hankel singular value (3.8) that the Hankel norm of the system is the largest Hankel singular value of the system, $\gamma_{\max}$,

$$\|G\|_h = \gamma_{\max} . \tag{4.4}$$

4.2 Properties

For flexible systems in the modal representation, the H_2, H_∞, and Hankel norms are expressed in terms of the norms of the modes. The decomposition of the system norms in terms of its modal norms is the basis of the dynamics and control algorithms presented in this book.

4.2.1 The H_2 Norm

Define $\Delta\omega_i$ as a half-power frequency at the *i*th resonance, $\Delta\omega_i = 2\zeta_i\omega_i$, see [15] and [26]. This variable is a frequency segment at the *i*th resonance for which the value of the power spectrum is one-half of its maximal value. The determination of the half-power frequency is illustrated in Fig. 4.1. The half-power frequency is the width of the shaded area in this figure, obtained as a cross section of the resonance peak at the height of $h_i/\sqrt{2}$, where h_i is the height of the resonance peak.

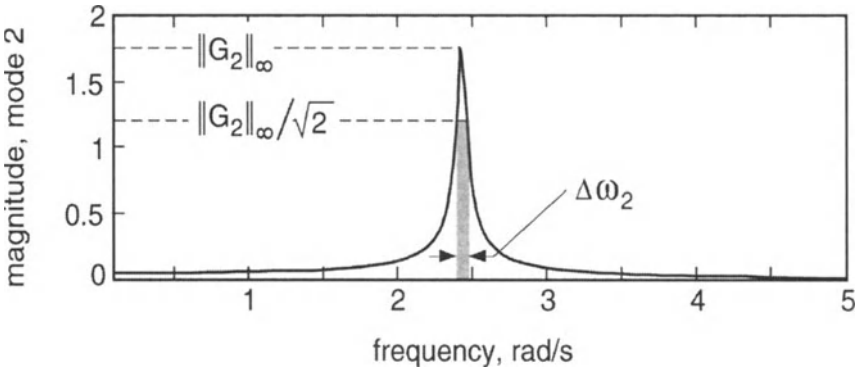

Figure 4.1. The determination of the half-power frequency.

Consider the *i*th natural mode and its state-space representation (A_i, B_i, C_i), see (2.32a,b). For this representation one obtains the following closed-form expressions:

Property 4.1(a) ***Mode Norm.*** *Let* $G_i(\omega) = C_i(j\omega I - A_i)^{-1}B_i$ *be the transfer function of the ith mode. The* H_2 *norm of the ith mode is*

$$\|G_i\|_2 \cong \frac{\|B_i\|_2\|C_i\|_2}{2\sqrt{\zeta_i\omega_i}} = \frac{\|B_i\|_2\|C_i\|_2}{\sqrt{2\Delta\omega_i}} \cong \gamma_i\sqrt{2\Delta\omega_i}\ . \tag{4.5}$$

Proof. From the definition of the H_2 norm and Eq.(3.20) one obtains

$$\|G_i\|_2 \cong \sqrt{\mathrm{tr}(C_i^T C_i W_{ci})} \cong (\|B_i\|_2\|C_i\|_2)/(2\sqrt{\zeta_i\omega_i})\ . \qquad \square$$

The norm of the second-order modal representation $(\omega_i, \zeta_i, b_i, c_i)$ is obtained by replacing B_i, C_i with b_i, c_i, respectively. Note also that $\|G_i\|_2$ is the modal cost of Skelton [97], [99]. The Matlab function *norm_2.m* in Appendix A.3 can be used to compute modal H_2 norms.

Property 4.1(b) ***System Norm.*** *Let* $G(\omega) = C(j\omega I - A)^{-1}B$ *be the transfer function of a structure, and let (A, B, C) be its modal state-space representation. The system* H_2 *norm is, approximately, the rms sum of the modal norms*

$$\|G\|_2 \cong \sqrt{\sum_{i=1}^{n}\|G_i\|_2^2}\ , \tag{4.6}$$

where n is the number of modes.

Proof. Since the controllability grammian W_c in modal coordinates is diagonally dominant, its H_2 norm is as follows:

$$\|G\|_2^2 = \mathrm{tr}(C^T C W_c) \cong \sum_{i=1}^{n}\mathrm{tr}(C_i^T C_i W_{ci}) = \sum_{i=1}^{n}\|G_i\|_2^2\ . \tag{4.7}$$

$\square$

Example 4.1. The determination of the H_2 norm for a simple system as in Fig. 1.2 is illustrated. For this system, the masses are $m_1 = 11$, $m_2 = 5$, and $m_3 = 10$, while the stiffness coefficients are $k_1 = 10$, $k_2 = 50$, $k_3 = 55$, and $k_4 = 10$. The damping matrix is proportional to the stiffness matrix $D = 0.01K$.

The single input u is applied, such that $f_1 = u$, $f_2 = 2u$, $f_3 = -5u$, the output is a linear combination of the mass displacements, $y = 2q_1 - 2q_2 + 3q_3$, where q_i is the displacement of the ith mass, and f_i is the force applied to that mass.

The transfer function of the system and of each mode is shown in Fig. 4.2. It is observed that each mode is dominant in the neighborhood of the mode natural frequency, thus the system transfer function coincides with the mode transfer function near this frequency. The shaded area shown in Fig. 4.3(a) is the H_2 norm of the mode. Note that this area is shown in the logarithmic scale for visualization purposes and that most of the actual area is included in the neighborhood of the peak; compare with the same plot in Fig.4.1 in the linear coordinates. The system H_2 norm is shown as the shaded area in Fig.4.3b, which is approximately a sum of areas of each of the modes.

The H_2 norms of the modes determined from the transfer function are: $\|G_1\|_2 = 1.9399$, $\|G_2\|_2 = 0.3152$, $\|G_3\|_2 = 0.4405$, and the system norm is $\|G\|_2 = 2.0141$. It is easy to check that these norms satisfy (4.6) since $\sqrt{2.0141^2 + 0.3152^2 + 0.4405^2} = 2.0141$.

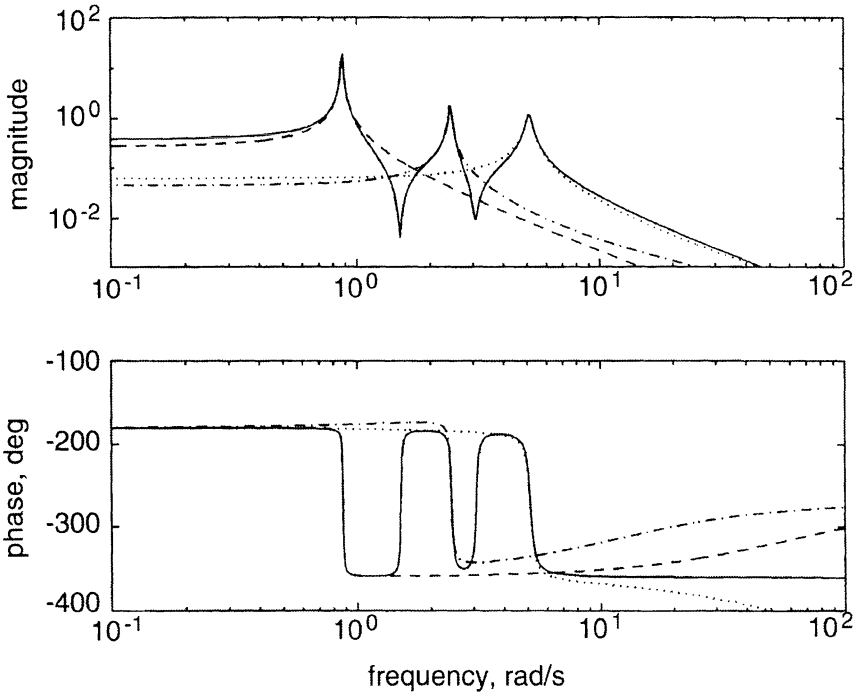

Figure 4.2. The transfer function of the system and of each mode.

In structural testing or in controller design a structure is often equipped with a filter that models disturbances or system performance. In the following we will analyze how the filter addition impacts the structural and modal norms. Consider a filter with a diagonal transfer function $F(\omega)$. The diagonal $F(\omega)$ of order s represents the input filter with no cross-coupling between the inputs. Similarly, the diagonal $F(\omega)$ of order r represents the output filter with no cross-coupling between the outputs. Denote by α_i the magnitude of the filter response at the ith natural frequency

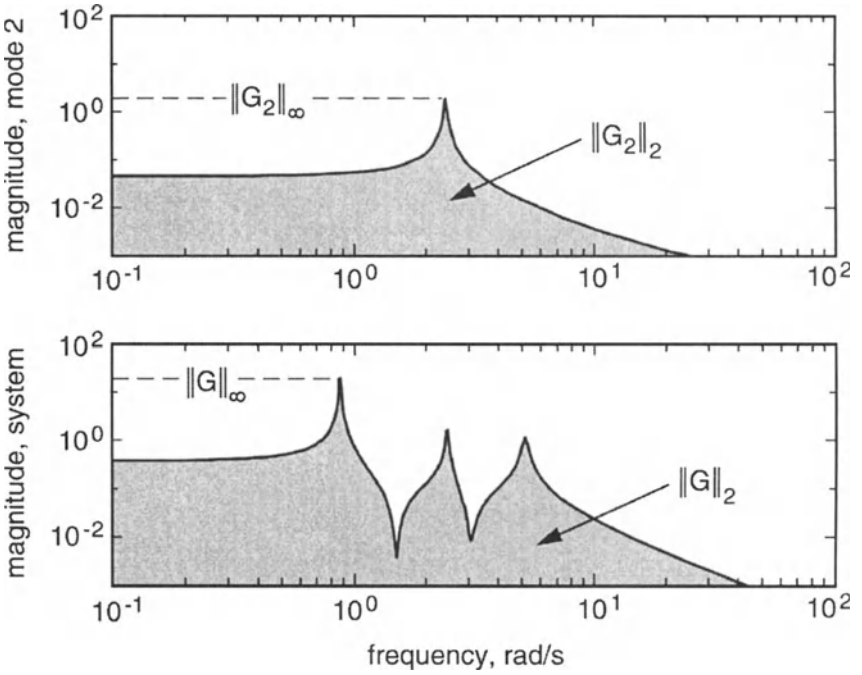

Figure 4.3. H_2 and H_∞ norms (a) of the second mode, and (b) of the system.

$$\alpha_i = |F(\omega_i)| = \sqrt{F^*(\omega_i)F(\omega_i)}\,. \tag{4.8}$$

The filter is smooth if the slope of its transfer function is small when compared to the slope of the structure near the resonance, that is, at the half-power frequency

$$\left|\frac{\partial \sigma_{\max}(F)}{\partial \omega}\right| << \left|\frac{\partial \sigma_{\max}(G)}{\partial \omega}\right| \qquad \text{for} \qquad \omega = \omega_i - 0.5\Delta\omega_i\,, \tag{4.9}$$

and $i = 1, \ldots, n$. Above, $\sigma_{\max}(X)$ denotes the maximal singular value of X and $\Delta\omega_i$ denotes the half-power frequency at the ith resonance. The smoothness property is illustrated in Fig. 4.4.

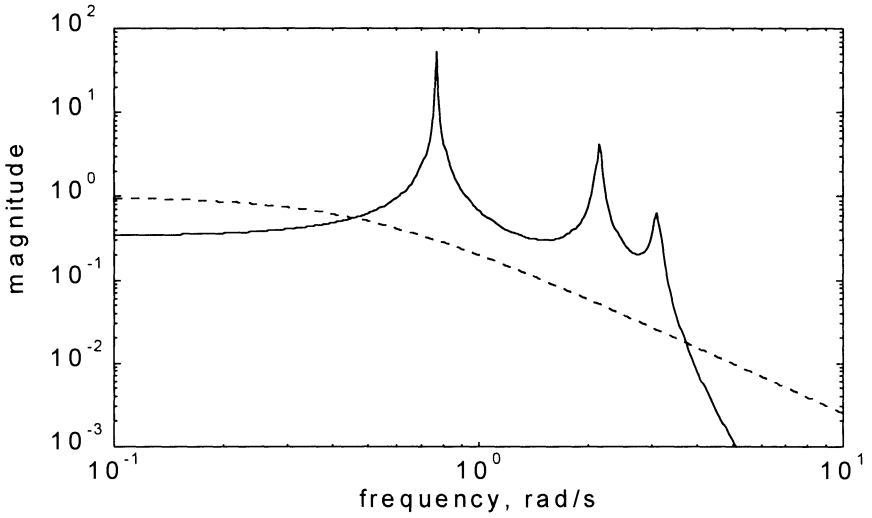

Figure 4.4. Magnitude of a transfer function of a structure (solid line) and a smooth filter (dashed line).

With the above assumptions the following property is valid:

Property 4.2 ***Structure with a Filter.*** *The norm of a structure with a smooth filter is approximately a rms sum of scaled modal norms*

$$\|GF\|_2^2 \cong \sum_{i=1}^{n} \|G_i \alpha_i\|_2^2 \ , \tag{4.10a}$$

and the norm of the ith mode with a smooth filter is a scaled norm

$$\|G_i F\|_2 \cong \|G_i \alpha_i\|_2 \ . \tag{4.10b}$$

Proof. Note that for the smooth filter the transfer function GF preserves the properties of a flexible structure given by Property 2.1, thus

$$\|GF\|_2^2 = \frac{1}{2\pi} \int_{-\infty}^{\infty} \mathrm{tr}(F^* G^* GF) d\omega$$

$$\cong \sum_{i=1}^{n} \frac{1}{2\pi} \int_{-\infty}^{\infty} \mathrm{tr}(F(\omega_i)F^*(\omega_i)G_i^*G_i)\, d\omega$$

$$= \sum_{i=1}^{n} \frac{1}{2\pi} \int_{-\infty}^{\infty} \mathrm{tr}(|F(\omega_i)|^2 G_i^*G_i)\, d\omega$$

$$= \sum_{i=1}^{n} \frac{1}{2\pi} \int_{-\infty}^{\infty} \mathrm{tr}(|F(\omega_i)|G_i^*G_i|F(\omega_i)|)\, d\omega = \sum_{i=1}^{n} \|G_i\alpha_i\|_2^2 . \qquad (4.11)$$

In the above approximation we used (4.2), the trace commutative property $\mathrm{tr}(AB) = \mathrm{tr}(BA)$, and the following inequality

$$\int_{-\infty}^{\infty} \mathrm{tr}(F^*G_j^*G_iF)\, d\omega << \int_{-\infty}^{\infty} \mathrm{tr}(F^*G_i^*G_iF)\, d\omega \qquad \text{for} \quad i \neq j . \qquad \square$$

Property 4.2 says that a norm of a smooth filter in series with a flexible structure is approximately equal to the norm of a structure scaled by the filter gains at natural frequencies. A similar result to Property 4.2 holds for a structure with a filter at the output.

Consider a flexible structure with s actuators (or s inputs) and n modes, so that the modal input matrix B consists of n block-rows of dimension $2 \times s$

$$B = \begin{bmatrix} B_1 \\ B_2 \\ \vdots \\ B_n \end{bmatrix}, \qquad (4.12)$$

and the ith block-row B_i of B that corresponds to the ith mode has the form

$$B_i = \begin{bmatrix} B_{i1} & B_{i2} & \cdots & B_{is} \end{bmatrix}, \qquad (4.13)$$

where B_{ik} corresponds to the kth actuator at the ith mode. The question arises as to how the two-norm of a structure with a single actuator corresponds to the two-norm of the same structure with a set of s actuators. The answer is in the following property:

Property 4.3 ***Additive Property of a Set of Actuators for Each Mode.*** *The two-norm of the ith mode of a structure with a set of s actuators is the rms sum of norms of the mode with each single actuator from this set, i.e.,*

$$\|G_i\|_2 \cong \sqrt{\sum_{j=1}^{s} \|G_{ij}\|_2^2}, \qquad i = 1, \ldots, n. \tag{4.14}$$

Proof. From (4.5) one obtains the norm of the ith mode with the jth actuator ($\|G_{ij}\|_2$), and the norm of the ith mode with all actuators ($\|G_i\|_2$)

$$\|G_{ij}\|_2 \cong \frac{\|B_{ij}\|_2 \|C_i\|_2}{2\sqrt{\zeta_i \omega_i}}, \qquad \|G_i\|_2 \cong \frac{\|B_i\|_2 \|C_i\|_2}{2\sqrt{\zeta_i \omega_i}}. \tag{4.15}$$

But, from the definition of the norm and from (4.13), it follows that

$$\|B_i\|_2 = \sqrt{\sum_{j=1}^{s} \|B_{ij}\|_2^2}, \tag{4.16}$$

introducing the above equation to (4.15), one obtains (4.14).
❐

A similar property can be derived for a structure.

Property 4.4 ***Additive Property of a Set of Actuators for a Structure.*** *The two-norm of a structure with a set of s actuators is the rms sum of norms of a structure with each single actuator from this set,*

$$\|G\|_2 \cong \sqrt{\sum_{j=1}^{s} \|G_j\|_2^2}. \tag{4.17}$$

Proof. From (4.7) and (4.14) one obtains

$$\|G\|_2 \cong \sqrt{\sum_{i=1}^{n} \|G_i\|_2^2} = \sqrt{\sum_{i=1}^{n} \sum_{j=1}^{s} \|G_{ij}\|_2^2} = \sqrt{\sum_{j=1}^{s} \left(\sum_{i=1}^{n} \|G_{ij}\|_2^2 \right)} = \sqrt{\sum_{j=1}^{s} \|G_j\|_2^2}. \tag{4.18}$$

❐

Similarly to the actuator properties one can derive sensor properties. For r sensors of an n mode structure the output matrix is as follows:

$$C = [C_1 \quad C_2 \quad \dots \quad C_n], \qquad C_i = \begin{bmatrix} C_{1i} \\ C_{2i} \\ \vdots \\ C_{ri} \end{bmatrix}, \tag{4.19}$$

where C_i is the output matrix of the ith mode, and C_{ji} is the 1×2 block of the jth output at the ith mode.

Property 4.5 ***Additive Property of a Set of Sensors for Each Mode.*** *The two-norm of the ith mode of a structure with a set of r sensors is the rms sum of norms of the mode with each single actuator from this set, i.e.,*

$$\|G_i\|_2 \cong \sqrt{\sum_{k=1}^{r} \|G_{ki}\|_2^2}, \qquad i = 1, \dots, n. \tag{4.20}$$

Proof. Denote the norm of the ith mode with the kth sensor ($\|G_{ki}\|_2$), and the norm of the ith mode with all sensors ($\|G_i\|_2$). From (4.5) we have

$$\|G_{ik}\|_2 \cong \frac{\|B_i\|_2 \|C_{ki}\|_2}{2\sqrt{\zeta_i \omega_i}}, \qquad \|G_i\|_2 \cong \frac{\|B_i\|_2 \|C_i\|_2}{2\sqrt{\zeta_i \omega_i}}. \tag{4.21}$$

From (4.19) it follows that

$$\|C_i\|_2^2 = \sum_{k=1}^{r} \|C_{ki}\|_2^2 . \tag{4.22}$$

Introducing the above equation to (4.21), one obtains (4.20). ❐

Property 4.6 ***Additive Property of a Set of Sensors for a Structure.*** *The two-norm of a structure with a set of r sensors is the rms sum of norms of a structure with each single actuator from this set,*

$$\|G\|_2 \cong \sqrt{\sum_{j=1}^{r} \|G_j\|_2^2} . \tag{4.23}$$

Proof. Similar to the proof of Property 4.4. ❐

Equations (4.17) and (4.23) show that the H_2 norm of a mode with a set of actuators (sensors) is the rms sum of the H_2 norms of this mode with a single actuator (sensor).

4.2.2 The H_∞ Norm

The H_∞ norm of a natural mode can be approximately expressed in the closed-form as follows:

Property 4.7(a) ***Mode Norm.*** *Consider the ith mode* (A_i, B_i, C_i), *or* $(\omega_i, \zeta_i, b_i, c_i)$ *with the corresponding Hankel singular value* γ_i. *Its* H_∞ *norm is estimated as*

$$\|G_i\|_\infty \cong \frac{\|B_i\|_2 \|C_i\|_2}{2\zeta_i\omega_i} = \frac{\|b_i\|_2 \|c_i\|_2}{2\zeta_i\omega_i}, \tag{4.24a}$$

or

$$\|G_i(\omega)\|_\infty \cong 2\gamma_i . \tag{4.24b}$$

Proof. In order to prove this, note that the largest amplitude of the mode is approximately at the *i*th natural frequency, thus

$$\|G_i\|_\infty \cong \sigma_{\max}(G_i(\omega_i)) = \frac{\sigma_{\max}(C_i B_i)}{2\zeta_i\omega_i} = \frac{\|B_i\|_2 \|C_i\|_2}{2\zeta_i\omega_i} . \tag{4.25}$$

Comparing (4.25) and (3.21), one obtains (4.24b). ❐

For a structure, the approximate H_∞ norm is proportional to its largest Hankel singular value $\gamma_{\max}$. The modal H_∞ norms can be calculated using the Matlab function *norm_inf.m* given in Appendix A.4.

Property 4.7(b) ***System Norm.*** *Due to the almost independence of the modes, the system* H_∞ *norm is the largest of the mode norms, i.e.,*

$$\|G\|_\infty \cong \max_i \|G_i\|_\infty \cong 2\gamma_{\max}, \qquad i = 1, \ldots, n. \tag{4.26}$$

This property says that the largest modal peak response of a lightly damped structure determines the worst-case response.

Example 4.2. The determination of the H_∞ norm of a simple structure, as in Example 4.1 and its modes, is illustrated. The H_∞ norm of the second mode is shown in Fig. 4.2(a) as the height of the second resonance peak. The H_∞ norm of the system is shown in Fig. 4.2(b) as the height of the highest (first in this case) resonance peak. The H_∞ norms of the modes, determined from the transfer function, are: $\|G_1\|_\infty \cong 18.9229$, $\|G_2\|_\infty \cong 1.7454$, $\|G_3\|_\infty \cong 1.2176$, and the system norm is $\|G\|_\infty \cong \|G_1\|_\infty \cong 18.9619$.

Similarly to the H_2 norm, consider a structure G with a smooth input filter F. The following property is valid:

Property 4.8 ***Structure with a Filter.*** *The H_∞ norm of a structure with a smooth filter is equal to the H_∞ norm of the structure with scaled modes*

$$\|GF\|_\infty \cong \max_i(\|G_i\alpha_i\|_\infty), \qquad i = 1, \ldots, n, \tag{4.27a}$$

and the norm of the ith mode with a smooth filter is equivalent to the norm of the scaled mode

$$\|G_iF\|_\infty \cong \|G_i\alpha_i\|_\infty, \tag{4.27b}$$

where the scaling factor α_i is defined in (4.8).

Proof. Note that for a smooth filter the transfer function GF preserves the properties of a flexible structure given by Property 2.1(b), thus

$$\begin{aligned}\|GF\|_\infty &= \sup_\omega \sigma_{\max}(G(\omega)F(\omega)) \cong \max_i \sigma_{\max}(G(\omega_i)F(\omega_i)) \\ &\cong \max_i \sigma_{\max}(G_i(\omega_i)\alpha_i) = \max_i(\|G_i\alpha_i\|_\infty).\end{aligned} \tag{4.28}$$

In the above approximation we took into consideration the fact that $\sigma_k(GF) = \sigma_k(G|F|)$, which can be proven as follows:

$$\sigma_k^2(GF) = \lambda_k(F^*G^*GF) = \lambda_k(FF^*G^*G)$$

$$= \lambda_k(|F|^2 G^* G) = \lambda_k(|F|G^* G|F|) = \sigma_k^2(G|F|)\,. \tag{4.29}$$

❐

This property says that a norm of a smooth filter in series with a flexible structure is approximately equal to the norm of a structure scaled by the filter gains at natural frequencies.

Consider a flexible structure with s actuators (or s inputs). Similarly to the H_2 norm, the question arises as to how the H_∞ norm of a structure with a single actuator corresponds to the H_∞ norm of the same structure with a set of s actuators. The answer is in the following property:

Property 4.9 ***Additive Property of a Set of Actuators for Each Mode.*** *The H_∞ norm of the ith mode of a structure with a set of s actuators is the rms sum of norms of the mode with each single actuator from this set, i.e.,*

$$\|G_i\|_\infty \cong \sqrt{\sum_{j=1}^{s} \|G_{ij}\|_\infty^2}\,, \qquad i = 1, \ldots, n. \tag{4.30}$$

Proof. From (4.24) one obtains the norm of the ith mode with the jth actuator ($\|G_{ij}\|_\infty$), and the norm of the ith mode with all actuators ($\|G_i\|_\infty$)

$$\|G_{ij}\|_\infty = \frac{\|B_{ij}\|_2 \|C_i\|_2}{2\zeta_i \omega_i}\,, \qquad \|G_i\|_\infty \cong \frac{\|B_i\|_2 \|C_i\|_2}{2\zeta_i \omega_i}\,. \tag{4.31}$$

Introducing (4.16) to the above equation, one obtains (4.30). ❐

Similarly to the actuator properties one can derive sensor properties.

Property 4.10 ***Additive Property of a Set of Sensors for Each Mode.*** *The H_∞ norm of the ith mode of a structure with a set of r sensors is the rms sum of norms of the mode with each single actuator from this set, i.e.,*

$$\|G_i\|_\infty \cong \sqrt{\sum_{k=1}^{r} \|G_{ki}\|_\infty^2}\,, \qquad i = 1, \ldots, n. \tag{4.32}$$

Proof. Denote the norm of the *i*th mode with the *k*th sensor ($\|G_{ki}\|_\infty$), and the norm of the *i*th mode with all sensors ($\|G_i\|_\infty$). From (4.24) we have

$$\|G_{ik}\|_\infty = \frac{\|B_i\|_2 \|C_{ki}\|_2}{2\zeta_i \omega_i}, \qquad \|G_i\|_\infty = \frac{\|B_i\|_2 \|C_i\|_2}{2\zeta_i \omega_i}. \tag{4.33}$$

Introducing (4.22) to the above equation, one obtains (4.32). ❐

Equations (4.30) and (4.32) show that the H_∞ norm of a mode with a set of actuators (sensors) is the rms sum of the H_∞ norms of this mode with a single actuator (sensor). Note however, that unlike the H_2 norm, this property does not hold for the whole structure.

4.2.3 The Hankel Norm

This norm is approximately evaluated from the following closed-form formula:

Property 4.11(a) ***Mode Norm.*** *Consider the ith mode in the state space form* (A_i, B_i, C_i), *or the corresponding second-order form* $(\omega_i, \zeta_i, b_i, c_i)$. *Its Hankel norm is determined from*

$$\|G_i\|_h = \gamma_i \cong \frac{\|B_i\|_2 \|C_i\|_2}{4\zeta_i \omega_i} = \frac{\|b_i\|_2 \|c_i\|_2}{4\zeta_i \omega_i}. \tag{4.34}$$

The modal H_∞ norms can be calculated using the Matlab function *norm_han.m* given in Appendix A.5.

For a structure the Hankel norm is obtained as follows.

Property 4.11(b) ***System Norm.*** *The Hankel norm of the system is the largest norm of its modes, i.e.,*

$$\|G\|_h \cong \max_i \|G_i\|_h = \gamma_{\max} = 0.5\|G\|_\infty, \tag{4.35}$$

where $\gamma_{\max}$ *is the largest Hankel singular value of the system.*

Since the Hankel norm is approximately one-half of the H_∞ norm: $\|G_i\|_h \cong 0.5\|G_i\|_\infty$ and $\|G\|_h \cong 0.5\|G\|_\infty$, therefore Properties 4.8–4.10 of the H_∞ norm apply to the Hankel norm as well, namely:

Property 4.12 ***Additive Property of a Set of Actuators for Each Mode.*** *The Hankel singular value (Hankel norm) of the ith mode of a structure with a set of s actuators is the rms sum of the Hankel singular values of the mode with each single actuator from this set, i.e.,*

$$\gamma_i = \sqrt{\sum_{j=1}^{s} \gamma_{ij}^2}\,, \qquad i = 1, \ldots, n. \tag{4.36}$$

Similar are the sensor properties.

Property 4.13 ***Additive Property of a Set of Sensors for Each Mode.*** *The Hankel singular value (Hankel norm) of the ith mode of a structure with a set of r sensors is the rms sum of the Hankel singular values of the mode with each single sensor from this set, i.e.,*

$$\gamma_i = \sqrt{\sum_{k=1}^{r} \gamma_{ki}^2}\,, \qquad i = 1, \ldots, n. \tag{4.37}$$

Finally, comparing (4.5), (4.24a), and (4.34) one obtains the approximate relationships between H_2, H_∞, and Hankel norms

$$\|G_i\|_\infty \cong 2\|G_i\|_h \cong \sqrt{\zeta_i \omega_i}\,\|G_i\|_2\,. \tag{4.38}$$

Example 4.3. Consider a truss presented in Fig. 1.3. Vertical control forces are applied at nodes 9 and 10, and the output rates are measured in the horizontal direction at nodes 4 and 5. For this structure the H_2 and H_∞ norms of each mode are given in Fig. 4.5.

From (4.38) it follows that the ratio of the H_∞ and H_2 norms is

$$\frac{\|G_i\|_2}{\|G_i\|_\infty} \cong \sqrt{\zeta_i \omega_i} = 0.707\sqrt{\Delta\omega_i}\,,$$

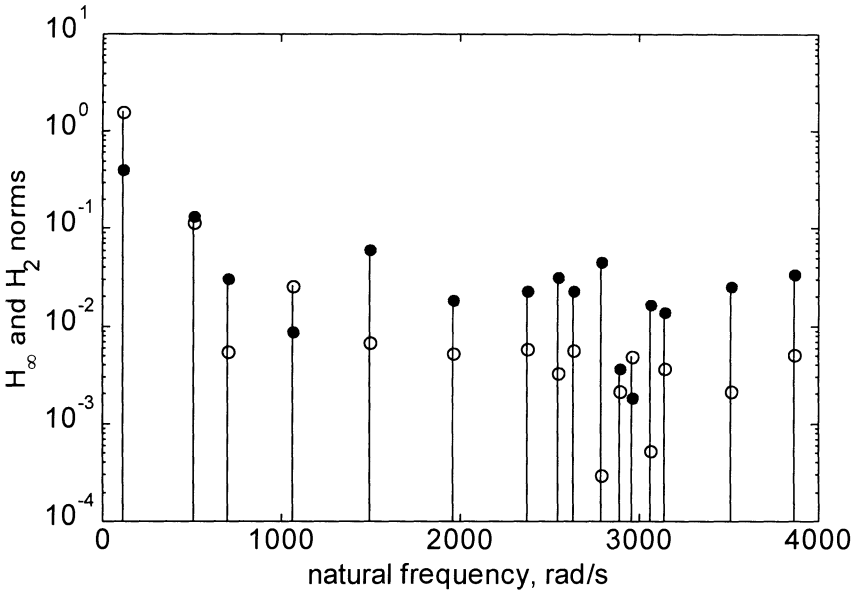

Figure 4.5. Approximate norms of the 2D truss: H_2 (o) and H_∞ (•).

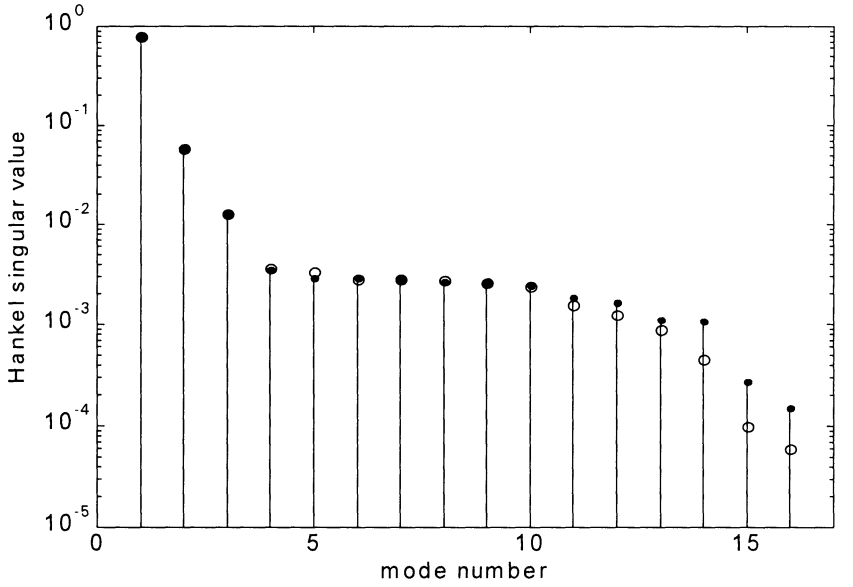

Figure 4.6. The exact (o) and the approximate (•) Hankel singular values of the 2D truss.

hence, the relationship between the H_∞ and H_2 norms depends on the width of the resonance. For a wide resonant peak (large $\Delta\omega_i$) the H_2 norm of the ith mode is larger than the corresponding H_∞ norm. For a narrow resonant peak (small $\Delta\omega_i$) the H_∞ norm of the ith mode is larger than the corresponding H_2 norm. This is visible in Fig. 4.5, where neither norm is dominant.

The exact Hankel singular values, and the approximate values, obtained from (4.3) and (4.36), respectively, are shown in Fig. 4.6. A good coincidence between the exact and approximate values is observed.

5
Model Reduction

Model reduction is a part of dynamic analysis, testing, and the control of flexible structures. Typically, a model with a large number of degrees of freedom, such as the one developed for the static analysis of structures, causes numerical difficulties in dynamic analysis, to say nothing of the high computational cost. In system identification, on the other hand, the order of the identified system is determined by the reduction of the initially oversized model that includes a noise model. Finally, in structural control the complexity and performance of a model-based controller depends on the order of the structural model. In all cases the reduction is a crucial part of the analysis and design. Thus, the reduced-order system solves the above problems if it acquires the essential properties of the full-order model.

Many reduction techniques have been developed. Some of them, as in [59], [110], and [111], give optimal results, but they are complex and computationally expensive. Other methods, comparatively simple, give results close to the optimal one. The latter include balanced and modal truncation, see [85], [55], [97], [98], [101], [112], [40], and [51], which are discussed later. Model reduction of flexible structures requires specific approach, and was studied by Gregory [55], Jonckheere [62], Skelton [98], Gawronski [38], [40], Gawronski and Williams [51], and Cottin, Prells, and Natke [17]. In this chapter the reduction in modal coordinates is discussed.

W. K. Gawronski, *Dynamics and Control of Structures*

5.1 Reduction Through Truncation

A reduced-order model is obtained here by truncating appropriate states in the modal coordinates. Denote by x the modal state vector of n modes ($N = 2n$ states), and by (A, B, C) the modal representation (the subscript m is dropped for simplicity of notation). Let x be partitioned as follows:

$$x = \begin{Bmatrix} x_r \\ x_t \end{Bmatrix}, \tag{5.1a}$$

where x_r is the vector of the retained states, and x_t is a vector of truncated states. If there are $k < n$ retained modes, x_r is a vector of $2k$ states, and x_t is a vector of $2(n–k)$ states. Let the state triple (A, B, C) be partitioned accordingly,

$$A = \begin{bmatrix} A_r & 0 \\ 0 & A_t \end{bmatrix}, \qquad B = \begin{bmatrix} B_r \\ B_t \end{bmatrix}, \qquad C = \begin{bmatrix} C_r & C_t \end{bmatrix}. \tag{5.1b}$$

The diagonally dominant modal grammian is divided similarly,

$$\Gamma \cong \begin{bmatrix} \Gamma_r & 0 \\ 0 & \Gamma_t \end{bmatrix}. \tag{5.2}$$

The reduced model is obtained by deleting the last $2(n–k)$ rows of A,B, and the last $2(n–k)$ columns of A,C. Formally, this operation is written as

$$A_r = LAL^T, \qquad B_r = LB, \qquad C_r = CL^T, \tag{5.3}$$

where $L = \begin{bmatrix} I_{2k} & 0 \end{bmatrix}$.

Modal reduction by truncation of stable models always produces a stable reduced model, since the poles of the reduced model are a subset of the full-order poles.

The problem is to order the states so that the retained states x_r will be the best reproduction of the full system response. The choice depends on the definition of the reduction index.

5.2 Reduction Errors

We use H_2 , H_∞, and Hankel norms to evaluate the reduction errors. The first approach, based on the H_2 norm, is connected to the Skelton reduction method, see [98]. The second method, based on the H_∞ and Hankel norms is connected to the Moore reduction method, see [85].

5.2.1 H_2 Model Reduction

The H_2 reduction error is defined as

$$e_2 = \|G - G_r\|_2 , \tag{5.4}$$

where G is the transfer function of the full model and G_r is the transfer function of the reduced model.

The squares of the mode norm are additive, see Property 4.1, therefore the norm of the reduced system with k modes is the root-mean-square (rms) sum of the mode norms

$$\|G_r\|_2^2 = \sum_{i=1}^{k} \|G_i\|_2^2 . \tag{5.5}$$

Thus, the reduction error is

$$e_2^2 = \|G\|_2^2 - \|G_r\|_2^2 = \sum_{i=k+1}^{n} \|G_i\|_2^2 . \tag{5.6}$$

It is clear from the above equation that the near-optimal reduction is obtained if the truncated mode norms $\|G_i\|_2$ for $i = k+1, \ldots, n,$ are the smallest ones. Therefore, the modal state vector is rearranged, starting from the mode with the largest H_2 norm and ending with the mode with the smallest norm. Truncation of the last n–k modes will give, in this case, a near-optimal reduced model of order k.

5.2.2 H_∞ and Hankel Model Reduction

It can be seen from (4.36) that the H_∞ norm is approximately twice the Hankel norm, hence the reduction using one of those norms is identical with the reduction using the other norm. Thus, we consider here the H_∞ reduction only.

The H_∞ reduction error is defined as

$$e_\infty = \|G - G_r\|_\infty . \tag{5.7}$$

It was shown by Glover [52] that the upper limit of the H_∞ reduction error is as follows:

$$e_\infty = \|G - G_r\|_\infty \le \sum_{i=k+1}^{n} \|G_i\|_\infty . \tag{5.8}$$

However, for the flexible structures in the modal coordinates the error can be estimated less conservatively. In this case the transfer function is a sum of its modes, see Property 2.1, therefore

$$G = \sum_{i=1}^{n} G_i \quad \text{and} \quad G_r = \sum_{i=1}^{k} G_i , \tag{5.9}$$

thus $G - G_r = \sum_{i=k+1}^{n} G_i = G_t$, where G_t is the transfer function of the truncated part. Therefore

$$e_\infty = \|G - G_r\|_\infty = \|G_t\|_\infty \cong \|G_{k+1}\|_\infty , \tag{5.10}$$

i.e., the error is equal to the H_∞ norm of the largest truncated mode. It is clear that the near-optimal reduction is obtained if the H_∞ norms of the truncated modes are the smallest ones.

Example 5.1. A simple system as in Example 2.5 is considered. For this system the H_∞ modal norms are obtained from (4.25), $\|G_1\|_\infty \cong 6.7586$ (mode of the natural frequency 1.3256 rad/s), $\|G_2\|_\infty \cong 4.9556$ (mode of the natural frequency 2.4493 rad/s), and $\|G_3\|_\infty \cong 2.6526$ (mode of the natural frequency

3.200 rad/s). The H_2 mode norms (see (4.5)) are as follows: $\|G_1\|_2 \cong 3.2299$, $\|G_2\|_2 \cong 3.3951$, $\|G_3\|_2 \cong 0.5937$. The reduction errors after the truncation of the last mode (of frequency 3.200 rad/s) are $e_\infty = 2.6526$ and $e_2 = 0.5937$, while the system norms are $\|G\|_\infty = 6.7586$ and $\|G\|_2 \cong 4.7235$.

Example 5.2. Consider a 2D truss as in Example 1.3. Its model has been reduced in the modal coordinates using the H_∞ norm. The approximate norms of the modes are shown in Fig. 5.1. From this figure the system norm (the largest of the mode norms) is $\|G\|_\infty = 1.6185$. Based on the modal norms it was decided that in the reduced-order model we reject all modes of the H_∞ norm less than 0.01. The area of the H_∞ norm less than 0.01 is in Fig. 5.1, below the dashed line, and the modes with the H_∞ norm in this area are deleted. Consequently, the reduced model consists of three modes. The transfer function of the full and reduced models (from the second input to the second output) is shown in Fig. 5.2(a), and the corresponding impulse response is shown in Fig. 5.2(b). Both figures indicate a small reduction error, which is obtained as $(\|G\|_\infty - \|G_r\|_\infty)/\|G\|_\infty \cong \|G_4\|_\infty / \|G\|_\infty = 0.0040$.

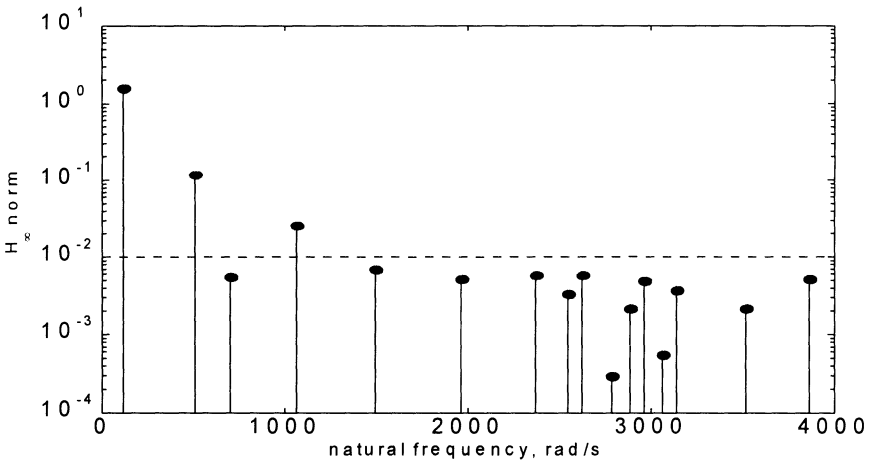

Figure 5.1. H_∞ norms of the 2D truss modes.

5.3 Systems with Integrators

Systems with integrators have poles at zeros, therefore the corresponding H_2, H_∞, and Hankel norms do not exist as their values tend to infinity. However, the infinite values of the norms of some modes should not be an obstacle in the

reduction process. These values indicate that the corresponding states should be retained in the reduced model, regardless of the norms of other modes. The reduction problem can be solved by determining the inverses of grammians, see [45]. Here two simple approaches are used for the reduction of systems with integrators.

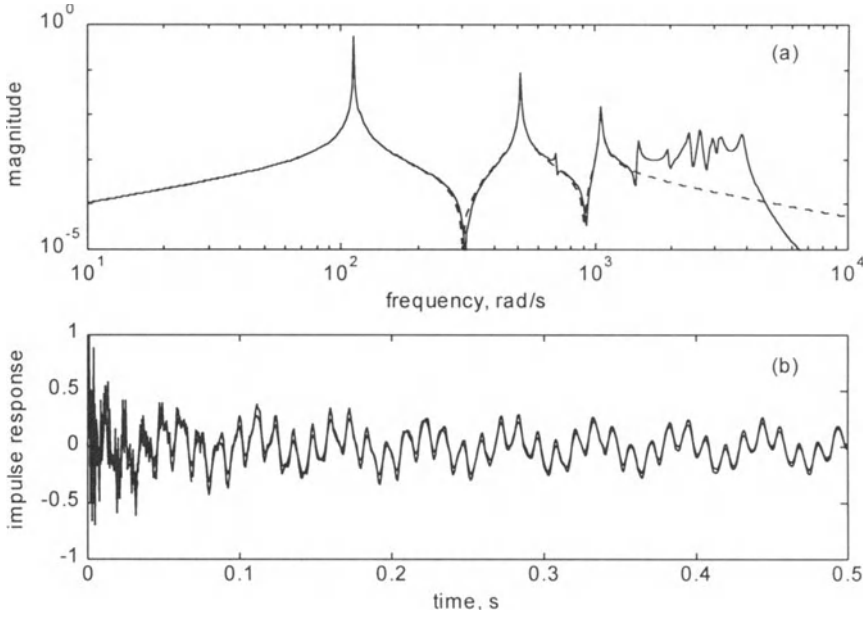

Figure 5.2. (a) Magnitude of the transfer function, and (b) impulse responses of the full (solid line) and reduced (dashed line) truss models.

In the first approach the system is represented in modal coordinates, represented by the following system triple (see Section 3.3):

$$A = \begin{bmatrix} 0_m & 0 \\ 0 & A_o \end{bmatrix}, \qquad B = \begin{bmatrix} B_r \\ B_o \end{bmatrix}, \qquad C = \begin{bmatrix} C_r & C_o \end{bmatrix}, \tag{5.11}$$

where 0_m is an $m \times m$ zero matrix. The triple (A_o, B_o, C_o) has no poles at zero. It is itself in modal coordinates. The vector of the corresponding modal H_∞ norms is denoted h_o. This vector is arranged in descending order, and the remaining infinite norms are added

$$h = \{\inf, \quad h_o\} \tag{5.12}$$

to obtain the vector of H_∞ norms of the (A, B, C) representation, where inf = $\{\infty, \infty, \ldots, \infty\}$ contains m values at infinity. The system is reduced by truncation, as described at the beginning of this chapter.

The second approach is based on the approximate evaluation of the H_∞ norms. From (4.25) one finds

$$\|G_i\|_\infty \cong \frac{\|B_{mi}\|_2 \|C_{mi}\|_2}{2\zeta_i \omega_i}, \tag{5.13}$$

and $\omega_i = 0$ for the poles at zero, thus $\|G_i\|_\infty \to \infty$. For nonzero poles the finite norms are determined from the above equation, and ordered in descending order. The corresponding state-space representation is reduced by truncation.

Example 5.3. A simple system is from Fig.1.2 with the following parameters: $m_1 = m_2 = 1$, $m_3 = 2$, $k_1 = k_4 = 0$, $k_2 = 0.3$, and $k_3 = 1$. Damping is proportional to the stiffness, $d_i = 0.03k_i$, i = 1, 2, 3, and the input force is applied at mass m_2, and the output rate is measured at the same location. This system has two poles at zero. Find its H_∞ norms, and reduce the system.

The modal representation, as in (5.11), is as follows:

$$A_o = \begin{bmatrix} -0.0264 & 1.3260 & 0 & 0 \\ -1.3260 & -0.0264 & 0 & 0 \\ 0 & 0 & -0.0051 & 0.5840 \\ 0 & 0 & -0.5840 & -0.0051 \end{bmatrix}, \quad B_o = \begin{bmatrix} -0.3556 \\ -1.1608 \\ -0.0072 \\ 0.1642 \end{bmatrix},$$

$$C_o = \begin{bmatrix} -0.161 & -0.5836 & -0.0043 & -0.0821 \end{bmatrix},$$

$$B_r = \begin{bmatrix} 6.0883 \times 10^7 \\ 35.8240 \end{bmatrix}, \qquad C_r = \begin{bmatrix} 4.1062 \times 10^{-9} & 0 \end{bmatrix},$$

with the following H_∞ norms $\|G_1\|_\infty \cong 13.9202$ and $\|G_2\|_\infty \cong 1.3247$. Therefore the vector of the norms of the modes of the (A_o, B_o, C_o) representation is

$$h_o = \{13.9202, \quad 13.9202, \quad 1.3247, \quad 1.3247\}$$

and the vector of H_∞ norms of the full system (A, B, C) is

$h = \{\infty, \quad \infty, \quad 13.9202, \quad 13.9202, \quad 1.3247, \quad 1.3247\}$.

By deleting the last two states in the state-space representation, related to the smallest norms, one obtains the reduced-order model as follows:

$$A_r = \begin{bmatrix} 0 & 0 & 0 & 0 \\ 0 & 0 & 0 & 0 \\ 0 & 0 & -0.0264 & -1.3260 \\ 0 & 0 & 1.3260 & -0.0264 \end{bmatrix}, \qquad B_r = \begin{bmatrix} 6.0883 \times 10^7 \\ 35.8240 \\ -0.3556 \\ -1.1608 \end{bmatrix},$$

$$C_r = \begin{bmatrix} 4.1062 \times 10^{-9} & 0 & -0.161 & -0.5840 \end{bmatrix}.$$

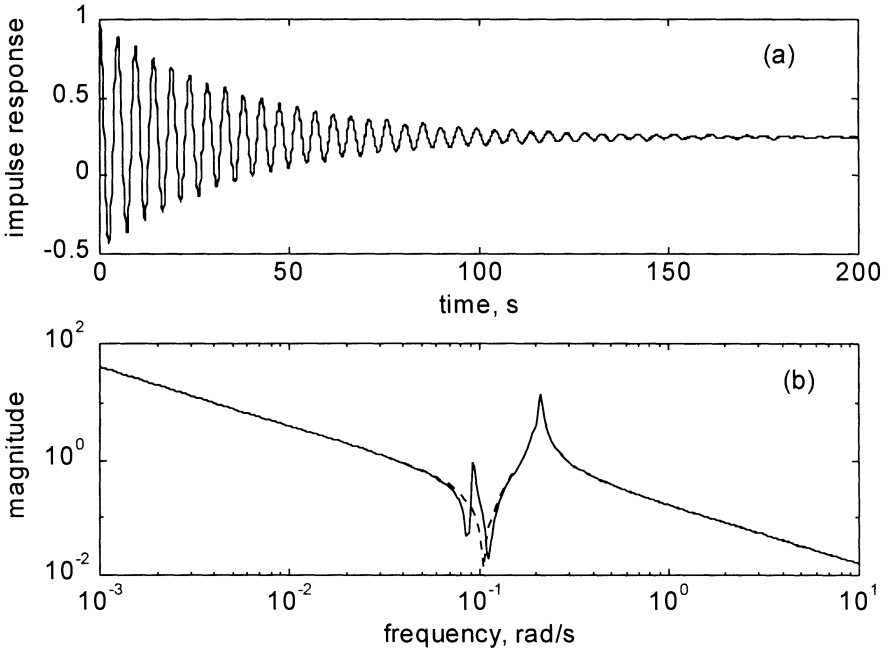

Figure 5.3. (a) Impulse responses and (b) magnitudes of the transfer function of the full (solid line) and reduced (dashed line) models of a simple structure with poles at zero.

The plots of the impulse response and the magnitude of the transfer function of the full and reduced models are shown in Fig. 5.3(a,b). The plots show that the error of the reduction is small. In fact, for the impulse response, the error was less than 1%, namely,

$$\varepsilon = \frac{\|y - y_r\|_2}{\|y\|_2} = 0.0021 .$$

In the above y denotes the impulse response of the full model, and y_r denotes the impulse response of the reduced model.

Example 5.4. Consider the Deep Space Network antenna azimuth model that has a pole at zero. The identified state-space representation of the open-loop model has n = 36 states, including states with a pole at zero. This model is reduced in modal coordinates, by determining the Hankel norms (or Hankel singular values) for states with nonzero poles. The plot of the Hankel singular values is shown in Fig. 5.4. By deleting the states with Hankel singular values smaller than 0.003 one obtains the 18-state model. The reduced model preserves properties of the full model, as is shown by the magnitude and phase of the transfer function in Fig.5.5(a,b). The state-space representation of the reduced antenna model is given in Appendix B.2.

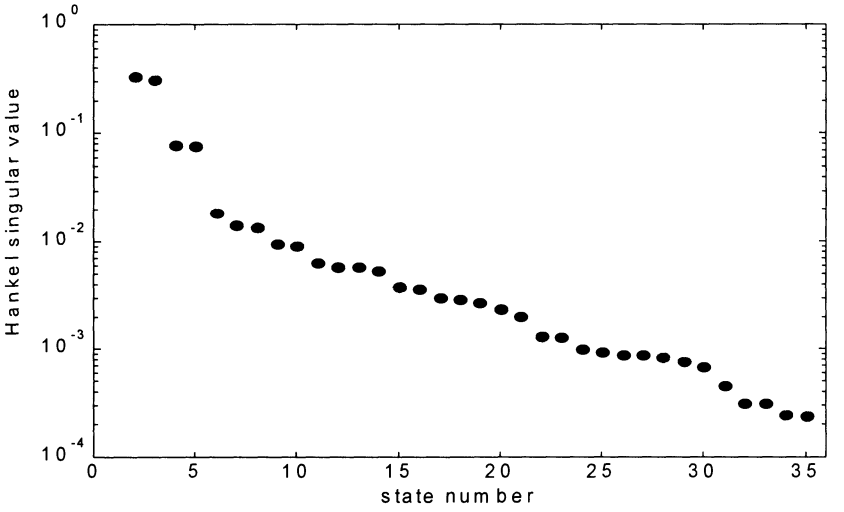

Figure 5.4. Hankel singular values of the DSS26 antenna rate-loop model.

5.4 Structures with Actuators and Sensors

A flexible structure in testing or in a closed-loop configuration is equipped with sensors and actuators. Does the presence of sensors and actuators impact the dynamics of a flexible structure, and consequently the process of model reduction? This question is answered for four important cases: sensors and

actuators in cascade connection with a structure, accelerometers as sensors, the proof-mass actuators, and centrifugal actuators attached to a structure.

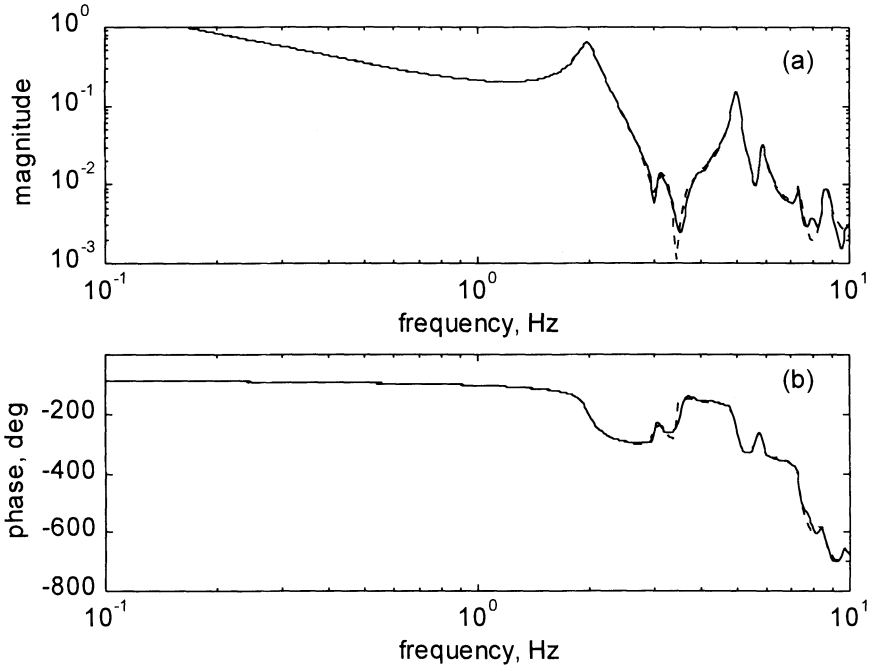

Figure 5.5. Transfer function: (a) magnitude (b) phase, of the full (solid line) and reduced-order (dashed line) models of the DSS26 antenna.

5.4.1 Actuators and Sensors in a Cascade Connection

Only actuator dynamics is considered. In particular, the reconstruction of the norms of modes and of a structure from the norms of the actuator-structure norms is discussed. The problem of sensors in a cascade connection with a structure is similar to the actuator case.

Properties of the actuators in series connection with structures are derivatives of the properties of a smooth filter in series connection with a structure, proven in Chapter 4. Let G_i and G_{si} be a transfer function of the ith mode with and without actuators, respectively. Additionally, let G and G_s be a transfer function of the structure with and without actuators, respectively. As a corollary of Property 4.2, the norms of modes and a structure for a smooth actuator transfer function are determined approximately as follows:

Property 5.1 ***H_2 Norms of a Mode and a Structure with an Actuator.***

(a) $$\|G_i\|_2 \cong \alpha_i \|G_{si}\|_2 , \tag{5.14a}$$

(b) $$\|G\|_2 \cong \sum_{i=1}^{n} \sqrt{\alpha_i^2 \|G_{si}\|_2^2} , \tag{5.14b}$$

where

$$\alpha_i = \|G_a(\omega_i)\|_2 , \tag{5.14c}$$

with ω_i being the ith resonance frequency, and G_a the transfer function of the actuator.

Similarly, based on Property 4.8, we have the following property of the H_∞ and Hankel norms of a mode and a structure with a smooth actuator.

Property 5.2 ***H_∞ Norms of a Mode and a Structure with an Actuator.***

(a) $$\|G_i\|_\infty \cong \alpha_i \|G_{si}\|_\infty , \tag{5.15a}$$

(b) $$\|G\|_\infty \cong \max_i (\alpha_i \|G_{si}\|_\infty). \tag{5.15b}$$

Property 5.3 ***Hankel Norms of a Mode and a Structure with an Actuator.***

(a) $$\|G_i\|_h \cong \alpha_i \|G_{si}\|_h , \tag{5.16a}$$

(b) $$\|G\|_h \cong \max_i (\alpha_i \|G_{si}\|_h). \tag{5.16b}$$

Example 5.5. Consider the 3D truss from Fig. 1.4, with the longitudinal (*x*-direction) input at node 21 and the longitudinal rate output at node 14. The actuator located at node 21 has the following smooth transfer function:

$$G_a(s) = \frac{0.1}{(1+0.01s)^2} .$$

The truss modal damping is identical for each mode, 0.5% ($\zeta_i = 0.005$), $i = 1,\ldots,72$. The H_∞ norms of the modes of the structure, with the actuator obtained from the definition (4.2), are marked by circles in Fig. 5.6. The

approximate H_∞ norms of the modes of the structure with the actuator were obtained from Property 5.2 (using Matlab function *norm_inf.m* from Appendix A.4), and plotted as dots in the same figure. The exact and approximate norms overlap each other in this figure, showing that the approximation error is negligible.

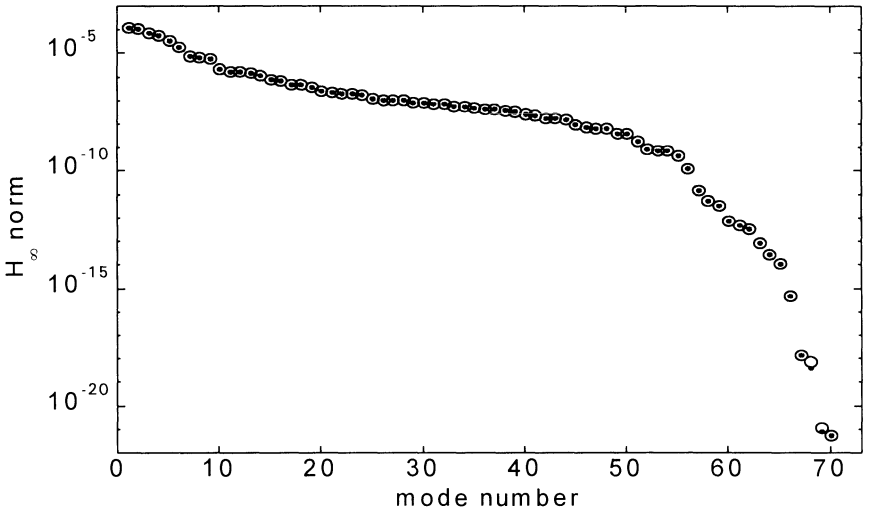

Figure 5.6. The H_∞ norms of the modes of the 3D truss with an actuator: exact (○), and approximate (•) values.

5.4.2 Accelerometers as Sensors

Accelerometers are frequently used as structural sensors due to their simplicity, and because they do not require a reference frame. However, they amplify high frequency parasitic noise. From the standpoint of analysis they introduce an additional difficulty – the feed-through term, D, in the state output equation. The output for the accelerometer sensors is in the form of $y = Cx + Du$, rather than $y = Cx$, as in (2.1). The difficulty with this equation follows from the fact that the grammians do not depend on matrix D. Thus the grammian-based model reduction does not reflect the presence of the accelerometers. However, this problem can be solved by using the series connection of a structure and sensors, and Properties 5.1-5.3.

A structure with the accelerometers can be considered as a structure with rate sensors cascaded with differentiating devices (the derivative of a rate gives acceleration). Thus, the norms of a structure equipped with accelerometers can be determined as the scaled norms of a structure with rate sensors. For simplicity of notation consider a structure with a single accelerometer. Denote

(A_r, B_r, C_r) and $G_r = C_r(sI - A_r)^{-1}B_r$ as the state space triple and as transfer function, respectively, of the structure with a rate sensor. The transfer function G_a of the structure with an accelerometer is therefore

$$G_a = j\omega G_r . \tag{5.17}$$

According to (5.14c) the scaling factor is $\alpha_i = \|j\omega_i\| = \omega_i$, thus from (5.14)–(5.16) the following property holds:

Property 5.4 ***Norms of Modes with Accelerometers.*** *The norms of modes with the accelerometers are related to the modes with the rate output as follows:*

$$\|G_{ai}\| \cong \omega_i \|G_{ri}\|, \qquad i = 1, \ldots, n \tag{5.18}$$

where ω_i is the ith natural frequency, and $\|.\|$ denotes either H_2, H_∞, or Hankel norms.

The above equations show that the norm of the *i*th mode with an accelerometer sensor is obtained as a product of the norm of the *i*th mode with a rate sensor and the *i*th natural frequency.

Example 5.6. The truss from the previous example is considered. The longitudinal input force is applied to node 21 and the longitudinal acceleration is measured at node 14. The H_∞ norms of the modes for the structure with the accelerometer are marked by circles in Fig. 5.7. The approximate H_∞ norms of the modes of the structure with the accelerometers were obtained from (5.18b), and plotted as dots in Fig. 5.7. The exact and approximate norms overlap each other in this figure, showing that the approximation error is negligible.

5.4.3 Proof-Mass Actuators

Proof-mass actuators are widely used in structural dynamics testing. In many cases, however, the actuator dynamics are not included in the model. Here, the relationship between the norms of a structure with a proof-mass actuator and the norms of the structure alone (i.e., with an ideal actuator) is studied, and the influence of the proof-mass actuator on model dynamics and reduction is analyzed.

The proof-mass actuator consists of mass *m*, and a spring with stiffness *k*, and they are attached to a structure at node, say, *na*. It is a reaction-type force

actuator, see [116], and [44]. It generates a force by reacting against the mass m, thus force f acts on the structure, and $-f$ acts on the mass m (Fig. 5.8(a)). It is assumed that the stiffness of the proof-mass actuator is much smaller than the dynamic stiffness of the structure (often it is zero).

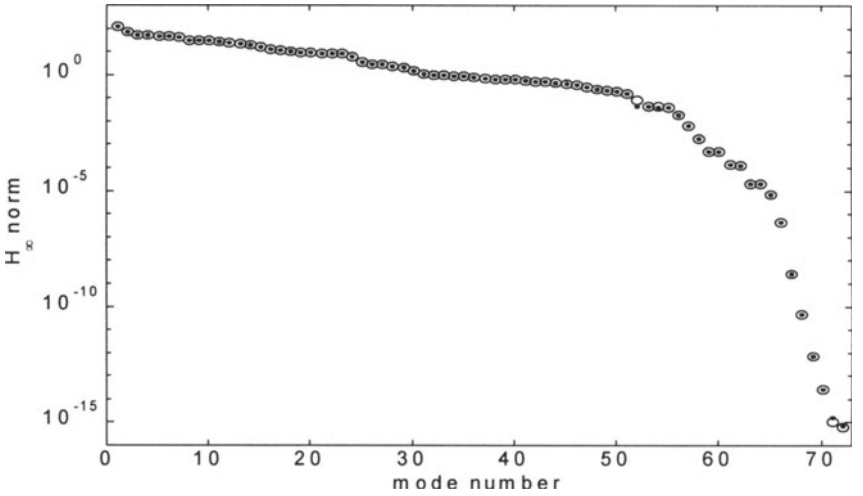

Figure 5.7. The H_∞ norms of the modes of the 3D truss with an accelerometer: exact (○), and approximate (•) values.

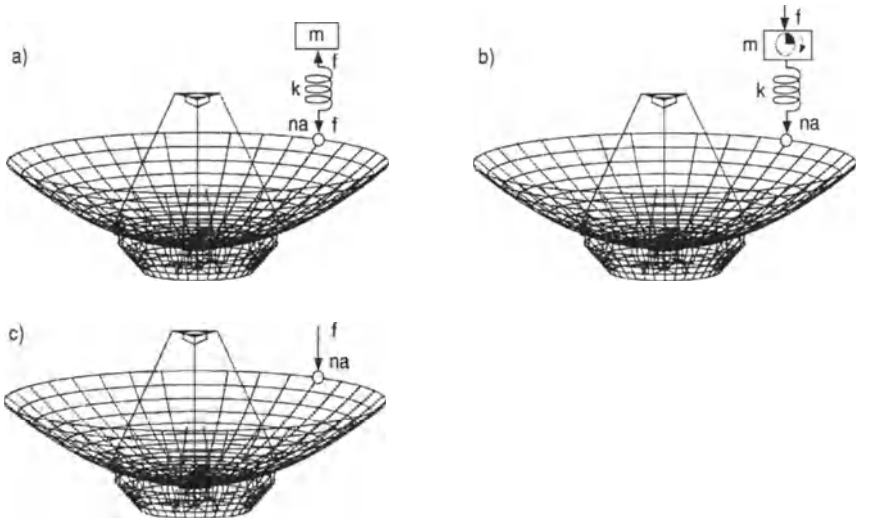

Figure 5.8. A structure with: (a) proof-mass actuator; (b) centrifugal actuator; and (c) ideal actuator.

Let us consider a structure with proof-mass actuator, shown in Fig. 5.8(a). Let M_s, D_s, and K_s, be the mass, damping, and stiffness matrices of the structure, respectively, and let B_s be the matrix of the actuator location,

$$B_s = \begin{bmatrix} 0 & 0 & \dots & 0 & 1 & 0 & \dots & 0 \end{bmatrix}^T \tag{5.19}$$

with a nonzero term at the actuator location *na*. Denote $G_s(\omega) = -\omega^2 M_s + j\omega D_s + K_s$ and $j = \sqrt{-1}$, then the dynamic stiffness of a structure at the actuator location is defined as

$$k_s = \frac{1}{B_s^T G_s^{-1} B_s}. \tag{5.20}$$

The dynamic stiffness is the inverse of the frequency response function at the actuator location. At zero frequency, it is reduced to the stiffness constant at the actuator location. Denote by q_a, m, k, d, the displacement, mass, stiffness, and damping of the actuator.

The structural dynamics of an "ideal" actuator is excited by the force f, as in Fig. 5.8(c). In contrast, the force generated by the proof-mass actuator consists of an additional force f_a, which is a reaction force from the actuator mount, see Fig. 5.9. Thus the total force f_o acting on the structure is

$$f_o = f + f_a. \tag{5.21}$$

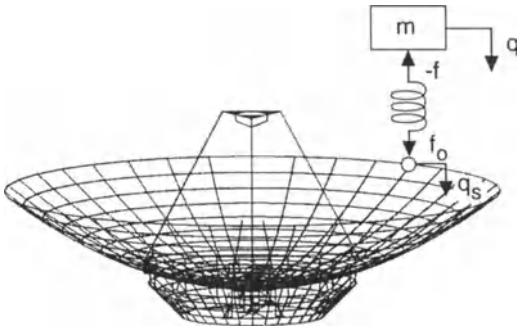

Figure 5.9. Displacements and forces at the proof-mass actuator mounting.

From Fig. 5.9 one finds

$$m\ddot{q} + k(q - q_s) = -f\,, \tag{5.22a}$$

$$f_a = k(q - q_s)\,, \tag{5.22b}$$

and the structural displacement q_s at node *na* is obtained from the dynamic stiffness of the structure

$$k_s q_s = f + f_a\,. \tag{5.23}$$

Combining the last three equations together, after a little algebra, one arrives at the following relationship:

$$f_a = \frac{\rho^2 - \beta}{1 + \beta - \rho^2} f\,, \tag{5.24a}$$

where

$$\rho = \frac{\omega_o}{\omega}, \qquad \omega_o = \sqrt{\frac{k}{m}}, \qquad \beta = \frac{k}{k_s}\,. \tag{5.24b}$$

Introducing (5.24a,b) into (5.21) one obtains the following relationship between the proof-mass actuator force (f_o) and the ideal actuator force (*f*)

$$f_o = \alpha_c f, \qquad \alpha_c = \frac{1}{1 + \beta - \rho^2}\,. \tag{5.25}$$

It follows from the above equation that the actuator force, f_o, approximately reproduces the ideal force *f* if $\alpha_c \cong 1$. This is obtained if

$$\beta << 1 \qquad \text{and} \qquad \rho << 1\,. \tag{5.26}$$

The above conditions are satisfied when the actuator stiffness is small (compared with the structural stiffness), and the actuator mass is large enough, such that the actuator natural frequency is smaller than the structural principal frequency. Hence, the above conditions can be replaced with the following ones:

$$k << k_s \qquad \text{and} \qquad \omega >> \omega_o\,. \tag{5.27}$$

If these conditions are satisfied, one obtains $f \cong f_o$, and consequently the transfer function of the system with the proof-mass actuator is approximately equal to the transfer function of the system without the proof-mass actuator. Based on these considerations the following norm properties are derived:

Property 5.5 ***Norms of a Mode with Proof-Mass Actuators.*** *Norms of the ith structural mode with a proof-mass actuator* (G_{ci}) *and of the ith structural mode alone* (G_{si}), *are related as follows:*

$$\|G_{si}\| = \frac{\|G_{ci}\|}{\alpha_{ci}}, \qquad i = 1,...,n, \tag{5.28}$$

where $\|.\|$ *denotes either* H_2, H_∞ *or Hankel norms,*

$$\alpha_{ci} = \frac{1}{1+\beta_i - \rho_i^2} \tag{5.29a}$$

and

$$\rho_i = \frac{\omega_o}{\omega_i}, \qquad \beta_i = \frac{k}{k_{si}}, \tag{5.29b}$$

while

$$k_{si} = k_s(\omega_i) = \frac{1}{B_s^T G_s^{-1}(\omega_i) B_s}. \tag{5.29c}$$

The variable k_{si} is the *i*th modal stiffness of the structure.

Proof. The force f_o acting on the structure is related to the actuator force f as in (5.25). Hence replacing f_o with f in the structural model gives (5.28). ❑

In addition to conditions (5.27), consider the following ones:

$$\omega_o << \omega_1 \qquad \text{and} \qquad k << \min_i k_{si}, \tag{5.30}$$

where ω_1 is the fundamental (lowest) frequency of the structure. These conditions say that the actuator natural frequency should be significantly lower than the fundamental frequency of the structure, and that the actuator stiffness

should be much smaller than the dynamic stiffness of the structure at any frequency of interest. If the aforementioned conditions are satisfied, one obtains $\alpha_{ci} \cong 1$ for $i = 1,\ldots,n$, thus the norms of the structure with the proof-mass actuator are equal to the norms of the structure without the proof-mass actuator. Also, the controllability and observability properties of the system are preserved. In particular, the presence of the proof-mass actuator will not affect the model order reduction. Note also that for many cases, whenever the first condition of (5.27) is satisfied, the second condition (5.30) is satisfied too.

Example 5.7. Consider the 3D truss, Fig. 1.4, with force input at node 21, acting in the *y*-direction, and with the rate output measured at node 14 in the *y*-direction. The magnitude of its transfer function is shown in Fig. 5.10(a), as a solid line. The Hankel singular values of the truss are shown as dots in Fig. 5.10(b) (and the modal H_∞ norm is twice the Hankel singular value). The proof-mass actuator was attached to node 21 to generate the input force. The mass of the proof-mass actuator is $m = 0.1\text{Ns}^2/\text{cm}$, and its stiffness is $k = 1\text{N/cm}$. Its natural frequency is $\omega_o = 3.1623\text{rad/s}$, much lower than the truss fundamental frequency, $\omega_1 = 32.8213\text{rad/s}$. The plot of the magnitude of the transfer function for the truss with the proof-mass actuator is shown in Fig. 5.10(a) as a dashed line. The figure shows perfect overlapping of the transfer functions for $f >> f_o$, where $f_o = \omega_o/2\pi = 0.5033\text{Hz}$. Hankel singular values of the truss with the proof-mass actuator are plotted by circles in Fig. 5.10(b). Observe that the Hankel singular values are the same for the truss without and with the proof-mass actuator, except for the first Hankel singular value, related to the proof-mass actuator itself.

5.4.4 Centrifugal Actuators

In the centrifugal actuator, force is proportional to the square of the excitation frequency. It consists of mass *m* and a spring with stiffness *k*, and they are attached to a structure at node, say, *na*. The force acts on mass *m* exclusively (Fig. 5.8(b)). It is assumed that the stiffness of the actuator is much smaller than the dynamic stiffness of the structure (often it is zero).

This configuration is shown in Fig. 5.8(b). The force acting on mass *m* is proportional to the squared frequency

$$f = \kappa\omega^2 \ , \tag{5.31}$$

where κ is a constant. The relationship between transfer functions of a structure without and without a centrifugal actuator is as follows:

$$H_c = \alpha_c H_s, \qquad \alpha_c = \frac{\kappa\omega_o}{1+\beta-\rho^2}, \tag{5.32}$$

which can be derived from the actuator equations

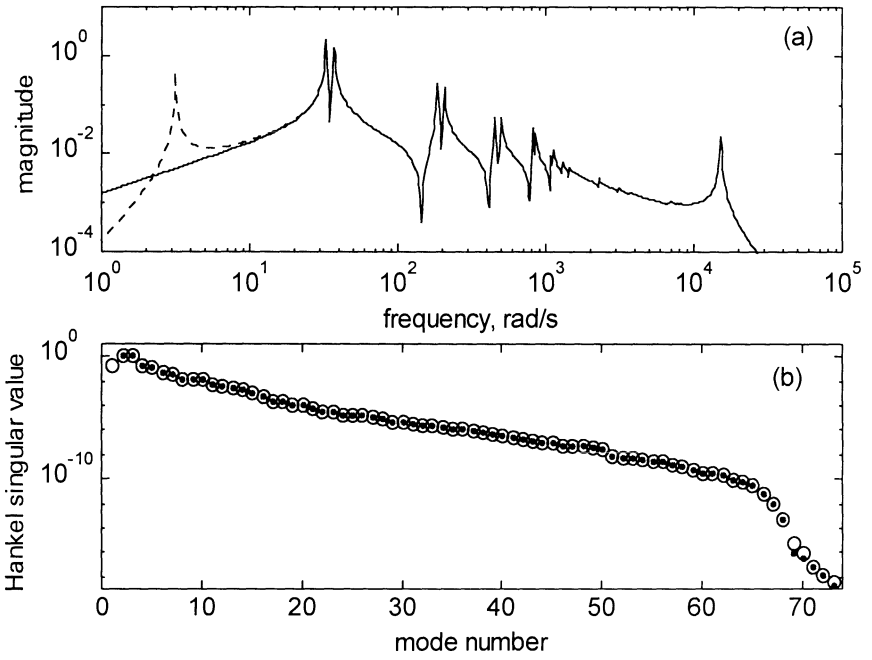

Figure 5.10. 3D truss: (a) magnitudes of the transfer function without (solid line) and with (dashed line) the proof-mass actuator; and (b) Hankel singular values without (o) and with (•) the proof-mass actuator.

$$m\ddot{q} + k(q - q_s) = \kappa\omega^2, \tag{5.33a}$$

$$f_o = f_a = k(q - q_s). \tag{5.33b}$$

For these equations one obtains

$$f_o = \alpha_c f, \qquad \alpha_c = \frac{\kappa\omega^2}{1+\beta-\rho^2}. \tag{5.34}$$

The above result shows that the structural transfer function with the centrifugal actuator is proportional to the structural transfer function without the actuator.

Property 5.6 ***Norms of Modes with Centrifugal Actuators.*** The norms of the ith structural mode (G_{si}), and of the ith structural mode with a centrifugal actuator (G_{ci}), are related as in (5.28), however the coefficient α_{ci} is now

$$\alpha_{ci} = \frac{\kappa\omega_o^2}{1+\beta_i-\rho_i^2} . \tag{5.35}$$

Proof. Similar to Property 5.5. ❑

With the conditions in (5.30) satisfied, one obtains $\alpha_{ci} = \kappa\omega_o^2$ for $i = 1,\ldots,n,$ thus the norms of the structure with the centrifugal actuator are proportional to the norms of the structure without the actuator. This scaling does not influence the results of model reduction, since the procedure is based on ratios of norms rather than their absolute values.

In applications measurement noise is unavoidable, thus care should be taken in the selection of the scaling factor. For instance, if the scaling factor is too small, modes with small norms cannot be detected, and the reduction procedure could be biased.

6
Assignment

The sensor and actuator locations of an open-loop system influence the controllability and observability properties of a system. Therefore one can modify the sensor and/or actuator locations to obtain the required (or assigned) values of the controllability and observability grammians. In particular, one can find the locations such that all Hankel singular values are identical. This is a case of a uniform controllability and observability assignment.

6.1 Problem Statement

For control system purposes, it is advantageous to have a tool to modify or shape the system controllability and observability properties. This can be done in two ways: by modifying the system properties, such as introducing a feedback loop, see [106]; or by determining proper sensor and/or actuator configurations, see [37] and [39]. The configuration includes the actuator and sensor locations, as well as the gains at each location. The latter method, called the grammian assignment, is addressed in this chapter.

Let the system be described by a stable system matrix A, and the location of the actuators and/or sensors is not yet known (thus B and/or C matrices are not yet known). The following problem is considered. For a positive definite matrix W, find the input (B) and output (C) matrices such that both grammians of the system are equal to W. It can be solved by finding B, C and a nonsingular transformation R, such that the grammians of the representation (A_1, B, C) are

W. K. Gawronski, *Dynamics and Control of Structures*

equal to W, and $A_1 = R^{-1}AR$. Depending on what is to be determined (sensors, actuators, or both), the question is divided into three separate problems.

Problem 6.1. Given A, B, find C and the transformation R, such that $W_{c1} = W_{o1} = W$ for the representation (A_1, B_1, C), where $A_1 = R^{-1}AR$ and $B_1 = R^{-1}B$.

Problem 6.2. Given A, C, find B and the transformation R, such that $W_{c1} = W_{o1} = W$ for the representation (A_1, B, C_1), where $A_1 = R^{-1}AR$ and $C_1 = CR$.

Problem 6.3. Given A, find B, C, and the transformation R, such that $W_{c1} = W_{o1} = W$ for the representation (A_1, B, C), where $A_1 = R^{-1}AR$.

Note that the matrices B and C include not only the actuator and sensor locations, but also the gain at each location (for the location-only problem the entries of B and C would be either 1 or 0).

The solution of the problems may or may not exist, since not every positive definite grammian can be obtained through the sensor or actuator placement. A matrix W, for which the solution exists, is an assignable one. Define

$$N_c = -AW - WA^T, \quad N_o = -A^T W - WA. \tag{6.1}$$

A symmetric positive semidefinite matrix W is assignable if N_c and N_o are positive semidefinite.

6.2 Algorithms

Assuming an assignable matrix W, the following algorithms solve Problems 6.1, 6.2, and 6.3, respectively.

Algorithm 6.1. *For given A, B, and assignable matrix W:*

1. *Determine W_c from the Lyapunov equations (3.5).*
2. *Find P_c and P from the decomposition of W_c and W:*

$$W_c = P_c P_c^T, \qquad W = PP^T. \tag{6.2}$$

3. *Find* A_1 *and* B_1 *from the following:*

$$A_1 = R^{-1}AR, \qquad B_1 = R^{-1}B, \tag{6.3a}$$

where

$$R = P_c P^{-1}. \tag{6.3b}$$

4. *Define*

$$N_o = -A_1^T W - WA_1, \tag{6.4}$$

and determine C from the decomposition of N_o:

$$N_o = C^T C \tag{6.5}$$

(note that N_o *is positive semidefinite if W is assignable).*

Proof. Note from step 4 that $A_1^T W + WA_1 + C^T C = 0$, i.e., W is the assigned observability grammian. For A_1 and B_1 from step 3 one obtains $A_1 W + WA_1^T + B_1 B_1^T = 0$, hence W is the assigned controllability grammian. ❑

A similar algorithm is obtained for determination of the actuator locations.

Algorithm 6.2. *For given A, C, and matrix W which is assignable and positive definite:*

1. *Determine* W_o *from the Lyapunov equation (3.5).*
2. *Find* P_o *and P such that*

$$W_o = P_o^T P_o, \qquad W = P^T P. \tag{6.6}$$

3. *Find* A_1 *and* C_1 *from the following:*

$$A_1 = R^{-1}AR, \qquad C_1 = CR, \tag{6.7a}$$

where

$$R = P_o^{-1} P. \tag{6.7b}$$

4. *Define*

$$N_c = -A_1 W - W A_1^T, \tag{6.8}$$

and determine B from the decomposition of N_c*:*

$$N_c = BB^T \tag{6.9}$$

(note that N_c *is positive semidefinite if W is assignable).*

Problem 6.3 is solved using the following algorithm:

Algorithm 6.3. *For W assignable and positive definite, the matrices B and C obtained from the decomposition of* N_c *and* N_o*:*

$$N_c = BB^T, \qquad N_o = C^T C, \tag{6.10}$$

are the solutions of Problem 6.3.

The essential difficulty is to make the grammians assignable. The assignability depends on the system representation. For flexible structures the approximate assignability is guaranteed for the system in the modal coordinates. Indeed, assume a diagonal grammian W. The controllability grammian W_c is diagonally dominant, therefore the transformation matrix R is diagonally dominant as well. For a block-diagonal matrix A in modal coordinates, as in (2.29), one obtains A_1 diagonally dominant from (6.3a), hence N_c and N_o are positive definite, since the off-diagonal entries of R are small.

Example 6.1. Consider the system in Fig. 1.2 with the masses $m_1 = m_2 = m_3 = 1$, stiffnesses $k_1 = k_2 = k_3 = k_4 = 50$, and the damping matrix D proportional to the stiffness matrix K, i.e., $D = 0.001K$. A single input force is applied at mass 3.

The grammian W = diag(10, 10, 7, 7, 1, 1) is assigned by determining the matrix C of sensor locations.

Using Algorithm 6.1, one obtains the triple (A_1, B_1, C)

$$A_1 = \begin{bmatrix} -0.00132 & 11.45430 & 0 & 0 & 0 & 0 \\ -11.42815 & -0.12958 & 0 & 0 & 0 & 0 \\ 0.00007 & -0.00071 & 0 & 9.99962 & 0 & 0 \\ 0.01922 & -0.19048 & -10.00038 & -0.10000 & 0 & 0 \\ 0.00182 & -0.01806 & -0.00007 & -0.01896 & -0.00629 & 4.37914 \\ -0.00260 & 0.02577 & 0.00010 & 0.0271 & -4.36118 & -0.01281 \end{bmatrix},$$

$$B_1^T = \begin{bmatrix} 0.16245 & -1.60986 & -0.00444 & -1.18321 & -0.11214 & 0.16006 \end{bmatrix},$$

$$C = \begin{bmatrix} 0.15749 & -1.56066 & -0.00379 & -1.01023 & -0.01383 & 0.01974 \\ -0.03985 & 0.39494 & -0.00231 & -0.61596 & -0.00896 & 0.01280 \\ 0.00001 & -0.00013 & 0.00002 & 0.00482 & -0.11092 & 0.15833 \\ 0.00000 & 0.00000 & 0.00000 & 0.00000 & 0.00000 & 0.00000 \\ 0.00000 & 0.00000 & 0.00000 & 0.00000 & 0.00000 & 0.00000 \\ 0.00000 & 0.00000 & 0.00000 & 0.00000 & 0.00000 & 0.00000 \end{bmatrix}.$$

For this representation the following grammians are obtained: $W_c = W_o$ = diag(10.00000, 10.00000, 7.00000, 7.00000, 1.00000, 1.00000); i.e., it is assigned.

Example 6.2. Consider the 2D truss in Fig. 1.3 with a proportional damping matrix $D = M + 10^{-5} K$. The input forces are applied at nodes 4 and 10, in a vertical direction. The last two modes (of highest frequency) are assigned with the Hankel singular values = 1, the remaining modes with the Hankel singular values = 10^{-8} (small nonzero values to avoid singularities in the algorithm). The output matrix C is of the form $C = \begin{bmatrix} C_o & 0_{2\times 28} \end{bmatrix}$, where

$$C_o = \begin{bmatrix} 16.8383 & -3.9675 & -2.9772 & 15.3972 \\ -1.1908 & 0.2806 & -1.2241 & 1.1379 \end{bmatrix}$$

and it assigns the above values, and was determined using Algorithm 6.1. The Hankel singular values of the assigned system are {1.00000 1.00000} and the remaining are zero. The magnitude of the transfer function of the assigned

system is plotted in Fig. 6.1. It shows that the system is indeed assigned with two Hankel singular values equal to 1, and the remaining Hankel singular values equal to zero, since it has only two resonance peaks. They are of magnitude 2 – which corresponds to two Hankel singular values of magnitude 1.

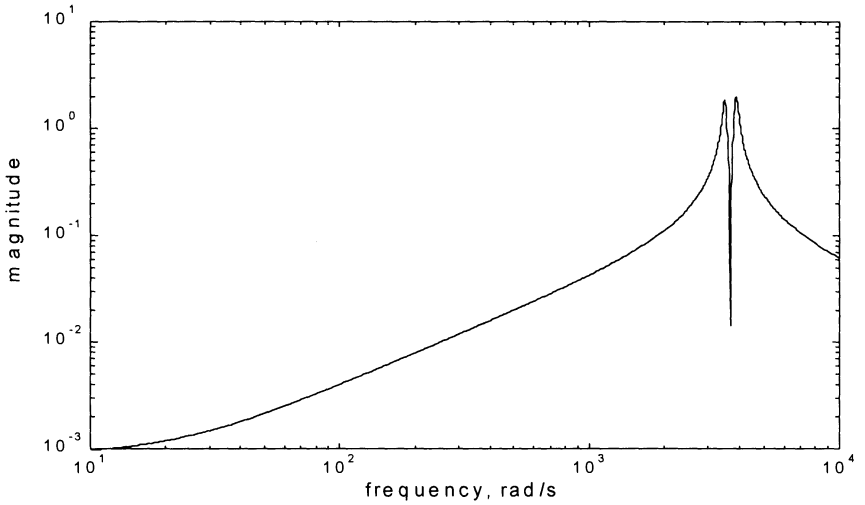

Figure 6.1. Magnitude of the transfer function of the assigned 2D truss.

6.3 Uniformly Balanced Systems

A system with all its states equally controllable and observable is a uniformly balanced system. All its Hankel singular values are equal, so that the grammians are in the form $W_c = W_o = \gamma I_N$, where γ is a positive scalar. For a stable A in modal coordinates the uniformly balanced system is always assignable. Indeed, in this case, $BB^T = C^T C = -\gamma(A + A^T)$ and $-A - A^T$ is positive definite, hence one can find B and C by decomposition of $-\gamma(A + A^T)$. The uniformly balanced system is determined as follows:

Algorithm 6.4. *Given A, B, the grammian $W = \gamma I_n$ is assigned with*

$$C = \gamma B^T W_c^{-1}, \tag{6.11}$$

where W_c is the controllability grammian of (A, B).

Algorithm 6.5. *Given A, C, the grammian* $W = \gamma I_n$ *is assigned with*

$$B = \gamma W_o^{-1} C^T, \tag{6.12}$$

where W_o *is the observability grammian of (A, C).*

Properties of the uniformly balanced systems are obtained from the following auxiliary attributes. Let $G(\omega) = C(j\omega I_n - A)^{-1} B$ be a transfer function of the triplet (A, B, C), with s inputs and r outputs. Let $j\omega$ be not a pole of an element of $G(j\omega)$. For $s \le r$ let the $s \times r$ matrix $U_1(\omega)$ have s orthonormal rows, i.e., $U_1(\omega)U_1^*(\omega) = I_s$, and for $s \ge r$ let the $s \times r$ matrix $U_2(\omega)$ have r orthonormal columns; i.e., $U_2(\omega)U_2^*(\omega) = I_r$.

Property 6.1 ***System Stability.*** *If* $rank(U_1(\omega)) = rank(G(\omega)) = s$ *for all real* ω, *and G satisfies the equation*

$$GU_1 + U_1^* G^* = \frac{GG^*}{\gamma}, \tag{6.13}$$

or if $rank(U_2(\omega)) = rank(G(\omega)) = r$ *and G satisfies the equation*

$$U_2 G + G^* U_2^* = \frac{G^* G}{\gamma}, \tag{6.14}$$

then the system is stable.

Proof. Introduce $G_1 = GU_1$ and $G_2 = U_2 G$. It follows from (6.13) that G_1 is positive real, and from (6.14) that G_2 is positive real, hence both are stable. But (A, BU_1, C) is the state-space representation of G_1, and $(A, B, U_2 C)$ is the state-space representation of G_2. The representations G, G_1, and G_2 include a stable matrix A, hence G, G_1, and G_2 are stable. ❑

Denote $\|.\|_u$ as a unitarily invariant norm, e.g., an H_∞ or H_2 norm. Now we can claim that the following property is valid:

Property 6.2 ***Uniformly Balanced Systems.*** *Transfer function* $G(\omega) = C(j\omega I_n - A)^{-1}B$ *of a uniformly balanced system (A,B,C) has the following properties:*

(a) *G is stable;*

(b) $\|G\|_u \le 2\gamma$; (6.15)

(c) *for a square system (the number of inputs is equal to the number of outputs, r) G is positive real; and*

(d) *a square system*

$$G_o = \frac{G}{\gamma} - I_r \qquad or \qquad (A, B, \frac{C}{\gamma}, -I_r) \tag{6.16}$$

is all-pass.

Proof.

(a) Note that G satisfies (6.13) and (6.14), hence it is stable.

(b) Note that from the left-hand side of (6.13) it follows that $\left\|GU + U^*G^*\right\|_u \le 2\|GU\|_u = 2\|G\|_u$. From the right-hand side of (6.13) one obtains $\left\|GG^*\right\|_u / \gamma = \|G\|_u^2 / \gamma$, thus $\|G\|_u^2 / \gamma \le 2\|G\|_u$, or $\|G\|_u \le 2\gamma$.

(c) The positive realness of the square uniformly balanced system follows from (6.13) and from the definition of positive-realness of a transfer function, see [2].

(d) The all-pass system G_o satisfies the following condition, $G_o G_o^* = I_r$, see [81, p. 260]. Note that

$$G_o G_o^* = \frac{GG^*}{\gamma^2} - \frac{G^*}{\gamma} - \frac{G}{\gamma} + I_r . \tag{6.17}$$

For a square system, (6.14) simplifies to the following one $G + G^* = G^*G/\gamma$. Introducing this into (6.17), one obtains $G_o G_o^* = I_r$, i.e., G_o is all-pass. ❑

The plot of the transfer function for a single-input–single-output uniformly balanced system is a circle of radius γ and center (γ, 0), and transfer function G_0 is a circle of radius γ, and center (0, 0).

The uniformly balanced representation is useful in the system identification, since in this representation the locations of sensors and/or actuators are such that all the states (modes) are equally excited and observed, hence they are equally "treated" when tested.

Example 6.3. The uniformly balanced representation with $\gamma = 1$ is determined for A and B as in Example 6.1. From Algorithm 6.5 we arrive at the following matrix C that uniformly balances the system

$$C = \begin{bmatrix} 0.0514 & -0.5091 & -0.0017 & -0.4472 & -0.1121 & 0.1601 \end{bmatrix}.$$

The plot of the magnitude of the system transfer function in Fig. 6.2 shows that Property 6.2(b) is satisfied.

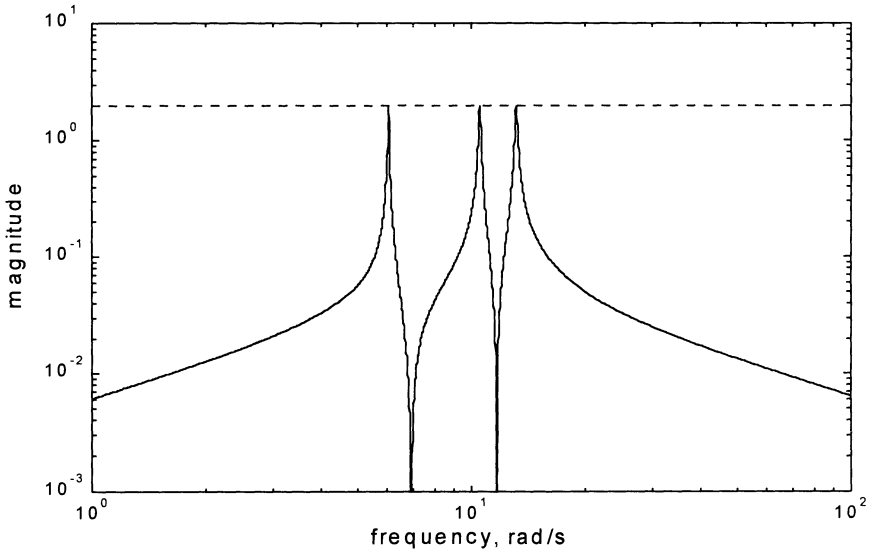

Figure 6.2. Magnitude of the transfer function of the uniformly balanced simple system.

Example 6.4. The 2D truss from Example 6.1 is uniformly balanced using Algorithm 6.4. All its Hankel singular values are equal to 1. The magnitude and phase of the transfer function of the uniformly balanced truss are shown in Fig. 6.3(a,b), solid line. The latter figures illustrates Property 6.2(b), where the magnitude of the transfer function does not exceed 2γ. The transfer function G_0 of the all-pass system created from the uniformly balanced truss using (6.16) is

presented in Fig. 6.3(a,b), dashed line. The figure illustrates the Property 6.2(d), showing the magnitude equal to 1. The Nyquist plots of uniformly balanced truss G (solid line) and the all-pass system G_o are shown in Fig. 6.4. Both circles are of radius 1, shifted by 1.

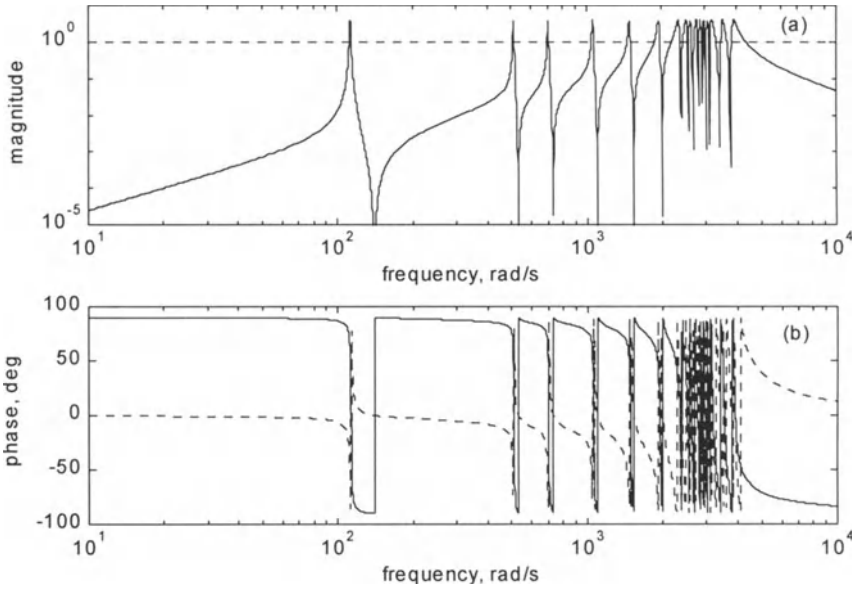

Figure 6.3. The transfer functions of the uniformly balanced (solid line) and all-pass (dashed line) trusses, (a) magnitude, and (b) phase.

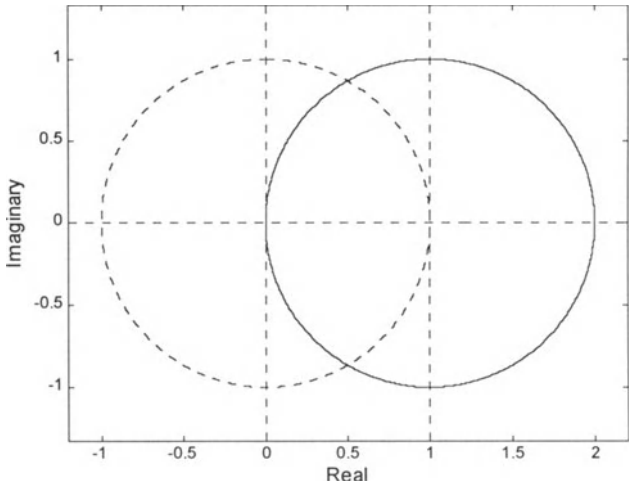

Figure 6.4. The Nyquist plots of the uniformly balanced (solid line) and all-pass (dashed line) trusses.

7
Actuator and Sensor Placement

A typical actuator and sensor location problem for structural testing can be described as follows. The structural test plan is based on the available information on the structure itself, on disturbances acting on the structure, and on the expected structural performance. The first information is typically in the form of a structural finite-element model. The disturbance information includes disturbance location and disturbance spectral contents. The structure performance is commonly evaluated through the displacements or accelerations at certain structural locations.

It is not possible in general to duplicate the dynamics of a real structure during testing. This happens not only due to physical restrictions or limited knowledge of disturbances, but also because the test actuators cannot be located at the disturbance locations and sensors cannot be placed at the performance evaluation locations. Thus, to obtain the performance of the test items close to the performance of a structure in a real environment one uses the available (or candidate) locations of actuators and sensors and formulates the selection criteria and selection mechanisms.

The control design problem of a structure can be defined in a similar manner. Namely, actuators are placed within the allowable locations, and they are not necessary collocated with the disturbance locations; sensors are placed at the sensor allowable locations, generally outside the locations of performance evaluation.

For simple test articles, an experienced test engineer can determine the appropriate sensor or actuator locations in an ad hoc manner. However, for the first-time testing of large and complex structures the placement of sensors and actuators is neither an obvious nor a simple task. In practice heuristic means are combined with engineering judgment and simplified analysis to determine

W. K. Gawronski, *Dynamics and Control of Structures*

actuator and sensor locations. In most cases the locations vary during tests (in a trial and error approach) to obtain acceptable data to identify target modes.

The actuator and sensor placement problem was investigated by many researchers, see, for example, [1], [7], [19], [34], [42], [66], [69], [70], [75], [76], [79], [80], [82], [83], and [100]. A typical solution to the location problem is found through a search procedure. For large numbers of locations the search for the number of possible combinations is overwhelming and only a small selected subset is searched. This is time consuming and not necessarily the optimal solution. The approach proposed here consists of the determination of the norm of each sensor (or actuator) for selected modes, and then grade them according to their participation in the system norm. This is a computational effective approach with a clear physical interpretation.

7.1 Problem Statement

Given a large set of sensors and actuators, the placement problem consists of determining the locations of a smaller subset of sensors or actuators such that the H_2 , H_∞, or Hankel norms of the subset is as close as possible to the norm of the original set. In this chapter the placement problem is solved in the modal coordinates using the previously derived structural properties. A comparatively simple methodology of choice of a small subset of sensors and/or actuators from a large set of possible locations is proposed.

Let $\mathcal{R}$ and $\mathcal{S}$ be the sets of the candidate sensor and actuator locations, respectively. These are chosen in advance as all allowable locations of actuators, of population S, and as all allowable locations of sensors, of population R. The placement of s actuators within the given $\mathcal{S}$ actuator candidate locations, and the placement of r sensors within the given $\mathcal{R}$ sensor candidate locations, is considered. Of course, the number of candidate locations is larger than the number of actuators or sensors, i.e., $R > r$ and $S > s$.

7.2 Additive Property of Modal Norms

The properties of modal norms that are used in the actuator and sensor placement procedures are discussed in this section.

7.2.1 The H_2 Norm

Consider a flexible structure in modal representation. The H_2 norm of the ith mode is given by (4.5), Chapter 4, i.e.,

$$\|G_i\|_2 \cong \frac{\|B_i\|_2 \|C_i\|_2}{2\sqrt{\zeta_i \omega_i}}, \tag{7.1}$$

where B_i and C_i are the input and output matrices of the ith mode. For S inputs and R outputs, these matrices are

$$B_i = \begin{bmatrix} B_{i1} & B_{i2} & \cdots & B_{iS} \end{bmatrix}, \qquad C_i = \begin{bmatrix} C_{1i} \\ C_{2i} \\ \vdots \\ C_{Ri} \end{bmatrix}, \tag{7.2}$$

and B_{ij} is the 2×1 block of the jth input, while C_{ji} is the 1×2 block of the jth output. From Properties 4.3 and 4.5 one obtains the following additive properties of the H_2 norm:

$$\|G_i\|_2^2 \cong \sum_{j=1}^{R} \|G_{ij}\|_2^2 \qquad \text{or} \qquad \|G_i\|_2^2 \cong \sum_{k=1}^{S} \|G_{ik}\|_2^2, \tag{7.3a}$$

where

$$\|G_{ij}\|_2 = \frac{\|B_{ij}\|_2 \|C_i\|_2}{2\sqrt{\zeta_i \omega_i}}, \qquad \|G_{ik}\|_2 = \frac{\|B_i\|_2 \|C_{ki}\|_2}{2\sqrt{\zeta_i \omega_i}}, \tag{7.3b}$$

are the H_2 norms of the ith mode with the jth actuator only, or the ith mode with the kth sensor only. Equation (7.3a) shows that the H_2 norm of a mode with a set of actuators (sensors) is the root-mean-square (rms) sum of the H_2 norms of this mode with a single actuator (sensor).

7.2.2 The H_∞ and Hankel Norms

A similar relationship can be obtained for the H_∞ norm. From (4.25) one obtains

$$\|G_i\|_\infty \cong \frac{\|B_i\|_2 \|C_i\|_2}{2\zeta_i \omega_i}, \tag{7.4}$$

and from Properties 4.9 and 4.10 the additive property of the H_∞ norm has the following form:

$$\|G_i\|_\infty^2 \cong \sum_{j=1}^{S} \|G_{ij}\|_\infty^2 \qquad \text{or} \qquad \|G_i\|_\infty^2 \cong \sum_{k=1}^{R} \|G_{ik}\|_\infty^2, \tag{7.5a}$$

where

$$\|G_{ij}\|_\infty = \frac{\|B_{ij}\|_2 \|C_i\|_2}{2\zeta_i \omega_i}, \qquad \|G_{ik}\|_\infty = \frac{\|B_i\|_2 \|C_{ki}\|_2}{2\zeta_i \omega_i}, \tag{7.5b}$$

are the H_∞ norms of the *i*th mode with the *j*th actuator only, or the *i*th mode with the *k*th sensor only. Equation (7.5a) shows that the H_∞ norm of a mode with a set of actuators (sensors) is the rms sum of the H_∞ norms of this mode with a single actuator (sensor).

Hankel norm properties are similar to the H_∞ norm properties.

7.3 Placement Indices and Matrices

Actuator and sensor placement are solved independently. Due to their similarity, in this section the actuator placement problem is considered only.

7.3.1 H_2 Placement Indices and Matrices

Denote by G the transfer function of the system with all S candidate actuators. The placement index σ_{2ki} that evaluates the *k*th actuator at the *i*th mode in terms of the H_2 norm is defined with respect to all the modes and all admissible actuators

$$\sigma_{2ki} = w_{ki} \frac{\|G_{ki}\|_2}{\|G\|_2}, \qquad k = 1, ..., S, \qquad i = 1, ..., n, \tag{7.6a}$$

where $w_{ki} \geq 0$ is the weight assigned to the *k*th actuator and the *i*th mode, and n is a number of modes. Matlab function *norm_2.m* given in Appendix A.3 determines modal H_2 norms. The weight reflects the importance of the mode and the actuator in applications, and reflects the dimensions of the inputs. In

applications it is convenient to represent the two-norm placement indices as a placement matrix

$$\Sigma_2 = \begin{bmatrix} \sigma_{211} & \sigma_{212} & \cdots & \sigma_{21k} & \cdots & \sigma_{21S} \\ \sigma_{221} & \sigma_{222} & \cdots & \sigma_{22k} & \cdots & \sigma_{22S} \\ \cdots & \cdots & \cdots & \cdots & \cdots & \cdots \\ \sigma_{2i1} & \sigma_{2i2} & \cdots & \sigma_{2ik} & \cdots & \sigma_{2iS} \\ \cdots & \cdots & \cdots & \cdots & \cdots & \cdots \\ \sigma_{2n1} & \sigma_{2n2} & \cdots & \sigma_{2nk} & \cdots & \sigma_{2nS} \end{bmatrix} \begin{matrix} \\ \\ \\ \Leftarrow \\ \\ \\ \\ \Uparrow \end{matrix} \begin{matrix} \\ \\ \\ i\text{th mode} \\ \\ \\ \\ k\text{th actuator} \end{matrix} \tag{7.7a}$$

where the kth column consists of indexes of the kth actuator for every mode, and the ith row is a set of the indexes of the ith mode for all actuators.

In the sensor placement procedure the placement index σ_{2ki} evaluates the kth sensor at the ith mode

$$\sigma_{2ki} = w_{ki} \frac{\|G_{ki}\|_2}{\|G\|_2}, \qquad k = 1, ..., R, \qquad i = 1, ..., n, \tag{7.6b}$$

where $w_{ki} \geq 0$ is the weight assigned to the kth sensor and the ith mode, and n is a number of modes. The sensor placement matrix is defined as follows

$$\Sigma_2 = \begin{bmatrix} \sigma_{211} & \sigma_{212} & \cdots & \sigma_{21k} & \cdots & \sigma_{21R} \\ \sigma_{221} & \sigma_{222} & \cdots & \sigma_{22k} & \cdots & \sigma_{22R} \\ \cdots & \cdots & \cdots & \cdots & \cdots & \cdots \\ \sigma_{2i1} & \sigma_{2i2} & \cdots & \sigma_{2ik} & \cdots & \sigma_{2iR} \\ \cdots & \cdots & \cdots & \cdots & \cdots & \cdots \\ \sigma_{2n1} & \sigma_{2n2} & \cdots & \sigma_{2nk} & \cdots & \sigma_{2nR} \end{bmatrix} \begin{matrix} \\ \\ \\ \Leftarrow \\ \\ \\ \\ \Uparrow \end{matrix} \begin{matrix} \\ \\ \\ i\text{th mode} \\ \\ \\ \\ k\text{th sensor} \end{matrix} \tag{7.7b}$$

where the kth column consists of indexes of the kth sensor for every mode, and the ith row is a set of the indexes of the ith mode for all sensors.

7.3.2 H_∞ and Hankel Placement Indices and Matrices

Similarly to the H_2 index, the placement index $\sigma_{\infty ki}$ evaluates the kth actuator at the ith mode in terms of the infinity-norm. It is defined in relation to all the modes and all admissible actuators

$$\sigma_{\infty ki} = w_{ki} \frac{\|G_{ki}\|_\infty}{\|G\|_\infty}, \qquad k = 1, ..., S, \qquad i = 1, ..., n, \tag{7.8a}$$

where $w_{ki} \geq 0$ is the weight assigned to the kth actuator and to the ith mode. The Matlab functions *norm_inf.m* and *norm_han.m* given in Appendix A.4 and A.5 determine the modal H_∞ and Hankel norms.

Using the above indices, one introduces the infinity-norm placement matrix, similar to the two-norm matrix introduced earlier

$$\Sigma_\infty = \begin{bmatrix} \sigma_{\infty 11} & \sigma_{\infty 12} & \cdots & \sigma_{\infty 1k} & \cdots & \sigma_{\infty 1S} \\ \sigma_{\infty 21} & \sigma_{\infty 22} & \cdots & \sigma_{\infty 2k} & \cdots & \sigma_{\infty 2S} \\ \cdots & \cdots & \cdots & \cdots & \cdots & \cdots \\ \sigma_{\infty i1} & \sigma_{\infty i2} & \cdots & \sigma_{\infty ik} & \cdots & \sigma_{\infty iS} \\ \cdots & \cdots & \cdots & \cdots & \cdots & \cdots \\ \sigma_{\infty n1} & \sigma_{\infty n2} & \cdots & \sigma_{\infty nk} & \cdots & \sigma_{\infty nS} \end{bmatrix} \begin{matrix} \\ \\ \\ \Leftarrow \\ \\ \\ \Uparrow \end{matrix} \begin{matrix} \\ \\ \\ i\text{th mode} \\ \\ \\ k\text{th actuator} \end{matrix} \tag{7.9a}$$

The Hankel placement index and matrix is one-half of the H_∞ placement index and Σ_∞ matrix, respectively.

In the sensor placement procedure the placement index $\sigma_{\infty ki}$ evaluates the kth sensor at the ith mode in terms of the infinity-norm

$$\sigma_{\infty ki} = w_{ki} \frac{\|G_{ki}\|_\infty}{\|G\|_\infty}, \qquad k = 1, ..., R, \qquad i = 1, ..., n, \tag{7.8b}$$

where $w_{ki} \geq 0$ is the weight assigned to the kth sensor and to the ith mode.

The infinity-norm placement matrix is similar to the two-norm matrix, i.e.,

$$\Sigma_\infty = \begin{bmatrix} \sigma_{\infty 11} & \sigma_{\infty 12} & \cdots & \sigma_{\infty 1k} & \cdots & \sigma_{\infty 1R} \\ \sigma_{\infty 21} & \sigma_{\infty 22} & \cdots & \sigma_{\infty 2k} & \cdots & \sigma_{\infty 2R} \\ \cdots & \cdots & \cdots & \cdots & \cdots & \cdots \\ \sigma_{\infty i1} & \sigma_{\infty i2} & \cdots & \sigma_{\infty ik} & \cdots & \sigma_{\infty iR} \\ \cdots & \cdots & \cdots & \cdots & \cdots & \cdots \\ \sigma_{\infty n1} & \sigma_{\infty n2} & \cdots & \sigma_{\infty nk} & \cdots & \sigma_{\infty nR} \end{bmatrix} \begin{matrix} \\ \\ \\ \Leftarrow \\ \\ \\ \end{matrix} \begin{matrix} \\ \\ \\ i\text{th mode} \\ \\ \\ \end{matrix} \qquad (7.9b)$$

$$\Uparrow$$

kth sensor

The Hankel placement index and matrix is one-half of the H_∞ placement index and Σ_∞ matrix, respectively.

7.3.3 Actuator/Sensor Indices and Modal Indices

For convenience in further discussion we denote by Σ the placement matrix either of the two- or of the infinity-norm. The placement matrix gives an insight into the placement properties of each actuator, since the placement index of the kth actuator is determined as the rms sum of the kth column of Σ. The vector of the actuator placement indices is defined as $\sigma_a = [\sigma_{a1} \quad \sigma_{a2} \quad \ldots \quad \sigma_{aS}]^T$, and its kth entry is the placement index of the kth actuator. In the case of the H_2 norm, it is the rms sum of the kth actuator indexes over all modes,

$$\sigma_{ak} = \sqrt{\sum_{i=1}^{n} \sigma_{ik}^2}, \qquad k = 1, \ldots, S, \qquad (7.10a)$$

and in the case of the H_∞ and Hankel norms it is the largest index over all modes

$$\sigma_{ak} = \max_i(\sigma_{ik}), \qquad i = 1, \ldots, n, \qquad k = 1, \ldots, S \qquad (7.10b)$$

Similarly, the vector of the sensor placement indices is defined as $\sigma_s = [\sigma_{s1} \quad \sigma_{s2} \quad \ldots \quad \sigma_{sR}]^T$, and its kth entry is the placement index of the kth sensor. In the case of the H_2 norm, it is the rms sum of the kth sensor indexes over all modes,

$$\sigma_{sk} = \sqrt{\sum_{i=1}^{n} \sigma_{ik}^2}, \qquad k = 1, \ldots, R, \tag{7.10c}$$

and in the case of the H_∞ and Hankel norms it is the largest index over all modes

$$\sigma_{sk} = \max_i(\sigma_{ik}), \qquad i = 1, \ldots, n, \qquad k = 1, \ldots, R \tag{7.10d}$$

The vector of the mode indices is defined as follows: $\sigma_m = [\sigma_{m1} \quad \sigma_{m2} \quad \ldots \quad \sigma_{mn}]^T$, and its ith entry is the index of the ith mode. This entry is a rms sum of the ith mode indices over all actuators

$$\sigma_{mi} = \sqrt{\sum_{k=1}^{S} \sigma_{ik}^2}, \qquad i = 1, \ldots, n, \tag{7.11a}$$

or a rms sum of the ith mode indices over all sensors

$$\sigma_{mi} = \sqrt{\sum_{k=1}^{R} \sigma_{ik}^2}, \qquad i = 1, \ldots, n, \tag{7.11b}$$

The actuator placement index, σ_{ak}, is a nonnegative contribution of the kth actuator at all modes to the H_2 or H_∞ norms of the structure. The sensor placement index, σ_{sk}, is a nonnegative contribution of the kth sensor at all modes to the H_2 or H_∞ norms of the structure. The mode index, σ_{mi}, is a nonnegative contribution of the ith mode for all actuators (or all sensors) to the H_2 or H_∞ norms of the structure. The determination of the H_2 actuator and modal indices for the pinned beam is illustrated in Fig. 7.1. Four actuators are located on the beam, and five modes are considered. The second mode index is the rms sum of indexes of all actuators for this mode, and the fourth actuator index is the rms sum of these actuator indices over five modes.

From the above properties it follows that the index σ_{ak} (σ_{sk}) characterizes the importance of the kth actuator (sensor), thus it serves as the actuator (sensor) placement index. Namely, the actuators (sensors) with small index σ_{ak} (σ_{sk}) can be removed as the least significant ones. Note also that the mode index σ_{mi} can also be used as a reduction index. Indeed, it characterizes the significance of

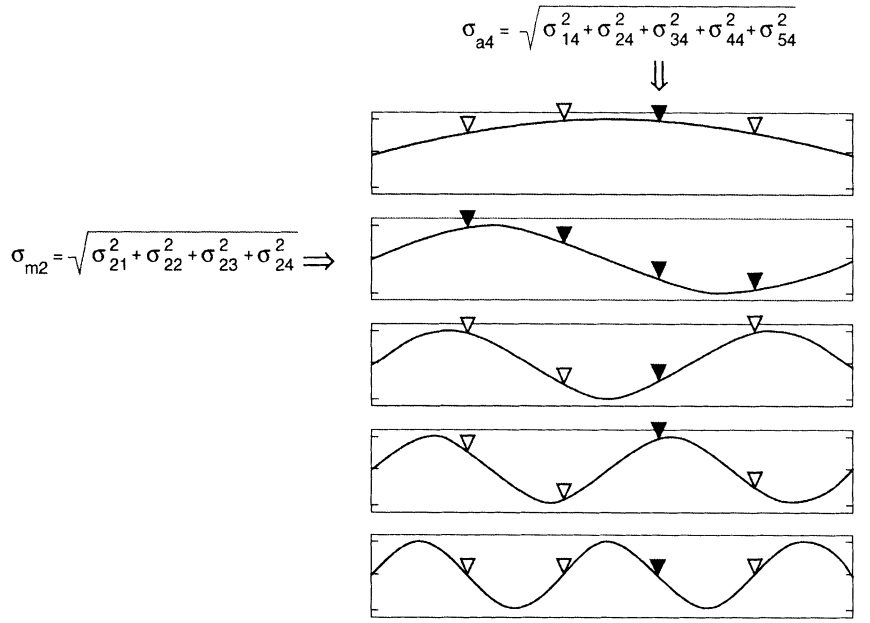

Figure 7.1. Determination of the H_2 actuator and modal indices of a pinned beam (∇ – actuator location; and ▼ – actuators used for the calculation of the indices).

the *i*th mode for the given locations of sensors and actuators. The norms of the least significant modes (those with the small index σ_{mi}) should either be enhanced by the reconfiguration of the actuators or sensors, or be eliminated.

Example 7.1. The 2D truss from Fig. 1.3 is considered. It is excited in the *y*-direction by an actuator located at node 4. Accelerometers serve as sensors. The task is to find four accelerometer locations within all 16 possible locations, that is, within all but 1 and 6 nodes, in the *x*- and *y*-directions. The unit weights are assumed for all modes, and the two-norm indices are used.

The placement indices σ_{si}, $i = 1, ..., 16$ of each accelerometer location are given in Fig. 7.2, for lower (2–5) nodes of the truss, and in Fig. 7.3, for upper (7–10) nodes of the truss. The left column of these figures represents the H_2 index σ_{si} for the *x*-direction accelerometers, while the right column represents the index for the *y*-direction accelerometers. The largest value indices are for the nodes 5, 10, 4, and 9, all in the *y*-direction. Note that the chosen locations are the nodes at the tip in the same direction, and that a single accelerometer would probably do the same job as the four put together. This problem is addressed in the following section.

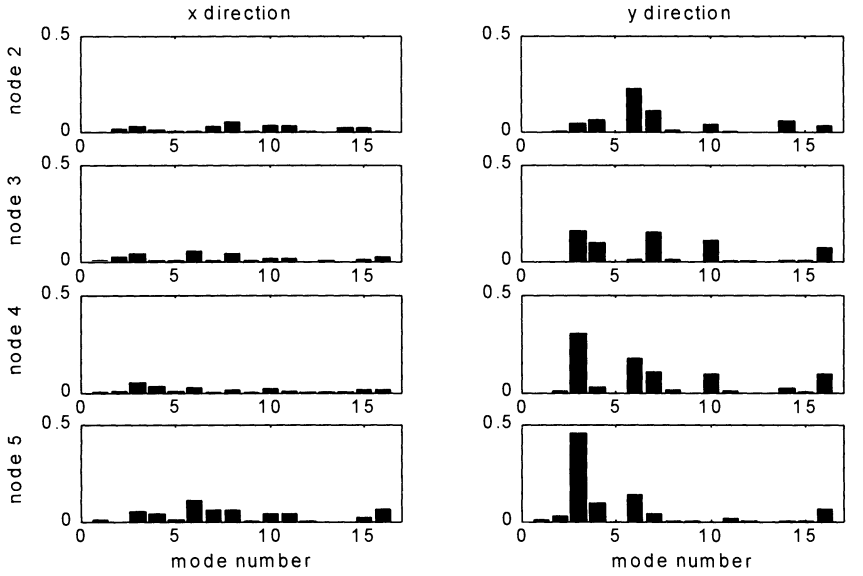

Figure 7.2. The 2D truss sensor indices for nodes 2–5.

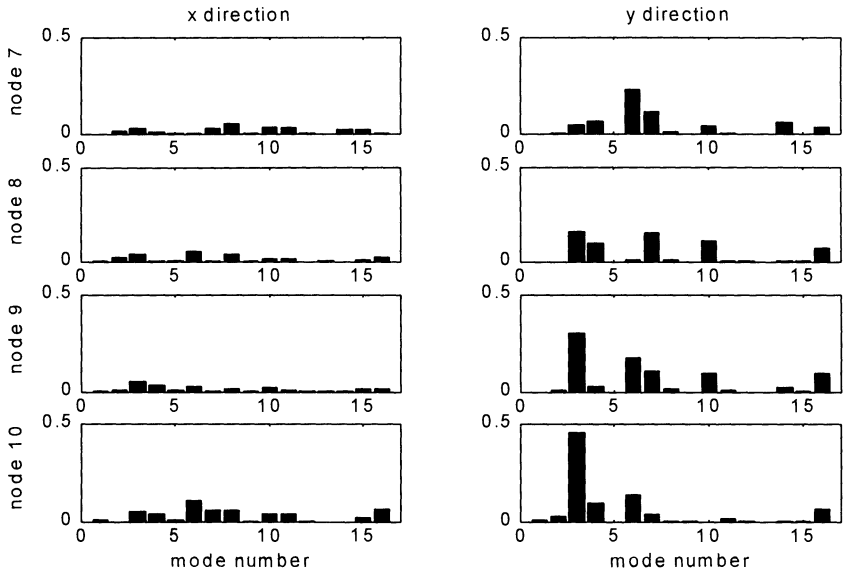

Figure 7.3. The 2D truss sensor indices for nodes 7–10.

7.4 Placement for Large Structures

In the case of the placement of a very large number of sensors, the maximization of the performance index alone may be neither a sufficient nor satisfactory criterion. Suppose that a specific sensor location gives a high-performance index. Inevitably, locations close to it will have a high-performance index as well. But the locations in the neighborhood of the original sensor are not necessarily the best choice, since the sensors at these locations can be replaced by the appropriate gain adjustment of the original sensor. One wants to find sensor locations that cannot be compensated for by original sensor gain adjustment. These locations can be determined using the additional criterion. It is based on the correlation of each sensor modal norm. Define a vector of the *i*th sensor norms, which is composed of the squares of the modal norms

$$g_i = \begin{bmatrix} \|G_{i1}\|^2 \\ \|G_{i2}\|^2 \\ \vdots \\ \|G_{in}\|^2 \end{bmatrix}, \tag{7.12}$$

where G_{ik} denotes the transfer function of the *k*th mode at the *i*th sensor. The norm $\|\cdot\|$ denotes either the H_2, H_∞, or Hankel norms. The correlation coefficient r_{ik} is defined as follows:

$$r_{ik} = \frac{g_i^T g_k}{\|g_i\|_2 \|g_k\|_2}, \qquad i = 1, \ldots, r, \qquad k = i+1, \ldots, R \quad . \tag{7.13}$$

Denote a small positive number, ε, say $\varepsilon = 0.01 - 0.20$. Denote the membership index $I(k)$, k=1,…,R, where R is the number of sensors. This index is determined as follows:

$$I(k) = \begin{cases} 0 & \text{if } r_{ik} > 1-\varepsilon \quad \text{and} \quad \sigma_k \le \sigma_i \quad \text{for } k > i \ , \\ 1 & \text{elsewhere} \ , \end{cases} \tag{7.14}$$

for $k > i$. If $I(k)$=1, the *k*th sensor is accepted, and if $I(k)$=0, the *k*th sensor is rejected (in this case the two locations *i* and *k* are either highly correlated, or the *i*th location has a higher performance σ_i).

Based on the above analysis the placement strategy is established. For technical and economical reasons the number of sensors exceeds significantly the number of actuators. Therefore, the actuator selection comes first, as a less flexible procedure.

7.4.1 Actuator Placement Strategy

1. Place sensors at all accessible degrees of freedom.
2. Based on engineering experience, technical requirements, and physical constraints select the possible actuator locations. In this way S candidate actuator locations are selected.
3. For each mode (k), and each selected actuator location (i), determine the actuator placement index $\sigma_k(i)$.
4. For each mode select the s_1 most important actuator locations (those with the largest $\sigma_k(i)$). The resulting number of actuators s_2 for all the modes in consideration (i.e., $s_2 \le n \times s_1$) is much smaller than the number of candidate locations S, i.e., $s_2 << S$.
5. Check the correlation indices for the remaining s_2 actuators. Reject all but one actuator with a correlation index higher than $1-\varepsilon$ (i.e., those with the zero membership index). The resulting number of actuators is now $s_3 < s_2$, typically $s_3 << s_2$.
6. If the already small number s_3 is still too large, the actuator importance index, and the modal importance index are recalculated. The actuator number is further reduced to the required one by reviewing the indices.

7.4.2 Sensor Placement Strategy

1. Actuator locations are already determined.
2. Select the areas where the sensors can be placed, obtaining the R candidate sensor locations.
3. Determine the sensor placement indices $\sigma_k(i)$ for all the candidate sensor locations ($i = 1, \ldots, R$), and for all the modes of interest ($k = 1, \ldots, n$).
4. For each mode, select r_1 for the most important sensor locations. The resulting number of sensors r_2 for all the modes considered (i.e., $r_2 \le n \times r_1$) is much smaller than the number of candidate locations, i.e., $r_2 << R$.
5. For the given small positive number ε check the correlation indices for the remaining r_2 sensors. Reject the sensors with correlation indices higher than $1-\varepsilon$ (i.e., those with the zero membership indices). The resulting number of sensors is $r_3 < r_2$, typically $r_3 << r_2$.

Example 7.2. The 2D truss accelerometer location as in Example 7.1 is reconsidered. Using $\varepsilon = 0.15$, the membership index I is determined for each location. The plot of the index is in Fig. 7.4 that indicates four accelerometer locations, namely, at nodes 2, 5, and 8 in the y-direction, and at node 7 in the x-direction. These are the locations that are not heavily correlated, and have the best detection of modes 6, 3, 7, and 8, respectively.

Example 7.3. *(International Space Station Structure).* This example is based on [90]. The Z1 module of the International Space Station structure, see Fig. 1.9, is shaped with a basic truss frame and numerous appendages and attachments such as control moment gyros and a cable tray. The total mass of the structure is around 30,000 lb.

The finite-element model of the structure consists of 11,804 degrees of freedom with 56 modes below the frequency of 70 Hz. The natural frequencies are listed in Table 7.1. The task is to identify all modes below 70 Hz by generating dynamic test data, with accelerometers used as sensors. This non-trivial undertaking requires extensive pretest analysis and careful planning of the actuator and sensor locations, especially if one does not have the freedom to repeat the test and modify the sensor/actuator location for retesting.

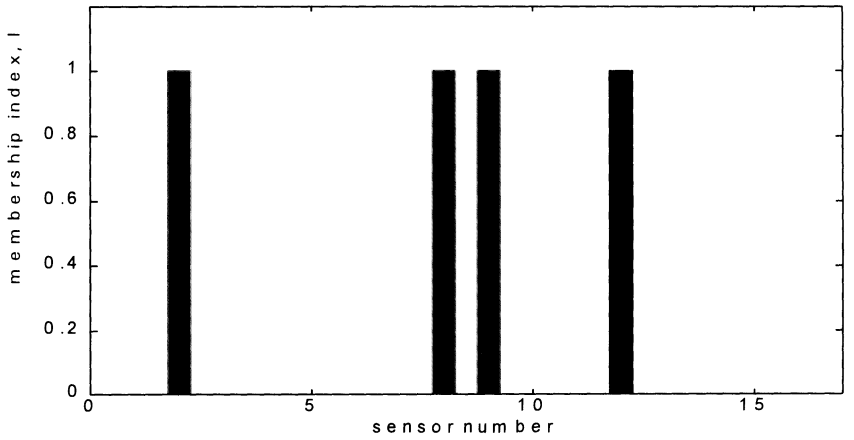

Figure 7.4. The 2D truss placement index *I*.

Actuator Placement. The first part of the analysis involves the selection of four actuator locations. The initial selection procedure combines engineering judgment, practical experience, and physical constraints including the following criteria:

- All target modes should be excited with relatively equal amplitudes.
- The structure is excited in three axes.

The structure drawings and the finite-element model were examined and 2256 actuator candidate locations were selected out of the 11,804 translational degrees of freedom. The selection was based on accessibility of the locations, strength of the structural parts, modal masses, and local flexibility. It was assumed at this stage of analysis that accelerometers were located at all degrees of freedom. The Hankel norms of each actuator were determined and used to

evaluate the actuator importance indices. For each of 56 modes the six most important actuators were selected, obtaining 268 actuator locations (it is less than 6×56, because some locations were the same for two or more modes). Next, the correlation coefficients of the Hankel norm vectors (see (7.13)) for each actuator location were obtained. Those highly correlated were discarded and the one with the highest placement index out of all the highly correlated actuators was kept.

Table 7.1. *Natural Frequencies (Hz) of the International Space Station Structure.*

9.34	28.93	35.07	40.71	49.78	60.91	65.91
16.07	29.44	35.16	41.18	50.98	61.53	66.79
19.21	30.19	36.43	42.10	51.39	62.92	67.05
21.14	30.42	37.21	42.46	54.82	63.25	67.26
22.67	31.21	37.61	43.34	57.02	63.46	67.49
23.81	32.25	38.30	44.83	57.61	64.22	67.63
25.24	33.88	39.79	46.42	58.42	64.70	69.17
26.33	34.71	40.37	47.34	59.24	65.23	69.67

In this process the number of actuators was reduced down to 52 locations. The next step of the selection process involved the re-evaluation of the importance indices of each actuator and their comparison with the threshold value. In this step the number of actuator locations was reduced to 7. The final step involved evaluation of the actual location of these actuators using the finite-element model simulations, along with determination of accessibility, structural strength, and the importance index. The final four actuators were located at the nodal points shown in Fig. 1.9 as black spots. These four locations are essentially near the four corners of the structure.

Sensor Placement. The sensor selection criteria includes:

- Establishing the maximum allowable number of sensors. In our case it was 400.
- Determination of the sensor placement indices for each mode. Sensors with the highest indices were selected.
- Using the correlation procedure to select uncorrelated sensors by evaluating the membership index.

The excitation level of each mode by the four selected actuators is represented by the Hankel norms, and is shown in Fig. 7.5(a). It can be seen that some modes are weakly excited, providing weaker measurement signal, thus they are more difficult to identify. Fig. 7.5(b) presents an overview of the sensor importance index for each sensor as the sum of the indices for all modes.

Sensors at the degrees of freedom with larger amplitude of modal vibrations have higher indices. By looking at the sensor importance indices for a particular mode one can roughly evaluate the participation of each mode at a particular sensor location. The highly participating modes have a high index at this location. The set of illustrations presented in Fig. 7.6 shows the placement indices of each sensor for the first 10 modes. The first mode (Fig. 7.6(a)) is a global (or system) mode with indices for all sensors almost identical. The second mode (Fig. 7.6(b)) is a global mode of more complex configuration. The third, fourth, fifth, and seventh modes (Fig. 7.6(c,d,e,g)) show more dominant responses from the cable tray attachment. The sixth mode is dominated by the local motion at locations 1000–2000, which correspond to the attachments and cross-beams near the circular dish on a side of the structure. The eighth and ninth modes (Figs. 7.6(h,i)) are local modes of the control moment gyros – see the four columns sticking up at the end. The last one (Fig. 7.6(j)) shows a highly dominant mode of a beam sticking out of the structure.

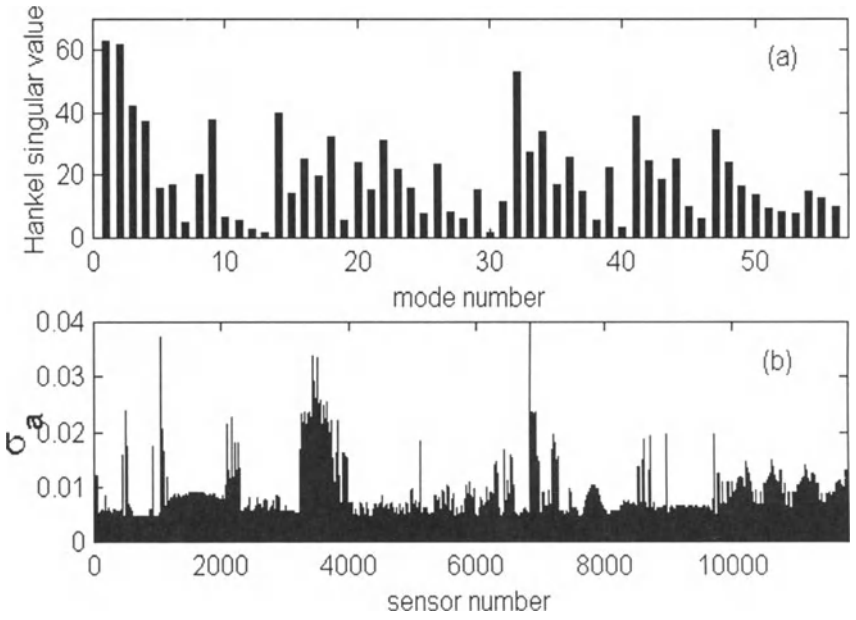

Figure 7.5. The International Space Station structure with four actuators: (a) the Hankel norms, and (b) the sensor index for all modes.

Figure 7.7 shows the membership index I which has nonzero values for 341 locations. Figure 7.8(a,b) indicates with triangles Δ the selected sensor locations. It can be observed that many of the sensors are located in and around the control moment gyros (see Fig. 7.8) and the cable tray (see Fig. 1.9), since

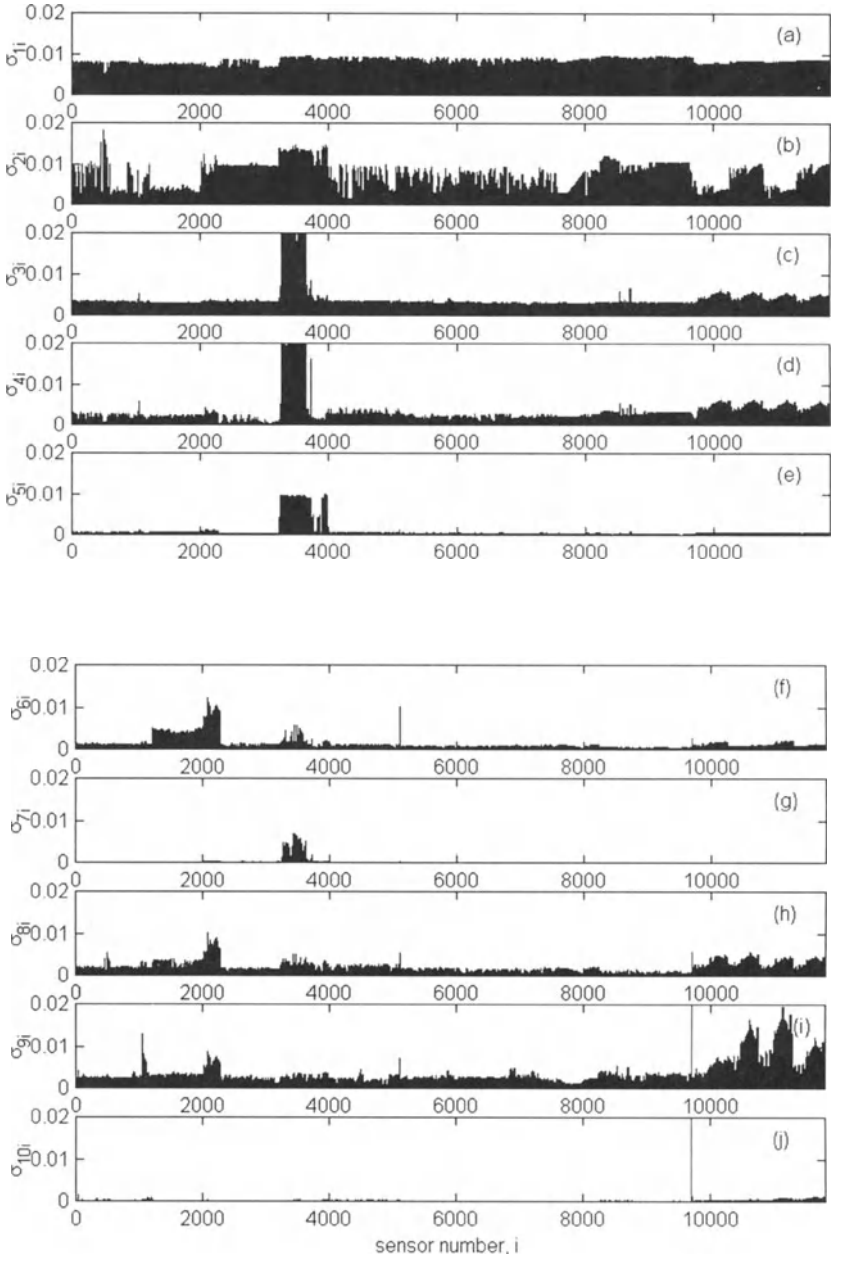

Figure 7.6. The placement index for the first ten modes: (a) mode 1; (b) mode 2; (c) mode 3; (d) mode 4; (e) mode 5; (f) mode 6; (g) mode 7; (h) mode 8; (i) mode 9; (j) mode 10.

13 out of the 56 modes involve extensive control moment gyro movement and 9 are mostly cable tray modes. Many of the 56 modes are local modes that require concentrations of sensors at the particular locations seen in Fig. 7.8.
In order to test the effectiveness of the procedure we compare the Hankel norms of each mode, for the structure with a full set of 11,804 sensors, and with the selected 341 sensors. The norms with the selected sensors should be proportional to the norms of the full set (they are always smaller than the norms of the full set, but proportionality indicates that each mode is excited and sensed comparatively at the same level). The norms are shown in Fig. 7.9, showing that the profile of the modal norms is approximately preserved.

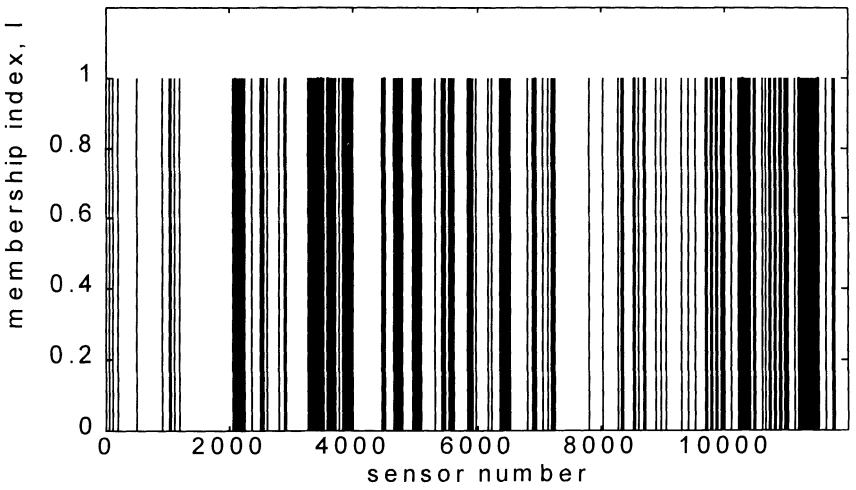

Figure 7.7. Membership index *I* for the International Space Station structure.

7.5 Placement for General Plant Configuration

The problem of actuator and sensor placement presented in this section refers to the more general problem which consists of selection of actuators not collocated with disturbances, and sensors not collocated with the performance outputs. This problem has its origin both in structural testing and control.

7.5.1 Structural Testing and Control

A typical actuator and sensor location problem for structural testing can be described as follows. The structural test plan is based on the available information on the structure itself, on disturbances acting on the structure, and on the expected structural performance. The first information is typically in a

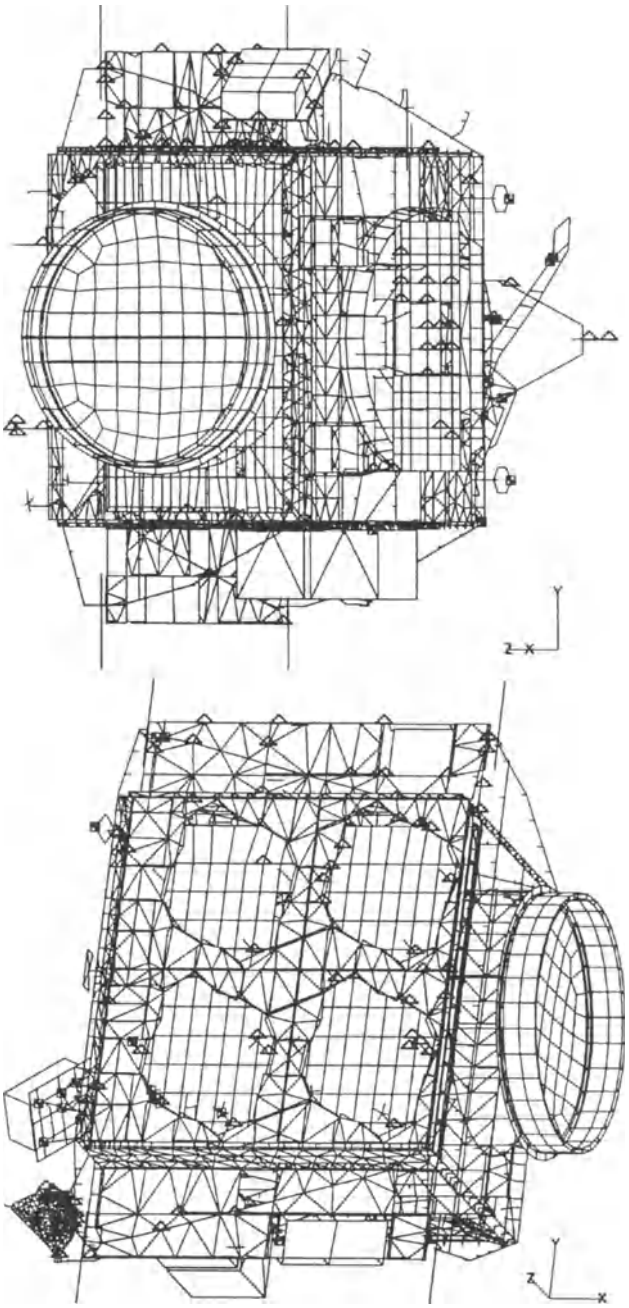

Figure 7.8. Two views of the sensor location for the International Space Station structure.

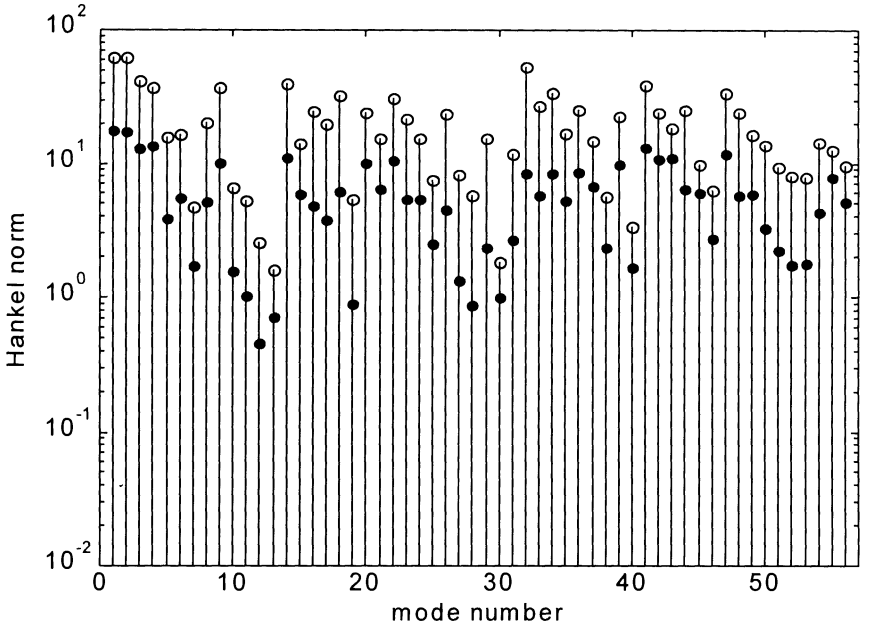

Figure 7.9. The modal Hankel norms of the full set of sensors (○), and the selected sensors (•) of the International Space Station truss.

form of a structural finite-element model. The disturbance information includes disturbance location and spectral contents. The structure performance is commonly evaluated through the displacements or accelerations at selected locations.

The formulation of structural testing is based on a block diagram as in Fig. 7.9. In this diagram the structure input is composed of two inputs not necessarily collocated: the vector of the disturbances (w), and the vector of the actuator inputs (u). Similarly, the plant output is divided into two sets: the vector of the performance (z), and the vector of the sensor output (y). The actuator inputs include forces and torque applied during a test. The disturbance inputs include disturbances, noises, and commands, known and unknown, but not applied during the test. The sensor signals consist of structure outputs recorded during the test. The performance output includes signals that characterize the system performance, and is not generally measured during the test.

It is not possible in general to duplicate the dynamics of a real structure during testing. This happens not only due to physical restrictions or limited knowledge of disturbances, but also because the test actuators cannot be placed at the disturbance locations and sensors cannot be placed at the performance evaluation locations. Thus, to obtain the performance of the test item close to the performance of a structure in a real environment one uses the available (or

candidate) locations of actuators and sensors and formulates the selection criteria to imitate the actual environment as close as possible.

The control design problem of a structure can be defined in a similar manner. The feedback loop is closed between the sensors and actuators of a structure. The actuators are placed within the allowable locations, and they are not necessarily collocated with the disturbance locations; sensors are placed at the sensor allowable locations, generally outside the locations of performance evaluation. In the control nomenclature u is the control input, y is the plant output accessible to the controller, w is the vector of disturbances, and z is the vector of the performance output, for example, see [12].

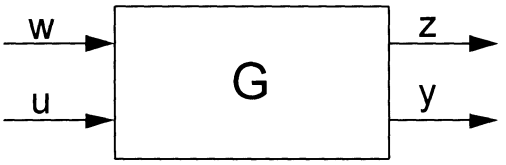

Figure 7.10. Structure configuration for testing and control.

7.5.2 Properties

In this section we address the two-input–two-output actuator and sensor location problem as applied to flexible structures. We derive the placement rules based on the properties of the structural norms, and illustrate their application with the truss sensor location. Let (A, B, C) be the modal representation of a structure, with s inputs, r outputs, n modes, and $N = 2n$ states.

Consider a plant as in Fig. 7.10, with inputs w and u, and outputs z and y. Let G_{wz} be the transfer matrix from w to z, *let* G_{wy} be the transfer matrix from w to y, let G_{uz} be the transfer matrix from u to z, and let G_{uy} be the transfer matrix from u to y. Let G_{wzi}, G_{uyi}, G_{wyi}, and G_{uzi} be the transfer functions of the ith mode. The following multiplicative properties of modal norms hold:

Property 7.1 ***Modal Norms of a General Plant.*** *The following norm relationships hold:*

$$\|G_{wzi}\|\|G_{uyi}\| \cong \|G_{wyi}\|\|G_{uzi}\| \tag{7.15}$$

for $i = 1, \ldots, n$, *where* $\|.\|$ *denotes either* H_2, H_∞, *or Hankel norms.*

Proof. Denote by B_w and B_u the modal input matrices of w and u, respectively, and let C_z and C_y be the modal output matrices of z and y, respectively, and let B_{wi}, B_{ui}, C_{zi}, and C_{yi} be their ith blocks related to the ith mode. The H_∞ norms are approximately determined from (4.25) as

$$\|G_{wzi}\|_\infty \cong \frac{\|B_{wi}\|_2 \|C_{zi}\|_2}{2\zeta_i \omega_i}, \qquad \|G_{uyi}\|_\infty \cong \frac{\|B_{ui}\|_2 \|C_{yi}\|_2}{2\zeta_i \omega_i}, \tag{7.16a}$$

$$\|G_{wyi}\|_\infty \cong \frac{\|B_{wi}\|_2 \|C_{yi}\|_2}{2\zeta_i \omega_i}, \qquad \|G_{uzi}\|_\infty \cong \frac{\|B_{ui}\|_2 \|C_{zi}\|_2}{2\zeta_i \omega_i}. \tag{7.16b}$$

Introducing the above equations to (7.15) the approximate equality is proven by inspection. The H_2 and Hankel norm properties are proven similarly, using (4.5) and (4.34) instead of (4.25). ❑

Property 7.1 shows that for each mode the product of norms of the performance loop (i.e. from the disturbance to the performance) and the control loop (i.e. from the actuators to the sensors) is approximately equal to the product of the norms of the cross-couplings: between the disturbance and sensors, and between the actuators and performance. The physical meaning of this property lies in the fact that by increasing the actuator–sensor connectivity, one increases automatically the cross-connectivity for the ith mode: actuator-to-performance, and disturbance-to-sensors. It shows that sensors not only respond to the actuator input, but also to disturbances, and actuators not only impact the sensors, but also the performance.

This property is important for the closed-loop design. For the plant as in Fig. 7.10 one obtains

$$z = G_{wz} w + G_{uz} u, \qquad y = G_{wy} w + G_{uy} u. \tag{7.17}$$

The closed-loop transfer matrix G_{cl} from w to z, with the controller K such that $u = Ky$, is as follows:

$$G_{cl} = G_{wz} + G_{uz} K (I - G_{uy})^{-1} G_{wy}. \tag{7.18}$$

From the second part of the right-hand side of the above equation it follows that the controller impacts the closed-loop performance not only through the

action from u to y, but also through the cross-actions from u to z, and from w to y. Therefore, if the transfer matrices G_{wy} or G_{uz} are zero, the controller has no impact whatsoever on the performance z. Thus the controller design task consists of simultaneous gain improvement between u and y, w and y, and u and z. However, Property 7.1 shows that the improvement in G_{uy} automatically leads to the improvement of G_{wy} and G_{uz}. Thus, the task of actuator and sensor location simplifies to the manipulation of G_{uy} alone.

The impact of G_{uy} on the overall system performance can be shown in the following properties of the modal norms. Let G_i denote the transfer function of the ith mode, from the combined input $\{w,\ u\}$ to the combined output $\{z, y\}$. It is easy to show that for the ith mode the following holds:

$$\|G_i\|^2 \cong \|G_{uzi}\|^2 + \|G_{uyi}\|^2 + \|G_{wzi}\|^2 + \|G_{wyi}\|^2. \tag{7.19}$$

where $\|.\|$ denotes either H_2, H_∞, or Hankel norms. Consider S actuator locations, generating S inputs $\{u_1 \quad \dots \quad u_S\}$. The actuators impact only the first two terms of (7.19), and the last two are constant. Denote these two terms as $\|G_{ui}\|^2$, i.e.,

$$\|G_{ui}\|^2 \cong \|G_{uzi}\|^2 + \|G_{uyi}\|^2. \tag{7.20}$$

From the definitions of norms (7.3) and (7.5) one obtains the following property:

Property 7.2(a) ***Additive Property of Actuators of a General Plant.***

$$\|G_{ui}\|^2 \cong \alpha_{wi}^2 \sum_{k=1}^{S} \|G_{u_k yi}\|^2, \tag{7.21a}$$

where $G_{u_k yi}$ is the transfer function of the ith mode from the kth actuator to the output y, and α_{wi} is the disturbance weight of the ith mode, defined as

$$\alpha_{wi} = \sqrt{1 + \frac{\|G_{wzi}\|^2}{\|G_{wyi}\|^2}}. \tag{7.21b}$$

Proof. From (7.3), or (7.5), it follows that

$$\|G_{uzi}\|^2 \cong \sum_{k=1}^{S} \|G_{u_k zi}\|^2 \qquad \text{and} \qquad \|G_{uyi}\|^2 \cong \sum_{k=1}^{S} \|G_{u_k yi}\|^2, \tag{7.22}$$

where $G_{u_k zi}$ is the transfer function of the ith mode from the kth actuator to the performance z. Introducing the above equations to (7.20) one obtains

$$\|G_{ui}\|^2 \cong \sum_{k=1}^{S} \left(\|G_{u_k zi}\|^2 + \|G_{u_k yi}\|^2 \right). \tag{7.23}$$

Next, using Property 7.1 one obtains

$$\|G_{u_k zi}\| \cong \frac{\|G_{u_k yi}\| \|G_{wzi}\|}{\|G_{wyi}\|}$$

which, introduced to the above equation, gives (7.21). ❑

Note that the disturbance weight α_{wi} does not depend on the actuator location. It characterizes structural dynamics caused by the disturbances w.

Similarly, one obtains the additive property of the sensor locations of a general plant. Consider R sensor locations with R outputs $\{y_1 \ \ldots \ y_R\}$. The sensors impact only the second and fourth terms of (7.19), and the remaining are constant. Denote the second and fourth terms by $\|G_{yi}\|^2$, that is,

$$\|G_{yi}\|^2 \cong \|G_{wyi}\|^2 + \|G_{uyi}\|^2, \tag{7.24}$$

then the following property holds:

Property 7.2(b) ***Additive Property of Sensors of a General Plant.***

$$\|G_{yi}\|^2 \cong \alpha_{zi}^2 \sum_{k=1}^{R} \|G_{uy_k i}\|^2, \tag{7.25a}$$

where

$$\alpha_{zi} = \sqrt{1 + \frac{\|G_{wzi}\|^2}{\|G_{uzi}\|^2}} \tag{7.25b}$$

is the performance weight of the ith mode.

Note that the performance weight α_{zi} characterizes part of the structural dynamics that is observed at the performance output. It does not depend on the sensor location.

7.5.3 Placement Indices and Matrices

Properties 7.2(a,b) are the basis of the actuator and sensor search procedure of a general plant. The actuator index that evaluates the actuator usefulness in test is defined as follows:

$$\sigma_{ki} = \frac{\alpha_{ui}\left\|G_{u_k yi}\right\|}{\left\|G_u\right\|}, \tag{7.26a}$$

where $\left\|G_u\right\|^2 = \left\|G_{uy}\right\|^2 + \left\|G_{uz}\right\|^2$, while the sensor index is

$$\sigma_{ki} = \frac{\alpha_{yi}\left\|G_{uy_k i}\right\|}{\left\|G_y\right\|}, \tag{7.26b}$$

where $\left\|G_y\right\|^2 = \left\|G_{uy}\right\|^2 + \left\|G_{wy}\right\|^2$.

The indices are the building blocks of the actuator placement matrix Σ

$$\Sigma = \begin{bmatrix} \sigma_{11} & \sigma_{12} & \cdots & \sigma_{1k} & \cdots & \sigma_{1S} \\ \sigma_{21} & \sigma_{22} & \cdots & \sigma_{2k} & \cdots & \sigma_{2S} \\ \cdots & \cdots & \cdots & \cdots & \cdots & \cdots \\ \sigma_{i1} & \sigma_{i2} & \cdots & \sigma_{ik} & \cdots & \sigma_{iS} \\ \cdots & \cdots & \cdots & \cdots & \cdots & \cdots \\ \sigma_{n1} & \sigma_{n2} & \cdots & \sigma_{nk} & \cdots & \sigma_{nS} \end{bmatrix} \Leftarrow \text{ith mode} \tag{7.27a}$$

$\Uparrow$

*k*th actuator

or the sensor placement matrix

$$\Sigma = \begin{bmatrix} \sigma_{11} & \sigma_{12} & \cdots & \sigma_{1k} & \cdots & \sigma_{1R} \\ \sigma_{21} & \sigma_{22} & \cdots & \sigma_{2k} & \cdots & \sigma_{2R} \\ \cdots & \cdots & \cdots & \cdots & \cdots & \cdots \\ \sigma_{i1} & \sigma_{i2} & \cdots & \sigma_{ik} & \cdots & \sigma_{iR} \\ \cdots & \cdots & \cdots & \cdots & \cdots & \cdots \\ \sigma_{n1} & \sigma_{n2} & \cdots & \sigma_{nk} & \cdots & \sigma_{nR} \end{bmatrix} \Leftarrow \; i\text{th mode} \qquad (7.27b)$$

$$\Uparrow$$

kth sensor

The placement index of the kth actuator (sensor) is determined from the kth column of Σ. In the case of the H_2 norm it is the rms sum of the kth actuator indexes over all modes,

$$\sigma_k = \sqrt{\sum_{i=1}^{n} \sigma_{ik}^2}, \qquad k = 1,\ldots,S \text{ or } R, \qquad (7.28a)$$

and in the case of the H_∞ and Hankel norms it is the largest index over all modes

$$\sigma_k = \max_i(\sigma_{ik}), \qquad i = 1, \ldots, n, \qquad k = 1, \ldots, S \text{ or } R. \qquad (7.28b)$$

This property shows that the index for the set of sensors/actuators is determined from the indexes of each individual sensor or actuator. This decomposition allows for the evaluation of an individual sensor/actuator through its participation in the performance of the whole set of sensors/actuators.

For the placement of a large number of sensors the maximization of the performance index alone is not a satisfactory criterion. These locations can be selected using the correlation of each sensor modal norm. Define the kth sensor norm vector, which is composed of the squares of the modal norms

$$g_{uyk} = \begin{bmatrix} \left\| G_{uy_k 1} \right\|^2 \\ \left\| G_{uy_k 2} \right\|^2 \\ \vdots \\ \left\| G_{uy_k n} \right\|^2 \end{bmatrix}, \qquad (7.29)$$

where $G_{uy_k i}$ denotes the transfer function of the ith mode at the kth sensor. The norm $\|.\|$ denotes either the H_2, H_∞, or Hankel norm. The sensor locations can be additionally selected using the correlation coefficient r_{ik}, defined as follows:

$$r_{ik} = \frac{g_{uyi}^T g_{uyk}}{\|g_{uyi}\|_2 \|g_{uyk}\|_2}, \qquad i = 1, \ldots, r, \quad k = i+1, \ldots, r \tag{7.30}$$

Denote a small positive number ε, say $\varepsilon = 0.01 - 0.20$. The membership index $I(k)$, $k = 1, \ldots, r$, is defined as follows:

$$I(k) = \begin{cases} 0 & \text{if } r_{ik} > 1-\varepsilon \text{ and } \sigma_k \le \sigma_j \\ 1 & \text{elsewhere,} \end{cases} \tag{7.31}$$

for $k > j$ and r is the number of sensors. If $I(k) = 1$ the kth sensor is accepted, and if $I(k) = 0$ the kth sensor is rejected (in this case the two locations j and k are either highly correlated, or the jth location has higher performance σ_j).

From Property 7.2 the following search procedure for the sensor placement follows:

1. The norms of the transfer functions G_{wzi}, $G_{uy_k i}$ are determined (for all modes and for each sensor) along with the norm of G_y (for all actuators and all sensors).
2. The performance σ_k of each sensor is determined from (7.26b).
3. Check if the chosen location is highly correlated with the previously selected locations by determining the correlation coefficient r_{ik} from (7.30), and the membership index $I(k)$, from (7.31). Highly correlated sensors are rejected.

Example 7.4. Consider the 3D truss as in Fig.1.4. The disturbance w is applied at node 7 in the horizontal direction. The performance z is measured as rates of all nodes. The input u is applied at node 26 in the vertical direction, and the candidate sensor locations are at the nodes 5, 6, 7, 12, 13, 14, 19, 20, 21, 26, 27, and 28, in all three directions (total of 36 locations). Using the first 50 modes, the task is to select a minimal number of sensors that would measure, as close as possible, the disturbance-to-performance dynamics.

First, the H_∞ norms of each mode of G_{wz}, G_{wy}, G_{uz}, and G_{uy} are determined, and presented in Fig. 7.11(a,b). Next, Property 7.1 is checked. Indeed, (7.15b) holds since the plots of $g_1(k) = \|G_{wzk}\|_\infty \|G_{uyk}\|_\infty$ and of $g_2(k) = \|G_{wyk}\|_\infty \|G_{uzk}\|_\infty$ overlap in Fig. 7.12.

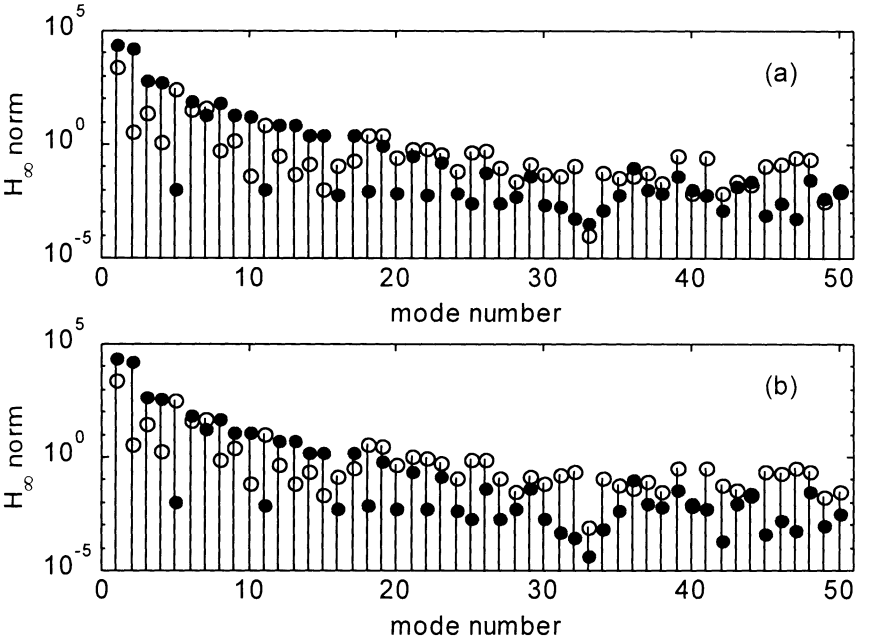

Figure 7.11. The H_∞ norms of the 3D truss modes: (a) G_{wz} (•) and G_{uy} (○); and (b) G_{wy} (•) and G_{uz} (○).

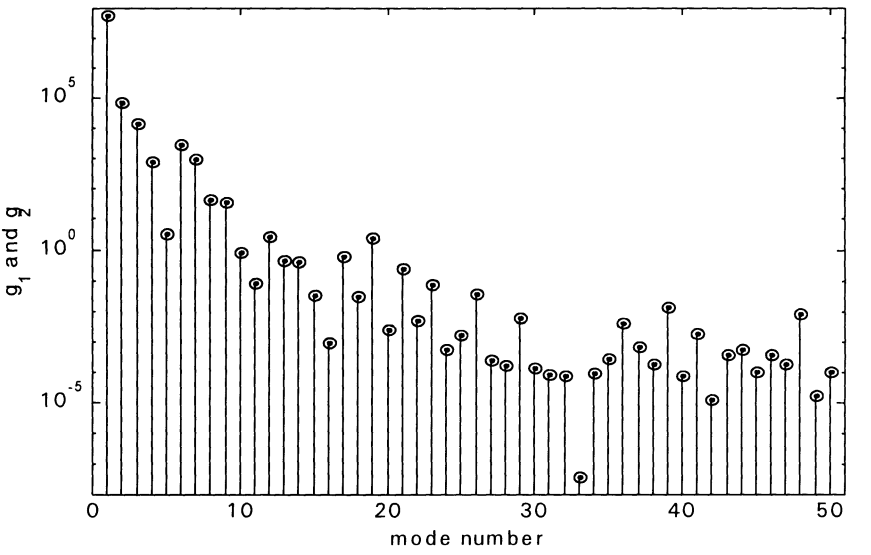

Figure 7.12. Overlapped plots of $g_1(k)$ (•) and $g_2(k)$ (○).

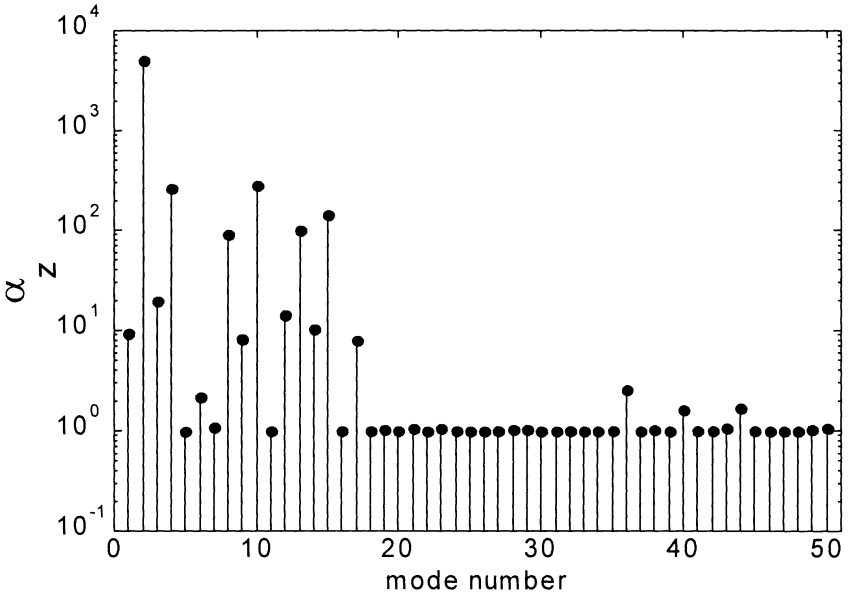

Figure 7.13. Modal weights for the 3D truss.

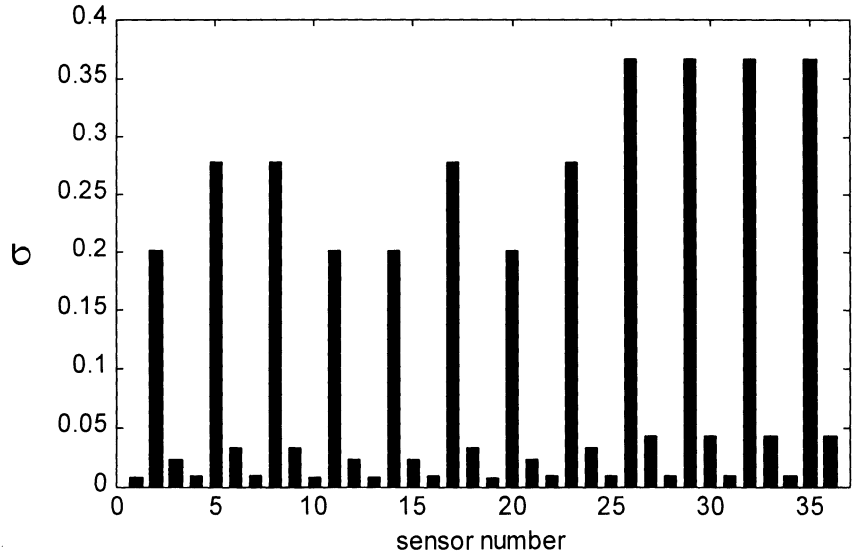

Figure 7.14. Sensor indices for the 3D truss.

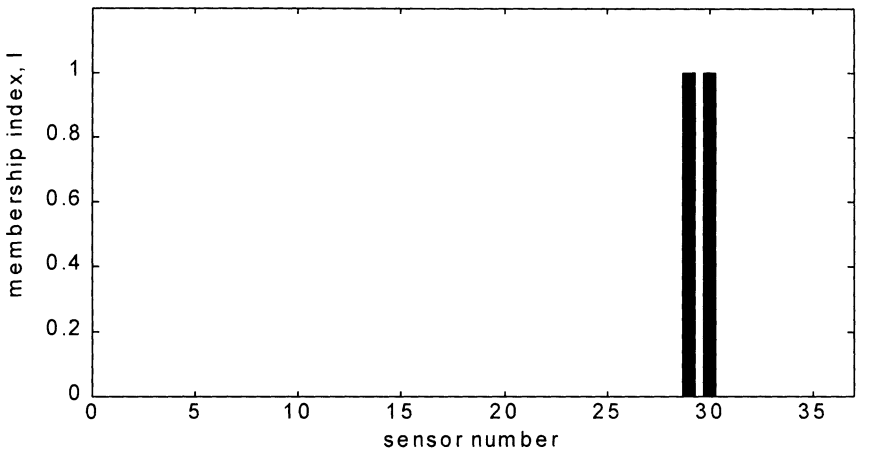

Figure 7.15. Membership index I for the 3D truss.

In the following the sensor modal weights α_{yi} are determined for each mode, and shown in Fig. 7.13. The placement indices σ_k for each sensor are determined from (7.28b), and their plot is shown in Fig. 7.14. Note that although there are sensors with a high value of σ_k, they can be highly correlated. Therefore the membership index $I(k)$ is determined, assuming $\varepsilon = 0.03$. The index is shown in Fig. 7.15. Its only nonzero values are for $k = 29$ and $k = 30$, that correspond to node 14, in the y- and z-directions. Thus the rate sensors at node 14 in the y- and z-directions are chosen for this particular task.

Part 2

Control

8
Dissipative Controllers

The most direct approach to controller design is to implement a proportional gain between the input and output. This approach, however, seldom gives a superior performance, since the performance enhancement in this case is tied to the reduction of the stability margin. If some conditions are satisfied, one obtains a special type of proportional controllers – dissipative ones. As stated by Joshi [64, p. 45] "the stability of dissipative controllers is guaranteed regardless of the number of modes controlled (or even modeled), and regardless of parameter errors." Therefore, for safety reasons, they are the most convenient candidates for implementation. However, the simplicity of the control law does not simplify the design. For example, in order to obtain the required performance a multi-input–multi-output controller with a large number of inputs and outputs has to be designed. Determining the gains for this controller is not an obvious task. In this chapter we investigate the properties of the dissipative controllers, and show how to design dissipative controllers for flexible structures in order to meet certain objectives.

8.1 Definition and Properties

Dissipative controllers and their properties are based on Popov's theory of hyperstability, [91], subsequently developed as a positive real property of the control systems [2], [10], and as the dissipative (passive) property of the systems [107], [108], and [21]. The terms: dissipative, passive, positive real, and

W. K. Gawronski, *Dynamics and Control of Structures*

hyperstable systems are synonyms, and their inter-relations are discussed by Wen [105]. In this chapter the above systems are called dissipative systems.

Consider a square stable plant (A,B,C), i.e., a linear system with the number of inputs equal to the number of outputs. An open-loop square system with simple poles is dissipative, see Ref.[2], if there exist a symmetric positive definite matrix P and a matrix Q that satisfy the following equations:

$$A^T P + PA = -Q^T Q, \qquad B^T P = C. \tag{8.1}$$

The system is strictly dissipative if $Q^T Q$ is positive definite.

The above definition allows for the simple determination of a dissipative system (at least in theory). Given A and B, the matrix Q is selected. Next, one solves the first of (8.1) for P, and the output matrix C is found from the second equation (8.1).

Three particular cases of the dissipative systems are discussed. In the first case, when $Q = B^T$ is chosen to obtain

$$P = W_c \quad \text{and} \quad C = B^T W_c \tag{8.2a}$$

and W_c is the controllability grammian. In this case the actuators are weighted proportionally to the system controllability grammian. In the second case the matrix $Q = CW_o^{-1}$ is chosen, where W_o is the observability grammian. Thus

$$P = W_o^{-1} \quad \text{and} \quad B = W_o C^T. \tag{8.2b}$$

In this case the sensors are weighted proportionally to the system observability grammian.

In the third case $Q = (-A - A^T)^{1/2}$ is chosen, therefore one obtains

$$P = I \quad \text{and} \quad B = C^T. \tag{8.2c}$$

In this particular case the actuators and sensors are collocated. This case is most frequently used, since it requires simple actuator and sensor collocation to guarantee the closed-loop system stability.

The guaranteed stability of the closed-loop system is the most useful property of the dissipative system. It was shown by Desoer [21], and by Benhabib, Iwens, and Jackson [10] that, for the square and strictly dissipative plant and the square and dissipative controller (or vice versa: the square and dissipative plant and the square and strictly dissipative controller), the closed-

loop system is asymptotically stable. In particular, if the feedback gain matrix is positive definite, the closed-loop system is asymptotically stable.

As a corollary, consider a dissipative system with the state-space representation (A,B,C) which has collocated sensors and actuators, that is, $C = B^T$. In this case a closed-loop system with the feedback gain

$$u = -Ky, \tag{8.3}$$

where $K = \text{diag}(k_i)$, $i = 1, \ldots, r$ and $k_i > 0$, is stable. This particularly useful configuration can be used only if there is the freedom to choose the collocated sensors and actuators, and if the number of the available sensors and actuators is large enough to satisfy the performance requirements.

The stability property allows one to design simple and stable controllers, regardless of the plant parameter variations. However, one has to be aware, that stability does not imply performance, and sometimes the performance of these controllers can be poor, as reported by Hyland [58].

8.2 Dissipative Controllers for Flexible Structures

Consider a structure with the state-space representation (A,B,C) and with an equal number of sensors and actuators. According to the previously introduced property, the collocation of sensors and actuators and positive definite gain makes it dissipative. However, flexible structures inherit a property, which restricts the collocation of sensors and actuators. The restriction follows from its state-space representation, as in (2.28). In this representation the upper half of the matrix B is equal to zero regardless of the configuration of applied forces. Thus, in order to satisfy the collocation requirement, the left half of C must be equal to zero. But the displacement measurements are located in this part (while the right part locates the rates). Consequently, a flexible structure is dissipative if the force inputs and the rate outputs are collocated.

When designing dissipative controllers one has to collocate the sensors and actuators. When working with an analytical model it is beneficial to choose the actuators first, and determine subsequently the sensor locations by introducing $C = B^T$. In this way a physically realizable dissipative system is obtained. In the case when the outputs are determined first and the inputs are picked afterward as $B = C^T$, one still deals with a dissipative system, but not necessarily a physically realizable one. Note also that the collocation of force actuators and rate sensors is a sufficient but by no means necessary condition of dissipativeness. For example, if the weighted collocation is used the system with displacement sensors is dissipative.

For flexible structures we will consider the low-authority controllers. Let the plant have r inputs and outputs. Denote by $K = \text{diag}(k_i)$, $k_i > 0$, $i = 1, ..., r$ the gain matrix of a dissipative controller, then its closed-loop matrix is $A_c = A - BKB^T$. Let A be in the modal form 2, and let b_i be the ith column of B. The dissipative controller is of low authority if for the closed-loop matrix A_c one obtains $\text{eig}(A_c) \cong \text{eig}(A - \sum_{i=1}^{r} k_i \text{diag}(b_i b_i^T))$. In other words, for the low-authority controller one can replace BKB^T with its diagonal terms. For the flexible structures the dissipative controller has the following property:

Property 8.1 ***Relationship Between A, B, and C for the Low-Authority Dissipative Controller.*** *For* $\max(k_i) \le k_o$ *and a controllable and observable flexible system there exists* $k_o > 0$ *such that the dissipative controller is of low authority. Furthermore, if A is in the almost-balanced modal form 2, the following holds:*

$$BB^T \cong -\Gamma(A + A^T) = \text{diag}(\gamma_1\alpha_1, \gamma_1\alpha_1, \gamma_2\alpha_2, \gamma_2\alpha_2, ..., \gamma_n\alpha_n, \gamma_n\alpha_n), \tag{8.4a}$$

$$C^T C \cong -\Gamma(A + A^T) = \text{diag}(\gamma_1\alpha_1, \gamma_1\alpha_1, \gamma_2\alpha_2, \gamma_2\alpha_2, ..., \gamma_n\alpha_n, \gamma_n\alpha_n), \tag{8.4b}$$

or, for the ith block, it can be written as

$$B_i B_i^T \cong -\gamma_i(A_i + A_i^T) = \gamma_i\alpha_i I_2, \tag{8.5a}$$

$$C_i^T C_i \cong -\gamma_i(A_i + A_i^T) = \gamma_i\alpha_i I_2, \tag{8.5b}$$

where $\alpha_i = 2\zeta_i\omega_i$, B_i *is the ith two-row block of B, and* C_i *is the two-column block of C.*

Proof. Note that $b_i K b_j^T$ is the ijth term of BKB^T. Since $(b_i K b_j^T)^2 \le (b_i K b_i^T)(b_j K b_j^T)$, therefore, for A in the modal form 2, and for small gain K such that $\max(k_i) \le k_o$, the off-diagonal terms of BKB^T do not influence the eigenvalues of A_c, and they can be ignored. Equations (8.4) and (8.5) follow from the Lyapunov equations (3.5). ❑

In order to determine the properties of the dissipative controllers in modal coordinates, consider further the dissipativity conditions (8.1) for a structure in

the modal coordinates in the form 2. Consider also a feedback as in (8.3). In this case the closed-loop equations are as follows:

$$\dot{x} = (A - BKC)x + Bu_o, \qquad y = Cx, \tag{8.6}$$

where u_o is a control command ($u_o \equiv 0$ in the case of vibration suppression). Since the matrix A is in the modal form 2, and K is diagonal, $K = \text{diag}(k_1,...,k_r)$, then in the modal coordinates with collocated sensors and actuators one obtains the closed-loop matrix $A_c = A - BKB^T$ in the form

$$A_c = A - \sum_{j=1}^{r} k_j b_j b_j^T, \tag{8.7}$$

where b_j is the jth column of B. In the modal coordinates matrix A_c is block-diagonal, that is, $A_c = \text{diag}(A_{c1},..., A_{cn})$, where A_{ci} is the ith 2×2 block. For this block (8.7) is as follows:

$$A_{ci} \cong A_i - \sum_{j=1}^{r} k_j b_{ji} b_{ji}^T, \tag{8.8}$$

where b_{ji} is the ith block of the jth column of B. In this equation the cross terms $b_{jk} b_{ji}^T$ (for $k \neq i$) are omitted as negligible for the low-authority controllers in the modal coordinates, see Property 8.1. Also, from Property 8.1, the following holds $b_{ji} b_{ji}^T \cong -\gamma_{ji} (A_i + A_i^T)$, where γ_{ji} is the ith Hankel singular value obtained for the jth column of B, i.e., for the triplet (A, b_j, b_j^T). Thus, (8.8) is now

$$A_{ci} \cong A_i + 2k_j \gamma_{ji} (A_i + A_i^T). \tag{8.9}$$

For A_i as in (2.30b), one obtains $A_i + A_i^T = -2\zeta_i \omega_i I_2$, and re-writes (8.9) as follows:

$$A_{ci} \cong \begin{bmatrix} -\beta_i \zeta_i \omega_i & -\omega_i \\ -\omega_i & -\beta_i \zeta_i \omega_i \end{bmatrix}, \tag{8.10a}$$

with the parameter β_i given as

$$\beta_i = 1 + 2\sum_{j=1}^{r} k_j \gamma_{ji} \,. \tag{8.10b}$$

Comparing the closed-loop matrix as in (8.10a), and the open-loop matrix as in (2.30b), it can be seen that β_i is a measure of the shift of the *i*th pair of poles. Denote the closed-loop pair of poles $(\lambda_{cri} \pm j\lambda_{cii})$ and the open-loop pair $(\lambda_{ori} \pm j\lambda_{oii})$, then it follows from (8.10) that they are related

$$(\lambda_{cri} \pm j\lambda_{cii}) \cong (\beta_i \lambda_{ori} \pm j\lambda_{oii}), \qquad i = 1, \ldots, n \,. \tag{8.11}$$

The above equation shows that the real part of the *i*th pair of poles is shifted, while the imaginary part is stationary. The shift is proportional to the gain of each input, and to the *i*th Hankel singular values associated with each input.

Equation (8.10) sets the basic limitation for the dissipative controller design: that the number of inputs (and outputs) limits the number of controlled modes (or controlled pairs of poles). In order to illustrate this, we assume a single-input–single-output system. In this case $\beta_{1i} = 1 + 2k_1\gamma_{1i}$ and the scalar gain k_1 is the only free parameter available for the design. Thus only one pole can be shifted to the required position. If more than one pair should be shifted, their placement would be a least-squares compromise, which typically would be nonsatisfactory. Thus, in order to avoid this rough approximation, it is often required for the dissipative controllers to have a large number of sensors and actuators to meet the required performance criteria.

The pole-shift coefficient β_i is also interpreted as a ratio of the variances of the open-loop (σ_{oi}^2) and closed-loop (σ_{ci}^2) states excited by the white noise input, i.e.,

$$\beta_i \cong \frac{\sigma_{oi}^2}{\sigma_{ci}^2} \,. \tag{8.12}$$

Since $\beta_i \geq 1$, it is therefore a relative measure of the noise suppression of the closed-loop system with respect to the open-loop system. This interpretation follows from the closed-loop Lyapunov equation

$$(A - BKB^T)W_{cc} + W_{cc}(A - BKB^T)^T + BB^T = 0 \,, \tag{8.13a}$$

where W_{cc} is the closed-loop controllability grammian. For the ith pair of variables the above equation is as follows:

$$\left(A_i - \sum_{j=1}^{r} k_j B_{ji} B_{ji}^T\right) w_{cci} + w_{cci}\left(A_i - \sum_{j=1}^{r} k_j B_{ji} B_{ji}^T\right)^T + B_i B_i^T \cong 0 . \tag{8.13b}$$

Introducing (8.5), after some algebra, one obtains

$$w_{cci} + 2 w_{cci}\left(\sum_{j=1}^{r} k_j \gamma_{ji}\right) - w_{oci} \cong 0 , \tag{8.14}$$

where $w_{oci} \cong \gamma_i$ is the diagonal entry of the open-loop controllability grammian. Finally one obtains

$$\frac{w_{oci}}{w_{cci}} = \frac{\sigma_{oi}^2}{\sigma_{ci}^2} \cong 1 + 2\sum_{j=1}^{r} k_j \gamma_{ji} = \beta_i . \tag{8.15}$$

Based on (8.10b), (8.11), and (8.12) a tool for the pole placement of the dissipative controllers is developed. The task is to determine gains k_j, $j = 1, \ldots, r$, such that the selected poles are placed at the required location (or as close as possible in the least-squares sense). Equivalently, the task is to determine gains k_j, j = 1, ..., r, such that the input noise of the selected modes is suppressed at ratio β_i. The approach follows from (8.10b), since one can determine the gains such that q poles are shifted by β_i, $i = 1, \ldots, q$, i.e., $\lambda_{cri} \cong \beta_i \lambda_{ori}$, or the noise can be suppressed by β_i, i.e., $\sigma_{oi}^2 \cong \beta_i \sigma_{ci}^2$. Define the gain vector k

$$k = \begin{bmatrix} k_1 & k_2 & \ldots & k_r \end{bmatrix}, \tag{8.16}$$

so that Eq.(8.10b) can be rewritten as

$$d\beta \cong Gk, \tag{8.17}$$

where $d\beta$ is the vector of the pole shifts

$$d\beta = \begin{bmatrix} \beta_1 - 1 \\ \beta_2 - 1 \\ \vdots \\ \beta_q - 1 \end{bmatrix} \tag{8.18a}$$

and G is the matrix of the system Hankel singular values for each actuator and sensor location

$$G = 2\begin{bmatrix} \gamma_1 & \gamma_2 & \cdots & \gamma_r \end{bmatrix} = 2\begin{bmatrix} \gamma_{11} & \gamma_{21} & \cdots & \gamma_{r1} \\ \gamma_{12} & \gamma_{22} & \cdots & \gamma_{r2} \\ \cdots & \cdots & \cdots & \cdots \\ \gamma_{1q} & \gamma_{2q} & \cdots & \gamma_{rq} \end{bmatrix}, \tag{8.18b}$$

where $\gamma_i = \begin{bmatrix} \gamma_{i1} & \gamma_{i2} & \cdots & \gamma_{iq} \end{bmatrix}^T$ is the set of Hankel singular values for the ith actuator/sensor location, and γ_{ij} is the jth Hankel singular value for the ith actuator/sensor location.

The least-squares solution of (8.17) is obtained

$$k \cong G^+ d\beta, \tag{8.19}$$

where G^+ is the pseudoinverse of G. The set of equations (8.17) is either overdetermined ($q > r$, or rank(G) = r), or square ($q = r$ = rank(G)), or underdetermined ($q < r$, or rank(G) = q), see [54]. The form of the pseudoinverse depends on the number of inputs and outputs r, and the number of poles shifted, q, that is, on the rank of the matrix G.

8.3 Design Examples

Two examples of modal dissipative controller design are presented: the controller design for the simple flexible system, and for the 2D truss structure. The dissipative controller for the Deep Space Network antenna is not investigated, since the antenna predefined inputs and outputs are not suitable for this kind of design.

8.3.1 A Simple Structure

The system is shown in Fig. 1.2, with masses $m_1 = m_2 = m_3 = 1$, stiffness $k_1 = 10$, $k_2 = k_4 = 3$, $k_3 = 4$, and the damping matrix D as a linear

combination of the mass and stiffness matrices, $D = 0.004K+0.001M$. The input force is applied to mass m_3, and the output is the rate of the same mass. The poles of the open-loop system are

$$\lambda_{o1,o2} = -0.0024 \pm j0.9851,$$
$$\lambda_{o3,o4} = -0.0175 \pm j2.9197,$$
$$\lambda_{o5,o6} = -0.0295 \pm j3.8084.$$

The system Hankel singular values are as follows:

$$\gamma_1 = [63.6418, 63.6413, 4.9892, 4.9891, 0.2395, 0.2391]^T.$$

It is required to shift the first pole by increasing its damping twofold, and leave the other poles stationary. For this shift the coefficients are $\beta_1 = 2$, and $\beta_2 = \beta_3 = 1$, therefore $d\beta = [1 \quad 1 \quad 0 \quad 0 \quad 0 \quad 0]^T$. Also for this case $G = 2\gamma_1$, thus the gain $k = 0.0078$ is obtained from (8.19). For this gain, the closed-loop eigenvalues were computed

$$\lambda_{c1,c2} = -0.0049 \pm j0.9851,$$
$$\lambda_{c3,c4} = -0.0189 \pm j2.9197,$$
$$\lambda_{c5,c6} = -0.0296 \pm j3.8084,$$

and from this result one can see that the actual shifts $\beta_1 = 1.9939$, $\beta_2 = 1.0779$, and $\beta_3 = 1.0037$ are close to the required ones.

Next, consider a design that increases the first and the second pole damping twofold, and leaves the third stationary. In this case $\beta_1 = \beta_2 = 2$ and $\beta_3 = 1$ is required, therefore $d\beta = [1 \quad 1 \quad 1 \quad 1 \quad 0 \quad 0]^T$. The gain $k = 0.0084$ is obtained from (8.19), and the closed-loop eigenvalues for this gain are computed:

$$\lambda_{c1,c2} = -0.0051 \pm j0.9851,$$
$$\lambda_{c3,c4} = -0.0190 \pm j2.9197,$$
$$\lambda_{c5,c6} = -0.0296 \pm j3.8084.$$

Comparing the open- and closed-loop poles, one can see that the actual shifts, $\beta_1 = 2.0718$, $\beta_2 = 1.0840$, and $\beta_3 = 1.0040$, are almost the same as in the first case. Thus, we hardly meet the requirements. This case shows that for the underdetermined problem (the number of inputs is smaller than the number

of poles to be shifted), the obtained least-squares result is the best but not satisfactory.

8.3.2 The 2D Truss

The 2D truss is presented in Fig. 1.3, with the damping matrix proportional to the mass and stiffness matrix, $D = 0.3M + 0.00002K$. Control forces are applied at node 4, directed horizontally, and at node 10, directed vertically. The rate output is collocated with the force. The system has 16 modes. The two most controllable and observable modes are suppressed by increasing their damping 60 times. The required feedback gain is obtained from (8.19). Note that in this case $\beta_1 = \beta_2 = 60$, and the remaining β's are equal to 1. Let γ_1 and γ_2 be vectors of the Hankel singular values for the first input and output, and for the second input and output, respectively. Then $G = 2[\gamma_1 \quad \gamma_2]$. For this case $d\beta = [59 \quad 59 \quad 59 \quad 59 \quad 0 \quad 0 \quad \ldots \quad 0]^T$, and one obtains from (8.19) the gain matrix $k = \text{diag}(4.3768, \quad 385.0546)$.

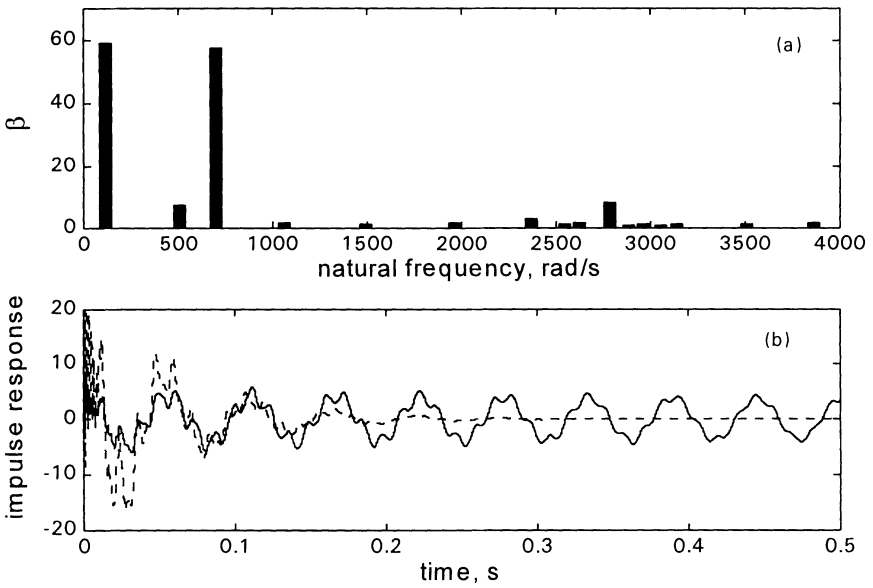

Figure 8.1. A dissipative controller for the 2D truss: (a) coefficient β_i; and (b) open-loop (solid line) and closed-loop (dashed line) impulse responses.

For this gain the closed-loop poles were determined, and the pole shift was obtained as a ratio of real parts of the closed- and open-loop poles, as in

definition (8.11), i.e., $\beta_i = \lambda_{cri}/\lambda_{ori}$. The plot of β_i in Fig. 8.1 shows that $\beta_1 = 58.94$ and $\beta_2 = 57.46$ are close to the assigned value of 60. The damping of the two poles increased 60 times, while the other poles changed insignificantly.

9
LQG Controllers

The control issues for flexible structures include the maintenance of precise positioning or tracking. It is expected that these requirements should be satisfied for structures with natural frequencies within the controller bandwidth and within the disturbance spectra. LQG controllers (Linear system, Quadratic cost, Gaussian noise) are often used for tracking and disturbance rejection purposes. A good insight into the problems of analysis and design of LQG controllers can be obtained from the books by Kwakernaak and Sivan [71], Maciejowski [81], Anderson and Moore [3], Furuta and Sano [31], Lin [78], Skogestad and Postlethwaite [102], and Dorato et al. [22].

Two issues in LQG controller design are of special importance: the determination of the weights of the performance index, and controller order reduction. The first issue – weight determination – ultimately impacts the closed-loop system performance, in terms of the tracking accuracy and the disturbance rejection properties. If the weights of the LQG performance index are inappropriately chosen, the LQG controller performance will not satisfy the requirements. The selection of weights is most often not an easy task. As stated by Lin [78, p. 93] "It takes a great deal of experience to transform design requirements and objectives to the performance index that will produce the desired performance." Our task is to replace experience with analytical tools.

The second issue – controller order reduction – impacts the implementation in terms of complexity and accuracy of the controller software. These problems are especially important for flexible structures, since the structure models are typically of high order, making order reduction a necessity. The order of the controller is equal to the order of the plant, which is often unacceptably high.

W. K. Gawronski, *Dynamics and Control of Structures*

In this chapter both problems: weight determination and controller order reduction, are solved in the modal coordinates. The properties of flexible structures that allow one to solve the two mentioned problems efficiently are subsequently derived.

9.1 Definition and Gains

A block diagram of an LQG controller is shown in Fig. 9.1, where a stable plant is described as follows:

$$\dot{x} = Ax + Bu + v, \qquad y = Cx + w\,. \tag{9.1}$$

The plant is perturbed by random disturbances, v, and the output is noise-corrupted, w. The noise v, called process noise, has covariance $V = E(vv^T)$, the measurement noise w has covariance $W = E(ww^T)$, and both noises are uncorrelated, i.e., $E(vw^T) = 0$, where $E(.)$ is the expectation operator. Without loss of generality, it is assumed further that $W = I$. The plant state vector is denoted x and the estimated state is denoted $\hat{x}$. The performance of the system is shaped by the estimator gain (K_e) and the controller gain (K_p). The task is to determine the controller and estimator gains such that the performance index J

$$J^2 = E\left(\int_0^\infty (x^T Qx + u^T Ru)\, dt \right) \tag{9.2}$$

is minimal, where R is a positive definite input weight matrix, and Q is a positive semidefinite state weight matrix. It is assumed further that $R = I$ without loss of generality.

The estimated state is obtained from the following equations:

$$\dot{\hat{x}} = A\hat{x} + Bu + K_e(y - C\hat{x})\,. \tag{9.3}$$

The minimum of J is obtained for the feedback

$$u = -K_c\hat{x}, \tag{9.4}$$

with the gain matrix,

$$K_c = B^T S_c\,, \tag{9.5a}$$

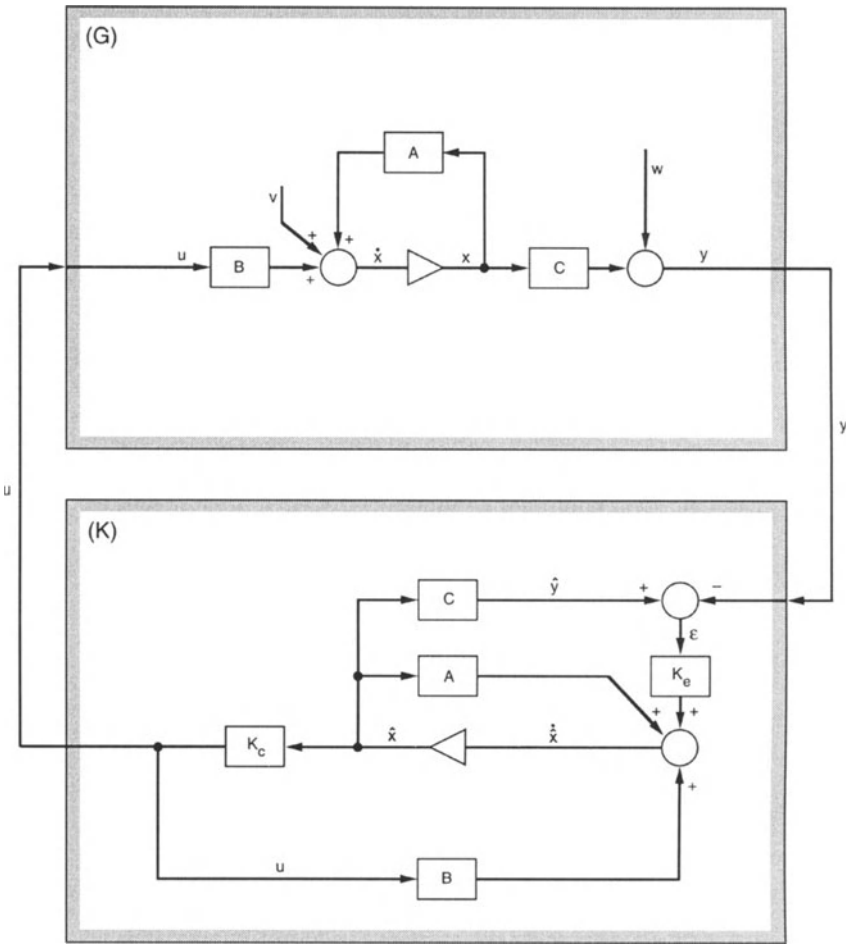

Figure 9.1. The LQG closed-loop system.

and S_c is the solution of the controller algebraic Riccati equation (CARE)

$$A^T S_c + S_c A - S_c B B^T S_c + Q = 0 . \tag{9.6a}$$

The optimal estimator gain is given by

$$K_e = S_e C^T , \tag{9.5b}$$

where S_e is the solution of the filter (or estimator) algebraic Riccati equation (FARE)

$$AS_e + S_e A^T - S_e C^T C S_e + V = 0. \tag{9.6b}$$

The controller state-space representation $(A_{lqg}, B_{lqg}, C_{lqg})$ from input y to output u is as follows:

$$A_{lqg} = A + BK_c + K_e C, \tag{9.7a}$$

$$B_{lqg} = -K_e, \tag{9.7b}$$

$$C_{lqg} = K_c. \tag{9.7c}$$

9.2 Balanced LQG Controller

For a controllable and observable system there exists a state-space representation such that the CARE and FARE solutions are equal and diagonal, see [63], [89], and [36]

$$S_c = S_e = \mathrm{M} = \mathrm{diag}(\mu_1, \mu_2, ..., \mu_N), \qquad \mu_1 \geq \mu_2 \geq \cdots \geq \mu_N > 0 \tag{9.8}$$

where M is a diagonal positive definite $\mathrm{M} = \mathrm{diag}(\mu_i)$, $i = 1, \ldots, N$, $\mu_i > 0$. A state-space representation with condition (9.8) satisfied is an LQG balanced representation, and μ_i, $i = 1, \ldots, N$, are its LQG singular (or characteristic) values.

Let R be the transformation of the state x such that $x = R\bar{x}$. Then the solutions of CARE and FARE, and the weighting matrices in the new coordinates, are as follows:

$$\bar{S}_c = R^T S_c R, \qquad \bar{S}_e = R^{-1} S_e R^{-T}, \tag{9.9a}$$

$$\bar{Q}_c = R^T Q_c R, \qquad \bar{Q}_e = R^{-1} Q_e R^{-T}. \tag{9.9b}$$

The transformation R to the LQG balanced representation is obtained as follows. Decompose S_c and S_e,

$$S_c = P_c^T P_c, \qquad S_e = P_e P_e^T, \tag{9.10a}$$

and form a matrix H, such that

$$H = P_c P_e \,. \tag{9.10b}$$

Find the singular value decomposition of H

$$H = V\mathrm{M}U^T, \tag{9.10c}$$

then the transformation matrix is obtained either as

$$R = P_e U\mathrm{M}^{-1/2} \tag{9.10d}$$

or

$$R = P_c^{-1} V\mathrm{M}^{1/2} \,. \tag{9.10e}$$

Proof. By inspection. Introduce R to (9.9a) to show that (9.8) is satisfied. ❑

The Matlab function *bal_LQG* which transforms a representation (A,B,C) to the LQG balanced representation (A_b, B_b, C_b) is given in Appendix A.6.

9.3 Weights of Special Interest

We discuss here weighting matrices of special form, and the corresponding CARE/FARE solutions. First, for a fully controllable system, consider the weights Q and V as follows:

$$Q = 2W_c^{-1} BB^T W_c^{-1}, \qquad V = 2W_o^{-1} C^T C W_o^{-1} \,. \tag{9.11}$$

In this case one obtains the inverses of the controllability and observability grammians as the CARE and FARE solutions

$$S_c = W_c^{-1}, \qquad S_e = W_o^{-1} \,. \tag{9.12}$$

This can be proved by introduction of (9.11) and (9.12) into CARE, which gives

$$A^T S_c + S_c A + S_c BB^T S_c = 0 \,. \tag{9.13}$$

Introducing $S_c = W_c^{-1}$ gives the Lyapunov equations (3.5). A similar proof can be shown for the solution of FARE.

The weights as in (9.11) penalize each state reciprocally to its degree of controllability and observability. Particularly, when the weights Q and V are determined in the open-loop balanced modal representation, one obtains from (9.11) that the system is LQG balanced, with $S_c = S_e = \mathrm{M} = \Gamma^{-1}$.

Next, define the closed-loop performance. Let $W_c = \mathrm{diag}(w_{ci} I_2)$, and $W_{cl} = \mathrm{diag}(w_{cli} I_2)$, $i = 1, \ldots, n$, be the matrices of open- and closed-loop controllability grammians. The matrix B, defined as follows:

$$\mathrm{B} = W_c W_{cl}^{-1} = \mathrm{diag}(\beta_i) = \mathrm{diag}\left(\frac{w_{ci}}{w_{cli}}\right) \tag{9.14}$$

is the ratio of open-loop (w_{ci}) and closed-loop (w_{cli}) state variances excited by the white noise input.

For the weights as in (9.11), and a system in the modal coordinates, one obtains each state of the plant and estimator, equally influenced by the feedback. As a result

$$\mathrm{B} = 3I\,. \tag{9.15}$$

This follows from the Lyapunov equations for the closed-loop controllability grammian W_{cl}, which is obtained from the following equation:

$$(A - BB^T S_c) W_{cl} + W_{cl}(A^T - S_c BB^T) + BB^T = 0\,. \tag{9.16a}$$

According to (9.12), $S_c = W_c^{-1}$, and introducing $W_{cl} = W_c/3$ to (9.16a), one obtains

$$AW_c + W_c A^T + BB^T = 0\,, \tag{9.16b}$$

which shows that $W_{cl} = W_c/3$ is a solution of (9.16a), and consequently that $B = 3I$.

Consider another set of weights of a fully controllable system, namely

$$Q = C^T C + W_o BB^T W_o, \qquad V = BB^T + W_c C^T C W_c\,, \tag{9.17}$$

then one obtains the observability and controllability grammians as solutions of CARE and FARE

$$S_c = W_o, \qquad S_e = W_c. \tag{9.18}$$

This can be proved simply by the introduction of (9.18) to the CARE and FARE equations. If the system is in the open-loop balanced representation, then the system is LQG balanced, with the Hankel singular values and the LQG singular values identical, $S_c = S_e = \mathrm{M} = \Gamma$.

9.4 Low-Authority LQG Controller

The design of the LQG controller seems to be a straightforward task. It goes as follows: given weights Q and V one obtains the gains K_c and K_e from (9.5a) and (9.5b), and the controller representation from (9.7). However, from the implementation point of view, this approach is not appropriately defined. The weights that meet requirements are not known, thus the gains cannot be determined. The design process starts from the definition of the required closed-loop system performance, such as the norm of the tracking error, or the location of the closed-loop poles. Thus, one has to find appropriate weights Q and V that meet the performance requirements. This task does not have an analytical solution in general, and is frequently solved using a trial-and-error approach. In the following sections this problem is solved using the properties of flexible structures.

The low-authority property of a flexible structure under LQG control can be formulated as follows. Let (A,B,C) be the open-loop modal representation of a flexible structure (in the modal form 1 or 2), and let $A_{c1} = A - BB^T S_c$, $A_{c2} = A - S_e C^T C$ be the closed-loop matrices, where S_c and S_e are the solutions of the CARE and FARE equations, respectively. Denote by b_i the ith row of B. The LQG controller is of low authority if the closed-loop matrices are as follows $A_{c1} \cong \mathrm{eig}(A - \mathrm{diag}(BB^T)S_c)$ and $A_{c2} \cong \mathrm{eig}(A - S_e \mathrm{diag}(C^T C))$. In other words, for the low-authority controller, BB^T and $C^T C$ can be replaced with their diagonal terms. The low-authority LQG controller has the following property:

Property 9.1 ***Relationship Between A, B, and C for the Low-Authority LQG Controller.*** *Let* $\|S_c\|_2 \le s_o$ *and* $\|S_e\|_2 \le s_o$. *For a controllable and observable flexible system there exists* $s_o > 0$ *such that the controller is of low authority. Furthermore, if A is in the modal form 1, one can use the following replacement for* BB^T *(or* $C^T C$*)*

$$BB^T \cong -W_c(A+A^T) = \text{diag}\,(0,2w_{c1}\alpha_1,0,2w_{c2}\alpha_2,...,0,2w_{cn}\alpha_n), \tag{9.19a}$$

$$C^TC \cong -W_o(A+A^T) = \text{diag}\,(0,2w_{o1}\alpha_1,0,2w_{o2}\alpha_2,...,0,2w_{on}\alpha_n), \tag{9.19b}$$

or, for the ith block,

$$B_iB_i^T \cong -w_{ci}(A_i+A_i^T) = w_{ci}\begin{bmatrix}0 & 0\\ 0 & 2\alpha_i\end{bmatrix}, \tag{9.20a}$$

$$C_i^TC_i \cong -w_{oi}(A_i+A_i^T) = w_{oi}\begin{bmatrix}0 & 0\\ 0 & 2\alpha_i\end{bmatrix}, \tag{9.20b}$$

where $\alpha_i = 2\zeta_i\omega_i$. *If A is in the modal form 2 the following replacement is used*

$$BB^T \cong -W_c(A+A^T) = \text{diag}\,(w_{c1}\alpha_1,w_{c1}\alpha_1,w_{c2}\alpha_2,w_{c2}\alpha_2,...,w_{cn}\alpha_n,w_{cn}\alpha_n) \tag{9.21a}$$

$$C^TC \cong -W_o(A+A^T) = \text{diag}\,(w_{o1}\alpha_1,w_{o1}\alpha_1,w_{o2}\alpha_2,w_{o2}\alpha_2,...,w_{on}\alpha_n,w_{on}\alpha_n) \tag{9.21b}$$

or, for the ith block,

$$B_iB_i^T \cong -w_{ci}(A_i+A_i^T) = w_{ci}\alpha_i I_2, \tag{9.22a}$$

$$C_i^TC_i \cong -w_{oi}(A_i+A_i^T) = w_{oi}\alpha_i I_2, \tag{9.22b}$$

B_i *is the ith two-row block of B, and* C_i *is the two-column block of C.*

Proof. Note that for the positive semidefinite matrix BB^T one obtains $(b_ib_j^T)^2 \le (b_ib_i^T)(b_jb_j^T)$, i.e., that the off-diagonal terms do not exceed the geometric mean value of the corresponding diagonal terms. Therefore, if A is in modal form 1 or 2, and for small S_c such that $\|S_c\|_2 \le s_o$, the off-diagonal terms of BB^T do not influence the eigenvalues of A_{c1}, i.e., $A_{c1} = \text{eig}(A - BB^TS_c)$. If the matrix BB^T is obtained from the Lyapunov equations (3.5) and replaced by its diagonal terms, one obtains (9.19) – (9.22). Similar applies to the eigenvalues of $A - S_eCC^T$. ❑

The low authority property is illustrated with the LQG controller for a simple structure as in Fig. 1.2. The root locus for the third mode and for the increasing values of the matrix S_c is marked "o" in Fig. 9.2. The approximate root-locus, using the diagonal part of BB^T is marked "•" in the same figure.

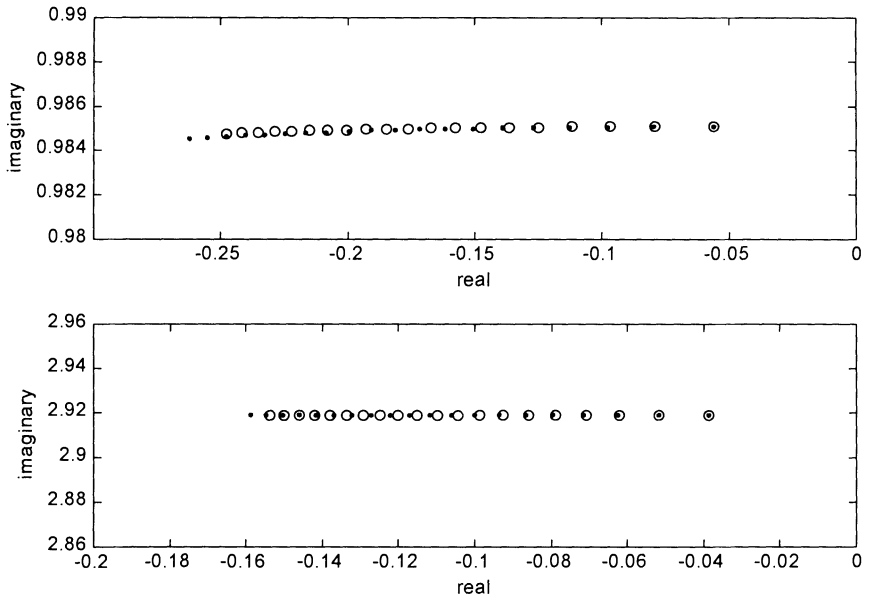

Figure 9.2. The exact (o) and approximate (•) root-locus of a simple system: (a) first pole, (b) second pole.

The figure shows good agreement between the exact and approximate roots for small S_c.

9.5 Approximate Solutions of CARE and FARE

For the LQG design in modal coordinates we use diagonal weight matrices Q and V. This significantly simplifies the design process, and can be justified as follows. The term $E\int_0^\infty x^T Qx dt$ represents the participation of weight Q in the performance index J. It is evaluated as follows:

$$E\int_0^\infty x^T Qx dt = E\int_0^\infty \sum_{i,j=1}^{N} q_{ij} x_i x_j \, dt \,, \tag{9.23}$$

where x_i is the ith component of x. For the positive definite matrix Q one obtains

$$q_{ij}^2 \le q_i q_j, \tag{9.24}$$

and in the modal coordinates the grammians are diagonally dominant, see Property 3.1, therefore the modal coordinates are almost orthogonal, that is,

$$\left(E\int_0^\infty x_i x_j\, dt\right)^2 << \left(E\int_0^\infty x_i^2\, dt\right)\left(E\int_0^\infty x_j^2\, dt\right). \tag{9.25a}$$

Introducing (9.24) and (9.25) to (9.23), one obtains

$$E\int_0^\infty x^T Q x\, dt \cong E\int_0^\infty \sum_{i=1}^{N} q_{ii} x_i x_j\, dt = E\int_0^\infty x^T Q_d x\, dt, \tag{9.25b}$$

where Q_d is a diagonal matrix that consists of the diagonal entries of Q.

Due to the duality of Q and V, the same applies to the matrix V, that is, in modal coordinates the full matrix V can be replaced with its diagonal part V_d, and the system performance remains almost unchanged.

Next, based on Property 9.1, it will be shown that the low-authority controllers in the modal representation produce diagonally dominant solutions of the CARE and FARE equations.

Property 9.2(a) ***Approximate Solution of CARE.*** *Assume a diagonal weight matrix* $Q = \text{diag}(q_i I_2)$, $i = 1,\dots,n$, *then there exist* $q_i \le q_{oi}$, *where* $q_{oi} > 0$, $i = 1,\dots,n$, *such that*

(a) $$S_c \cong diag(s_{ci} I_2) \tag{9.26a}$$

is the solution of (9.6a), and

(b) $$s_{ci} \cong \frac{\beta_{ci} - 1}{2w_{ci}}, \qquad \beta_{ci} = \sqrt{1 + \frac{2q_i w_{ci}}{\zeta_i \omega_i}}. \tag{9.26b}$$

Proof. (a) Note that for $Q = 0$ one obtains $S_c = 0$. For small Q the CARE transforms into the following Lyapunov equation $A^T S_c + S_c A + Q = 0$. For a modal matrix A and diagonal Q the solution of this equation is diagonally dominant, see Property 3.1. Thus there exist $q_i \le q_{oi}$, where $q_{oi} > 0$, $i = 1,\dots,n$, such that (9.26a) holds.

(b) For diagonally dominant S_c, (9.6a) turns into a set of the following equations:

$$s_{ci}(A_i + A_i^T) - s_{ci}^2 B_i B_i^T + q_i I_2 \cong 0, \qquad i = 1,...,n. \tag{9.27a}$$

For a low-authority controller in modal coordinates one obtains $B_i B_i^T \cong -w_{ci}(A_i + A_i^T)$ and $A_i + A_i^T = -2\zeta_i \omega_i I_2$, see (9.22a). Therefore the above equation is now in the following form

$$s_{ci}^2 + \frac{s_{ci}}{w_{ci}} - \frac{q_i}{2\zeta_i \omega_i w_{ci}} \cong 0, \qquad i = 1,...,n. \tag{9.27b}$$

There are two solutions of the above equation, but for a stable system and for $q_i = 0$ it is required that $s_{ci} = 0$, therefore (9.26) is the unique solution of (9.27b). ❑

A similar result is obtained for the FARE equation.

Property 9.2(b) ***Approximate Solution of FARE.*** *For a diagonal V, $V = \text{diag}(v_i I_2)$, $i = 1,\ldots,n$, there exist $v_i \le v_{oi}$ where $v_{oi} > 0$, $i = 1,\ldots,n$, such that*

(a) $$S_e \cong diag(s_{ei} I_2) \tag{9.28a}$$

is the solution of (9.6b), where

(b) $$s_{ei} \cong \frac{\beta_{ei} - 1}{2w_{oi}}, \quad \text{where} \quad \beta_{ei} = \sqrt{1 + \frac{2v_i w_{oi}}{\zeta_i \omega_i}}. \tag{9.28b}$$

Equations (9.26) and (9.28) allow one to determine the LQG singular values as follows:

$$\mu_i \cong \frac{\sqrt{(\beta_{ci} - 1)(\beta_{ei} - 1)}}{2\gamma_i}, \qquad i = 1,\ldots,n. \tag{9.29}$$

Also, the diagonally dominant solutions of CARE and FARE allow one to determine the relationship between the weights and the root-locus, which is a useful tool of controller design.

Property 9.3(a) ***LQG Root-Locus.*** *Let the weight Q be*

$$Q = \text{diag}(0,0,\ldots,q_i I_2,\ldots,0,0), \tag{9.30}$$

then for the low-authority controller $(q_i \le q_{oi})$ the closed-loop pair of flexible poles $(\lambda_{cri} \pm j\lambda_{cii})$ relates to the open-loop poles $(\lambda_{ori} \pm j\lambda_{oii})$ as follows:

$$(\lambda_{cri} \pm j\lambda_{cii}) \cong (\beta_{ci}\lambda_{ori} \pm j\lambda_{oii}), \qquad i = 1,\ldots,n, \tag{9.31}$$

where β_{ci} is defined in (9.26).

Proof. For small weight q_i the matrix A of the closed-loop system is diagonally dominant, i.e., $A_c \cong \text{diag}(A_{ci})$, $i = 1,\ldots,n$, and $A_{ci} = A_i - B_i B_i^T s_{ci}$. Introducing (9.22a), one obtains

$$A_{ci} \cong A_i + 2s_{ci}\gamma_i(A_i + A_i^T) \tag{9.32a}$$

and introducing A_i as in (3.2) to the above equation one obtains

$$A_{ci} \cong \begin{bmatrix} -\beta_{ci}\zeta_i\omega_i & -\omega_i \\ \omega_i & -\beta_{ci}\zeta_i\omega_i \end{bmatrix}, \tag{9.32b}$$

with β_{ci} as in (9.26). ❑

This result implies that the weight Q as in (9.30) shifts the ith pair of complex poles of the flexible structure, and leaves the remaining pairs of poles almost unchanged. Only the real part of the pair of poles is changed (just moving the pole apart from the imaginary axis and stabilizing the system), and the imaginary part of the poles remains unchanged.

The above proposition has additional interpretations. Note that the real part of the ith open-loop pole is $\lambda_{oi} = -\zeta_i\omega_i$, and that the real part of the ith closed-loop pole is $\lambda_{ci} = -\zeta_{ci}\omega_i$; note also that the height of the open-loop resonant peak is $\alpha_{oi} = \kappa/2\zeta_i\omega_i$, where κ is a constant, and the closed-loop resonant peak is $\alpha_{ci} = \kappa/2\zeta_{ci}\omega_i$. From (9.31) one obtains $\beta_{ci} = \lambda_{cri}/\lambda_{ori}$, hence

$$\beta_{ci} = \frac{\zeta_{ci}}{\zeta_i} = \frac{\alpha_{oi}}{\alpha_{ci}} \tag{9.33}$$

is a ratio of the closed- and open-loop damping factors, or it is a ratio of the open- and closed-loop resonant peaks. Therefore, if a suppression of the *i*th resonant peak by the factor β_{ci} is required, the appropriate weight q_i is determined from (9.26), obtaining

$$q_i \cong \frac{(\beta_{ci}^2 - 1)\zeta_i \omega_i}{2w_{ci}} . \tag{9.34}$$

The coefficient β_{ci} is also interpreted as a ratio of the variances of open-loop (σ_{oi}^2) and closed-loop (σ_{ci}^2) states excited by the white noise input

$$\beta_{ci} \cong \frac{w_{oci}}{w_{cci}} = \frac{\sigma_{oi}^2}{\sigma_{ci}^2} . \tag{9.35}$$

This interpretation follows from the closed-loop Lyapunov equations

$$(A - BB^T S_c)W_c + W_c(A - BB^T S_c)^T + BB^T = 0, \tag{9.36a}$$

which for the *i*th pair of variables is as follows:

$$(A_i - B_i B_i^T s_{ci})w_{cci} + w_{cci}(A_i - B_i B_i^T s_{ci})^T + B_i B_i^T \cong 0 . \tag{9.36b}$$

Introducing (9.22a) gives

$$w_{cci} + 2w_{cci} w_{oci} s_{ci} - w_{oci} \cong 0 \tag{9.36c}$$

or

$$\frac{w_{oci}}{w_{cci}} \cong 1 + s_{ci} w_{oci} = \beta_{ci} . \tag{9.36d}$$

The plots of β_{ci} with respect to the weight q_i and for the controllability coefficient of the *i*th mode, $w_{ci} = 1$ are shown in Fig. 9.3. One obtains the same plot with respect to w_{ci} for $q_i = 1$.

The estimator poles are shifted in a similar manner.

Property 9.3(b) ***Estimator Root Locus.*** *Denote*

$$V = \text{diag}(0,0,...,v_i I_2,...,0,0), \tag{9.37}$$

then for moderate weights $(v_i \le v_{oi})$, *and the estimator pair of poles* $(\lambda_{eri} \pm j\lambda_{eii})$ *relates to the open-loop poles* $(\lambda_{ori} \pm j\lambda_{oii})$ *as follows:*

$$(\lambda_{\text{eri}}, \pm j\lambda_{\text{eii}}) \cong (\beta_{ei}\lambda_{\text{ori}}, \pm j\lambda_{\text{oii}}), \qquad i = 1,...,n, \tag{9.38}$$

where β_{ei} *is defined in (9.28).*

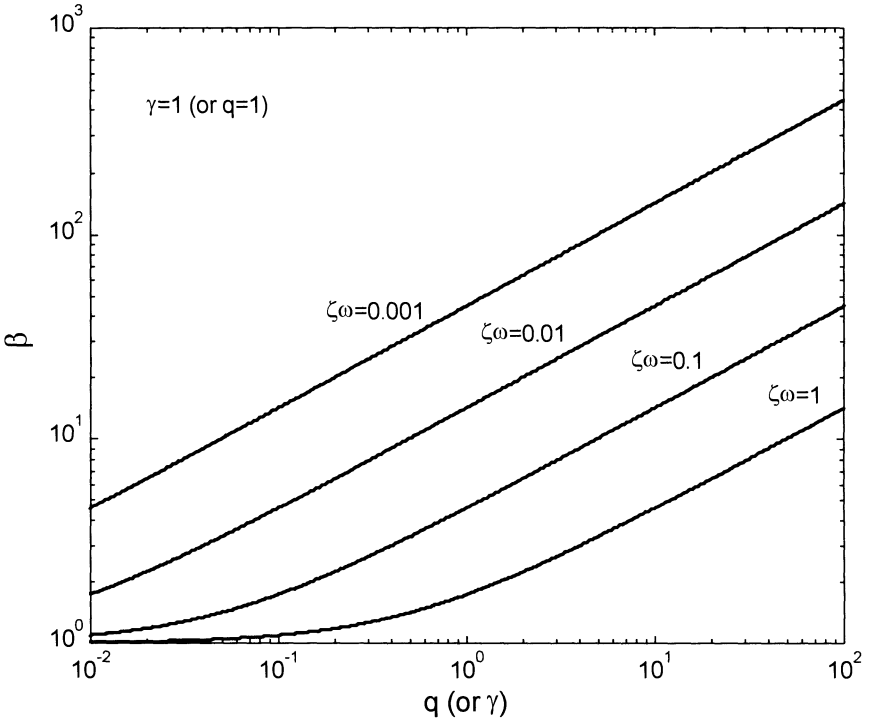

Figure 9.3. Coefficient β versus weight q for $\gamma = 1$, or versus the Hankel singular value γ for $q = 1$.

The above applies for controllers with limited damping authority, i.e., controllers that modify only moderately the system natural frequencies, as defined by Aubrun and Marguiles, see [5] and [6]. The controller authority is limited by the values q_{oi} and v_{oi} such that for the limited damping authority one has $q_i \le q_{oi}$ and $v_i \le v_{oi}$. The limiting values q_{oi} and v_{oi} are not difficult

to determine. There are several symptoms that the weight q_i approaches q_{oi} (or that v_i approaches v_{oi}). Namely, q_{oi} is the weight at which the ith pair of complex poles of the plant departs significantly from the horizontal trajectory in the root-locus plane and approaches the real axis. Alternatively, it is a weight at which the ith resonant peak of the plant transfer function disappears (the peak is flattened). A similar result applies to the estimator weights v_{oi}.

9.6 Almost-LQG-Balanced Modal Representation

For the diagonally dominant solutions of CARE and FARE in modal coordinates ($S_c \cong \text{diag}(s_{ci}I_2)$, $S_e \cong \text{diag}(s_{ei}I_2)$, $i = 1, ..., n$), an approximately balanced solution M of CARE and FARE is obtained. It is diagonally dominant as a geometric mean of CARE and FARE, i.e.,

$$\text{M} \cong \text{diag}(\mu_i I_2), \qquad \text{where} \qquad \mu_i = \sqrt{s_{ci}s_{ei}}, \qquad i = 1,...,n. \tag{9.39}$$

The transformation R from the modal representation (A,B,C) to the LQG balanced representation $(A_{lqg},B_{lqg},C_{lqg})$ is diagonally dominant as well,

$$R \cong diag(r_1 I_2, r_2 I_2,...,r_n I_2), \qquad r_i = \left(\frac{s_{ei}}{s_{ci}}\right)^{1/4}, \tag{9.40}$$

where the LQG balanced representation is approximately obtained from the following transformation $(A_{lqg},B_{lqg},C_{lqg}) \cong (A, R^{-1}B, CR)$. Note that this transformation requires only a rescaling of the modes, or the state input and output matrices.

Property 9.4 ***Weights that Approximately LQG Balance the Modal Representation.*** *If the system is in the almost-balanced modal representation, and the weights Q and V are equal and diagonal, $Q = V = \text{diag}(q_i)$, the solutions of the Riccati equations are almost identical*

$$s_{ci} \cong s_{ei}, \qquad i = 1,...,n, \tag{9.41a}$$

and the open-loop and LQG balanced representations approximately coincide, i.e.,

$$(A_{lqg},B_{lqg},C_{lqg}) \cong (A,B,C). \tag{9.41b}$$

Proof. Introducing $q_i = v_i$ and $w_{ci} = w_{oi}$ to (9.26) and (9.28) one finds that $s_{ci} \cong s_{ei}$, $i = 1,...,n$. In this case, from (9.40) it follows that $R \cong I$, hence the open-loop and LQG balanced representations are approximately identical. ❐

9.7 Three Ways to Compute LQG Singular Values

From the above analysis one can use one of three ways to compute LQG singular values.

1. From the algorithm in Section 9.2. This algorithm gives the exact LQG singular values. However, the relationship between the LQG singular value and the corresponding natural mode it represents is neither explicit nor obvious.
2. From (9.39). This is an approximate value that gives a connection between the LQG singular values and the corresponding modes.
3. From (9.29). This is an approximate value related to a specific mode. It is a closed-form equation that gives an explicit relationship between structural parameters and the singular value.

9.8 The Tracking LQG Controller

Previously considered LQG controllers were designed for vibration suppression purposes. A more complex task includes a tracking controller with a required tracking performance in addition to vibration suppression properties. This is the case of controllers for radar and microwave antennas, such as the NASA Deep Space Network antennas. A configuration for this kind of controller should assure zero steady-state tracking error, which is achieved by adding an integral of the plant position to the plant state-space representation, as reported in [4], [28], [29], [61], [92], and [114]. This closed-loop system configuration of the tracking LQG controller is shown in Fig. 9.4. In this figure (A,B,C) is the plant state-space triple, x is the state, $\hat{x}$ is the estimated state, $\hat{x}_f$ is the estimated state of a flexible part, r is the command, u is the control input, y is the output, $\hat{y}$ is the estimated output, $e = r - \hat{y}$ is the servo error, e_i is the integral of servo error, v is the process noise of intensity V, and the measurement noise w is of intensity W. Both v and w are uncorrelated: $E(vw^T) = 0$, $V = E(vv^T)$, $W = E(ww^T) = I$, $E(v) = 0$, and $E(w) = 0$.

For the open-loop state-space representation (A,B,C) of a flexible structure divide the state vector x into the tracking, x_t, and flexible, x_f, parts

$$x = \begin{pmatrix} x_t \\ x_f \end{pmatrix}. \tag{9.42}$$

For this division the system triple can be presented as follows (see [46]):

$$A = \begin{bmatrix} A_t & A_{tf} \\ 0 & A_f \end{bmatrix}, \qquad B = \begin{bmatrix} B_t \\ B_f \end{bmatrix}, \qquad C = \begin{bmatrix} C_t & 0 \end{bmatrix}. \tag{9.43a}$$

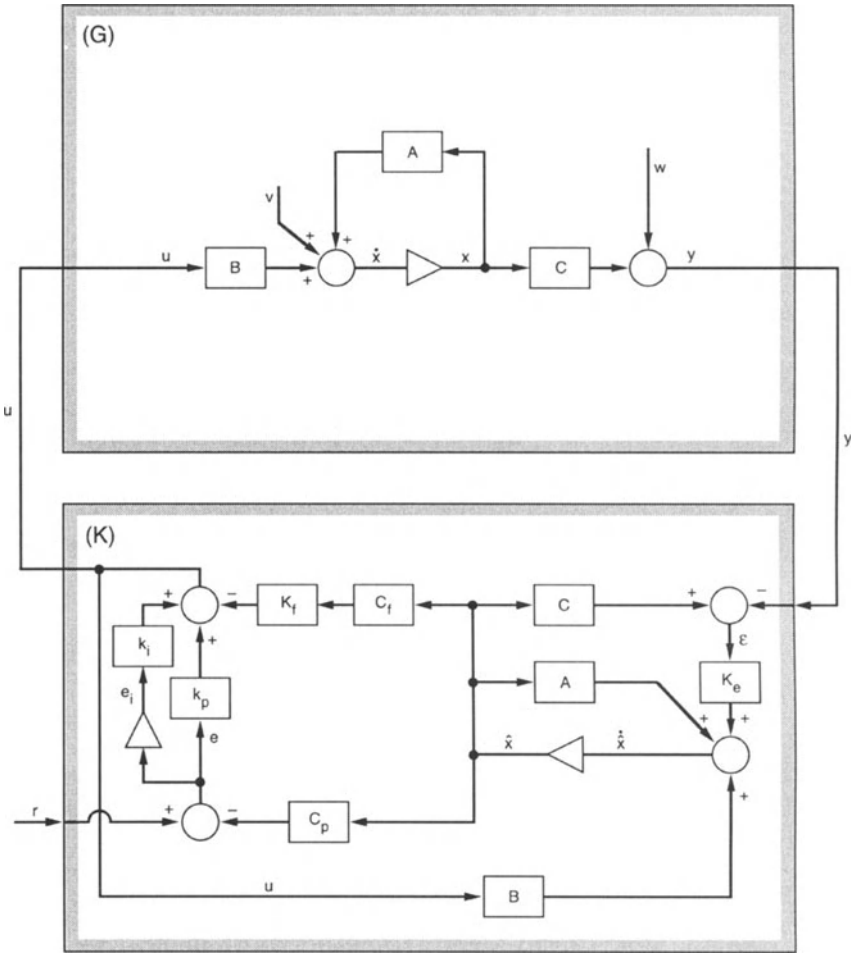

Figure 9.4. The tracking LQG controller with an integral upgrade.

The gain, K_c, the weight, Q, and solution of CARE, S_c, are divided similarly to x

$$K_c = \begin{bmatrix} K_{ct} & K_{cf} \end{bmatrix}, \qquad Q = \begin{bmatrix} Q_t & 0 \\ 0 & Q_f \end{bmatrix}, \qquad \text{and} \qquad S_c = \begin{bmatrix} S_{ct} & S_{ctf} \\ S_{ctf}^T & S_{cf} \end{bmatrix}. \tag{9.43b}$$

The tracking system is considered to be of low authority, if the flexible weights are much smaller than the tracking ones, i.e., such that $\|Q_t\| >> \|Q_f\|$. It was shown by Collins et al., [16] that for $Q_f = 0$ one obtains $S_{cf} = 0$ and $S_{ctf} = 0$. It means that the gain of the tracking part, K_{ct}, does not depend on the flexible part. And for the low-authority tracking system (with small Q_f), one obtains weak dependence of the tracking gains on the flexible weights, due to the continuity of the solution. Similar conclusions apply to the FARE equation (9.6b).

This property can be validated by observation of the closed-loop transfer functions for different weights for the Deep Space Network antenna, as in Fig. 9.5. Denote by I_n and 0_n the identity and zero matrices of order n, then the magnitude of the closed-loop transfer function (azimuth angle to azimuth command) for $Q_t = I_2$ and $Q_f = 0_{10}$ is shown as a solid line, for $Q_t = I_2$ and $Q_f = 5 \times I_{10}$ as a dashed line, and for $Q_t = 8 \times I_2$ and $Q_f = 0_{10}$ as a dot–dashed line in Fig. 9.5. It follows from the plots that variations in Q_f changed the properties of the flexible subsystem only, while variations in Q_t changed the properties of both subsystems.

Note, however, that the larger Q_f increases dependency of the gains on the flexible system; only a quasi-independence in the final stage of controller design is observed, while separation in the initial stages of controller design is still strong. The design consists therefore of the initial choice of weights for the tracking subsystem, and determination of the controller gains of the flexible subsystem. It is followed by the adjustment of weights of the tracking subsystem, and a final tuning of the flexible weights, if necessary.

This approach is similar to the high-/low-authority controller design, reported in [5], [6], and [104]. The high-authority controller is designed to assure required performance, while the low-authority controller is used as a robust inner loop for suppressing the plant responses outside the high-authority controller bandwidth. The low-authority controller has limited damping authority, i.e., it is allowed to modify only moderately the system poles, see [6].

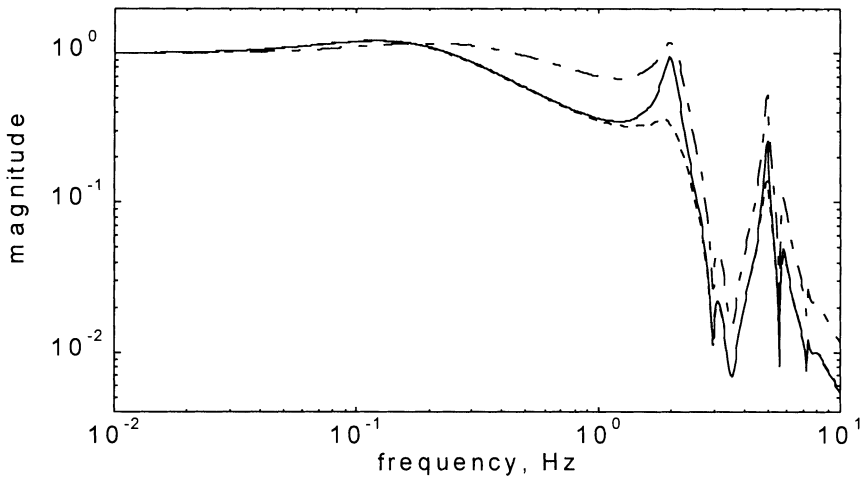

Figure 9.5. Magnitudes of the transfer function of a closed-loop system for different LQG weights.

9.9 Frequency Weighting

The LQG controller can be designed to meet stringent tracking requirements and, at the same time, maintain the binding disturbance rejection properties. In order to achieve this, the problem should be appropriately defined in quantitative terms. For this purpose the frequency shaping filters are used to define tracking requirements, or disturbance rejection performance of the closed-loop system. These filters are used only in the controller design stage. They add to the complexity of the problem, since in the process of design the number of system equations varies and their parameters are modified. As stated by Voth et al. [104, p. 55] "The selection of the controller gains and filters as well as the controller architecture is an iterative, and often tedious, process that relies heavily on the designers' experience."

We will show in this section that this complex task can be simplified in the case of flexible structure control. Flexible structures have special properties that allow for a comparatively simple incorporation of filters. Namely, for the system in modal representation, the addition of a filter is equivalent to the multiplication of each row of the input matrix (or input gains) by a constant. The ith constant is the filter gain at the ith natural frequency of the structure. In this way each natural mode is weighted separately. This approach addresses the system performance at the mode level, which simplifies an otherwise ad hoc and tedious process.

Let (A,B,C) be the state-space representation of G, with s inputs and r outputs, and let (A_i,B_i,C_i) and G_i be the state-space representation of the ith mode and its transfer function, respectively. Introduce the transfer function

$$\overline{G} = \sum_{i=1}^{n} \overline{G}_i , \tag{9.44}$$

where

$$\overline{G}_i = C_i(j\omega I - A_i)^{-1}\overline{B}_i \tag{9.45a}$$

and

$$\overline{B}_i = B_i\alpha_i , \qquad \alpha_i = |F(\omega_i)| . \tag{9.45b}$$

Above, $\overline{G}_i$ is a transfer function G_i with the scaled input matrix B_i.

For the LQG controller the H_2 norm of the transfer function GF is used as a system performance measure. In the modal representation this norm is approximated as follows:

Property 9.5(a) ***LQG Input Filtering.*** *The H_2 norm of a structure with a smooth input filter is approximately equal to the H_2 norm of a structure with a scaled input matrix B*

$$\|GF\|_2 \cong \|\overline{G}\|_2 . \tag{9.46}$$

Proof. Using Property 4.2 one obtains

$$\|GF\|_2^2 \cong \sum_{i=1}^{n} \|G_i\alpha_i\|_2^2 = \sum_{i=1}^{n} \|\overline{G}_i\|_2^2 = \|\overline{G}\|_2^2 . \qquad \square$$

Equation (9.46) shows that the application of the input filter for the H_2 performance modeling is equivalent to the scaling of the $2\times s$ modal input matrix B_i with α_i.

Property 9.5(b) ***LQG Output Filtering.*** *The H_2 norm of a structure with a smooth output filter is approximately equal to the H_2 norm of a structure with a scaled output matrix C*

$$\|FG\|_2 \cong \|\overline{G}\|_2, \tag{9.47}$$

where

$$\overline{G} = \sum_{i=1}^{n} \overline{G}_i, \tag{9.48a}$$

$$\overline{G}_i = \overline{C}_i (j\omega I - A_i)^{-1} B_i, \tag{9.48b}$$

and

$$\overline{C}_i = \alpha_i C_i. \tag{9.48c}$$

Proof. Similar to the one of Property 9.5(a). ❐

Note that Property 9.5 preserves the order and physical (modal) interpretation of the transfer function, and the corresponding state variables. This simplifies the controller design process, since the relationship between filter gains and system performance is readily available.

9.10 Reduced-Order LQG Controller

The size of a plant determines the size of a controller. However, the size of the plant is often too large to be acceptable for implementation. It is crucial to obtain a controller of the smallest possible order that preserves the stability and performance of the full-order controller. However, the plant model should not be reduced excessively in advance, in order to assure the quality of the closed-loop system design. Therefore, controller reduction is a part of controller design. The modal LQG design procedure provides this opportunity.

9.10.1 The Reduction Index

In order to perform controller reduction successfully, an index of the importance of each controller mode is introduced. In the open-loop case, modal norms served as reduction indices. In the closed-loop case, LQG singular values were

used as reduction indices by Jonckheere and Silverman, [63] for symmetric and passive systems. Unfortunately, they produce unstable controllers. This is illustrated by the simple structure example in this section, where the most important controller mode has the lowest LQG singular value.

In this chapter the effectiveness of the closed-loop system is evaluated by the degree of suppression of flexible motion of the structure. The suppression, in turn, depends on the pole mobility to the left-hand side of the complex plane. Therefore, if a particular pair of poles is moved easily (i.e., when a small amount of weight is required to move the poles), the respective states are easy to control and estimate. On the contrary, if a particular pair of poles is difficult to move (i.e., even a large amount of weight moves the poles insignificantly), the respective states are difficult to control and to estimate. In the latter case, the action of the controller is irrelevant, and the states which are difficult to control and estimate are reduced; this demonstrates heuristically the rationale of the choice of the pole mobility as an indicator of the importance of controller states.

For the LQG system in modal coordinates the reduction index σ_i is defined as a product of a Hankel singular value and the LQG singular value of the system

$$\sigma_i = \gamma_i \mu_i . \tag{9.49}$$

It combines the observability and controllability properties of the open-loop system and the controller performance. This choice is a result of the fact that σ_i is a measure of the ith pole mobility. In order to show it note, from (9.29), and (9.49), that σ_i is the geometric mean of the plant and the estimator pole mobility indexes, i.e.,

$$\sigma_i \cong 0.5\sqrt{(\beta_{ci}-1)(\beta_{ei}-1)} . \tag{9.50}$$

This equation reveals, for example, that for $\beta_{ci} = 1$ the ith controller pole is stationary, and σ_i is equal to zero. Similarly, for $\beta_{ei} = 1$ the ith estimator pole is stationary, and σ_i is equal to zero. However, for a shifted pole one obtains $\beta_{ci} > 1$, $\beta_{ei} > 1$, hence the index is also "shifted," that is, $\sigma_i > 0$.

Denote by σ_{oi}^2 the variance of the open-loop response to white noise, and by σ_{ci}^2 the variance of the closed-loop response to white noise, and note that $w_{oci} = \sigma_{oi}^2$ and $w_{cci} = \sigma_{ci}^2$, where w_{oci} and w_{cci} are the diagonal entries of the open- and closed-loop controllability grammians. Denote $\Delta\sigma_i^2 = \sigma_{oi}^2 - \sigma_{ci}^2$ the change of the response of the open- and closed-loop systems due to white noise. Then a useful interpretation of the reduction index follows from (9.36d):

$$\sigma_i \cong \frac{\Delta\sigma_i^2}{2\sigma_{ci}^2}. \tag{9.51}$$

This equation shows that the reduction index is proportional to the relative change of the response of the open- and closed-loop systems due to white noise. Having defined σ_i as the controller performance evaluation tool, the reduction technique is developed.

In order to find the reduction index from (9.49) the problem of the determination of Hankel singular values and LQG singular values arises. They are found as follows. In modal coordinates the Hankel singular values are approximately equal to the geometric mean of the corresponding controllability and observability grammians, i.e.,

$$\gamma_i \cong \sqrt{w_{cii} w_{oii}}, \tag{9.52}$$

where w_{cii} and w_{oii} are the ith diagonal entries of the controllability and observability grammians, respectively. Similarly, in modal coordinates the solutions of the CARE and FARE equations are approximately equal to the geometric mean of the corresponding CARE and FARE solutions

$$\mu_i \cong \sqrt{s_{cii} s_{eii}}, \tag{9.53}$$

where s_{cii} and s_{eii} are the ith diagonal entries of the CARE and FARE solutions, respectively.

9.10.2 The Reduction Technique

In order to introduce the controller reduction technique, the matrix Σ of the reduction indices is defined as $\Sigma = \mathrm{diag}(\sigma_1, \sigma_2, \ldots, \sigma_N)$, and from (9.49) it follows immediately that

$$\Sigma = \Gamma \mathrm{M}. \tag{9.54}$$

Next, the diagonal entries σ_i in Σ are put in descending order, i.e., $\sigma_i > 0$, $\sigma_i \geq \sigma_{i+1}$, $i = 1, \ldots, N$, and the matrix is divided as follows:

$$\Sigma = \begin{bmatrix} \Sigma_r & 0 \\ 0 & \Sigma_t \end{bmatrix}, \tag{9.55}$$

where Σ_r consists of the first k entries of Σ, and then Σ_l the remaining ones. If the entries of Σ_l are small in comparison with the entries of Σ_r, the controller can be reduced by truncating its last $N-k$ states.

Note that the value of the index σ_i depends on the weight q_i, so that the reduction depends on the weight choice. For example, if for a given weight a particular resonant peak is too large to be accepted (or a pair of poles is too close to the imaginary axis, or the amplitudes of vibrations at this resonance frequency are unacceptable high), the weighting of this particular mode should be increased to suppress this mode. The growth of weight increases the value of σ_i, which can save this particular mode from reduction.

9.10.3 Stability of the Reduced-Order Controller

The question of stability of the closed-loop system with the reduced-order controller should be answered before implementation of the controller. In order to answer this question, consider the closed-loop system as in Fig.9.1. Denoting the state

$$x_o = \begin{Bmatrix} x \\ \varepsilon \end{Bmatrix} \tag{9.56}$$

and $\varepsilon = x - \hat{x}$, one obtains the following closed-loop equations:

$$\dot{x}_o = A_o x_o + B_o r + B_v v + B_w w, y = C_o x_o + w, \tag{9.57a}$$

where

$$A_o = \begin{bmatrix} A - BK_c & BK_c \\ 0 & A - K_e C \end{bmatrix}, \tag{9.57b}$$

$$B_o = \begin{bmatrix} B \\ 0 \end{bmatrix}, \qquad B_v = \begin{bmatrix} I \\ I \end{bmatrix}, \qquad B_w = \begin{bmatrix} 0 \\ -K_e \end{bmatrix}, \qquad C_o = \begin{bmatrix} C & 0 \end{bmatrix}. \tag{9.57c}$$

Let the matrices A, B, C of the estimator be partitioned conformingly to Σ in (9.55)

$$A = \begin{bmatrix} A_r & 0 \\ 0 & A_l \end{bmatrix}, \qquad B = \begin{bmatrix} B_r \\ B_l \end{bmatrix}, \qquad C = \begin{bmatrix} C_r & C_l \end{bmatrix} \tag{9.58a}$$

then the reduced controller representation is (A_r, B_r, C_r). The controller gains are divided similarly

$$K_c = \begin{bmatrix} K_{cr} & K_{cl} \end{bmatrix}, \qquad K_e = \begin{bmatrix} K_{er} \\ K_{el} \end{bmatrix}, \tag{9.58b}$$

and the resulting reduced closed-loop system is as follows:

$$A_{or} = \begin{bmatrix} A - BK_p & BK_{pr} \\ 0 & A_r - K_{er}C_r \end{bmatrix}, \tag{9.59a}$$

$$B_{or} = \begin{bmatrix} B \\ 0 \end{bmatrix}, \qquad B_{vr} = \begin{bmatrix} I \\ I_r \end{bmatrix}, \qquad B_w = \begin{bmatrix} 0 \\ -K_{er} \end{bmatrix}, \qquad C_o = \begin{bmatrix} C & 0_r \end{bmatrix}. \tag{9.59b}$$

Define the stability margin of matrix A_o as follows:

$$m(A_o) = \min_i(-\mathrm{Re}(\lambda_i(A_o))), \tag{9.60}$$

where Re(.) denotes a real part of a complex variable, and $\lambda_i(.)$ is the ith eigenvalue of a matrix.

Property 9.6 ***Stability of the Reduced-Order Controller.*** *For* $\|\Sigma_l\| << \|\Sigma_r\|$, *one obtains* $m(A_o) \cong m(A_{or})$, *where* A_{or} *is a closed-loop matrix of a system with the reduced controller, and* A_l *is the state matrix of the truncated part. Hence the reduced-order controller is stable.*

Proof. Introduce (9.58) and (9.59) to (9.57b) to obtain

$$A_o = \begin{bmatrix} A_{or} & A_{o1} \\ A_{o2} & A_l - K_{el}C_l \end{bmatrix}, \tag{9.61a}$$

where

$$A_{o1} = \begin{bmatrix} B_r K_{cl} \\ B_l K_{cl} \\ -K_{er}C_l \end{bmatrix}, \qquad A_{o2} = \begin{bmatrix} 0 & 0 & -K_{el}C_r \end{bmatrix}. \tag{9.61b}$$

The matrix A_o is divided into four blocks, with the upper left block A_{or}. Thus in order to prove that $m(A_o) \cong m(A_{or})$, it is sufficient to show that: (a) in the lower left block $\|K_{et}C_r\| \cong 0$; and (b) $m(A_t) \geq m(A_o)$; i.e., that in the lower right block $\|K_{et}C_t\| \cong 0$. But for (a) from (9.22) one obtains $\|K_{et}C_r\| = \|M_t C_t^T C_r\| << \|M_t C_t^T C_t\| \cong \|\Sigma_t\| \cong 0$; similarly, for (b) $\|K_{et}C_t\| = \|M_t C_t^T C_t\| \cong \|\Sigma_t\| \cong 0$. ❑

9.10.4 Performance of the Reduced-Order Controller

In addition to the stability evaluation, the performance of the reduced-order controller is assessed. Denote by $\varepsilon^T = \begin{bmatrix} \varepsilon_r^T & \varepsilon_t^T \end{bmatrix}$ the estimation error of the full-order controller and by ε_{rr} the estimation error of the reduced-order controller.

Property 9.7 ***Performance of the Reduced-Order Controller.*** *If the states with small reduction indices are truncated, then one obtains*

$$\varepsilon_r \cong \varepsilon_{rr} \qquad \text{and} \qquad \varepsilon_t \cong 0 . \tag{9.62}$$

Proof. Note that for A_o as in (9.61a) the estimation error is

$$\dot{\varepsilon}_r = (A_r - K_{er}C_r)\varepsilon_r - K_{er}C_t\varepsilon_t \quad \text{and} \quad \dot{\varepsilon}_t = K_{et}C_r\varepsilon_r + (A_t - K_{et}C_t)\varepsilon_t . \tag{9.63a}$$

But, from (9.59) the error of the reduced-order controller is

$$\dot{\varepsilon}_{rr} = (A_r - K_{er}C_r)\varepsilon_{rr} . \tag{9.63b}$$

As shown previously $\|K_{er}C_t\| \cong 0$, and $\|K_{et}C_t\| \cong 0$ for small σ_i, thus $\varepsilon_r \cong \varepsilon_{rr}$. Additionally, one obtains $\dot{\varepsilon}_t \cong A_t\varepsilon_t$, imposing that for stable A_t the truncation error vanishes ($\varepsilon_t \to 0$) with elapsing time ($t \to \infty$). ❑

The above property implies that for $\|\Sigma_t\| << \|\Sigma_r\|$ the performance of the reduced- and full-order controllers is approximately the same. The performance of the full- and reduced-order controllers is compared in the design examples section.

9.11 Design Examples

Examples of modal LQG controller design are presented for the simple flexible system for the 3D truss structure, and for the Deep Space Network antenna.

9.11.1 A Simple Structure

The system is shown in Fig. 1.2, with masses $m_1 = m_2 = m_3 = 1$, stiffnesses $k_1 = 10$, $k_2 = 3$, $k_3 = 4$, and $k_4 = 3$, and a damping matrix $D = 0.004K + 0.001M$, where K, M are the stiffness and mass matrices, respectively. The input force is applied to mass m_3, the output is the displacement of the same mass, and the poles of the open-loop system are

$$\lambda_{o1,o2} = -0.0024 \pm j0.9851,$$
$$\lambda_{o3,o4} = -0.0175 \pm j2.9197,$$
$$\lambda_{o5,o6} = -0.0295 \pm j3.8084.$$

The system Hankel singular values for each mode are: $\gamma_1 = 64.60$, $\gamma_2 = 1.71$, and $\gamma_3 = 0.063$.

The weight matrix Q and the covariance matrix V are chosen as follows: $Q = V = \text{diag}(0.5, 0.5, 1, 1, 2.5, 2.5)$. For these matrices the solution S_c of CARE and the solution S_e of FARE are diagonally dominant,

$$S_c \cong \text{diag}(1.32,\ 0.84,\ 2.54,\ 2.71,\ 12.94,\ 13.38),$$
$$S_e \cong \text{diag}(2.09,\ 1.60,\ 6.72,\ 6.60,\ 29.65,\ 29.51).$$

The approximate LQG singular values are obtained from (9.35), as a geometric mean of the CARE/FARE solutions

$$M_{al} \cong (S_c S_e)^{1/2} \cong \text{diag}(1.66,\ 1.16,\ 4.13,\ 4.23,\ 19.59,\ 19.87),$$

while the exact LQG singular values are

$$M = \text{diag}(1.60,\ 1.10,\ 3.90\,,4.20,\ 19.55,\ 19.86)\,.$$

The approximate LQG singular values obtained from (9.29) and the exact ones (from the algorithm in Section 9.2) are plotted in Fig. 9.6(a).

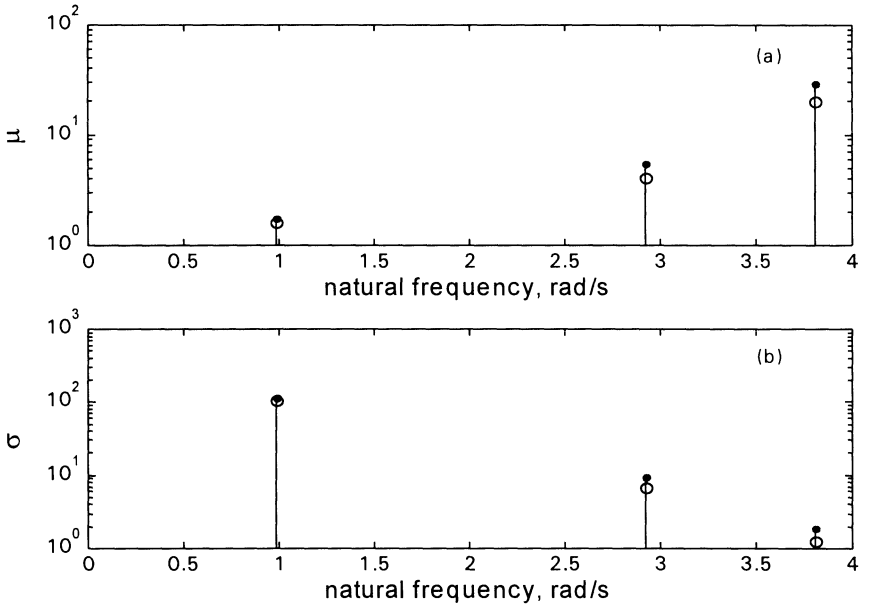

Figure 9.6. A simple system: (a) the LQG singular values, exact (o) and approximate (•); and (b) the controller reduction index, exact (o) and approximate (•).

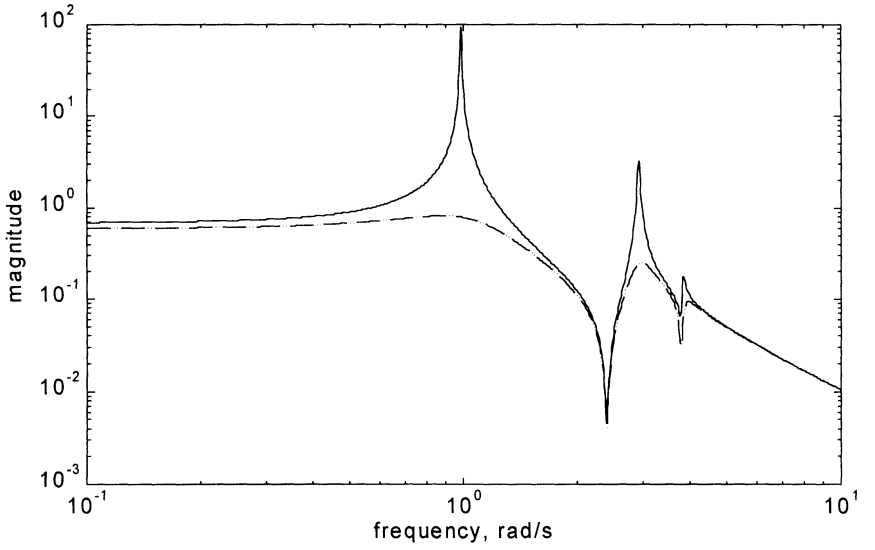

Figure 9.7. Magnitudes of the transfer function of the open-loop (solid line), and closed-loop (dashed line) simple structure.

The magnitudes of the open- and closed-loop transfer functions are shown in Fig. 9.7. The weights Q and V shift the poles to the right, so that the peaks of the open-loop transfer function (solid line in Fig. 9.7) are flattened, see the closed-loop transfer function (dashed line in Fig. 9.7).

The controller reduction matrix Σ is obtained as $\Sigma = M\Gamma$ from the exact and approximate values of M and Γ. Their plots are shown in Fig. 9.6(b). The approximate values of Σ are not quite close enough to the true ones, but the obtained accuracy is good enough to select the truncated modes. The third mode with the smallest reduction index ($\sigma_3 = 1.25$) is truncated, and the reduced LQG controller with a two-mode estimator is applied. The closed-loop transfer functions with full- and reduced-order controllers coincide, as shown in Fig. 9.8, solid and dashed lines, respectively.

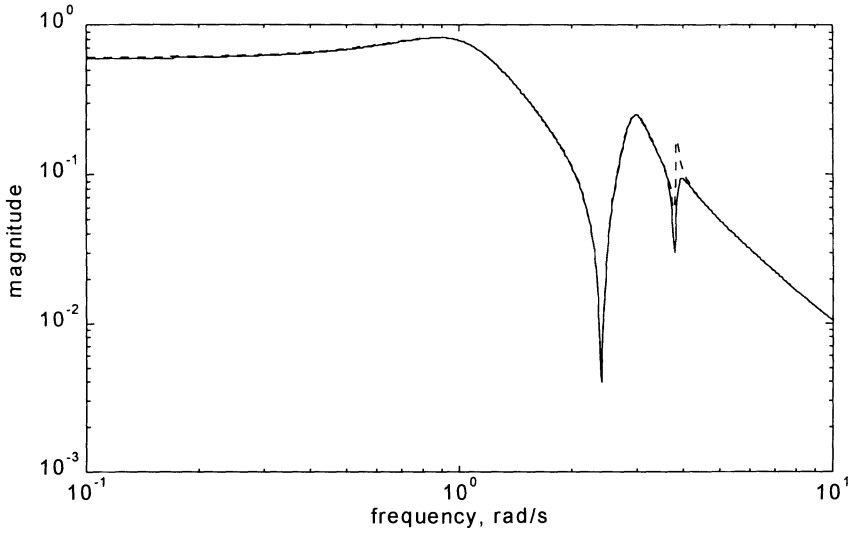

Figure 9.8. Magnitudes of the transfer function of the closed-loop simple structure with full-order (solid line), and reduced-order (dashed line) LQG controller.

9.11.2 The 3D Truss

The 3D truss as presented in Fig. 1.4 is analyzed. A vertical control force is applied at nodes 18 and 24 (the first input), and a horizontal force is applied at nodes 6 and 18 (the second input). The combined vertical displacement at nodes 6 and 12 is the first output, and the combined horizontal displacement at nodes 5 and 17 is the second output. The system is in modal almost-balanced representation, and it has (after reduction) 34 states (or 17 modes). The weight

(Q) and the covariance (V) matrices were assumed equal and diagonal, $Q = V = \text{diag}(q_1, q_1, q_2, q_2, \ldots, q_{17}, q_{17})$ where $q_1 = q_2 = 400$, $q_3 = q_4 = 4000$, $q_5 = q_6 = 40000$, $q_7 = \cdots = q_{17} = 400$. In this case the CARE and FARE solutions are approximately equal and diagonally dominant, as stated in Section 9.5. The resulting LQG singular values, exact and approximate from (9.29), show in Fig. 9.9(a) a satisfactory coincidence. Poles of the open- as well the closed-loop system and the estimator are shown in Fig. 9.10. For the modal almost-balanced controller the poles of the closed-loop system and the estimator overlap.

The open-loop (solid line) and closed-loop (dashed line) impulse responses from the first input to the first output show, in Fig. 9.11(a), good damping properties of the closed-loop system. The open-loop transfer function (solid line in Fig. 9.11(b)) and the closed-loop transfer function (dashed line in the same figure) show that the oscillatory motion of the structure is damped out. The diagonal entries of the reduction matrix Σ are shown in Fig. 9.9(b). They were obtained from (9.54) using exact and approximate values of Γ and M. The controller is reduced by truncating 18 states, which correspond to the small reduction indices ($\sigma_i < 0.01$). The resulting reduced-order controller has 16 states. The magnitude of the transfer function of the full- (solid line) and reduced-order (dashed line) controller overlap in Fig.9.12.

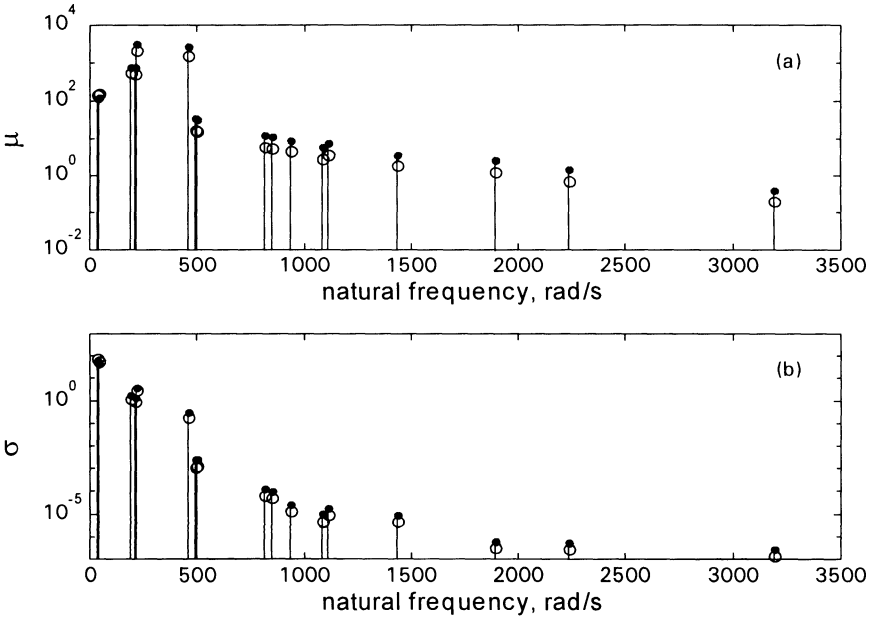

Figure 9.9. The 3D truss: (a) LQG singular values, exact (o) and approximate (•); and (b) controller reduction index, exact (o) and approximate (•).

9.11.3 The 3D Truss with Input Filter

Consider a steel truss as in Fig. 1.4. The disturbance is applied at node 7 in the z-direction, the performance is measured at node 21, in the z-direction; the input u is applied at node 20 in the z-direction, and the output y is a displacement of node 28, in the z-direction. The open-loop transfer function from the disturbance to the performance is shown in Fig. 9.13 (solid line). The disturbance input is filtered with a low-pass filter, $F(s) = 1/(1+0.011s)$, and the magnitude of its transfer function is shown in the same figure by a dot–dashed line. The resulting transfer function of the structure and filter is represented by the dotted line.

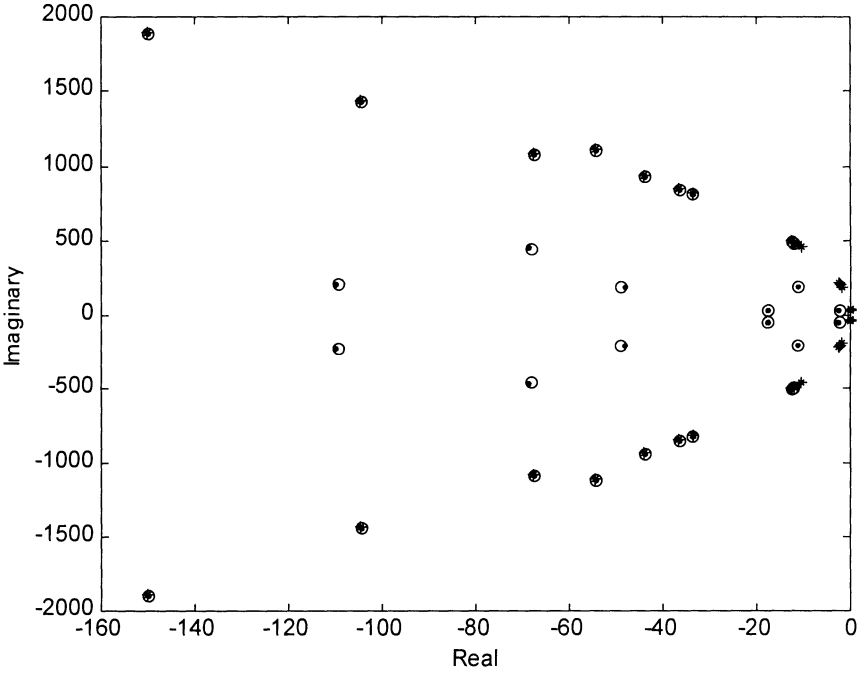

Figure 9.10. Poles of the open-loop truss (∗), the closed-loop truss (•), and poles of the estimator (○).

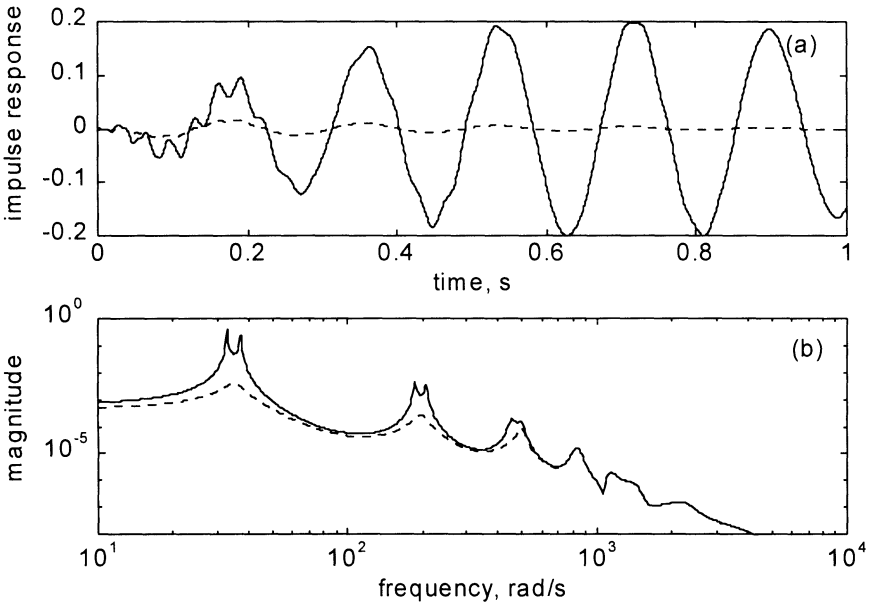

Figure 9.11. The 3D truss: (a) impulse responses; and (b) magnitudes of the transfer function of the open-loop (solid line) and closed-loop (dashed line) truss, from the first input to the first output.

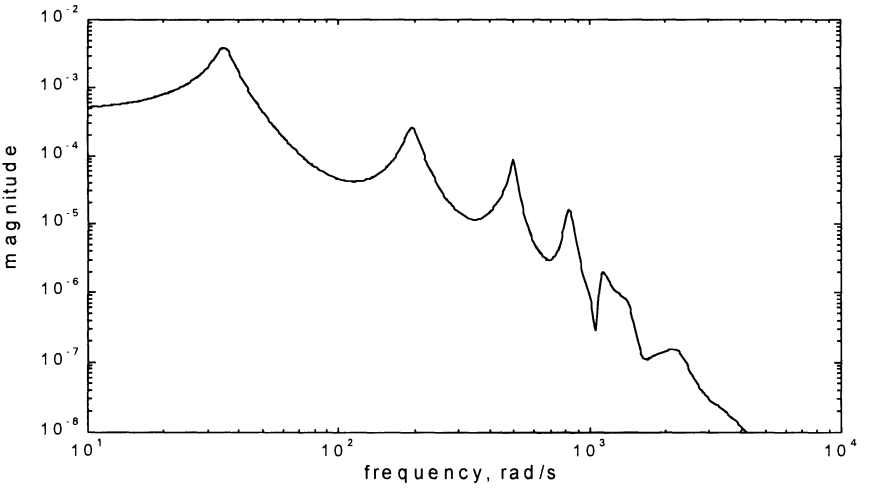

Figure 9.12. Overlapped magnitudes of the transfer function of the closed-loop truss with a full-order (solid line), and reduced-order (dashed line) LQG controller.

The equivalent structure with the filter was obtained by scaling the disturbance input, according to (9.45a,b), and the magnitude of its transfer function is shown in Fig. 9.13 (dashed line). It is clear from that figure that the structure with the filter, and the structure with the scaled disturbance input, have similar frequency characteristics, and their norms are $\|G\|_2 = 453.2945$ for the structure with the filter, and $\|G\|_2 = 453.5661$ for the structure with the scaled disturbance input.

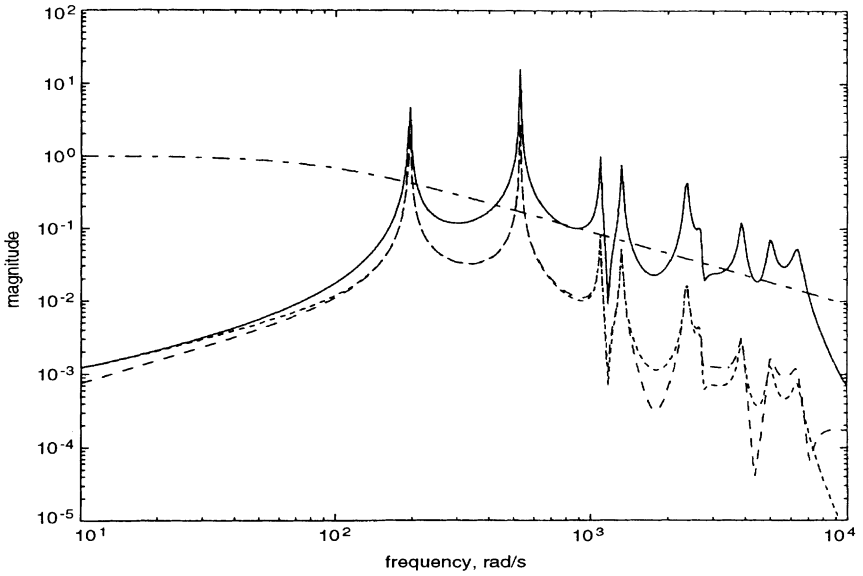

Figure 9.13. Magnitudes of the transfer function of the truss (solid line), filter (dash–dot line), truss with filter (dotted line), and truss with scaled disturbance input (dashed line).

Two frequency weighted LQG controllers for this structure were designed. The first one is based on the structure with a filter, while the second is based on the structure with a scaled input matrix. The closed-loop H_2 norms are as follows: $\|G_{cl}\|_2 = 108.6295$ for the structure with the filter, and $\|G_{cl}\|_2 = 108.7181$ for the structure with the scaled disturbance input.

9.11.4 The Deep Space Network Antenna

The design of a modal LQG controller is illustrated by the Deep Space Network antenna. For this design the 18-state reduced antenna modal model obtained in Chapter 5 is used. The weight, Q, and plant noise covariance, V, are assumed equal and diagonal.

The Deep Space Network antenna model is upgraded with the integral-of-the-position state, thus it consists of two tracking states in azimuth (azimuth angle and its integral), a state with the real pole that corresponds to the drive dynamics, and eight flexible modes (or 16 states). The preliminary weights $q_1 = q_2 = 1$ for the tracking subsystem (for the angle y and its integrals y_i) the drive state weight is $q_3 = 33$, and the weights for the flexible subsystem were chosen such that the flexible modes were damped ($q_4 = \cdots = q_7 = 33$, $q_8 = \cdots = q_{19} = 10$). The step response of the closed-loop system is shown in Fig. 9.14(a), with 8 s settling time. The closed-loop transfer function is shown in Fig. 9.14(b), with a bandwidth of 0.2 Hz.

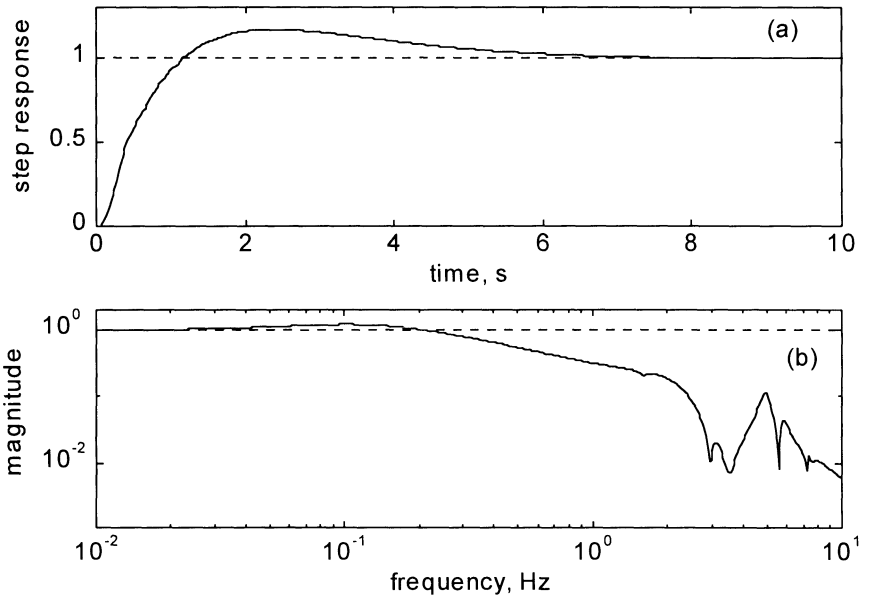

Figure 9.14. Initial design of the antenna LQG controller: (a) closed-loop step response; and (b) closed-loop magnitude of the transfer function.

In the next step, the tracking properties of the system are improved by the additional weight adjustment of the tracking subsystem. By setting the proportional and integral weight to $q_1 = q_2 = 100$ the tracking properties are improved, as is visible in the step response in Fig. 9.15(a) (small overshoot and settling time of 3 s) and in the magnitude of the transfer function Fig. 9.15(b) (extended bandwidth up to 2 Hz).

The reduced-order controller is obtained through evaluation of controller reduction indices σ_i. The plot of σ_i is shown in Fig. 9.16. Reducing the order of the estimator to 10 states (the first two are tracking states, and the next eight

are flexible mode states) yields a stable and accurate closed-loop system. The reduced-order controller is compared with the full-order controller in the step response plots in Fig. 9.15(a) and with the transfer function plots in Fig. 9.15(b), showing satisfactory accuracy.

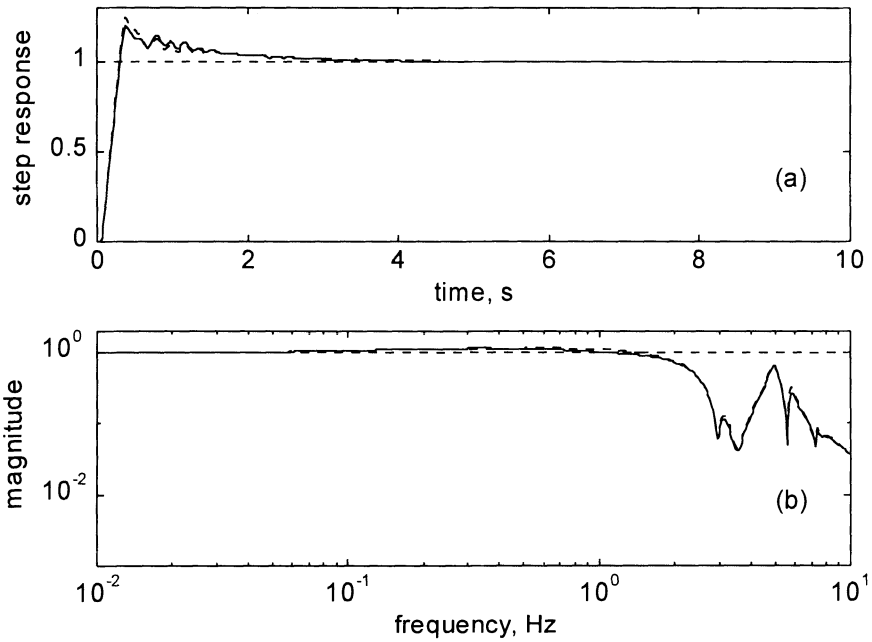

Figure 9.15. Final design of the antenna LQG controller, full-order controller – solid line, reduced-order controller – dashed line: (a) closed-loop step response; and (b) closed-loop magnitude of the transfer function.

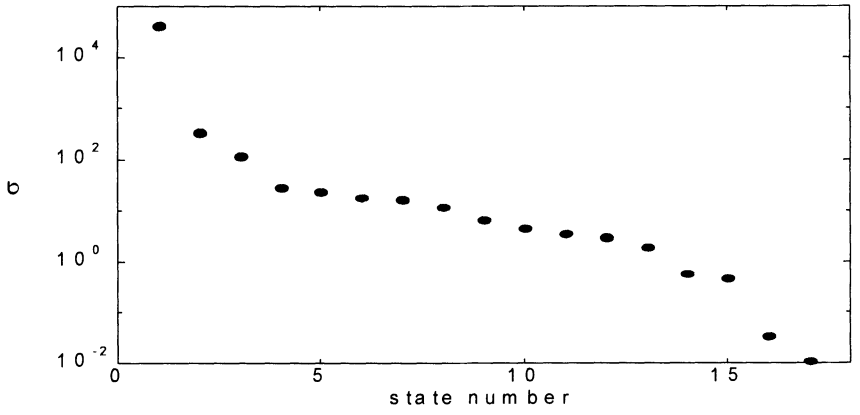

Figure 9.16. Controller reduction index for the Deep Space Network antenna.

10
H_∞ and H_2 Controllers

In the LQG controller design we assumed that the control inputs are collocated with disturbances, and that the control output was collocated with the performance. This assumption imposes significant limits on the LQG controller possibilities and applications. The locations of control inputs do not always coincide with the disturbance locations, and the locations of controlled output are not necessarily collocated with the location where the system performance is evaluated. The H_2 and H_∞ controllers address the controller design problem in its general configuration of noncollocated disturbance and control inputs, and non-collocated performance and control outputs. Many books and papers have been published addressing different aspects of H_∞ controller design, and [24], [81], [73], [78], [12], [77], [95], and [102] explain the basic issues of the method. The H_∞ method addresses wide range of the control problems, combining the frequency and time-domain approaches. The design is an optimal one in the sense of minimization of the H_∞ norm of the closed-loop transfer function. The H_∞ model includes colored measurement and process noise. It also addresses the issues of robustness due to model uncertainties, and is applicable to the single-input-single–output systems as well as to the multiple-input–multiple-output systems.

In this chapter the H_∞ controller design for flexible structures is presented. A modal approach to H_∞ controller design is chosen. It allows for the determination of a stable reduced-order H_∞ controller with performance close to the full-order controller.

W. K. Gawronski, *Dynamics and Control of Structures*

10.1 Definition and Gains

The closed-loop system architecture is shown in Fig. 10.1. In this figure G is the transfer function of a plant, K is the transfer function of a controller, w is the exogenous input (commands, disturbances), u is the actuator input, z is the regulated output (at which performance is evaluated), and y is the sensed (or controlled) output. The H_∞ control problem consists of determining K such that the H_∞ norm of the closed-loop transfer function G_{wz} from w to z is minimized over all realizable controllers K, that is,

find a realizable K such that $\|G_{wz}(K)\|_\infty$ is minimal. (10.1)

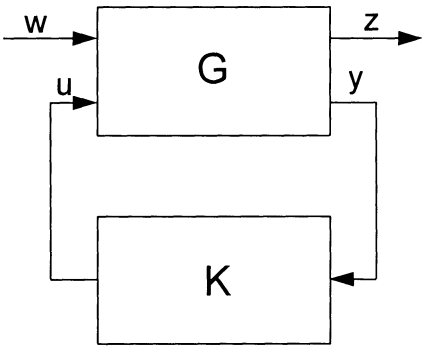

Figure 10.1. Closed-loop system configuration.

For a closed-loop system as in Fig. 10.1 the plant transfer function $G(s)$, and the controller transfer function $K(s)$ are such that

$$\begin{pmatrix} z(s) \\ y(s) \end{pmatrix} = G(s) \begin{pmatrix} w(s) \\ u(s) \end{pmatrix}, \qquad u(s) = K(s)y(s), \tag{10.2}$$

where u, w are control and exogenous inputs and y, z are measured and controlled outputs, respectively. The related state-space equations are as follows:

$$\dot{x} = Ax + B_1 w + B_2 u, \qquad z = C_1 x + D_{12} u, \qquad y = C_2 x + D_{21} w\,. \tag{10.3}$$

Hence, the state-space representation in the H_∞ controller description consists of the quintuple (A, B_1, B_2, C_1, C_2). For this representation (A, B_2) is stabilizable and (A, C_2) is detectable, and the conditions

$$D_{12}^T \begin{bmatrix} C_1 & D_{12} \end{bmatrix} = \begin{bmatrix} 0 & I \end{bmatrix}, \qquad D_{21} \begin{bmatrix} B_1^T & D_{21}^T \end{bmatrix} = \begin{bmatrix} 0 & I \end{bmatrix}, \tag{10.4}$$

are satisfied. The latter conditions make the H_∞ controller the central one. These are quite common assumptions and in the H_2 control they are interpreted as the absence of cross terms in the cost function $(D_{12}^T C_1 = 0)$, and the process noise and measurement noise are uncorrelated $(B_1 D_{21}^T = 0)$.

Let G_{wz} be the transfer function of the closed-loop system from w to z, then there exists an admissible controller such that $\|G_{wz}\|_\infty < \rho$, where ρ is the smallest number such that the following four conditions hold:

1. $S_{\infty c} \geq 0$ solves the following central H_∞ controller algebraic Riccati equation (HCARE)

$$S_{\infty c} A + A^T S_{\infty c} + C_1^T C_1 - S_{\infty c} (B_2 B_2^T - \rho^{-2} B_1 B_1^T) S_{\infty c} = 0. \tag{10.5a}$$

2. $S_{\infty e} \geq 0$ solves the following central H_∞ filter (or estimator) algebraic Riccati equation (HFARE)

$$S_{\infty e} A^T + A S_{\infty e} + B_1 B_1^T - S_{\infty e} (C_2^T C_2 - \rho^{-2} C_1^T C_1 S_{\infty e} = 0. \tag{10.5b}$$

3.

$$\lambda_{\max}(S_{\infty c} S_{\infty e}) < \rho^2, \tag{10.5c}$$

where $\lambda_{\max}(X)$ is the largest eigenvalue of X.

4. The Hamiltonian matrices

$$\begin{bmatrix} A & \rho^{-2} B_1 B_1^T - B_2 B_2^T \\ -C_1^T C_1 & -A^T \end{bmatrix}, \quad \begin{bmatrix} A^T & \rho^{-2} C_1^T C_1 - C_2^T C_2 \\ -B_1 B_1^T & -A \end{bmatrix}, \tag{10.5d}$$

do not have eigenvalues on the $j\omega$-axis.

With the above conditions satisfied the closed-loop system is as in Fig. 10.2, and the controller state-space representation $(A_\infty, B_\infty, C_\infty)$, from the input y to the output u, is given as

$$A_\infty = A + \rho^{-2} B_1 B_1^T S_{\infty c} + B_2 K_c + K_e C_2, \tag{10.6a}$$

$$B_\infty = -K_e, \tag{10.6b}$$

$$C_\infty = K_c, \tag{10.6c}$$

where

$$K_c = -B_2^T S_c \tag{10.6d}$$

and

$$K_e = -S_o S_{\infty e} C_2^T, \qquad S_o = (I - \rho^{-2} S_{\infty e} S_{\infty c})^{-1}. \tag{10.6e}$$

The size of the controller is equal to the size of the plant. The gain K_c is called the controller gain, while K_e is the filter (estimator) gain. Note that the form of the solution is similar to the LQG solution. However the LQG gains are determined independently, while the H_∞ gains are coupled through the inequality (10.5c), and through the component S_o in (10.6e).

10.2 The Balanced H_∞ Controller

A balanced H_∞ controller was investigated by Mustafa and Glover (see [86]) for collocated control and exogenous inputs, and for collocated measured and controlled outputs (i.e., as in the LQG configuration), and was extended in [43] for a general case.

An H_∞ controller is balanced if the related HCARE and HFARE solutions are equal and diagonal, i.e., if

$$S_{\infty c} = S_{\infty e} = \mathrm{M}_\infty, \qquad \mathrm{M}_\infty = \mathrm{diag}(\mu_{\infty 1}, \mu_{\infty 2}, ..., \mu_{\infty N}), \tag{10.7}$$

$\mu_{\infty 1} \geq \mu_{\infty 2} \geq \cdots \geq \mu_{\infty N} > 0$, where $\mu_{\infty i}$ is the ith H_∞ singular (or characteristic) value.

The transformation R to the H_∞ balanced representation is determined as follows. Let $P_{\infty c}$ and $P_{\infty e}$ be the square roots of the HCARE and HFARE solutions

$$P_{\infty c} = S_{\infty c}^{1/2}, \qquad P_{\infty e} = S_{\infty e}^{1/2}, \tag{10.8}$$

and denote $N_\infty = P_{\infty c} P_{\infty e}$. The singular value decomposition of N_∞ is found,

$$N_\infty = V_\infty M_\infty U_\infty^T, \tag{10.9}$$

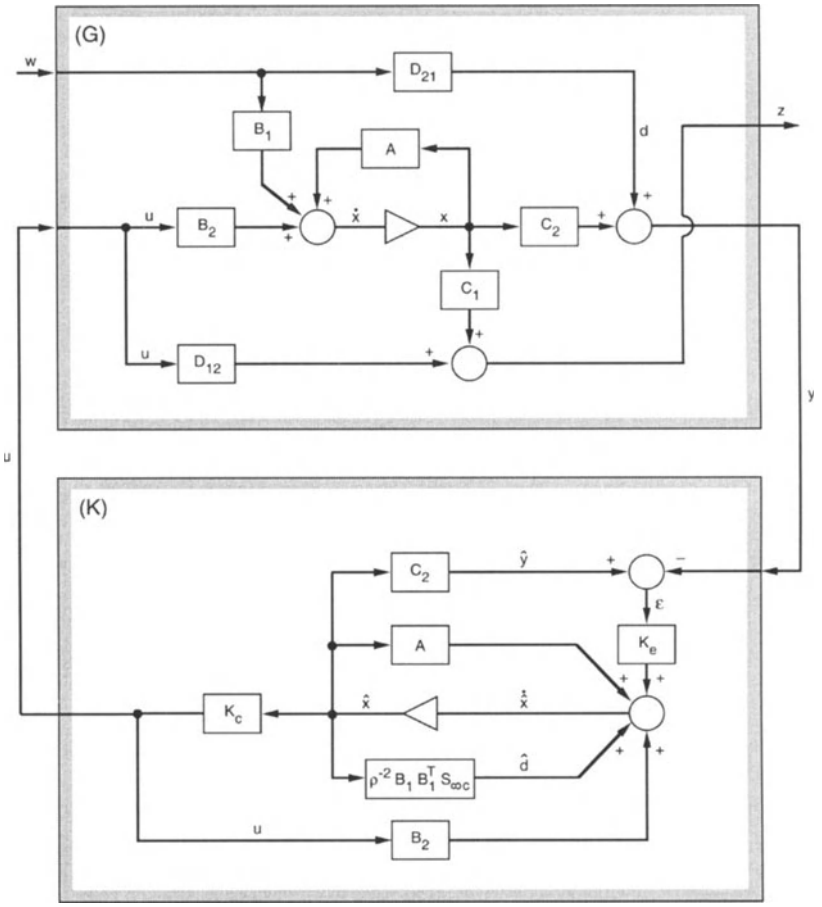

Figure 10.2. An H_∞ closed-loop system.

to obtain the transformation R in the following form:

$$R = P_{\infty e} U_{\infty} \mathrm{M}_{\infty}^{-1/2} = P_{\infty c}^{-1} V_{\infty} \mathrm{M}_{\infty}^{1/2} . \tag{10.10}$$

For the state $\bar{x}$ such that $\bar{x} = Rx$, the state-space representation $(R^{-1}AR, R^{-1}B_1, R^{-1}B_2, C_1R, C_2R)$ is H_{∞} balanced.

In order to prove this, note that the solutions of HCARE and HFARE in new coordinates are $\bar{S}_{\infty c} = R^T S_{\infty c} R$, $\bar{S}_{\infty e} = R^{-1} S_{\infty e} R^{-T}$. Introducing R, as in (10.10), gives the balanced HCARE and HFARE solutions.

The Matlab function *bal_H_inf.m* that transforms a representation (A, B_1, B_2, C_1, C_2) to the H_{∞} balanced representation $(A_b, B_{b1}, B_{b2}, C_{b1}, C_{b2})$ is given in Appendix A.7.

For the H_{∞} balanced solution, the condition in (10.5c) simplifies to

$$\mu_{\infty 1} < \rho \qquad \text{and} \qquad \mu_{\infty n} > 0. \tag{10.11}$$

The relationship between H_{∞} singular values and open-loop (Hankel) singular values is established. Denote the matrix inequality by $X_1 > X_2$ if the matrix $X_1 - X_2$ is positive definite, and by $X_1 \geq X_2$ if the matrix $X_1 - X_2$ is positive semidefinite. For asymptotically stable A, and for $V > 0$, consider two Riccati equations:

$$A^T S_1 + S_1 A - S_1 W_1 S_1 + V = 0 , \tag{10.12a}$$

$$A^T S_2 + S_2 A - S_2 W_2 S_2 + V = 0 . \tag{10.12b}$$

If $W_2 > W_1 > 0$, then one obtains

$$S_1 \geq S_2 \geq 0 , \tag{10.13}$$

see [20].

Property 10.1 ***H_{∞} and Hankel Singular Values.*** *Let Γ_1 be a matrix of Hankel singular values of the state representation (A, B_1, C_1), and let M_{∞} be a matrix of H_{∞} singular values defined in (10.7). Then for an asymptotically stable A, and for $B_2 B_2^T - \rho^{-2} B_1 B_1^T \geq 0$, $C_2^T C_2 - \rho^{-2} C_1^T C_1 \geq 0$, one obtains*

$$\mathrm{M}_{\infty} \leq \Gamma_1 \qquad \text{or} \qquad \mu_{\infty i} \leq \gamma_{1i}, \qquad i = 1, \ldots, N. \tag{10.14}$$

Proof. Note that (10.14) is a consequence of the property given by (10.13). This property is applied to (10.5a), and to the Lyapunov equation $W_o A + A^T W_o + C_1^T C_1 = 0$. It is also a consequence of property (10.13) applied to (10.5b), and to the Lyapunov equation $W_c A^T + A W_c + B_1 B_1^T = 0$. In this way one obtains $W_{c1} \geq S_{\infty e}$ and $W_{o1} \geq S_{\infty c}$. From the latter inequalities it follows that $\lambda_i(W_{c1}) \geq \lambda_i(S_{\infty e})$ and $\lambda_i(W_{o1}) \geq \lambda_i(S_{\infty c})$ (see [56, p. 471]), thus $\lambda_i(W_{c1} W_{o1}) \geq \lambda_i(S_{c1} S_{\infty e})$, or $M_\infty \leq \Gamma_1$. ❑

10.3 The H_2 Controller

The H_2 controller is a generalization of the LQG controller. It minimizes the H_2 norm similarly to the LQG index, but its two-input–two-output structure (disturbance and control inputs are not collocated and performance and sensor outputs are not collocated either) is similar to the H_∞ controller. Its representation is similar to the H_∞ system as in (10.3), and its matrices $A, B_1, B_2, C_1, C_2, D_{21}, D_{12}$ are defined in the following, based on [12].

It consists of state x, control input u, measured output y, exogenous input $w^T = \begin{bmatrix} v_u^T & v_y^T \end{bmatrix}$, and regulated variable $z = C_1 x + D_{12} u$, where v_u and v_y are process and measurement noises, respectively. The noises v_u and v_y are uncorrelated, and have constant power spectral density matrices V_u and V_y, respectively. For the positive semidefinite matrix V_u, matrix B_1 has the following form:

$$B_1 = \begin{bmatrix} V_u^{1/2} & 0 \end{bmatrix}. \tag{10.15}$$

The task is to determine the controller gain (K_c) and the estimator gain (K_e), such that the performance index (J) as in (9.2) is minimal, where R is a positive definite input weight matrix and Q is a positive semidefinite state weight matrix. Matrix C_1 is defined through the weight Q

$$C_1 = \begin{bmatrix} 0 \\ Q^{1/2} \end{bmatrix} \tag{10.16}$$

and, without loss of generality, assume $R = I$ and $V_y = I$, obtaining

$$D_{12} = \begin{bmatrix} I \\ 0 \end{bmatrix}, \qquad D_{21} = \begin{bmatrix} 0 & I \end{bmatrix}. \tag{10.17}$$

The minimum of J is achieved for the feedback with gain matrices (K_c and K_e) as follows:

$$K_c = -B_2^T S_{2c}, \tag{10.18a}$$

$$K_e = -S_{2e} C_2^T, \tag{10.18b}$$

where S_{2c} and S_{2e} are solutions of the controller Riccati equation (CARE) and the estimator Riccati equation (FARE), respectively, which in this case are as follows:

$$S_{2c}A + A^T S_{2c} + C_1^T C_1 - S_{2c} B_2 B_2^T S_{2c} = 0, \tag{10.19a}$$

$$S_{2e}A^T + A S_{2e} + B_1 B_1^T - S_{2e} C_2^T C_2 S_{2e} = 0. \tag{10.19b}$$

Note by comparing (10.5) and (10.19) that the H_2 solution is a special case of the H_∞ solution by assuming $\rho^{-1} = 0$.

10.4 The Balanced H_2 Controller

An H_2 controller is balanced if the related CARE and FARE solutions are equal and diagonal. The relationship between the H_∞ and H_2 characteristic values is derived as follows:

Property 10.2 ***The Relationship Between H_∞, H_2, and Hankel Singular Values.***

$$\mathrm{M}_2 \le \mathrm{M}_\infty \quad \text{or} \quad \mu_{2i} \le \mu_{\infty i}, \qquad i = 1, \ldots, N, \tag{10.20}$$

$$\mathrm{M}_2 \le \Gamma_1 \quad \text{or} \quad \mu_{2i} \le \gamma_{1i}, \qquad i = 1, \ldots, N. \tag{10.21}$$

Proof. Let $\beta = \inf\{\rho : \mathrm{M}_\infty(\rho) \ge 0\}$. Then on the segment $(\beta, +\infty)$ all H_∞ characteristic values are smooth nonincreasing functions of ρ, and the maximal

characteristic value $\mu_{\infty 1}$ is a nonincreasing convex function of ρ, see [74]. As a consequence, for $\rho \to \infty$, one obtains $M_\infty \to M_2$. However, $\mu_{\infty i}$ are increasing functions of ρ, and $\mu_{\infty i} \to \mu_{2i}$ as $\rho \to \infty$, thus $\mu_{2i} \le \mu_{\infty i}$.

The second part is a direct consequence of (10.20) and Property 10.1. ❑

10.5 The Low-Authority H_∞ Controller

The properties of flexible structures are now extended to H_∞ control design. These properties are valid for a low-authority controller of moderate action. In this case flexible structure properties are reflected in the properties of the H_∞ controller. Let (A, B_1, B_2, C_1, C_2) be the open-loop modal representation of a flexible structure (in the modal form 1 or 2), and let $A_{c1} = A - B_2 B_2^T S_{\infty c}$, $A_{c2} = A - S_o S_{\infty e} C_2 C_2$ be the closed-loop matrices, where $S_{\infty c}$ and $S_{\infty e}$ are the solutions of the HCARE and HFARE equations, respectively, and $S_o = (I - \rho^{-2} S_{\infty e} S_{\infty c})^{-1}$. Denote by b_i the ith row of B. The H_∞ controller is of low authority if for the closed-loop matrix A_{c1} one obtains $A_{c1} \cong \text{eig}(A - \text{diag}(BB^T S_c)$. In other words, for the low-authority controller one can replace BB^T with its diagonal terms. Similarly, for the low-authority H_∞ controller one can replace $C^T C$ with its diagonal terms, obtaining $A_{c2} \cong \text{eig}(A - S_o S_e \text{ diag}(C^T C))$.

One can find a positive scalar s_o such that for $\|S_c\|_2 \le s_o$ and $\|S_e\|_2 \le s_o$, the H_∞ controller is of low authority. For a low-authority controller the following property holds:

Property 10.3 ***HCARE and HFARE in Modal Coordinates.*** *For the low-authority H_∞ controller the solutions of HCARE and HFARE in modal coordinates are diagonally dominant*

$$S_{\infty c} \cong \text{diag}(s_{\infty ci} I_2), \qquad S_{\infty e} \cong \text{diag}(s_{\infty ei} I_2), \qquad i = 1, \ldots, n, \tag{10.22a}$$

and the H_∞ singular values are obtained as follows:

$$\mu_{\infty i} = \sqrt{s_{\infty ci} s_{\infty ei}}, \qquad i = 1, \ldots, n. \tag{10.22b}$$

Furthermore, if A is in the modal form 2, one can use (9.21) and (9.22) as replacements for BB^T *(or* C^TC*).*

Proof. The proof is similar to the proof of Property 9.1. The second part follows from the diagonally dominant solutions of HCARE and HFARE . ❑

The diagonal solutions of HCARE and HFARE are obtained under low-authority assumption. Often, for low values of the parameter ρ, some modes do not satisfy the low-authority conditions. The HCARE and HFARE solutions for these modes are no longer diagonal, and the total solution is in the block-diagonal form, as in Fig. 10.3. This block-diagonal form is equally useful in applications, since it remains diagonally dominant for the low-authority modes. These modes are subjected to truncation in the controller reduction process. They are weakly correlated with the remaining modes and small, and that makes the truncation stable and the truncation error small.

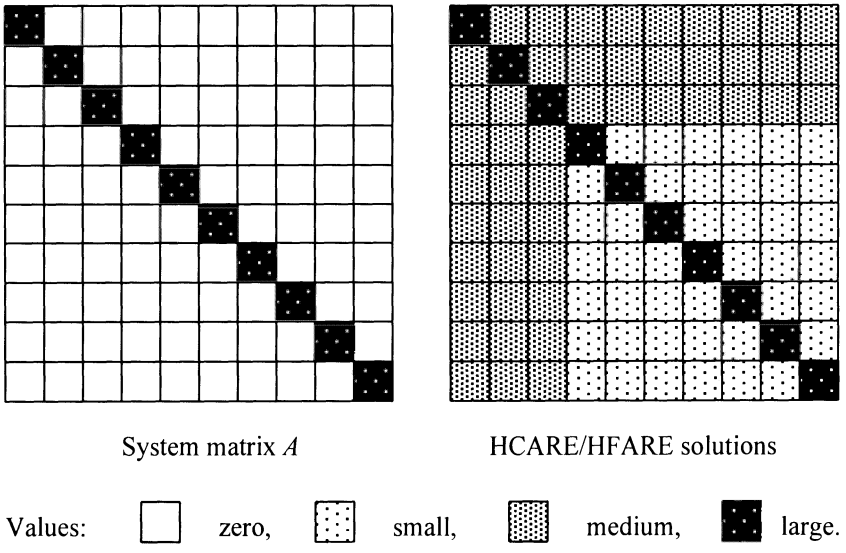

Figure 10.3. Modal matrix A and HCARE/HFARE solutions for the partially low authority H_∞ controller.

10.6 Approximate Solutions of HCARE and HFARE

For flexible structures in modal coordinates, one can use Properties 10.3 and 9.1 to obtain the Riccati equations (10.5a,b) in the following form:

$$\kappa_{ci} s_{c\infty i}^2 + s_{c\infty i} - w_{o1i} \cong 0, \qquad i = 1,\ldots,n, \tag{10.23a}$$

$$\kappa_{ei} s_{e\infty i}^2 + s_{e\infty i} - w_{c1i} \cong 0, \qquad i = 1,\ldots,n, \tag{10.23b}$$

where

$$\kappa_{ci} = w_{c2i} - \frac{w_{c1i}}{\rho^2}, \qquad \kappa_{ei} = w_{o2i} - \frac{w_{o1i}}{\rho^2}. \tag{10.24}$$

The solutions of the ith equation are

$$s_{c\infty i} \cong \frac{\beta_{ci} - 1}{2\kappa_{ci}} \quad \text{and} \quad s_{e\infty i} \cong \frac{\beta_{ei} - 1}{2\kappa_{ei}}, \tag{10.25}$$

where

$$\beta_{ci} = \sqrt{1 + 4 w_{o1i} \kappa_{ci}} = \sqrt{1 + 4\gamma_{21i}^2 - 4\rho^{-2}\gamma_{11i}^2}, \tag{10.26a}$$

$$\beta_{ei} = \sqrt{1 + 4 w_{c1i} \kappa_{ei}} = \sqrt{1 + 4\gamma_{12i}^2 - 4\rho^{-2}\gamma_{11i}^2}, \tag{10.26b}$$

and γ_{jki} is the ith Hankel singular value between the jth input and the kth output. The H_∞ singular values are real and positive for $\kappa_{ci} > 0$ and $\kappa_{ei} > 0$.

From (10.23), one obtains $\kappa_{ci} s_{c\infty i}^2 + s_{c\infty i} \cong w_{o1i}$ and $\kappa_{ei} s_{e\infty i}^2 + s_{e\infty i} \cong w_{c1i}$. Thus

$$s_{c\infty i} \le w_{o1i} \quad \text{for} \quad \kappa_{ci} \ge 0 \tag{10.27a}$$

and

$$s_{e\infty i} \le w_{c1i} \quad \text{for} \quad \kappa_{ei} \ge 0. \tag{10.27b}$$

Introducing (10.25) to (10.22b) one obtains the approximate H_∞ singular values as follows:

$$\mu_{\infty i} \cong \frac{\sqrt{(\beta_{ci}-1)(\beta_{ei}-1)}}{2\kappa_i}, \tag{10.28}$$

where

$$\kappa_i = \sqrt{\gamma_{22i}^2 - \rho^{-2}\gamma_{12i}^2 - \rho^{-2}\gamma_{21i}^2 + \rho^{-4}\gamma_{11i}^2}\,. \tag{10.29}$$

Consider a specific case of the equal cross-coupling between the two-inputs and two-outputs, i.e., $\gamma_{12} = \gamma_{21}$. For this case, $\beta_{ci} = \beta_{ei} = \beta$, and $\gamma_{12}^2 = \gamma_{21}^2 = \gamma_{11}\gamma_{22}$, therefore

$$\mu_{\infty i} \cong \frac{\beta - 1}{2\kappa_i}, \qquad \kappa_i = \gamma_{22} - \rho^{-2}\gamma_{11}. \tag{10.30}$$

Setting $\rho^{-1} = 0$ specifies the above results for the H_2 systems. Thus for the H_2 controller $\kappa_{ci} = w_{c2i}$, and for $\kappa_{ei} = w_{o2i}$ from (10.25) and (10.26), it follows that:

$$s_{c2i} = \frac{\beta_{2ci} - 1}{2w_{c2i}}, \qquad s_{e2i} = \frac{\beta_{2ei} - 1}{2w_{o2i}}, \tag{10.31}$$

are the approximate solutions of the modal H_2 Riccati equations, and

$$\beta_{2ci} = \sqrt{1 + 4\gamma_{21i}^2}\,, \qquad \beta_{2ei} = \sqrt{1 + 4\gamma_{12i}^2}\,. \tag{10.32}$$

Thus $\mu_{2i} = \sqrt{s_{c2i}s_{e2i}}$ is the ith characteristic value of an H_2 system, obtained from (10.27) for $\rho^{-1} = 0$

$$\mu_{2i} \cong \frac{\sqrt{(\beta_{2ci}-1)(\beta_{2ei}-1)}}{\gamma_{22i}}. \tag{10.33}$$

Also, from (10.30) one obtains

$$\mu_{2i} \le \mu_{\infty i} \le \gamma_{1i}^2 \qquad \text{and} \qquad \mu_{21} \le \rho \le \gamma_{11}^2 \tag{10.34}$$

for $\kappa_{ci} > 0$ and $\kappa_{ei} > 0$.

10.7 Almost-H_∞-Balanced Modal Representation

For the diagonally dominant solutions of HCARE and HFARE in modal coordinates see (10.22), it is not difficult to find an approximately balanced solution M_∞ of HCARE and HFARE, which is also diagonally dominant, i.e.,

$$M_\infty \cong \text{diag}(\mu_{\infty i} I_2) \quad \text{where} \quad \mu_{\infty i} = \sqrt{s_{\infty ci} s_{\infty ei}}, \qquad i = 1,\ldots,n. \tag{10.35}$$

The modal representation for which the solutions of HCARE and HFARE are approximately equal is called the almost H_∞ balanced representation. The transformation R from the modal representation (A, B_1, B_2, C_1, C_2) to the H_∞ almost balanced representation $(A_{abh}, B_{abh1}, B_{abh2}, C_{abh1}, C_{abh2})$ is diagonal

$$R = \text{diag}(r_1 I_2, r_2 I_2, \ldots, r_n I_2), r_i = \left(\frac{s_{\infty ei}}{s_{\infty ci}} \right)^{1/4}, \tag{10.36}$$

and

$$(A_{abh}, B_{abh1}, B_{abh2}, C_{abh1}, C_{abh2}) = (A, R^{-1}B_1, R^{-1}B_2, C_1 R, C_2 R). \tag{10.37}$$

Note that this transformation requires only a rescaling of the input and output matrices.

Indeed the modal representation $(A, R^{-1}B_1, R^{-1}B_2, C_1 R, C_2 R)$ is almost H_∞ balanced, and the HCARE, HFARE solution M_∞ is diagonally dominant in the modal almost-balanced coordinates. This is easily proven by noting that the solutions of HCARE and HFARE are $S_{\infty ch} = R_h^T S_{\infty c} R_h$ and $S_{\infty eh} = R_h^{-1} S_{\infty e} R_h^{-T}$, and introducing R, as in (10.36), one obtains a balanced solution as in Eq.(10.37). Note that the values of $s_{\infty ci}$ and $s_{\infty ei}$ depend on the choice of coordinates, but their product does not.

10.8 Three Ways to Compute H_∞ Singular Values

The above analysis allows for the computation of the H_∞ singular values in three different ways.

1. From the algorithm in Section 10.2. This algorithm gives the exact H_∞ singular values. However, the relationship between the H_∞ singular value and the corresponding natural mode it represents is not explicit.

2. From (10.22a,b). These approximate values give a straightforward connection between H_∞ singular values and natural modes.
3. From (10.28). This is an approximate value related to a specific mode. The largest singular values may be inaccurate, but the closed-form equation gives an explicit relationship between structural parameters and the singular value.

10.9 Tracking H_∞ Controller

The tracking control problem differs from the regulation problem because controller performance depends not only on the plant parameters, but also on the tracking command profile (its rate, acceleration, etc.). It is useful to formulate the tracking problem such that the requirements are met by definition. One important requirement for tracking systems is to maintain zero steady-state error. This requirement can be satisfied by upgrading the plant with an integrator. This approach was already discussed in the LQG design, Chapter 9. An H_∞ tracking controller with an integral upgrade is presented in Fig. 10.4. This design approach is similar to the LQG tracking controller design presented earlier.

10.10 Frequency Weighting

Loop shaping pre- and post-compensating filters are needed to meet specified performance requirements. Typically, filters are smooth, i.e., their transfer function satisfies conditions (4.9), and for smooth filters Property 4.8 is valid. This property says that the H_∞ norm of a smooth filter in series with a flexible structure is approximately equal to the norm of a structure alone with the input (output) matrices scaled by the filter gains at natural frequencies.

Denote by $\overline{G}_i$ a transfer function of the ith mode G_i with the scaled input matrix B_i, see (9.45). One can show that the H_∞ norms of both transfer functions are approximately equal.

Property 10.4(a) ***H_∞ Input Filtering.*** *The H_∞ norm of a structure with a smooth input filter is approximately equal to the H_∞ norm of a structure with a scaled input matrix B*

$$\|GF\|_\infty \cong \|\overline{G}\|_\infty, \tag{10.38}$$

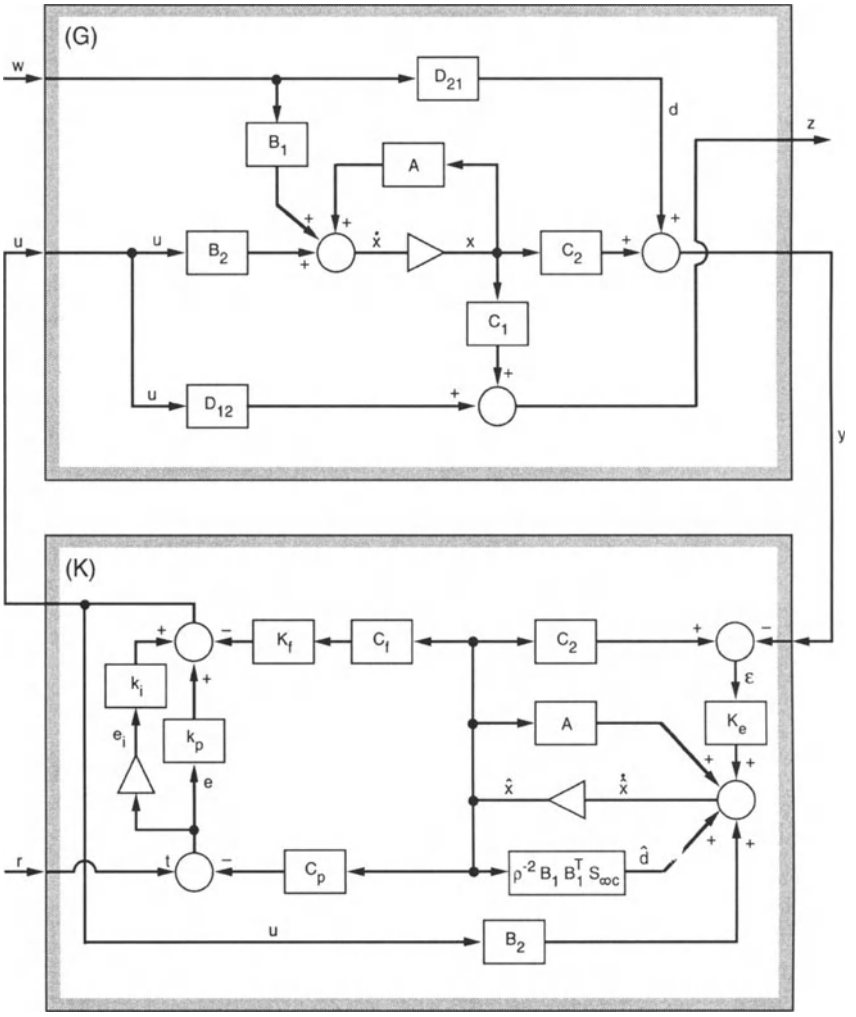

Figure 10.4. Tracking H_∞ controller with an integral upgrade.

where

$$\overline{G} = \sum_{i=1}^{n} \overline{G}_i \,, \qquad \overline{G}_i = C_i(j\omega I - A_i)^{-1}\overline{B}_i \,, \tag{10.39a}$$

and

$$\overline{B}_i = B_i \alpha_i, \qquad \alpha_i = |F(\omega_i)|. \tag{10.39b}$$

Proof. From Property 4.8 one obtains

$$\|GF\|_\infty \cong \max_i \|G_i \alpha_i\|_\infty = \max_i \|\overline{G}_i\|_\infty \cong \|\overline{G}\|_\infty, \qquad i = 1, \ldots, n. \tag{10.40}$$

❐

Equation (10.38) shows that the application of the input filter for the H_∞ performance modeling is equivalent to the scaling of the $2 \times n$ input matrix B_i with α_i, where α_i is the magnitude of the filter transfer function at the resonant frequency ω_i, $\alpha_i = |F(\omega_i)|$, see (4.8).

Property 10.4(b) ***H_∞ Output Filtering.*** *The H_∞ norm of a structure with a smooth output filter is approximately equal to the H_∞ norm of a structure with a scaled output matrix C*

$$\|FG\|_\infty \cong \|\overline{G}\|_\infty, \tag{10.41a}$$

where

$$\overline{G} = \sum_{i=1}^{n} \overline{G}_i, \tag{10.41b}$$

$$\overline{G}_i = \overline{C}_i (j\omega I - A_i)^{-1} B_i, \tag{10.41c}$$

and

$$\overline{C}_i = \alpha_i C_i. \tag{10.41d}$$

Proof. Similar to Property 10.4(a). ❐

Equation (10.41) shows that the application of the output filter for the H_∞ performance modeling is equivalent to the scaling of the $2 \times n$ output matrix C_i with α_i, where α_i is the magnitude of the filter transfer function at the resonant frequency.

10.11 The Closed-Loop System

The state-space equations of the open-loop system follow from (10.3):

$$\dot{x} = Ax + B_1 w + B_2 u\,, \tag{10.42a}$$

$$z = C_1 x + D_{12} u\,, \tag{10.42b}$$

$$y = C_2 x + D_{21} w\,, \tag{10.42c}$$

$$u = K_c \hat{x}\,, \tag{10.42d}$$

and the state-space equations of the central H_∞ controller are as follows, see [53] and [25]:

$$\dot{\hat{x}} = (A + K_e C_2 + \rho^{-2} B_1 B_1^T S_{\infty c} + B_2 K_c)\hat{x} - K_e y\,, \tag{10.43}$$

where

$$K_c = -B_2^T S_{\infty c}\,, \tag{10.44a}$$

$$K_e = -S_o S_{\infty e} C_2^T\,, \tag{10.44b}$$

$$S_o = (I - \rho^{-2} S_{\infty e} S_{\infty c})^{-1}\,. \tag{10.44c}$$

Defining a new state variable

$$x_o = \begin{Bmatrix} x \\ \varepsilon \end{Bmatrix}, \tag{10.45}$$

where $\varepsilon = x - \hat{x}$, one obtains the closed-loop state-space equations in the following form

$$\dot{x}_o = A_o x_o + B_o w\,, \tag{10.46a}$$

$$z = C_o x_o\,, \tag{10.46b}$$

where

$$A_o = \begin{bmatrix} A + B_2 K_c & -B_2 K_c \\ -\rho^{-2} B_1 B_1^T S_{\infty c} & A + K_e C_2 + \rho^{-2} B_1 B_1^T S_{\infty c} \end{bmatrix}, \tag{10.47a}$$

$$B_o = \begin{bmatrix} B_1 \\ B_1 - K_c D_{21} \end{bmatrix}, \tag{10.47b}$$

$$C_o = \begin{bmatrix} C_1 + D_{12} K_c & -D_{12} K_c \end{bmatrix}. \tag{10.47c}$$

The block diagram of the closed-loop system is shown in Fig. 10.2. Assuming $\rho^{-1} = 0$ in (10.46) and (10.47), one obtains the H_2 system.

10.12 The Reduced-Order H_∞ Controller

The order of the H_∞ controller is equal to the order of the plant, which is often too large for implementation. Order reduction is therefore an important design issue. The reduction of a generic H_∞ controller is not a straightforward task, however an H_∞ controller for flexible structures inherits special properties that are used for controller reduction purposes.

10.12.1 The Reduction Index

The following reduction index is introduced for H_∞ controller reduction purposes

$$\sigma_{\infty i} = \gamma_{22i} \mu_{\infty i}, \tag{10.48}$$

where γ_{22i} is the ith Hankel singular value of (A, B_2, C_2). The index $\sigma_{\infty i}$ serves as an indicator of importance of the ith mode of the H_∞ controller. If $\sigma_{\infty i}$ is small, the ith mode is considered negligible and can be truncated.

For an H_2 system, when $\rho^{-1} = 0$, one gets $\sigma_{\infty i} = \sigma_{2i}$, with

$$\sigma_{2i} = \gamma_{22i} \mu_{2i}. \tag{10.49}$$

The above choice of reduction index is justified by the properties of the closed-loop system, presented below.

10.12.2 Closed-Loop Poles

Let $(A_\infty,B_\infty,C_\infty)$ be the state-space representation of the central H_∞ controller as in (10.6). Defining the closed-loop state variable as in (10.45), one obtains the closed-loop modal state-space equations as in (10.46). Divide A_o into submatrices

$$A_o = \begin{bmatrix} A_{11} & A_{12} \\ A_{21} & A_{22} \end{bmatrix}, \tag{10.50}$$

where

$$A_{11} = A + B_2 K_c, \qquad A_{12} = -B_2 K_c, \tag{10.51a}$$

$$A_{21} = -\rho^{-2} B_1 B_1^T \mathrm{M}_\infty, \qquad A_{22} = A + K_e C_2 + \rho^{-2} B_1 B_1^T \mathrm{M}_\infty, \tag{10.51b}$$

to prove the following property:

Property 10.5 ***Closed-Loop Poles.*** *If*

$$\sigma_{\infty i} << \sigma_{\infty 1} \qquad \text{for} \qquad i = k+1, \ldots, n, \tag{10.52}$$

then the ith pole is shifted approximately by $2\sigma_{\infty i}$ *with respect to the open-loop location, i.e.,*

$$A_{22i} \cong A_i - 2\sigma_{\infty i} I_2 . \tag{10.53}$$

Proof. In modal coordinates, A is diagonal and the following components are diagonally dominant:

$$B_2 K_c = B_2 B_2^T \mathrm{M}_\infty \cong \mathrm{diag}(2\zeta_i \omega_i w_{c2i} \mu_{\infty i}), \tag{10.54a}$$

$$K_e C_2 = \mathrm{M}_\infty C_2^T C_2 \cong \mathrm{diag}(2\zeta_i \omega_i w_{o2i} \mu_{\infty i}), \tag{10.54b}$$

$$\rho^{-2} B_1 B_1^T \mathrm{M}_\infty \cong \mathrm{diag}\left(\frac{2\zeta_i \omega_i w_{c1i} \mu_{\infty i}}{\rho^2} \right), \tag{10.54c}$$

thus each of the four blocks of A_o is diagonally dominant. If $\sigma_{\infty i} << \sigma_{\infty 1}$ for $i = k+1,\ldots,n$, then the ith diagonal components of A_{12} and A_{21} are small for $i = k+1,\ldots,n$. Thus for those components the separation principle is valid and gains k_{ci} and k_{ei} are independent. Furthermore, the ith diagonal block A_{22i} of the matrix A_{22} is as follows:

$$A_{22i} \cong A_i - s_{oi}\mu_{\infty i}C_{2i}^T C_{2i} - \rho^{-2}B_{1i}B_{1i}^T\mu_{\infty i} \ , \tag{10.55}$$

where A_i is given by (2.30b). Note in addition that $s_{oi} \cong 1$ for $\sigma_{\infty i} << \sigma_{\infty 1}$, that $\mu_{\infty i}C_{2i}^T C_{2i} \cong 2\zeta_i\omega_i w_{o2i}\mu_{\infty i}I_2$, and that $\rho^{-2}B_{1i}B_{1i}^T\mu_{\infty i} \cong 2\zeta_i\omega_i\rho^{-2}w_{c1i}\mu_{\infty i}I_2$. Consequently, (10.55) now becomes $A_{22i} \cong A_i - 2\sigma_{\infty i}I_2$, or (10.53). ❑

10.12.3 Controller Performance

Let the error vector ε be partitioned as follows:

$$\varepsilon = \begin{Bmatrix} \varepsilon_r \\ \varepsilon_l \end{Bmatrix}, \tag{10.56}$$

with ε_r of dimension n_r, ε_l of dimension n_l, such that $n_r + n_l = n$. Let the matrix of the reduction indices be arranged in decreasing order, $\Sigma_\infty = \text{diag}(\sigma_{\infty 1}I_2,\ldots,\sigma_{\infty n}I_2)$, $\sigma_{\infty i} \geq \sigma_{\infty i+1}$, and be divided consistently by ε,

$$\Sigma_\infty = \begin{bmatrix} \Sigma_{\infty r} & 0 \\ 0 & \Sigma_{\infty l} \end{bmatrix}, \tag{10.57}$$

where $\Sigma_{\infty r} = \text{diag}(\sigma_{\infty 1}I_2,\ldots,\sigma_{\infty k}I_2)$, $\Sigma_{\infty l} = \text{diag}(\sigma_{\infty k+1}I_2,\ldots,\sigma_{\infty n}I_2)$. Divide the matrix M_∞ accordingly, $\mathrm{M}_\infty = \text{diag}(\mathrm{M}_{\infty r}, \mathrm{M}_{\infty l})$. The closed-loop system representation (A_o, B_o, C_o) is rearranged according to the division of ε, i.e.,

$$A_o = \begin{bmatrix} A_{or} & A_{ort} \\ A_{otr} & A_{ot} \end{bmatrix}, \qquad B_o = \begin{bmatrix} B_{or} \\ B_{ot} \end{bmatrix}, \qquad C_o = \begin{bmatrix} C_{or} & C_{ot} \end{bmatrix}. \tag{10.58}$$

Hence the closed-loop states of the reduced-order system are now

$$x_o = \begin{Bmatrix} x_r \\ \varepsilon_t \end{Bmatrix} \quad \text{and} \quad x_r = \begin{Bmatrix} x \\ \varepsilon_r \end{Bmatrix}. \tag{10.59}$$

The reduced-order controller representation is (A_{or}, B_{or}, C_{or}), and let the closed-loop system state be denoted by $\bar{x}_r$.

If condition (10.52) is satisfied, the performance of the closed-loop system with the reduced-order controller is almost identical to the full-order controller in the sense that $\|x_r - \bar{x}_r\|_2 \cong 0$. It follows from (10.54) that for $\sigma_{\infty i} << \sigma_{\infty 1}$ $(i = k+1, \ldots, n)$ one obtains $\|A_{otr}\| \cong \|A_{ort}\| \cong 0$, and the closed-loop block A_{ot} is almost identical to the open-loop block A_t, i.e., $A_{ot} \cong A_t$. In this case, from (10.51) and (10.57), one obtains

$$\dot{x}_r = A_{or} x_r + A_{ort} \varepsilon_t + B_{or} w \cong A_{or} x_r + B_{or} w = \dot{\bar{x}}_r, \tag{10.60}$$

or, thus $x_r \cong \bar{x}_r$.

The above approximations hold for the controllers with limited damping authority, i.e., for the controllers that modify only moderately the system natural frequencies. Typically, the modes with largest H_∞ singular values do not fall under this category, but the modes with the smallest H_∞ singular values are under low-authority control. Thus the latter modes are the ones that are the most suitable for reduction. Therefore the presented reduction procedure is applicable in this case.

10.13 Design Examples

The H_∞ design method is illustrated by the simple flexible system, the truss structure, and the Deep Space Network antenna.

10.13.1 A Simple Structure

The design of an H_∞ controller for a system as in Fig. 1.2 is described. The system parameters are as follows: $m_1 = 3$, $m_2 = 1$, $m_3 = 2$, $k_1 = 30$, $k_2 = k_3 = k_4 = 6$, $D = 0.004\,K + 0.001M$, where M, K, and D are mass, stiffness, and damping matrices, respectively. The control input (u) acts at mass 2 and mass 3 in opposite directions. The first disturbance (w_1) acts at mass 2 and mass 3 in opposite directions, with an amplification factor of 3, the second disturbance (w_2) acts at mass 2, and the third disturbance (w_3) is the output

noise. The output (y) is a displacement of mass 2, and the controlled outputs (z_1, z_2, and z_3) are the displacement of mass 2 with an amplification factor of 3, a rate of mass 3, and an input u. Thus:

$$B_1 = \begin{bmatrix} 0 & 0 & 0 \\ 0 & 0 & 0 \\ 0 & 0 & 0 \\ 0 & 0 & 0 \\ 1 & 3 & 0 \\ 0 & -1.5 & 0 \end{bmatrix}, \qquad B_2 = \begin{bmatrix} 0 \\ 0 \\ 0 \\ 0 \\ 1 \\ -0.5 \end{bmatrix},$$

$$C_1 = \begin{bmatrix} 0 & 0 & 1 & 0 & 0 & 0 \\ 0 & 0 & 0 & 0 & 3 & 0 \\ 0 & 0 & 0 & 0 & 0 & 0 \end{bmatrix}, \qquad C_2 = \begin{bmatrix} 0 & 0 & 0 & 0 & 1 & 0 \end{bmatrix},$$

and $D_{12}^T = D_{21} = \begin{bmatrix} 0 & 0 & 1 \end{bmatrix}$.

The parameter ρ is determined, obtaining $\rho = 7.55$. The H_∞ singular values, the exact and approximate obtained from (10.28), are shown in Fig. 10.5, showing good coincidence for the two smallest values. The open- and closed-loop impulse responses are shown in Fig. 10.6(a) (from the first input to the first output), and the magnitudes of the transfer function of the open- and closed-loop systems are compared in Fig. 10.6(b), showing significant vibration suppression.

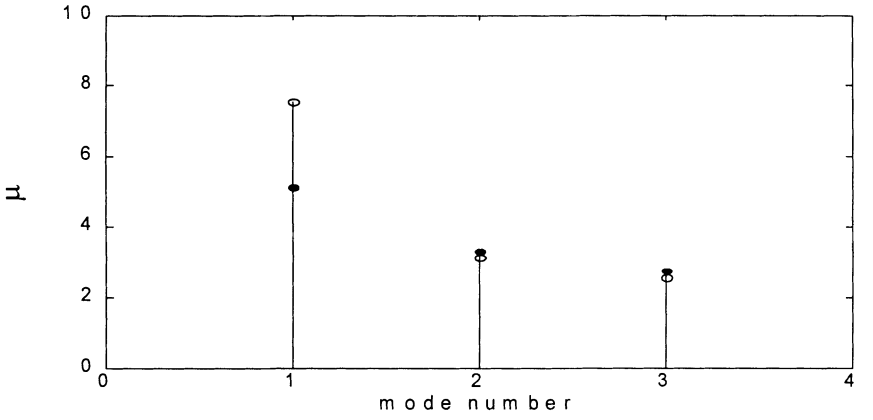

Figure 10.5. Exact (o) and approximate (•) H_∞ singular values of a simple system.

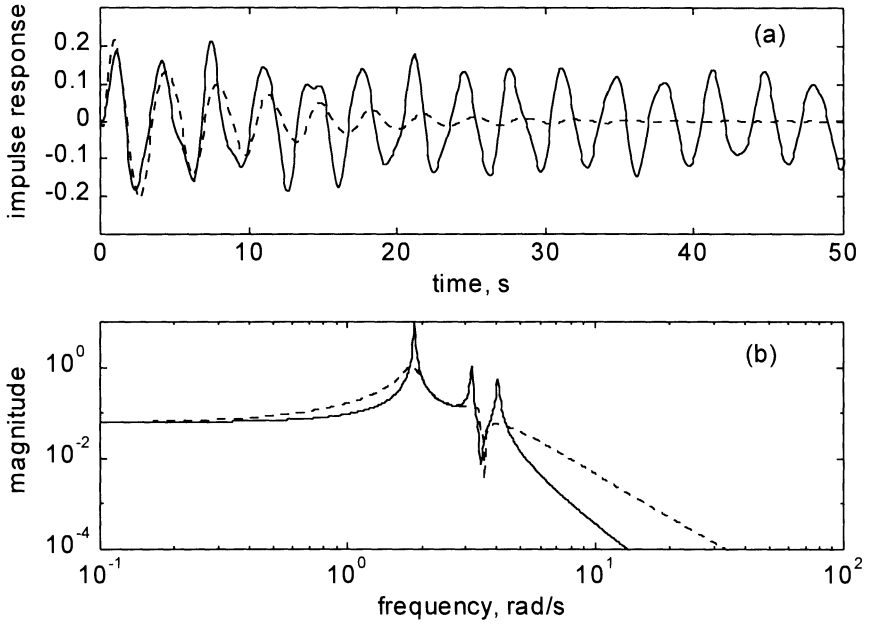

Figure 10.6. A simple system: (a) open- and closed-loop impulse responses; (b) magnitudes of the open- and closed-loop transfer functions.

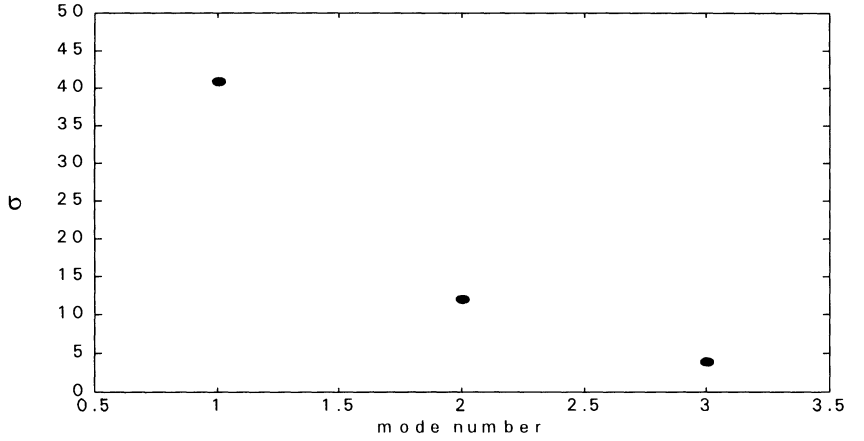

Figure 10.7. Reduction index of the simple system.

The controller is reduced, and the reduction indices are shown in Fig. 10.7. The third mode index is small, hence the controller order is reduced from 6 to 4

states. The obtained closed-loop system is stable, with comparable performance, as confirmed with the impulse responses of the full and reduced controller in Fig. 10.8 (from the first input to the first output).

10.13.2 The 2D Truss

The design of the H_∞ controller for the 2D truss structure, as shown in Fig. 1.3, is presented. The structural model has 16 modes, or 32 states. The control input, u, is applied to node 4 (vertical direction), the controller and the output y is collocated with u. The disturbances act at the input u with amplification factor of 90, and at node 10 (horizontal direction). The performance output z is measured at output y, and at node 9 (horizontal direction).

In Fig. 10.9 the system H_∞ singular values are compared with the approximate ones, obtained from (10.28). Similarly to the previous example, the small values show good coincidence and the large values diverge. This property is explained by the fact that for the largest singular values the closed-loop modal damping is large enough to diverge from the low-authority conditions. Nevertheless, this is not a significant obstacle, since only small H_∞ singular values are used to evaluate the modes subjected to reduction.

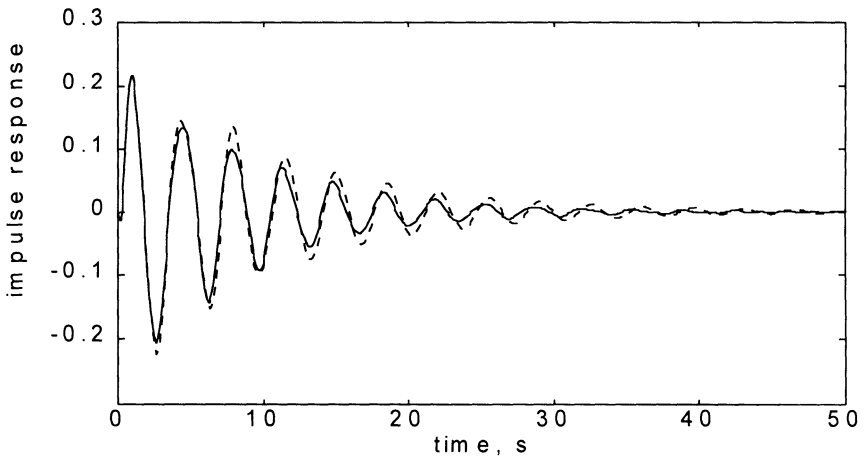

Figure 10.8. Impulse responses of the full (solid line) and reduced (dashed line) H_∞ closed-loop system.

Next, the H_∞ singular values (o), the H_2 singular values (•), and the Hankel singular values γ_{11i} (◊) are compared in Fig. 10.10, showing that Properties 10.1 and 10.2 hold. The critical value is ρ=125.1.

Open- and closed-loop impulse responses and magnitudes of the transfer functions are compared in Fig. 10.11, showing improved closed-loop performance.

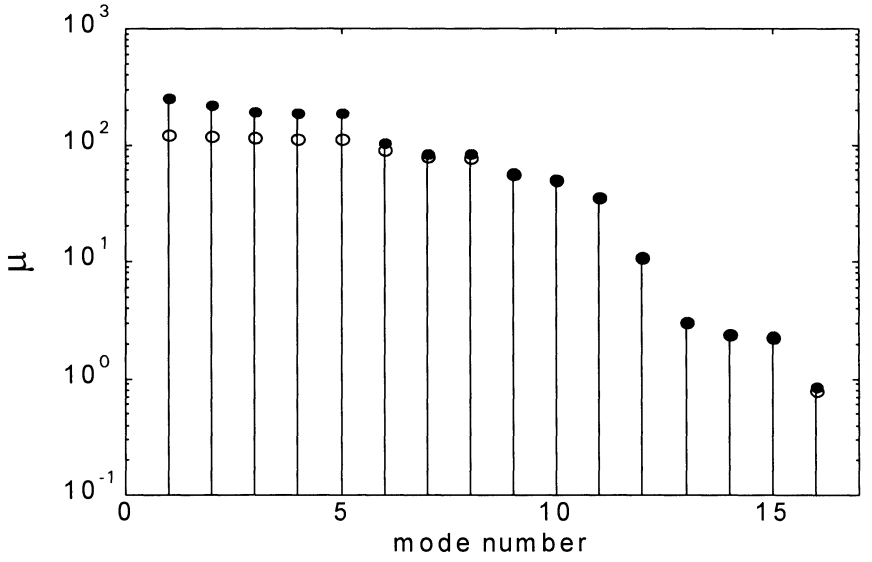

Figure 10.9. Exact (o) and approximate (•) H_∞ singular values of the 2D truss.

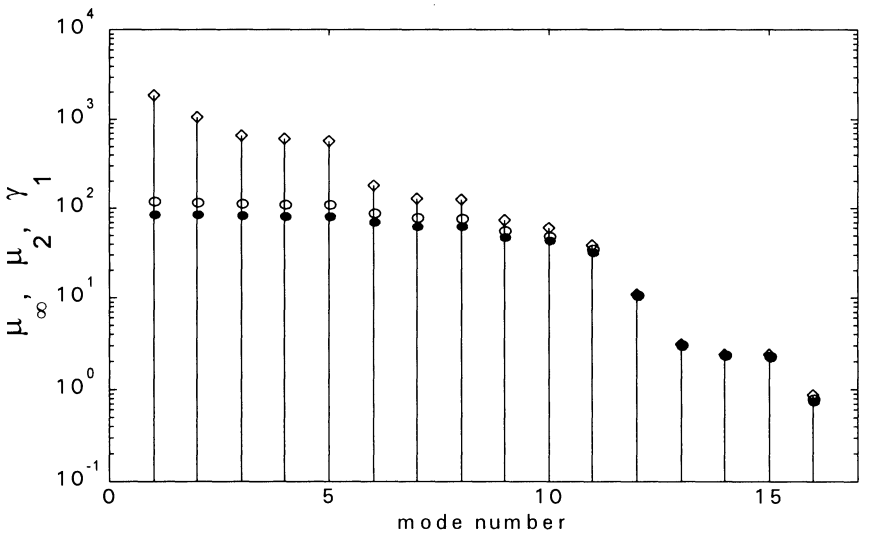

Figure 10.10. H_∞ (o), H_2 (•), and Hankel singular values (◊) of the 2D truss.

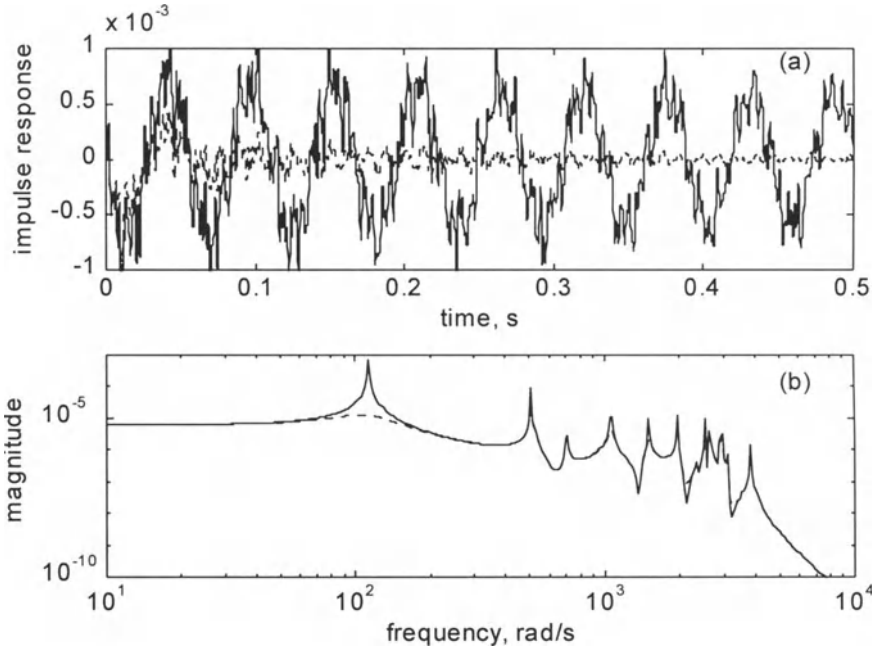

Figure 10.11. The 2D truss: (a) open-loop (solid line) and closed-loop (dashed line) impulse responses; and (b) magnitudes of the open-loop (solid line) and closed-loop (dashed line) transfer functions.

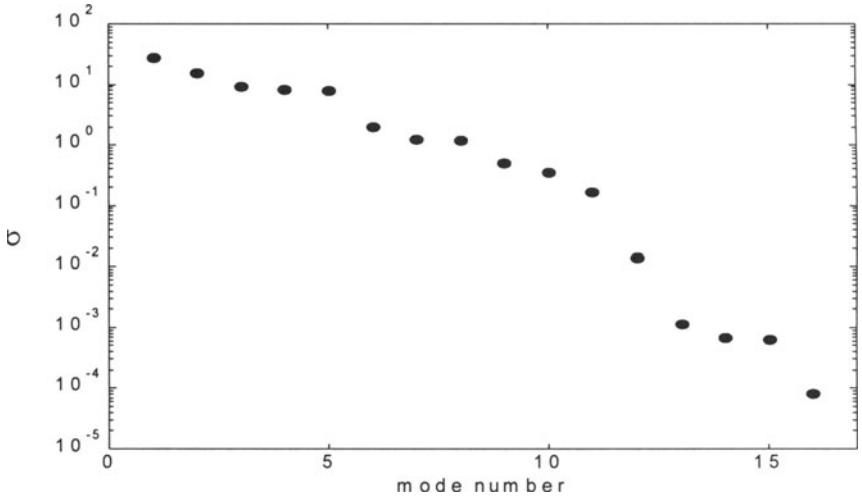

Figure 10.12. Reduction indices of the 2D truss.

The H_∞ reduction indices are shown in Fig. 10.12. The H_∞ reduction index satisfies the condition in (10.52) for k = 6, ..., 16, i.e., $\sigma_{\infty k} << \sigma_{\infty 1}$. Hence the reduced controller contains five modes. Indeed, the controller with five modes (of order 10) is stable, and its performance is almost identical to the full-order controller, since the closed-loop impulse responses of the full-order (see Fig. 10.11(a)) and reduced-order controllers overlap.

10.13.3 Filter Implementation Example

Consider the 3D truss with a filter as in Section 9.11.3. An equivalent structure with filter was obtained by scaling the disturbance input, according to (10.38), and the magnitude of its transfer function is shown in Fig. 9.13 (dashed line). It is clear from that figure that the structure with the filter, and the structure with the scaled disturbance input have very similar frequency characteristics, and their norms are as follows: $\|G\|_\infty = 2.6903$ for the structure with the filter, and $\|G\|_\infty = 2.6911$ for the structure with the scaled disturbance input.

Two frequency weighted H_∞ controllers for this structure were designed. The first one is based on a structure with a filter, while the second is based on a structure with scaled input matrix. The open- and closed-loop transfer functions are shown in Fig. 10.13. The closed-loop performance of the structure with the filter, and with the scaled input, is almost identical. The closed-loop H_∞ norms are as follows: $\|G_{cl}\|_\infty = 0.09681$ for the structure with the filter, and $\|G_{cl}\|_\infty = 0.09676$ for the structure with the scaled disturbance input.

10.13.4 Deep Space Network Antenna with Wind Disturbance Rejection Properties

A significant portion of the antenna tracking error is generated by the antenna vibrations excited by wind gusts. The LQG controller designed in Section 9.11.4 improved its tracking, but the disturbance rejection properties not addressed in the design process are rather moderate. The H_∞ controller allows for addressing simultaneously its tracking and disturbance rejection properties, as shown in the following.

In [35] the wind spectra were determined from the wind field data. For the antenna model in the modal representation the wind filter is added by appropriate scaling of the input matrix B_1 of the antenna. The scaling factors are the filter gains at the natural frequencies of the antenna.

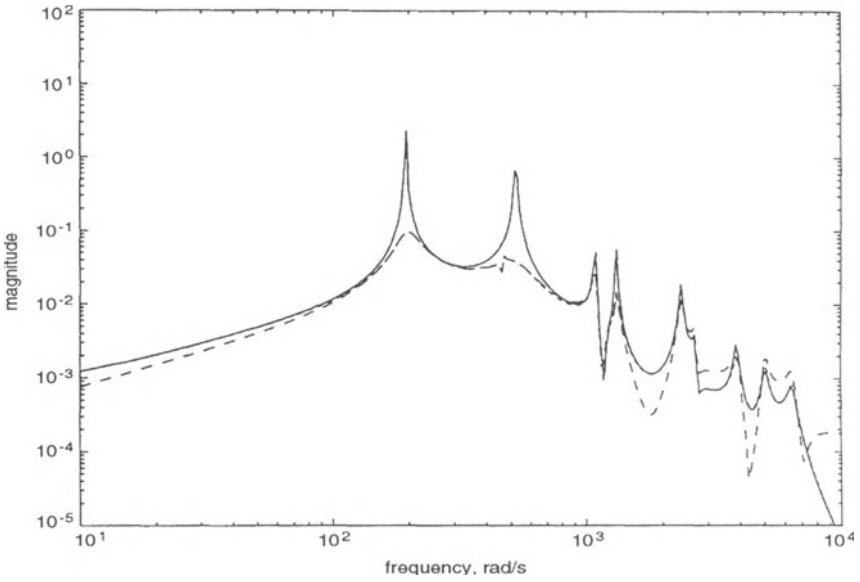

Figure 10.13. Magnitudes of the open-loop (solid line) and closed-loop transfer functions (with filter – dashed line, and with equivalent weights – dotted line).

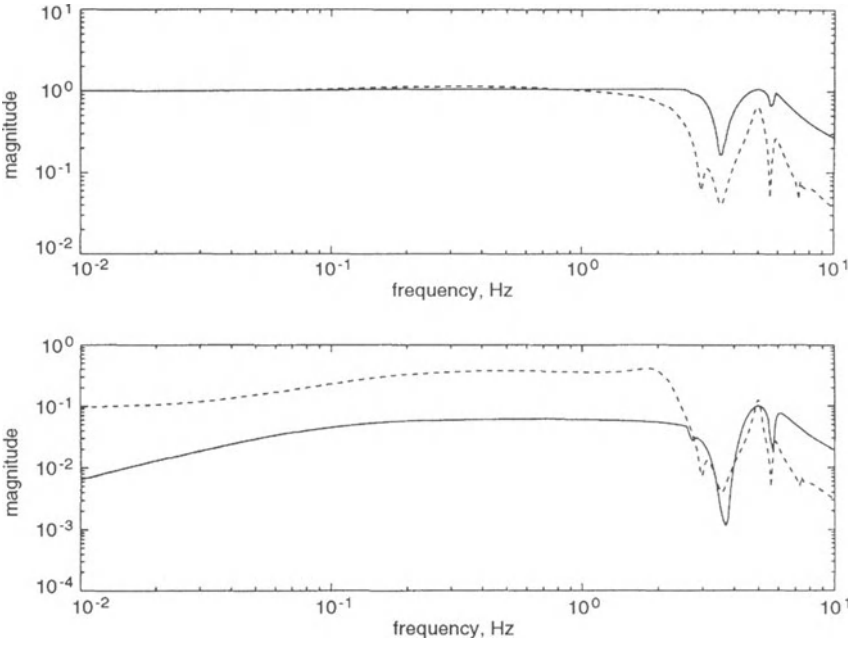

Figure 10.14. Magnitudes of the azimuth transfer functions of the H_∞ (solid line), and LQG (dashed line) controllers: (a) from the command input to the encoder output; and (b) from the wind disturbance input to the encoder output.

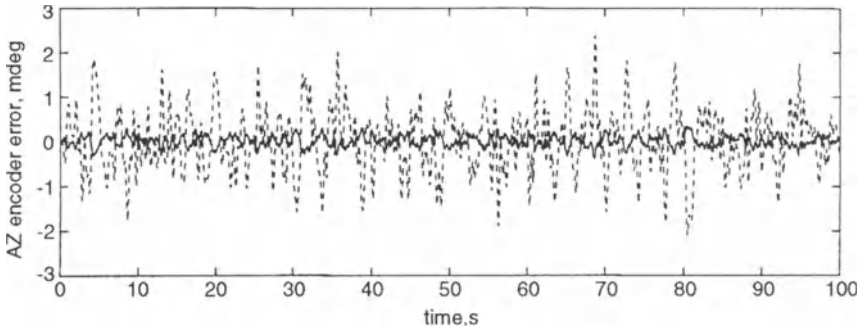

Figure 10.15. The azimuth tracking error due to wind gusts of the H_∞ (solid line), and LQG (dashed line) controllers.

The H_∞ controller for the azimuth axis was simulated, and its tracking performances are compared with the LQG controller performance using their transfer functions from the command input to the encoder output, see Fig. 10.14(a). The plot shows improved tracking performance of the H_∞ controller (the bandwidth is 2.2 Hz for the H_∞ controller and 1.2 Hz for the LQG controller). The wind disturbance rejection properties are illustrated by the transfer functions from the wind disturbance input to the encoder output, Fig. 10.14(b), and by the simulated wind gusts action on the antenna in Fig. 10.15, where the tracking errors of the H_∞ and LQG controllers are plotted. In Fig. 10.14(b) the H_∞ controller disturbance transfer function is about a decade lower than the LQG controller, showing improved disturbance rejection properties of the H_∞ controller. This is confirmed by the plot of the tracking error in a 50 km/h wind, see Fig. 10.15. The rms encoder error of the LQG controller is 0.70 mdeg, while the error of the H_∞ controller is 0.12 mdeg, showing an almost six-fold improvement.

Appendix A

Matlab Functions

The following Matlab® functions are given in this appendix:

- *realdiag*, for the determination of the modal form 2 of the state-space representation;
- *bal_op_loop*, for the determination of the open-loop balanced representation;
- *norm_2*, for the determination of modal H_2 norms;
- *norm_inf*, for the determination of modal H_∞ norms;
- *norm_Han*, for the determination of modal Hankel norms;
- *bal_LQG*, for the determination of the LQG balanced representation; and
- *bal_H_inf*, for the determination of the H_∞ balanced representation.

These functions use the following standard Matlab routines: *are, cdf2rdf, inv, lqe, lqr, lyap, norm, size, sqrt, svd.*

A.1 Transformation to the Modal Representation

```
% function [Am,Bm,Cm,Vm]=realdiag(A,B,C);
% This function finds the modal state-space representation of form 2
% The diagonal blocks of Am are in increasing order of imaginary part
% of the eigenvalues of A
% Vm is the transformation matrix from (A,B,C) to (Am,Bm,Cm)
%
function [Am,Bm,Cm,Vm]=realdiag(A,B,C);
%
[V,D]=eig(A);
```

```
[x,in]=sort(diag(abs(D)));
D=D(in,in);
V=V(in,in);
B=B(in,:);
C=C(:,in);
[Vm,Am]=cdf2rdf(V,D);
Bm=inv(Vm)*B;
Cm=C*Vm;
```

A.2 Open-Loop Balanced Representation

```
% function [Ab,Bb,Cb,Gamma,R]=bal_op_loop(A,B,C);
% This function finds the open-loop balanced representation (Ab,Bb,Cb)
% so that controllability (Wc) and observability (Wo) grammians
% are equal and diagonal:
%          Wc=Wo=Gamma
%
% Input parameters:
% (A,B,C)              - system state-space representation
%
% Output parameters:
% (Ab,Bb,Cb)           - balanced representation
% R                    - transformation to the balanced representation
% Gamma                - Hankel singular values
%
function [Ab,Bb,Cb,Gamma,R]=bal_op_loop(A,B,C);
%
Wc=lyap(A,B*B');                % controllability grammian
Wo=lyap(A',C'*C);               % observability grammian
[Uc,Sc,Vc]=svd(Wc);             % SVD of the controllability grammian
[Uo,So,Vo]=svd(Wo);             % SVD of the observability grammian
Sc=sqrt(Sc);
So=sqrt(So);
P=Uc*Sc;
Q=So*Vo';
H=Q*P;                          % Hankel matrix
[V,Gamma2,U]=svd(H);            % SVD of the Hankel matrix
Gamma=sqrt(Gamma2);             % Hankel singular values
R=P*U*inv(Gamma);               % transformation matrix R
Rinv=inv(Gamma)*V'*Q;           % inverse of R
Ab=Rinv*A*R;
Bb=Rinv*B;
Cb=C*R;                         % balanced representation (Ab,Bb,Cb)
```

A.3 H_2 Modal Norm

```
% function norm=norm_2(om,z,bm,cmq,cmr,cma);
%
%This function finds approximate H2 norm
% for each mode of a structure with displacement, rate, and acceleration sensors
%
% Input parameters:
% om    - vector of natural frequencies
% z     - vector of modal damping
% bm    - modal matrix of actuator location
% cmq   - modal matrix of displacement sensor location
% cmr   - modal matrix of rate sensor location
% cma   - modal matrix of accelerometer location
%
% Output parameter:
% norm - H2 norm
%
function norm=norm_2(om,z,bm,cmq,cmr,cma);
%
om2=diag(om.*om);
bb=diag(bm*bm');
cc=diag(cma'*cma*om2+cmr'*cmr+cmq'*cmq*inv(om2));
h=sqrt(bb.*cc)/2;
h=h./sqrt(z);
norm=h./sqrt(om);
```

A.4 H_∞ Modal Norm

```
% function norm=norm_inf(om,z,bm,cmq,cmr,cma);
%
%This function finds approximate H∞ norm
% for each mode of a structure with displacement, rate, and acceleration sensors
%
% Input parameters:
% om    - vector of natural frequencies
% z     - vector of modal damping
% bm    - modal matrix of actuator location
% cmq   - modal matrix of displacement sensor location
% cmr   - modal matrix of rate sensor location
% cma   - modal matrix of accelerometer location
%
```

```
% Output parameter:
% norm - H∞ norm
%
function norm=norm_inf(om,z,bm,cmq,cmr,cma);
%
om2=diag(om.*om);
bb=diag(bm*bm');
cc=diag(cma'*cma*om2+cmr'*cmr+cmq'*cmq*inv(om2));
h=sqrt(bb.*cc)/2;
h=h./z;
norm=h./om;
```

A.5 Hankel Modal Norm

```
% function norm=norm_han(om,z,bm,cmq,cmr,cma);
%
%This function finds approximate Hankel norm
% for each mode of a structure with displacement, rate, and acceleration sensors
%
% Input parameters:
% om    - vector of natural frequencies
% z     - vector of modal damping
% bm    - modal matrix of actuator location
% cmq   - modal matrix of displacement sensor location
% cmr   - modal matrix of rate sensor location
% cma   - modal matrix of accelerometer location
%
% Output parameter:
% norm - Hankel norm
%
function norm=norm_han(om,z,bm,cmq,cmr,cma);
%
om2=diag(om.*om);
bb=diag(bm*bm');
cc=diag(cma'*cma*om2+cmr'*cmr+cmq'*cmq*inv(om2));
h=sqrt(bb.*cc)/4;
h=h./z;
norm=h./om;
```

A.6 LQG Balanced Representation

```
% function [Ab,Bb,Cb,Mu,Kpb,Keb,Qb,Vb,R]=bal_LQG(A,B,C,Q,R,V,W)
%
% This function finds the LQG balanced representation (Ab,Bb,Cb)
% so that CARE (Sc) and FARE (Se) solutions are equal and diagonal:
%          Sc=Se=Mu
%
%
% Input parameters:
% (A,B,C)       - system state-space representation,
% Q             - state weight matrix,
% R             - input weight matrix,
% V             - process noise covariance matrix,
% W             - measurement noise covariance matrix.
%
% Output parameters:
% (Ab,Bb,Cb)    - LQG balanced representation,
% R             - LQG balanced transformation,
% Mu            - balanced CARE, FARE solution
% Qb            - balanced weight matrix,
% Vb            - balanced process noise covariance matrix,
% Kpb, Keb      - balanced gains.
%
%
function [Ab,Bb,Cb,Mu,Kpb,Keb,Qb,Vb,R]=bal_LQG(A,B,C,Q,R,V,W)
%
V1=V;
R1=R;
[n1,n2]=size(A);
[Kp,Sc,ec]=lqr(A,B,Q,R);                % solution of CARE
[Ke,Se,ee]=lqe(A,eye(n1),C,V,W);        % solution of FARE
[Uc,Ssc,Vc]=svd(Sc);
Pc=sqrt(Ssc)*Vc';                       % Pc
[Ue,Sse,Ve]=svd(Se);
Pe=Ue*sqrt(Sse);                        % Pe
H=Pc*Pe;                                % H
[V,Mu,U]=svd(H);                        % SVD of H
mu=sqrt(Mu);
R=Pe*U*inv(mu);                         % transformation R
Rinv=inv(mu)*V'*Pc;                     % inverse of R
Ab=Rinv*A*R;
Bb=Rinv*B;
Cb=C*R;                                 % LQG balanced representation
```

```
Qb=R'*Q*R;                          % balanced weight matrix
Vb=Rinv*V1*Rinv';                   % balan. process noise cov. matrix
[Kpb,Scb,ecb]=lqr(Ab,Bb,Qb,R1);
[Keb,Seb,eeb]=lqe(Ab,eye(n1),Cb,Vb,W);   % balanced gains
```

A.7 H_∞ Balanced Representation

```
% function [Ab,Bb1,Bb2,Cb1,Cb2,Mu_inf,R]=bal_H_inf(A,B1,B2,C1,C2,ro)
%
% This function finds the H_inf balanced representation
%       (Ab,Bb1,Bb2,Cb1,Cb2)
% so that HCARE (Sc) and HFARE (Se) solutions are equal and diagonal
%          Sc=Se=Mu_inf
%
% Input parameters:
% (A,B1,B2,C1,C2)              - system state-space representation
% ro                           - parameter in HCARE and HFARE
%
% Output parameters:
% (Ab,Bb1,Bb2,Cb1,Cb2)         - H_inf balanced representation,
% R                            - H_inf balanced transformation,
% Mu                           - balanced HCARE, HFARE solution,
%
%
function [Ab,Bb1,Bb2,Cb1,Cb2,Mu_inf,R]=bal_H_inf(A,B1,B2,C1,C2,ro)
%
[n1,n2]=size(A);
Qc=C1'*C1;
gi=1/(ro*ro);
Rc=B2*B2'-gi*B1*B1';
[Sc,sc1,sc2,wellposedc]=are(A,Qc,Rc,'eigen');      % HCARE solution
Qe=B1*B1';
Re=C2'*C2-gi*C1'*C1;
[Se,se1,se2,wellposef]=are(A',Qe,Re,'eigen');      % HFARE solution
%
if(norm(imag(Se))>1e-6 | norm(imag(Sc))>1e-6) ...
disp('non-positive solution');end
%
[Uc,Ssc,Vc]=svd(Sc);
Pc=sqrt(Ssc)*Vc';                                  % Pc
[Ue,Sse,Ve]=svd(Se);
Pe=Ue*sqrt(Sse);                                   % Pe
```

```
N=Pc*Pe;
[V,Mu_inf,U]=svd(N);
mu_inf=sqrt(Mu_inf);
R=Pe*U*inv(mu_inf);
Rinv=inv(mu_inf)*V'*Pc;
Ab=Rinv*A*R;
Bb1=Rinv*B1;
Bb2=Rinv*B2;
Cb1=C1*R;
Cb2=C2*R;                                   % H∞ balanced representation
```

Appendix B

Structural Parameters

This appendix provides the parameters of the 2D truss and the Deep Space Network antenna. They allow the reader to check the methods and to exercise her/his own ideas and modifications. No result is final, no approach is perfect.

B.1 Stiffness and Mass Matrices of the 2D Truss

Mass matrix, M:

$$M = \text{diag}(\ 0.41277,\ 0.41277,\ 0.41277,\ 0.41277,\ 0.41277,\ 0.41277,\ 0.23587,\ 0.23587,\ 0.41277,\ 0.41277,\ 0.41277,\ 0.41277,\ 0.41277,\ 0.41277,\ 0.23587,\ 0.23587).$$

Stiffness matrix, K:

$$K = \begin{bmatrix} K_1 & K_2 \end{bmatrix},$$

where

$K_1 = 10^6 \times$

```
[ 3.024  –1      0       0       0       0       0       0
  0      1.909   0       0       0       0       0       0
 –1      0       3.024   0      –1       0       0       0
  0      0       0       1.909   0       0       0       0
  0      0      –1       0       3.024   0      –1       0
  0      0       0       0       0       1.909   0       0
  0      0       0       0      –1       0       1.512  –0.384
  0      0       0       0       0       0      –0.384   1.621
  0      0      –0.512   0.384   0       0       0       0
  0     –1.333   0.384  –0.288   0       0       0       0
–0.512  –0.384   0       0      –0.512   0.384   0       0
–0.384  –0.288   0      –1.333   0.384  –0.288   0       0
  0      0      –0.512  –0.384   0       0      –0.512   0.384
  0      0      –0.384  –0.288   0      –1.333   0.384  –0.288
  0      0       0       0      –0.512  –0.384   0       0
  0      0       0       0      –0.384  –0.288   0      –1.333];
```

$K_2 = 10^6 \times$

```
[ 0      0      –0.512  –0.384   0       0       0       0
  0     –1.333  –0.384  –0.288   0       0       0       0
–0.512   0.384   0       0      –0.512  –0.384   0       0
  0.384 –0.288   0      –1.333  –0.384  –0.288   0       0
  0      0      –0.512   0.384   0       0      –0.512  –0.384
  0      0       0.384  –0.288   0      –1.333  –0.384  –0.288
  0      0       0       0      –0.512   0.384   0       0
  0      0       0       0       0.384  –0.288   0      –1.333
  3.024  0      –1       0       0       0       0       0
  0      1.909   0       0       0       0       0       0
 –1      0       3.024   0      –1       0       0       0
  0      0       0       1.909   0       0       0       0
  0      0      –1       0       3.024   0      –1       0
  0      0       0       0       0       1.909   0       0
  0      0       0       0      –1       0       1.512   0.384
  0      0       0       0       0       0       0.384   1.621];
```

B.2 State-Space Representation of the Deep Space Network Antenna

The state-space representation (A, B, C) of the Deep Space Network antenna in azimuth axis motion was obtained from the field test data. The following are the state matrices after reduction to 18 states. The state matrix A is in block-diagonal form. The first two diagonal entries are scalars, and the remaining eight diagonal blocks are of dimension 2×2.

$$
\begin{aligned}
A = diag\,(\ & 0 \\
& -1.104067 \\
& \\
& \begin{matrix} -0.348280 & 10.099752 \\ -10.099752 & -0.348280 \end{matrix} \\
& \\
& \begin{matrix} -0.645922 & 12.561336 \\ -12.561336 & -0.645922 \end{matrix} \\
& \\
& \begin{matrix} -0.459336 & 13.660350 \\ -13.660350 & -0.459336 \end{matrix} \\
& \\
& \begin{matrix} -0.934874 & 18.937362 \\ -18.937362 & -0.934874 \end{matrix} \\
& \\
& \begin{matrix} -0.580288 & 31.33133 \\ -31.331331 & -0.580288 \end{matrix} \\
& \\
& \begin{matrix} -0.842839 & 36.140547 \\ -36.140547 & -0.842839 \end{matrix} \\
& \\
& \begin{matrix} -0.073544 & 45.862202 \\ -45.862202 & -0.073544 \end{matrix} \\
& \\
& \begin{matrix} -3.569534 & 48.508185 \\ -48.508185 & -3.569534 \end{matrix});
\end{aligned}
$$

$$B = \begin{bmatrix} 1.004771 \\ -0.206772 \\ -0.093144 \\ 0.048098 \\ 0.051888 \\ 1.292428 \\ -0.024689 \\ 0.245969 \\ -0.234201 \\ 0.056769 \\ 0.540327 \\ -0.298787 \\ -0.329058 \\ -0.012976 \\ -0.038636 \\ -0.031413 \\ -0.115836 \\ 0.421496 \end{bmatrix};$$

$$C = \begin{bmatrix} 1.004771 & -0.204351 & 0.029024 & -0.042791 & -0.322601 & -0.545963 \\ -0.098547 & -0.070542 & 0.113774 & 0.030378 & 0.058073 & 0.294883 \\ 0.110847 & -0.109961 & -0.022496 & -0.009963 & 0.059871 & -0.198378 \end{bmatrix}.$$

References

[1] Aidarous, S.E., Gevers, M.R., and Installe, M.J., "Optimal Sensors' Allocation Strategies for a Class of Stochastic Distributed Systems," *International Journal of Control*, vol. 22, 1975, pp. 197-213.

[2] Anderson, B.D.O., "A System Theory Criterion for Positive Real Matrices," *J. SIAM Control*, vol. 5, 1967, pp. 171-182.

[3] Anderson, B.D.O., and Moore, J.B., *Optimal Control*, Prentice Hall, Englewood Cliffs, NJ, 1990.

[4] Athans, M., "On the Design of PID Controllers Using Optimal Linear Regulator Theory," *Automatica*, vol. 7, 1971, pp. 643-647.

[5] Aubrun, J.N., "Theory of the Control of Structures by Low-Authority Controllers," *Journal of Guidance, Control, and Dynamics*, vol. 3, 1980.

[6] Aubrun, J.N., and Margulies, G., "Low-Authority Control Synthesis for Large Space Structures," *NASA Contractor Report 3495*, Contract NAS1-14887, 1982.

[7] Basseville, M., Benveniste, A., Moustakides, G.V., and Rougee, A., "Optimal Sensor Location for Detecting Changes in Dynamical Behavior," *IEEE Trans. Automat. Control*, vol. AC-32, 1987, pp. 1067-1075.

[8] Bellos, J., and Inman, D.J., "Frequency Response of Nonproportionally Damped, Lumped Parameter, Linear Dynamic Systems," *ASME Journal of Vibration and Acoustics*, vol. 112, 1990, pp. 194-201.

[9] Bendat, J.S., and Piersol, A.G., *Random Data*, Wiley, New York, 1986.

[10] Benhabib, R.J., Iwens, R.P., and Jackson, R.L., "Stability of Large Space Structure Control Systems Using Positivity Concepts," *Journal of Guidance and Control*, vol. 4, 1981, pp. 487-494.

[11] Bhaskar, A., "Estimates of Errors in the Frequency Response of Non-Classically Damped Systems," *Journal of Sound and Vibration,* vol. 184, 1995, pp. 59-72.

[12] Boyd, S.P., and Barratt, C.H., *Linear Controller Design*, Prentice Hall, Englewood Cliffs, NJ, 1991.

[13] Chandrasekharan, P.C., *Robust Control of Linear Dynamical Systems*, Academic Press, London, 1996.

[14] Chung, R., and Lee, C.W., "Dynamic Reanalysis of Weakly Non-Proportionally Damped Systems," *Journal of Sound and Vibration*, vol. 111, 1986, pp. 37-50.

[15] Clough, R. W., and Penzien, J., *Dynamics of Structures*, McGraw-Hill, New York, 1975.

[16] Collins, Jr., E.G., Haddad, W.M., and Ying, S.S., "Construction of Low Authority, Nearly Non-Minimal LQG Compensators for Reduced-Order Control Design," *1994 American Control Conference*, Baltimore, MD, 1994.

[17] Cottin, N., Prells, U., and Natke, H.G. "On the Use of Modal Transformation to Reduce Dynamic Models in Linear System Identification," *IUTAM Symposium on Identification of Mechanical Systems*, Wuppertal, Germany, 1993.

[18] Cronin, L., "Approximation for Determining Harmonically Excited Response of Nonclassically Damped Systems," *ASME Journal of Engineering for Industry*, vol. 98, 1976, pp. 43-47.

[19] DeLorenzo, M.L., "Sensor and Actuator Selection for Large Space Structure Control," *Journal of Guidance, Control and Dynamics*, vol. 13, 1990, pp. 249-257.

[20] Derese, I., and Noldus, E., "Design of Linear Feedback Laws for Bilinear Systems," *International Journal of Control*, vol. 31, 1980, pp. 219-237.

[21] Desoer, C.A., and Vidyasagar, M., *Feedback Systems: Input-Output Properties,* Academic Press, New York, 1975.

[22] Dorato, P., Abdallah, C., and Cerone., V; *Linear Quadratic Control*, Prentice Hall, Englewood Cliffs, NJ, 1995.

[23] Dorf, R.C., *Modern Control Systems*, Addison-Wesley, Reading, MA, 1980.

[24] Doyle, J.C., Francis, B.A., and Tannenbaum, A.R., *Feedback Control Theory*, Macmillan, New York, 1992.

[25] Doyle, J. C., Glover, K., Khargonekar, P.P., and Francis, B.A., "State Space Solutions to Standard H_2 and H_∞ Control Problems," *IEEE Trans. Automat. Control*, vol. 34, 1989, pp. 831-847.

[26] Ewins, D.J., *Modal Testing*, Wiley, New York, 1984.

[27] Felszeghy, F., "On Uncoupling and Solving the Equations of Motion of Vibrating Linear Discrete Systems," *ASME Journal of Applied Mechanics*, vol. 60, 1993, pp. 456-462.

[28] Francis, B.A., and Wonham, W.M., "The Internal Model Principle of Control Theory," *Automatica*, vol. 12, 1976, pp. 457-465.

[29] Fukata, S., Mohri, A., and Takata, M., "On the Determination of the Optimal Feedback Gains for Multivariable Linear Systems Incorporating Integral Action," *International Journal of Control*, vol. 31, 1980, pp. 1027-1040.

[30] Fuller, C.R., Elliot, S.J., and Nelson, P.A., *Active Control of Vibrations,* Academic Press, London, 1996.

[31] Furuta, K., A. Sano, and D. Atherton, *State Variable Methods in Automatic Control.* Wiley, Chichester, 1988.

[32] Gawronski, W., "Almost-Balanced Structural Dynamics," *Journal of Sound and Vibration*, vol. 202, 1997, pp. 669-687.

[33] Gawronski, W., "Actuator and Sensor Placement for Structural Testing and Control," *Journal of Sound and Vibration*, vol. 206, 1997.

[34] Gawronski, W., *Balanced Control of Flexible Structures,* Springer-Verlag, London, 1996.

[35] Gawronski, W., "Wind Gusts Models Derived from Field Data," *Telecommunication and Data Acquisition Progress Report,* vol. 42-123, 1995, pp. 30-36 (NASA/JPL publication).

[36] Gawronski, W., "Balanced LQG Compensator for Flexible Structures," *Automatica*, vol. 30, 1994, pp. 1555-1564.

[37] Gawronski, W., "Balanced Systems and Structures: Reduction, Assignment, and Perturbations," in: *Control and Dynamics Systems*, ed. C.T. Leondes, vol. 54, Academic Press, San Diego, CA, 1992, pp. 373-415.

[38] Gawronski, W., "Model Reduction for Flexible Structures: Test Data Approach," *Journal of Guidance, Control, and Dynamics*, vol. 14, 1991, pp. 692-694.

[39] Gawronski, W., and Hadaegh, F.Y., "Balanced Input-Output Assignment," *International Journal for Systems Science*, vol. 24, 1993, pp. 1027-1036.

[40] Gawronski, W., and Juang, J.N., "Model Reduction for Flexible Structures," in: *Control and Dynamics Systems*, ed. C.T. Leondes, vol. 36, Academic Press, San Diego, CA, 1990, pp. 143-222.

[41] Gawronski, W., and Lim, K.B., "On Frequency Weighting for the H_∞ and H_2 Control Design of Flexible Structures," *AIAA Structures, Structural Dynamics, and Materials Conference/AIAA Adaptive Structures Forum*, Long Beach, CA, 1998.

[42] Gawronski, W., and Lim, K.B., "Balanced Actuator and Sensor Placement for Flexible Structures," *International Journal of Control*, vol. 65, 1996, pp. 131-145.

[43] Gawronski, W., and Lim, K.B., "Balanced H_∞ and H_2 Controllers," *Proc. 1994 IEEE American Control Conference*, Baltimore, MD, 1994, pp. 1116-1122.

[44] Gawronski, W., and Lim, K.B., "Controllability and Observability of Flexible Structures with Proof-Mass Actuators," *Journal of Guidance, Control, and Dynamics*, vol. 16, 1993, pp. 899-902.

[45] Gawronski, W., and Mellstrom, J.A., "Model Reduction for Systems with Integrators," *Journal of Guidance, Control, and Dynamics*, vol. 15, 1992, pp. 1304-1306.

[46] Gawronski, W., and Mellstrom, J.A., "Control and Dynamics of the Deep Space Network Antennas," in: *Control and Dynamics Systems*, ed. C.T. Leondes, vol. 63, Academic Press, San Diego, CA, 1994, pp. 289-412.

[47] Gawronski W., and Natke, H.G., "Realizations of the Transfer Function Matrix," *International Journal of Systems Science*, vol. 18, 1987, pp. 229-236.

[48] Gawronski, W., and Natke, H.G., "Balanced State Space Representation in the Identification of Dynamic Systems," in: *Application of System Identification in Engineering*, ed. H.G. Natke, Springer-Verlag, New York, 1988.

[49] Gawronski, W., Racho, C., and Mellstrom, J.A., "Application of the LQG and Feedforward Controllers to the Deep Space Network Antennas," *IEEE Trans. Control System Technology*, vol. 3, 1995, pp. 417-421.

[50] Gawronski, W., and Sawicki, J.T., "Response Errors of Non-Proportionally Lightly Damped Structures," *Journal of Sound and Vibration*, vol. 200, 1997, pp. 543-550.

[51] Gawronski, W., and Williams, T., "Model Reduction for Flexible Space Structures," *Journal of Guidance, Control, and Dynamics*, vol. 14, No.1, 1991, pp. 68-76.

[52] Glover, K., "All Optimal Hankel-Norm Approximations of Linear Multivariable Systems and their L^∞-Error Bounds," *International Journal of Control*, vol. 39, 1984, pp. 1115-1193.

[53] Glover, K., and Doyle, J.C., "State-Space Formulae for All Stabilizing Controllers That Satisfy an H_∞-Norm Bound and Relations to Risk Sensitivity," *Systems and Control Letters,* vol. 11, 1988, pp. 167-172.

[54] Golub, G.H., and Van Loan, C.F., *Matrix Computations*, The Johns Hopkins University Press, Baltimore, MD, 1989.

[55] Gregory, Jr., C.Z., "Reduction of Large Flexible Spacecraft Models Using Internal Balancing Theory," *Journal of Guidance, Control, and Dynamics*, vol. 7, 1984, pp. 725-732.

[56] Horn, R.A., and Johnson, C.R., *Matrix Analysis*, Cambridge University Press, Cambridge, England, 1985.

[57] Hwang, H., and Ma, F., "On the Approximate Solution of Nonclassically Damped Linear Systems," *ASME Journal of Applied Mechanics*, vol. 60, 1993, pp. 695-701.

[58] Hyland, D.C., "Distributed Parameter Modeling of Flexible Spacecraft: Where's the Beef?" *NASA Workshop on Distributed Parameter Modeling and Control of Flexible Aerospace Systems*, Williamsburg, VA, 1992, NASA Conference Publication 3242, 1994, pp. 3-23.

[59] Hyland, D.C., and Bernstein, D.S., "The Optimal Projection Equations for Model Reduction and the Relationships Among the Methods of Wilson, Skelton, and Moore," *IEEE Trans. Automat. Control*, vol. AC-30, 1985, pp. 1201-1211.

[60] Inman D.J., *Vibration with Control, Measurements, and Stability*, Prentice Hall, Englewood Cliffs, NJ, 1989.

[61] Johnson, C.D., "Optimal Control of the Linear Regulator with Constant Disturbances," *IEEE Trans. Automat. Control*, vol. 13, 1968, pp. 416-421.

[62] Jonckheere, E.A., "Principal Component Analysis of Flexible Systems – Open Loop Case," *IEEE Trans. Automat. Control*, vol. 27, 1984, pp. 1095-1097.

[63] Jonckheere, E.A., and Silverman, L.M., "A New Set of Invariants for Linear Systems – Application to Reduced Order Controller Design," *IEEE Trans. Automat. Control*, vol. AC-28, 1983, pp. 953-964.

[64] Joshi, S.M., *Control of Large Flexible Space Structures*, Springer-Verlag, Berlin, 1989.

[65] Juang, J.-N., *Applied System Identification*, Prentice Hall, Englewood Hills, NJ, 1994.

[66] Juang, J-N., and Rodriguez, G., "Formulations and Applications of Large Structure Actuator and Sensor Placements," *VPI/AIAA Symposium on Dynamics and Control of Large Flexible Spacecraft*, Blacksburg, 1979, pp. 247-262.

[67] Junkins, J.L., and Kim, Y., *Introduction to Dynamics and Control of Flexible Structures,* published by the American Institute of Aeronautics and Astronautics, Washington, DC, 1993.

[68] Kailath, T., *Linear Systems*, Prentice Hall, Englewood Cliffs, NJ, 1980.

[69] Kammer, D., "Sensor Placement for On-Orbit Modal Identification and Correlation of Large Space Structures," *Journal of Guidance, Control and Dynamics*, vol. 14, 1991, pp. 251-259.

[70] Kim, Y., and Junkins, J.L., "Measure of Controllability for Actuator Placement," *Journal of Guidance, Control and Dynamics*, vol. 14, 1991, pp. 895-902

[71] Kwakernaak, H., and Sivan, R., *Linear Optimal Control Systems*, Wiley, New York, 1972.

[72] Kwon, Y.W., and Bang, H., *The Finite Element Method Using Matlab,* CRC Press, Boca Raton, FL, 1997.

[73] Levine, W.S., and Reichert, R.T., "An Introduction to H_∞ Control Design," *Proc. 29th Conference on Decision and Control*, Honolulu, Hawaii, 1990, pp. 2966-2974.

[74] Li, X.P., and Chang, B.C., "On Convexity of H_∞ Riccati Solutions and its Applications," *IEEE Trans. Automat. Control*, vol. 38, 1993, pp. 963-966.

[75] Lim, K.B., "Method for Optimal Actuator and Sensor Placement for Large Flexible Structures," *Journal of Guidance, Control and Dynamics*, vol. 15, 1992, pp. 49-57.

[76] Lim, K.B., and Gawronski, W., "Actuator and Sensor Placement for Control of Flexible Structures," in: *Control and Dynamics Systems*, ed. C.T. Leondes, vol. 57, Academic Press, San Diego, CA, 1993, pp. 109-152.

[77] Lim, K.B., Maghami, P.G., and Joshi, S.M., "Comparison of Controller Designs for an Experimental Flexible Structure," *IEEE Control Systems Magazine*, June 1992, pp. 108-118.

[78] Lin, C.F., *Advanced Control Systems Design*, Prentice Hall, Englewood Cliffs, NJ, 1994.

[79] Lindberg Jr., R.E., and Longman, R.W., "On the Number and Placement of Actuators for Independent Modal Space Control," *Journal of Guidance, Control and Dynamics*, vol. 7, 1984, pp. 215-223.

[80] Longman, R. W., and Alfriend, K. T., "Energy Optimal Degree of Controllability and Observability for Regulator and Maneuver Problems," *Journal of the Astronautical Sciences*, vol. 38, 1990, pp. 87-103.

[81] Maciejowski, J.M., *Multivariable Feedback Design*, Addison-Wesley, Wokingham, England, 1989.

[82] Maghami, P.G., and Joshi, S.M., "Sensor/Actuator Placement for Flexible Space Structures," *IEEE American Control Conference*, San Diego, CA, 1990, pp. 1941-1948.

[83] Maghami, P.G., and Joshi, S.M., "Sensor-Actuator Placement for Flexible Structures with Actuator Dynamics," *AIAA Guidance, Navigation, and Control Conference*, New Orleans, LA, 1991, pp. 46-54.

[84] Meirovitch, L., *Dynamics and Control of Structures*, Wiley, New York, 1990.

[85] Moore, B.C., "Principal Component Analysis in Linear Systems, Controllability, Observability and Model Reduction," *IEEE Trans. Automat. Control*, vol. 26, 1981, pp. 17-32.

[86] Mustafa, D., and Glover, K., "Controller Reduction by H_∞-Balanced Truncation," *IEEE Trans. Automat. Control*, vol. 36, 1991, pp. 668-682.

[87] Natke, H.G., *Einfuehrung in die Theorie und Praxis der Zeitreihen- und Modalanalyse*, Vieweg, Braunschweig, 1992.

[88] Nicholson, W., "Response Bounds for Nonclassically Damped Mechanical Systems Under Transient Loads," *ASME Journal of Applied Mechanics* vol. 54, 1987, pp. 430-433.

[89] Opdenacker, P., and Jonckheere, E.A., LQG Balancing and Reduced LQG Compensation of Symmetric Passive Systems," *International Journal of Control*, vol. 41, 1985, pp. 73-109.

[90] Panossian, H., Gawronski, W., and Ossman, H., "Balanced Shaker and Sensor Placement for Modal Testing of Large Flexible Structures," *IMAC-XVI*, Santa Barbara, CA, 1998.

[91] Popov, V.M., *Hyperstability of Automatic Control Systems*, Springer-Verlag, New York, 1973.

[92] Porter, B., "Optimal Control of Multivariable Linear Systems Incorporating Integral Feedback," *Electronics Letters,* vol. 7, 1971.

[93] Porter, B., and Crossley R., *Modal Control*, Taylor and Francis, London, 1972.

[94] Preumont, A., *Vibration Control of Active Structures*, Kluwer Academic, Dordrecht, 1997.

[95] Shahian, B., and Hassul, M., *Control System Design Using Matlab*, Prentice Hall, Englewood Cliffs, NJ, 1993.

[96] Shahruz M., and Ma, F., "Approximate Decoupling of the Equations of Motion of Linear Underdamped Systems," *ASME Journal of Applied Mechanics*, vol. 55, 1988, pp. 716-720.

[97] Skelton, R.E., "Cost Decomposition of Linear Systems with Application to Model Reduction," *International Journal of Control*, vol. 32, 1980, pp. 1031-1055.

[98] Skelton, R.E., *Dynamic System Control: Linear System Analysis and Synthesis*, Wiley, New York, 1988.

[99] Skelton, R.E., and Hughes, P.C., "Modal Cost Analysis for Linear Matrix Second-Order Systems," *Journal of Dynamic Systems, Measurements and Control*, vol. 102, 1980, pp. 151-158.

[100] Skelton, R.E., and DeLorenzo, M.L., "Selection of Noisy Actuators and Sensors in Linear Stochastic Systems," *Journal of Large Scale Systems, Theory and Applications*, vol. 4, 1983, pp. 109-136.

[101] Skelton, R.E., Singh, R., and Ramakrishnan, J., "Component Model Reduction by Component Cost Analysis," *AIAA Guidance, Navigation and Control Conference*, Minneapolis, 1988, pp. 264-2747.

[102] Skogestad, S., and Postlethwaite, I., *Multivariable Feedback Control,* Wiley, Chichester, England, 1996.

[103] Uwadia, E., and Esfandiari, R.S., "Nonclassically Damped Dynamic Systems: An Iterative Approach," *ASME Journal of Applied Mechanics*, vol. 57, 1990, pp. 423-433.

[104] Voth, C.T., Richards, Jr., K.E., Schmitz, E., Gehling, R.N., and Morgenthaler, D.R., "Integrated Active and Passive Control Design Methodology for the LaRC CSI Evolutionary Model," *NASA Contractor Report 4580*, Contract NAS1-19371, 1994.

[105] Wen, J.T., "Time Domain and Frequency Domain Conditions for Strict Positive Realness," *IEEE Trans. Automat. Control*, vol. AC-33, 1988, pp. 988-992.

[106] Wicks, M.A., and DeCarlo, R.A., "Grammian Assignment of the Lyapunov Equation," *IEEE Trans. Automat. Control*, vol. AC-35, 1990, pp. 465-468.

[107] Willems, J.C., "Dissipative Dynamical Systems, Part I: General Theory, Part II: Linear Systems with Quadratic Supply Rates," *Arch. Rational Mech. Anal.,* vol. 45, 1972, pp. 321-351 and pp. 352-392.

[108] Willems, J.C., "Realization of Systems with Internal Passivity and Symmetry Constraints," *Journal of the Franklin Institute*, vol. 301, 1976, pp. 605-620.

[109] Williams, T., "Closed Form Grammians and Model Reduction for Flexible Space Structures," *IEEE Trans. Automat. Control*, vol. AC-35, 1990, pp. 379-382.

[110] Wilson, D.A., "Optimum Solution of Model-Reduction Problem," *IEE Proceedings*, vol. 119, 1970, pp. 1161-1165.

[111] Wilson, D.A., "Model Reduction for Multivariable Systems," *International Journal of Control*, vol. 20, 1974, pp. 57-60.

[112] Wortelboer, P., and van Oostveen, H., "Modal Reduction Guided by Hankel Singular Value Intervals," *Selected Topics in Identification, Modeling and Control*, vol. 1, 1990.

[113] Yae, H., and Inman, D. J., "Response Bounds for Linear Underdamped Systems," *ASME Journal of Applied Mechanics,* vol. 54, 1987, pp. 419-423.

[114] Yahagi, T., "Optimal Output Feedback Control in the Presence of Step Disturbances," *International Journal of Control*, vol. 26, 1977, pp. 753-762.

[115] Zhou, K., *Robust and Optimal Control*, Prentice Hall, Englewood Hills, NJ, 1995.

[116] Zimmerman, D.C, and Inman, D.J., "On the Nature of the Interaction Between Structures and Proof-Mass Actuators," *Journal of Guidance, Control, and Dynamics*, vol. 13, 1990, pp. 82-88.

Index

Mechanical Engineering Series *(continued)*

Laminar Viscous Flow
V.N. Constantinescu

Thermal Contact Conductance
C.V. Madhusudana

Transport Phenomena with Drops and Bubbles
S.S. Sadhal, P.S. Ayyaswamy, and J.N. Chung

Fundamentals of Robotic Mechanical Systems:
Theory, Methods, and Algorithms
J. Angeles

Electromagnetics and Calculations of Fields
J. Ida and J.P.A. Bastos

Mechanics and Control of Robots
K.C. Gupta

Wave Propagation in Structures:
Spectral Analysis Using Fast Discrete Fourier Transforms, 2nd ed.
J.F. Doyle

Fracture Mechanics
D.P. Miannay

Principles of Analytical System Dynamics
R.A. Layton

Composite Materials:
Mechanical Behavior and Structural Analysis
J.M. Berthelot

Modern Inertial Technology:
Navigation, Guidance, and Control, 2nd ed.
A. Lawrence

Dynamics and Control of Structures:
A Modal Approach
W.K. Gawronski